Physico-chimie des interfaces bactérie - solution aqueuse

Etienne Dague

UNIVERSITÉ HENRI POINCARÉ NANCY 1
- 2006 -

ÉCOLE DOCTORALE BIOLOGIE SANTÉ ENVIRONNEMENT
Spécialité : Chimie et Microbiologie de l'Eau

THÈSE

Présentée et soutenue publiquement
Le 6 novembre 2006

Pour obtenir le titre de

DOCTEUR DE L'UNIVERSITÉ HENRI POINCARÉ - NANCY 1

Par

Étienne DAGUE

Docteur en Pharmacie,
Titulaire du Diplôme d'Études Approfondies Chimie et Microbiologie de l'Eau

Sujet :

Physico - chimie des interfaces bactérie - solution aqueuse

MEMBRES DU JURY

Rapporteurs :

Pr Marie Noëlle Bellon-Fontaine, URBHM, INRA

Pr Paul Rouxhet, CIFA, UCL, Belgique

Examinateurs :

Pr Jean-Claude Block, Directeur de thèse, LCPME, UMR 7564 CNRS-UHP

Dr Fabien Gaboriaud, Co-encadrant de thèse, LCPME UMR 7564 CNRS-UHP

Dr Frédéric Jorand, Co-encadrant de thèse, LCPME, UMR 7564 CNRS-UHP

Dr Jérôme Duval, LEM, UMR 7569 CNRS-INPL

Membre invité :

Dr Job Ubbink, Centre de Recherche Nestlé, Lausanne, Suisse

Remerciements

Marie-Noelle Bellon-Fontaine a été le rapporteur de cette thèse ainsi que le président du jury. Je la remercie pour son analyse du travail, la discussion et sa gestion des débats qui ont suivi l'exposé oral.

Je remercie Paul Rouxhet d'avoir accepté d'être le rapporteur de ma thèse. Ses questions ont permis de mettre en relief le travail réalisé et de dégager, encore, d'autres perspectives attrayantes.

Merci à Job Ubbink d'avoir accepté de juger ce travail. Sa connaissance appliquée de l'interface des bactéries a permis d'élagir la discussion et d'envisager des applications potentielles.

Je remercie Jean-Claude Block, directeur du LCPME, pour m'avoir accueilli au laboratoire, m'avoir fait confiance en toutes circonstances et avoir su créer l'ambiance sereine nécessaire à la réalisation de ce travail de thèse. Je remercie également le chercheur-enseignant, le Professeur, qui ne perd jamais de vue la recherche, même dans son enseignement théorique, ce qui le rend différent des autres enseignants. Quand le contenu n'est plus si important que la façon de l'obtenir puis de le comprendre et de l'interpréter, la consommation de la science s'arrête et la recherche commence. Cette subtile transition se retrouve dans l'enseignement que j'ai reçu de Jean-Claude Block. Qu'il soit remercié pour cette richesse qu'il tente de partager avec les étudiants.

Fabien Gaboriaud a été le coencadrant de ce travail de thèse et je lui adresse ici toute l'expression de ma sincère amitié. Ces trois années passées à cogiter, expérimenter, recommencer, écrire ensemble ont été des moments privilégiés et précieux. Fabien Gaboriaud a su me faire progresser dans mon travail scientifique, mais aussi sur un plan plus personnel, par son ouverture d'esprit, sa capacité à faire la part des choses plus ou moins cruciales, sa remise en cause personnelle admirable. Merci pour la science, merci pour la leçon de vie.

Frédéric Jorand a été le coencadrant de cette thèse. Je le remercie pour sa présence et son soutien sans faille dans les moments difficiles de remise en cause, dans les réunions,

séminaires et auditions divers qui ont jalonné ces 3 années. Merci pour ta modération et ton recul en toutes circonstances.

La rencontre avec Jérome Duval a donné un élan supplémentaire à ce travail. Qu'il soit remercié pour sa patience (pour m'expliquer les subtilités de la modélisation), et sa capacité à prendre en compte les contraintes liées au caractère biologique des échantillons.

Bien sur la vie au laboratoire se déroule avec des condisciples. Les plus anciens accueillent les plus jeunes qui deviennent plus anciens etc etc. Pour ma part, j'ai été accueilli par Asfaw avec qui j'ai partagé le même bureau pendant 3 ans. Cette cohabitation s'est faite d'abord dans un respect mutuel admirable puis a glissé vers une franche amitié. Asfaw, je te remercie pour ta patience, ton calme, ta sagesse dans mes moments (fréquents ?) d'agacement, d'énervement, de révolte. Ta capacité à prendre rapidement du recul est impressionnante et devrait bien me servir d'exemple. Je penserai souvent à toi quand la moutarde me montera au nez dans le futur.
Asfaw et moi avons ensuite accueillie la thésarde suivante dans notre bureau, Lucie. J'espère qu'elle n'a pas trop souffert de sa situation et je lui souhaite de réussir un beau doctorat, en évitant les pièges de la forêt tropicale engloutie par son barrage guyanais préféré. Qu'il ne devienne pas un barrage contre le Pacifique, jeune Padawan. Dans la famille des anciens thésards du LCPME, je veux remercier les plus anciens de l'équipe spectroscopie : Emmanuel et Marie Camille dont la bonne humeur quotidienne et la percolation d'un café puissant m'ont permis une intégration rapide à l'équipe dont j'ai fait à moitié partie (les caprices de l'organigramme à la française : non content d'avoir 3 universités à Nancy, les laboratoires sont aussi découpés en sous fractions dénommées équipes. Et les thésards comme moi, sans doute les plus retors, vont jusqu'à être répartis par moitié dans les équipes... Etrange sensation de cul entre 2 chaises, mélangé à la possibilité de bouffer à 2 râteliers : intéressante expérience). Dans la catégorie des plus jeunes, je tiens à saluer ici Emilie qui m'a soutenu durant les mois d'été qui ont précédé le dépôt de cette thèse. L'art et la science se confondent souvent, car il n'y a pas de place pour une science laide. Ta persévérance à artistiquement fleurir le bureau m'a servi d'exemple pour terminer ce manuscrit dans les délais ... J'associe à ces remerciements Cyril, Frédéric, Lydie, Sébastien et Nathalia qui ont constitué la bande de joyeux doctorants, avec Asfaw, Lucie et Emilie, des 2 dernières années. Je crois que cette équipe laissera des souvenirs au laboratoire. Merci à Jean-Paul Moulin pour nous avoir ouvert le laboratoire et sa cave les soirs de fête, réglé les problèmes d'alarme incendie et intrusion les

soirs de raclette, avoir chanté avoir moi les lacs du Connemara un certain soir. Surtout merci pour l'assistance pratique et technique quasi quotidienne à laquelle il faut associer Gérard Paquot. Précieux hommes que ceux qui sont compétents dans leur domaine, font la part des choses, connaissent les limites et nous font parfois redescendre sur terre, dans la réalité. Dans le même contexte, je tiens à remercier l'équipe « administrative » du LCPME (Christelle, Marie, Jacqueline et Monique) grâce a qui le calvaire des missions, billets de train, d'avion, visa, etc se traverse avec un minimum d'efforts.

La thèse est une aventure scientifique et humaine. Les hommes et les femmes doivent s'accorder et s'entendre pour cheminer sur la voie de la recherche. J'ai toujours trouvé au laboratoire une atmosphère chaleureuse et efficace. Ces trois années resteront particulières pour moi. De prime abord, rien ne ressemble plus à un laboratoire qu'un autre laboratoire. Et bien, les hommes et les femmes qui le font vivre font la différence. Je remercie tous les membres du laboratoire pour cette ambiance propice à un travail agréable et efficace.

Sommaire

1. Introduction générale

Le développement des biofilms s'opère sur n'importe quels matériaux en contact avec de l'eau : canalisations [1, 2], pipelines, roches, dents [3, 4], parois d'aquarium, coques des bateaux, systèmes de refroidissement, façades des monuments [5], racines, feuilles des arbres [6, 7] ou troncs d'arbres immergés dans un barrage (biofilms épiphytes), bassins contenant des déchets radioactifs [8], cathéters [9, 10], prothèses [9, 11, 12]. La croissance de ces films biologiques est plus au moins rapide, mais inexorable, manifestant la puissance du vivant à coloniser les environnements les plus variés en terme de température, pression, osmolarité. Ces environnements paraissent parfois franchement hostiles. Dans de nombreux cas, le développement des biofilms induit soit un dysfonctionnement d'une installation industrielle, une surconsommation d'énergie, soit un risque pour la santé humaine. Ils apparaissent donc comme le plus souvent néfastes et de nombreuses recherches ont pour objet d'endiguer la colonisation des surfaces, d'éliminer les films formés, d'élaborer des matériaux moins propices à la fixation des cellules. Cependant, la meilleure connaissance de ce mode de vie sédentaire des bactéries conduit aujourd'hui à utiliser des biofilms maîtrisés, de composition plus ou moins bien connue, à des fins positives (en station d'épuration des eaux usées urbaines par exemple). Quoi qu'il en soit, il en ressort qu'un grand nombre de domaines industriels est concerné par la question des biofilms et donc par l'étape initiale de leur formation : l'adhésion des micro-organismes.

L'adhésion des micro-organismes aux surfaces est un problème majeur [13]. Cette question est étudiée depuis plus de 20 ans et malgré les approches pluridisciplinaires mises en oeuvre, les mécanismes régissant l'adhésion microbienne sont encore assez mal connus. Une meilleure compréhension des phénomènes conduisant à l'adhésion d'une cellule sur une surface est nécessaire pour limiter la formation des biofilms ou contrôler leur composition dans les usines de traitement des eaux usées, par exemple. La première étape de développement d'un biofilm est l'interaction d'une cellule planctonique avec un support. Au cours de cette étape, les processus biologiques sont peu impliqués, même si certaines bactéries sont capables de synthétiser des appendices comme les pili [14] ou d'autres extensions cellulaires [15] décrits comme augmentant les capacités d'adhésion des cellules. Ainsi, l'étude des propriétés physico-chimiques de l'interface entre la bactérie et son environnement liquide est un enjeu majeur pour aboutir à une meilleure compréhension de l'étape initiale de formation des biofilms, c'est-à-dire l'adhésion d'une bactérie planctonique à un support.

Les échanges de matière et les interactions moléculaires, impliqués dans les phénomènes d'adhésion, mais également de biominéralisation ou de reconnaissance spécifique de surface se situent au niveau de l'interface entre les bactéries et leur environnement. Dans ce contexte, le concept d'interface nécessite d'être clairement défini. La notion d'interface présume l'existence de deux systèmes : d'une part la bactérie et d'autre part, son environnement. Cette interface n'est cependant pas une surface ou une aire marquant nettement la séparation entre la cellule bactérienne et le milieu environnant. Nous inclurons dans l'interface bactérienne l'ensemble des structures de transition entre la cellule et le milieu liquide. La notion d'interface fait ici référence à une zone en trois dimensions, possédant une épaisseur, au sein de laquelle s'opère la transition entre 2 systèmes et sous la double influence du métabolisme bactérien et des conditions physico-chimiques de l'environnement. Nous reviendrons en détail sur le concept de surface et d'interface dans le paragraphe 2.2 interface bactérienne.

Au cours des vingt dernières années, l'interface de nombreux systèmes biologiques a été sondée selon des approches expérimentales majoritairement globales [16, 17] donnant accès à la connaissance des propriétés moyennes d'une population bactérienne. Ainsi, l'hydrophobie [16, 18-22], la charge et ou le potentiel de surface [23-26], la composition chimique de l'interface de nombreux micro-organismes ont été explorées [3, 27-30]. Beaucoup de travaux traitent la question de l'adhésion en qualifiant le caractère hydrophobe des cellules [16, 20-23, 31-37]. La méthode la plus simple et la plus fréquemment utilisée est le test d'adhésion microbien aux hydrocarbures [38]. Ce test est d'une mise en oeuvre aisée ce qui peut expliquer sa popularité. Cependant, il n'est pas que spécifique du caractère hydrophobe et cette analyse basée sur la partition solvant-phase aqueuse est fortement dépendante de la charge de surface des particules en interaction [35, 39-41].

Les interactions entre une bactérie et une surface, conduisant à son adhésion, sont un mélange complexe de différentes contributions physico-chimiques, principalement l'hydrophobie et les interactions électrostatiques [24, 42-44]. La charge électrostatique des cellules microbiennes peut être appréhendée de deux manières. Les titrages potentiométriques donnent une information indirecte sur la charge globale des cellules *via* la consommation protonique globale d'une suspension de micro-organismes. Les mobilités électrophorétiques, mesurées individuellement, permettent d'appréhender des hétérogénéités à l'échelle de la population microbienne, mais aussi de quantifier les propriétés électrocinétiques (densité de charge, hydrodynamique) de ces mêmes populations.

L'originalité de notre approche expérimentale réside, d'une part, dans l'utilisation de méthodes globales, couplées à des méthodes locales (du nanomètre au micromètre), préservant au mieux l'échantillon biologique (AFM en milieu liquide ou MET après cryofixation) qui permettent de sonder les cellules individuelles. La confrontation des résultats aux différentes échelles permet de donner une nouvelle approche des phénomènes d'adhésion des bactéries sur un support. Cette avancée a pu être réalisée, en partie, grâce au développement théorique de modèles tenant compte du caractère diffus, c'est-à-dire hétérogène, et souple des cellules bactériennes.

Le modèle choisi pour l'étude de l'interface entre les bactéries et leur environnement liquide est le genre *Shewanella.* Quatre souches (*Shewanella putrefaciens* CIP 8040 et CN32, *Shewanella oneidensis* MR4, *Shewanella algae* BrY) ont été sélectionnées, sur la base de clichés de Microscopie Electronique à Transmission (MET), car elles présentent des ultrastructures interfaciales différentes. Les propriétés physico-chimiques des différentes souches sont donc, *a priori*, différentes, laissant présumer des comparaisons intéressantes. De plus, ce genre bactérien a une importance environnementale, car il participe au cycle bio-géo-chimique du fer [45], particulièrement étudié au LCPME [46, 47]. En effet, la bioréduction anaérobie des oxydes de fer par les bactéries du genre *Shewanella,* conduit à différents minéraux comme la rouille verte ou la magnétite [45, 48] potentiellement utilisables en dépollution des sols. D'autre part, le genre *Shewanella* est retrouvé, sous forme de biofilms, dans l'industrie agroalimentaire notamment poissonnière [49, 50]. L'adaptation de certaines souches au froid, comme *Shewanella oneidensis* MR1 [51], induisent la contamination d'aliments conservés en atmosphère réfrigérée. Enfin, l'espèce *algae* a été rapportée comme pathogène opportuniste [52]. Ainsi ces 4 souches possédant différentes structures de l'interface, et présentant également des intérêts d'un point de vue géochimique, et sanitaires représentent un modèle d'étude idéal.

Ce mémoire est organisé en six parties. La partie « contexte scientifique » a pour but de faire le point sur la connaissance de l'interface des bactéries Gram négatives, et en particulier, sur les caractéristiques du genre *Shewanella.* Les méthodes expérimentales employées dans ce mémoire pour déterminer les propriétés physico-chimiques de l'interface des micro-organismes, à différentes échelles, y sont aussi présentées succinctement. Les résultats sont ensuite exposés sous la forme d'articles scientifiques. Le lecteur trouvera, en préambule à la

publication, un résumé en français reprenant l'essentiel de la problématique, de la démarche scientifique, des résultats et de leur interprétation. Une synthèse sous forme de schémas est également proposée en préambule à l'article lui-même. Les résultats obtenus sur les quatre souches à l'échelle locale, à différentes valeurs de pH et force ionique, font l'objet de la partie intitulée : « Quantification des propriétés nanomécaniques et électrohydrodynamiques des interfaces de *Shewanella* spp ». L'étude multiéchelle réalisée sur la souche de *Shewanella putrefaciens* CIP 8040 est décrite dans la quatrième partie ; elle consiste à expliquer les phénomènes macroscopiques par les observations à l'échelle micro voire nanoscopique. Le cinquième chapitre est consacré à la mise en œuvre des phénomènes observés et mesurés dans les deux chapitres précédents. La synergie et complémentarité entre l'approche électrocinétique et nanomécanique est envisagée. La dernière partie intitulée « Discussion générale, perspectives et conclusions» reprend les points forts des travaux exposés précédemment, mais aussi les éléments discutables qu'il s'agit de mettre en perspective avec d'autres travaux, utilisant d'autres approches.

Ces travaux pluridisciplinaires ont été menés en équipe, au sein du Laboratoire de Chimie Physique et Microbiologie pour l'Environnement. Il est le fruit de la collaboration interne entre l'équipe spectrochimie des interfaces et l'équipe microbiologie et physique. Les développements théoriques et les modélisations ont été réalisés en association avec Jérôme Duval du Laboratoire Environnement et Minéralurgie. Enfin les résultats présentés dans le premier article ont été obtenus au cours du DEA de Sidney Bailet. La coordination des compétences et spécialités de chacun des acteurs a permis de dégager une synergie scientifique conduisant à la vision novatrice de l'interface des bactéries présentée dans ce mémoire.

NB : les références bibliographiques rassemblées à la fin de ce mémoire regroupent la littérature citée dans l'introduction générale, le contexte scientifique et la discussion générale, perspectives et conclusions. La bibliographie relative aux articles scientifiques se trouve à la fin de chacun d'eux, formatée selon les recommandations des éditeurs.

2. Contexte scientifique

2.1. Morphologie de l'enveloppe des bactéries Gram négatives

Les bactéries Gram négatives présentent, de l'extérieur vers l'intérieur, une membrane externe, une fine couche de peptidoglycane et enfin une membrane interne ou cytoplasmique. Le résultat, dit négatif, de la coloration selon Gram est une conséquence de cette organisation. Lors de l'étape de lavage à l'alcool de la méthode de Gram, le cristal violet n'est pas retenu par la faible quantité de peptidoglycane et la cellule prend la couleur rose du colorant appliqué dans un deuxième temps (la fuchsine ou la safranine). Ce sont donc bien les structures de l'interface qui sont à la base de la classification des procaryotes [53].

L'espace entre les deux bicouches phospholipidiques (membrane externe et membrane interne) est appelé espace périplasmique ou périplasme. Cet espace ne fait pas partie du cytoplasme puisqu'il en est séparé par la membrane interne, mais ce n'est pas non plus le milieu extérieur duquel la membrane externe le sépare. Il s'agit d'un compartiment des bactéries Gram négatives soumis aux fluctuations du milieu environnant, jouant le rôle de filtre sélectif pour la bactérie, mais aussi permettant à la cellule des synthèses qu'elle ne pourrait pas faire dans son cytoplasme [54]. Le périplasme caractérise bien la notion de transition entre la cellule vivante et l'environnement physico-chimique.

Une des particularités de la membrane externe est son asymétrie. La face externe contient les lipopolysaccharides (LPS) alors que la face interne présente la majorité des phospholipides. Les LPS sont enchâssés dans la membrane interne par le lipide A et sont en mouvement constant (*cf.* Figure 1). La membrane externe laisse librement diffuser les ions et les molécules de petite taille grâce aux porines [55]. Cependant, elle ne doit pas laisser échapper des constituants, vitaux pour la cellule, présents dans l'espace périplasmique tel que les protéines affines ou les cytochromes.

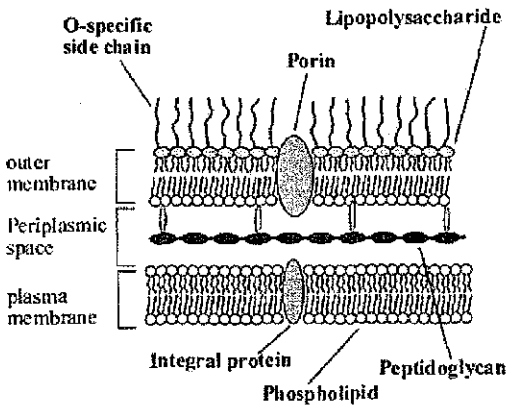

Figure 1 : Schéma de la membrane externe et du LPS des bactéries gram négatives [56, 57]

Des structures supplémentaires à la périphérie de la membrane externe des bactéries Gram négatives ont été décrites : S-Layer, capsule, etc [58] ; elles peuvent être considérées comme faisant partie de l'interface, car synthétisées et remaniées par la cellule, mais sous l'influence des conditions physico-chimiques du milieu. Enfin, notons que certaines bactéries Gram négatives sont capables de synthétiser des appendices plus ou moins longs dans un but bien précis. Citons : les fimbriae ou pili, qui sont des structures protéiniques tubulaires connues pour augmenter considérablement les capacités d'adhésion des bactéries et pouvant participer au processus de conjugaison bactérienne ; les flagelles de différents types, dont le rôle est d'assurer une certaine motricité aux cellules bactériennes planctoniques.

2.2. L'interface bactérienne

La définition de l'interface bactérienne est une question délicate. Ce même terme est employé par plusieurs communautés scientifiques, pour décrire des notions différentes. Les spécialistes des biofilms [2, 59, 60] entendent par interface la matrice d'exopolymères qui forment un gel emprisonnant les cellules. Dans ce cas l'interface est aussi une réserve de nutriments, un piège à oxydants, le siège de transferts de gènes et d'informations entre les bactéries. L'interface est représentée en trois dimensions, mais à l'échelle du µm voir de la dizaine de µm.

Pour la communauté des physico-chimistes, l'interface se définit comme un plan de transition entre 2 phases, par exemple un solide et un gaz. L'échelle de taille est alors de la dizaine de nanomètres. On comprend bien, alors, la difficulté à trouver une définition de l'interface bactérienne commune à ces deux communautés appelées à collaborer autour de la caractérisation des propriétés physico-chimiques des interfaces bactériennes... L'introduction générale, propose une définition possible, mais discutable à l'infini, de l'interface des bactéries qui ont servi de modèles dans notre étude. L'interface est considérée comme une zone de transition multidimensionnelle, de 5 à 120 nm d'épaisseur, basée sur la connaissance des structures non cytoplasmiques des bactéries Gram négatives, découlant des observations en microscopie électronique. La membrane cytoplasmique, le périplasme contenant le peptidoglycane, la membrane externe et les LPS sont les structures composant l'interface (*cf.* Figure 1).

Au final, cette définition de l'interface englobe les structures de la bactérie qui font géographiquement la transition entre deux systèmes (vivant et inerte), mais aussi les structures influencées à la fois par le métabolisme de la bactérie et les conditions physico-chimiques de son environnement.

2.3. Présentation du modèle bactérien : quatre souches du genre *Shewanella*

Les bactéries du genre *Shewanella* sont des bacilles (*cf.* Figure 2) à coloration de Gram négatives, positives ou négatives pour le test à l'oxydase, aérobies anaérobies facultatives non fermentatives, organo-hétérotrophes [61]. Elles ont un caractère ubiquitaire et se retrouvent dans des environnements aussi variés que l'eau de mer ou l'eau douce, les sédiments et les sols, les canalisations d'eau potable, l'industrie agro-alimentaire (en particulier les poissonneries) ou les intestins des animaux supérieurs dont l'homme.

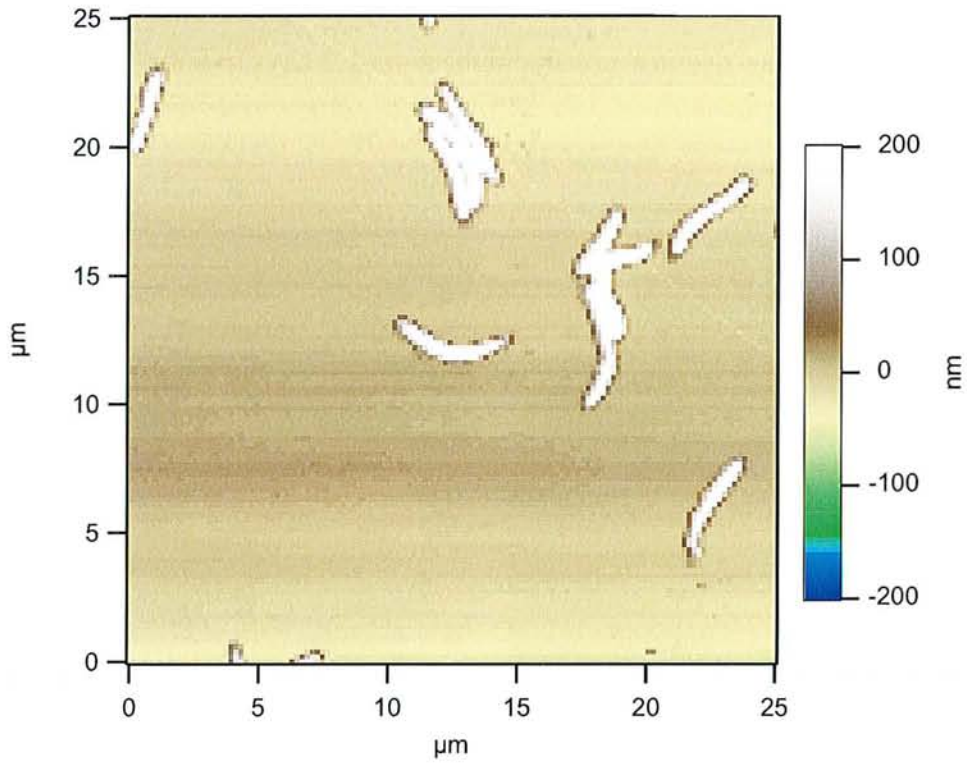

Figure 2 : *Shewanella putrefaciens* CIP 8040 imagée par microscopie à force atomique (image réalisée à l'école de Chimie de l'Université de Melbourne au cours d'une collaboration). L'image en trois dimensions est obtenue en mode contact et en milieu liquide, sur des cellules potentiellement vivantes. Le code couleur, à droite de l'image, indique la hauteur.

Dans l'environnement, *Shewanella putrefaciens* participe au cycle bio-géo-chimique des métaux par sa capacité à les utiliser comme accepteur d'électrons (par exemple le Fe (III) et le Mn (IV), l'U(VI), le Cr(VI), le Se(IV)) lors de la respiration anaérobie [62, 63]. Longtemps considéré comme physiologiquement possible, c'est seulement en 1988 que le couplage de la bioréduction du manganèse à la production d'énergie a été démontré chez *Shewanella putrefaciens* MR1 [62, 64]. Le génome de cette souche a maintenant été totalement séquencé ce qui ne permet pas, pour autant, de connaître les gènes impliqués dans les structures de l'interface, encore moins les propriétés physico-chimiques de cette interface (*cf.* discussion générale) et le rôle qu'elles jouent dans les processus de respiration anaérobie.

De plus, *S. putrefaciens* est capable d'adhérer et de former des biofilms sur différentes surfaces comme l'acier inoxydable [50]. La combinaison de ces deux phénomènes (adhésion à l'acier et bioréduction du Fe(III)) font du genre *Shewanella* un sujet d'étude de première importance dans le domaine de la biocorrosion.

La Figure 3 présente les quatre souches qui ont été utilisées dans notre étude. L'ultrastructure, fine et fragile, de leur interface est visualisable sur ces clichés de MET grâce à la technique de préparation des échantillons décrites au paragraphe 2.4.3.1.2 Cryofixation, Cryosubstitution, Cryomicroscopie page 18.

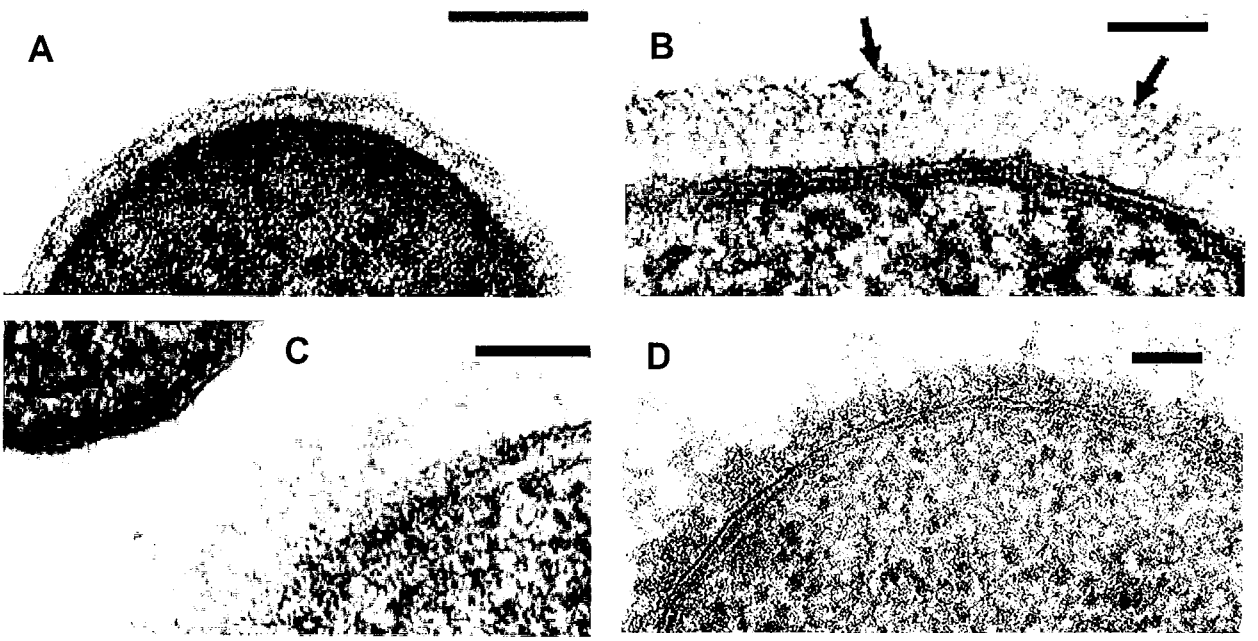

Figure 3 : Ultrastructure de l'interface de 4 souches du genre *Shewanella* mise en évidence par MET et cryosubstitution (la barre noire représente 100 nm). A : *S. putrefaciens* CN32 ; B : *S. oneidensis* MR4 ; C : *S. algae* BrY^{DL} ; D : *S. putrefaciens* CIP 8040. Les clichés A, B et C sont extraits de la référence [65]. Le cliché D a été réalisé au cours de nos travaux en collaboration avec A. Korenevsky et T.J. Beveridge de l'Université de Guelph, Canada.

La souche CN32 (*cf.* Figure 3 A) ne présente aucun polymère visible, MR4 (*cf.* Figure 3 B) montre une frange polymérique de 70 à 130 nm d'épaisseur. BrY^{DL} (*cf.* Figure 3 C) a la caractéristique de posséder deux phénotypes : le premier est doté d'un polymère de 90 nm d'épaisseur alors que le second, comme dans le cas de CN32, est dépourvu de structures visibles au MET, plus externes que la membrane externe. Enfin, CIP 8040 (*cf.* Figure 3 D) possède une frange polymérique de 50 à 70 nm d'épaisseur. Le Tableau 1 résume ces différentes caractéristiques.

Tableau 1 : Epaisseur de la frange polymérique de 4 souches de bactéries du genre *Shewanella* [65]

Souche	Frange polymérique
Shewanella putrefaciens CN32	Invisible au MET
Shewanella oneidensis MR4	70 à 130 nm
Shewanella algae BrY^{FC}	90 nm et invisible au MET
Shewanella putrefaciens CIP 8040	50 à 70 nm

Ce système biologique constitue notre modèle pour étudier les propriétés physico-chimiques de l'interface bactérie-solution. Ce choix se base sur la diversité des longueurs et densités des polymères observés au MET, sur l'importance environnementale du genre *Shewanella* (notamment sur sa capacité de bioréduction), et sur sa capacité à former des biofilms.

2.4. Méthodes expérimentales d'analyse physico-chimique des interfaces bactérie – solution aqueuse

Pour apprécier les propriétés physico-chimiques des interfaces bactériennes, plusieurs approches méthodologiques ont été retenues depuis plusieurs décennies [17, 21, 36, 66-68]. L'objectif de ces études a été de qualifier, globalement, les interfaces étudiées selon deux propriétés : leur caractère hydrophobe, ou hydrophobie, et leur charge de surface généralement mesurée par microélectrophorèse ou titrage potentiométrique. Parallèlement, les techniques de microscopie et spectroscopie ont été développées ces dernières années pour visualiser et quantifier les structures et les propriétés des cellules. Parmi ces techniques (comme la microscopie confocale, la spectroscopie de photoélectron X, la microscopie électronique), la microscopie à force atomique est une technique de choix permettant, non seulement de réaliser des images des bactéries, mais donnant aussi accès aux propriétés nanomécaniques de l'interface grâce à la spectroscopie de force.

2.4.1. Caractère hydrophobe

La définition étymologique de l'hydrophobie est la peur (phobie) de l'eau (hydro). Ce terme est également utilisé en psychiatrie pour désigner une peur pathologique de l'eau et aussi en séméiologie pour qualifier un des symptômes terminaux de la rage. Mais dans le domaine qui nous concerne, Rosenberg [69] retient une définition où l'hydrophobie est basée sur l'organisation du solvant (le plus souvent l'eau) autour de la molécule dite hydrophobe.

L'hydrophobie est, dans cette définition, un terme utilisé pour rendre compte du comportement de molécules apolaires dans l'eau. Les molécules d'eau s'organisent autour des molécules apolaires formant ainsi une cavité. Cette organisation du solvant autour des molécules apolaires conduit à une baisse du désordre ou entropie, thermodynamiquement défavorable. Ainsi les molécules hydrophobes auront tendance à se rassembler pour présenter à l'eau une surface proportionnellement plus faible et permettre de diminuer le volume d'eau « organisée ».

Pour une interface bactérienne, le problème devient plus complexe. Les structures de l'interface bactérienne présente à la fois des domaines hydrophobes et des domaines hydrophiles. Il vaut alors mieux parler de balance hydrophile-hydrophobe. De plus, certaines bactéries expriment des pili qui peuvent augmenter considérablement l'hydrophobie mesurée alors qu'ils ne représentent qu'une très faible surface. Bien que l'hétérogénéité des interfaces bactériennes rendent la mesure de l'hydrophobie difficile, ce paramètre est considéré comme un élément essentiel pour prédire la capacité d'adhésion microbienne à des surfaces [18, 23, 26, 31, 70]. La mesure du caractère hydrophile-hydrophobe a été tenté par différentes approches : tests d'adhésion des bactéries à des gouttelettes d'hydrocarbures, mesure de l'angle de contact entre un tapis bactérien et une goutte de liquide hydrophobe ou hydrophile, chromatographie d'interaction hydrophobe, mesure de l'adhésion à une surface hydrophobe, ...[22].

Le Test d'Adhésion Microbienne aux Hydrocarbures (MATH) a été développé, en 1980, par Rosenberg *et al.* [34, 71], comme une mesure de l'hydrophobie des cellules bactériennes [4, 34, 69]. Ce test consiste à mettre en contact, par vortex, une suspension bactérienne avec un hydrocarbure (initialement de l'hexadécane). Le mélange est laissé au repos et les deux phases se séparent. La phase aqueuse est alors précautionneusement prélevée et sa densité optique mesurée. Par différence avec la densité optique de la phase aqueuse avant le mélange, le pourcentage d'adhésion à l'hydrocarbure est calculé.

Une variante a été proposée par Bellon-Fontaine *et al.* [38, 72, 73] ; ces auteurs ont étendu la technique pour mesurer les propriétés acido-basiques, au sens de Lewis (c'est-à-dire accepteur-donneur d'électron), des interfaces bactériennes. Cette méthode appelée MATS (Microbial Adhesion Test to Solvants) est basée sur la comparaison de l'affinité des cellules microbiennes pour un solvant monopolaire (accepteur ou donneur d'électrons) et un solvant

apolaire : les deux solvants ayant par ailleurs des propriétés de van der Waals identiques. Dans le MATS, l'adhésion microbienne est considérée comme la résultante d'interactions électrostatiques, de van der Waals et donneur-accepteur d'électrons. Ainsi, en absence d'interactions électrostatiques et en considérant les forces de van der Waals négligeables, la différence observée dans l'adhésion aux solvants polaires ou apolaires peut être attribuée à des interactions acide-base de Lewis favorables ou défavorables. Une augmentation de l'adhésion à un solvant polaire traduirait des interactions de Lewis favorable et inversement pour les solvants apolaires.

Cette démonstration est basée sur l'absence d'interactions électrostatiques entre les cellules et les gouttelettes d'hydrocarbure. Busscher *et al.* en 1995 [39] ont démontré que la majorité des hydrocarbures utilisés dans les tests MATS présentent une charge dans les conditions de pH généralement utilisées pour ces essais d'hydrophobie disqualifiant le MATH et MATS comme une simple mesure de l'hydrophobie des cellules bactériennes.

D'autres approches expérimentales visant à qualifier l'hydrophobie des bactéries ont été développées, comme la mesure de l'angle de contact entre un tapis bactérien et une goutte de solvant ou la chromatographie d'interaction hydrophobe. Citons à ce propos l'étude de Ahimou *et al.* [74] qui ont combiné la mesure de l'hydrophobie selon le test MATH, la chromatographie d'interaction hydrophobe (CIH) et la mesure de l'angle de contact. Leur conclusion est également que le MATH et la chromatographie d'interaction hydrophobe sont très influencés par les interactions électrostatiques et que la corrélation entre ces trois méthodes n'est pas évidente. Aucune n'est spécifique de la balance hydrophile-hydrophobe, et chacune subit notamment, l'influence des interactions électrostatiques.

2.4.2. Mesures de la charge des cellules

Les interactions électrostatiques entre les bactéries et un support conditionnent grandement la réactivité de la particule bactérienne. La détermination du potentiel de surface des cellules s'est donc avérée être un enjeu majeur pour comprendre les phénomènes d'adhésion [43, 75-79]. La difficulté posée par la notion d'interface apparaît ici cruciale car le potentiel de surface présume l'existence d'une surface. Comme nous l'avons déjà dit, apprécier la surface d'une bactérie est un exercice périlleux. La notion de surface portant les charges ne peut pas s'appliquer à une cellule bactérienne recouverte de LPS car les charges ne

sont pas localisées sur un plan bidimensionnel bien défini mais plutôt dans un volume interfacial.

Une approche expérimentale pour mesurer la charge globale de l'interface est de réaliser des titrations potentiométriques. D'un point de vue pratique, une suspension bactérienne, de concentration connue, est amenée à pH 3 par addition d'acide chlorhydrique. Le pH de la solution est ensuite mesuré après chaque ajout de soude pour en déduire la surconsommation faite par les cellules et ainsi remonter à une charge surfacique [80]. Cependant, il a été montré que *Shewanella putrefaciens* placée à pH 8 ou 10 [81] est capable de supporter des ajouts de base considérables avant que le pH ne change. Dans une moindre mesure, le même genre de comportement a été observé dans des conditions acides. De plus, les courbes de titration sont fonction du délai entre chaque ajout de solution titrante (acide ou base). De sorte que, la consommation de solution titrante est augmentée quand le délai entre chaque ajout est allongé. Il ressort de ces expériences que *Shewanella putrefaciens* est capable de fournir une réponse métabolique active, lors du processus de titration. L'interprétation des courbes de titration est alors rendue délicate si bien que cette technique nous a semblé peu appropriée dans le cas de *Shewanella*. Pour étayer ce choix, mentionnons l'étude de Haas [82] qui s'est intéressé à l'influence des conditions de culture (phase de croissance, condition aérobie ou anaérobie) de *Shewanella putrefaciens* sur les titrations potentiométriques. Dans cette étude, de nombreuses précautions sont prises pour minimiser les hystérèses : la gamme de pH est restreinte (4 à 10) et un chelatant (EDTA) est utilisé pour neutraliser les cations basiques [83, 84]. L'auteur finit par conclure que les conditions de culture de *Shewanella putrefaciens* (notamment condition aérobie *versus* anaérobie) peuvent influencer le pouvoir tampon des bactéries. Aucune conclusion sur les charges de surface n'est proposée.

Néanmoins, les titrations ne doivent pas être définitivement disqualifiées pour les applications biologiques. Des travaux de titration sur *Streptococcus salivarius* [85], *Escherichia coli* [86], ou encore *Bacillus subtilis* [87] et *B. brevis* [86] ont été menés avec succès. Par exemple, Duval *et al.* [85] ont réalisé une analyse poussée des propriétés interfaciales, de *Streptococci* fibrillés et non fibrillés, basée sur les résultats de titrations et de microélectrophorèse, mettant en évidence les pk_a des groupements chargés distribués dans l'interface molle.

Un autre moyen d'accéder aux charges des cellules est la mesure des mobilités électrophorétiques. Expérimentalement, cette technique de microélectrophorèse consiste, d'une façon ou d'une autre, à mesurer la vitesse de déplacement d'une particule (bactérie ou minéral) dans un champ électrique. A partir de cette mesure, le potentiel au plan de

cisaillement ou potentiel zéta peut être calculé à l'aide des équations de Smoluchowski ou de Hüquel. Dans un cas comme dans l'autre, le passage de la mobilité au potentiel zéta est obtenu en tenant compte de la viscosité du milieu et de sa constante diélectrique. Cette méthode a été beaucoup employée [19, 23, 28, 42, 74, 78, 88] et a permis des comparaisons qualitatives intéressantes, entre micro-organismes. Cependant, ces équations ont été développées pour des applications liées aux particules dures et leur transposition directe à des bactéries, qui présentent une certaine souplesse de l'interface, requiert de grandes approximations [89]. Ainsi, il est impossible d'obtenir des valeurs quantitatives des propriétés électrostatiques de l'interface molle des bactéries en se basant sur ces calculs. Récemment, la mobilité élecrophorétique de particules molles a été décrites selon des modèles prenant en compte une particule centrale dure recouverte d'une couche de polymère « souple » [90-95]. Ces développements théoriques permettent de mesurer quantitativement la densité de charge contenue dans la couche de polymères souples ainsi que de déterminer la capacité du flux hydrodynamique à pénétrer dans l'enchevêtrement de polymères de la couche souple [75, 85, 96]. Les dernières avancées dans ce domaine considèrent une interface souple et diffuse (c'est à dire que la densité de polymère diminue en s'éloignant de la surface du centre dur) et la géométrie de la particule dure peut être soit sphérique (en première approximation bactéries Gram positives) soit cylindrique (en première approximation bactéries Gram négatives) [89].

2.4.3. Approche locale des interfaces bactériennes

Les techniques décrites précédemment s'intéressent à l'ensemble d'une population bactérienne. Les informations obtenues sont collectives et traduisent un comportement général de la population de bactéries individuelles. La microscopie permet d'observer les bactéries à l'échelle locale et donc de déterminer des propriétés individuelles qui induisent le comportement général.

2.4.3.1. Microscopie Electronique à Transmission (MET)

La MET est la méthode de choix pour l'observation des structures de l'interface des bactéries. Cette microscopie nécessite un échantillon très fin « transparent » aux électrons. La réalisation de coupes ultraminces est la solution technique de référence. Pour les préparer, il est nécessaire de fixer instantanément, d'une façon ou d'une autre, les molécules de la membrane et de dénaturer ou d'empêcher l'action des enzymes qui pourraient altérer la structure de la membrane des bactéries. Au cours de cette même étape, les ultrastructures de la

membrane doivent être maintenues et préservées au mieux. Ces deux contraintes sont contradictoires. Les techniques classiques de préparation des échantillons qui sont décrites dans le paragraphe suivant sont agressives et modifient les ultra structures de l'interface des bactéries. La cryofixation et cryosubstitution sont des techniques qui permettent de préserver au mieux l'ultrastructure des interfaces bactériennes.

2.4.3.1.1. Préparation conventionnelle

La technique conventionnelle de préparation consiste, dans une première étape, à fixer chimiquement l'échantillon. Le glutaraldéhyde est généralement utilisé en association avec le tétra oxyde d'osmium pour assurer la formation de liaisons covalentes capables de supporter l'étape suivante de déshydratation par des solutions d'alcool de plus en plus concentrées (50, 75, 95 et 100 %). Une fois déshydraté, l'échantillon est enrobé, généralement à température ambiante.

Ces trois étapes, fixation, déshydratation et enrobage dans la résine, sont basés sur la diffusion rapide d'agents chimiques dans l'échantillon (à température ambiante). Les structures délicates de la membrane des bactéries sont mal conservées [97], les éléments du périplasme sont extraits et la membrane externe présente à un aspect ondulé habituel des bactéries Gram négatives soumises à la préparation conventionnelle (*cf.* Figure 4) [58].

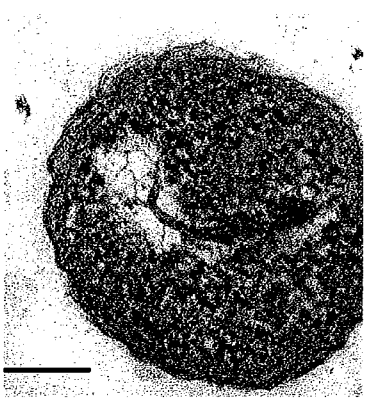

Figure 4 : *S. putrefaciens* CIP 8040 MET, préparation conventionnelle [35]. Notons l'aspect ondulé de la membrane externe inhérent à cette préparation (la barre représente 100 nm).

Cette méthode de préparation induit donc de nombreux artefacts principalement dus aux molécules chimiques très agressives utilisées pour la fixation et à la lenteur des processus de déshydratation et enrobage au cours desquels l'eau, les macromolécules, les ions sont redistribués.

En conclusion, la préparation conventionnelle ne permet pas de préserver les ultrastructures fines de l'interface qui nous intéressent dans ce mémoire. Toutefois, des informations

précieuses peuvent être obtenues en utilisant des marquages spécifiques des constituants cellulaires [98].

2.4.3.1.2. Cryofixation, Cryosubstitution, Cryomicroscopie

Au cours du processus de cryofixation, la température de l'échantillon passe brutalement, en 20 ms, de la température ambiante à la température de l'éthane liquide (-196 °C). En même temps, la pression est brutalement accrue de la pression atmosphérique à 2000 bars. [99, 100]. Ainsi l'eau contenue dans l'échantillon est instantanément transformée en glace amorphe ou glace micro cristalline. Aucune redistribution de l'eau ne peut avoir lieu et les ultrastructures de surface sont immédiatement piégées dans leur dernier état. Une fois l'échantillon fixé sous haute pression et à basse température, il peut être directement utilisé pour l'observation en cryomicroscopie [101]. Cette technique a été récemment mise en œuvre par Matias et Beveridge [100] et a permis de visualiser pour la première fois un espace périplasmique chez *Staphylococcus aureus*, pourtant une bactérie Gram positive ! La cryomicroscopie requiert tout un équipement microscopique refroidi à la température de l'azote liquide, encore peu répandu.

La cryosubstitution est l'étape au cours de laquelle l'échantillon est déshydraté. Ici le processus se déroule à froid (de -80°C à -30°C) et lentement (au moins 5 jours). La température est augmentée par palier alors que l'échantillon est placé dans un mélange dont la composition de base est acétone et acétate d'uranyl. L'impact de la composition du milieu de cryosubstitution sur la qualité des images obtenues a été largement discuté dans les années 1990 alors que la technique venait d'être mise au point [102, 103]. C'est grâce à cette technique que les ultrastructures des souches de *Shewanella* présentées au paragraphe 2.3 (Présentation du modèle bactérien : quatre souches du genre *Shewanella*) ont été élucidées. Citons enfin le travail de Hunter et Beveridge qui ont, grâce à cette technique, récemment réaliser des observations à haute résolution de biofilm de *Pseudomonas aeruginosa* [99].

2.4.3.2. Microscopie à Force Atomique (AFM)

La Microscopie à Force Atomique a été développée à partir de la découverte de l'effet tunnel par Binnig et Quate en 1986 [104]. Dès 1988, les premières applications de la microscopie à force atomique au monde de la biologie était décrite [105]. Le microscope (*cf.* Figure 5 [106]) est constitué d'une céramique piézo-électrique déplaçable dans les trois dimensions de l'espace (x,y et z). Un levier portant une pointe (ou l'échantillon, selon le microscope) est placé sur la céramique piézo-électrique. Cette pointe est ensuite mise en contact avec

l'échantillon. La déformation subie par le levier lors du balayage de la surface par la céramique piézo-électrique est mesurée par la déviation de la réflexion d'un faisceau laser sur un photodétecteur.

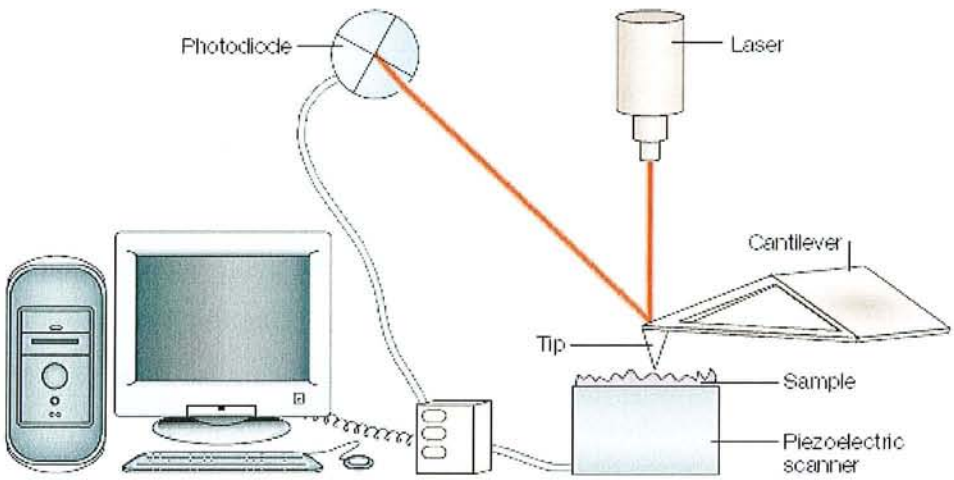

Figure 5 : Schéma de principe d'un microscope à force atomique [106, 107]

2.4.3.2.1. Préparation des échantillons biologiques pour l'AFM

Pour observer les bactéries dans leur état d'origine, l'immobilisation des cellules par simple adsorption à un support est généralement inappropriée. En effet, l'aire de contact entre la cellule et le support est trop faible ce qui conduit, sauf à laisser un temps de contact prolongé entre les bactéries et le support, à l'arrachage des cellules lors du balayage de l'échantillon par la pointe. Pour surmonter cette difficulté, des stratégies agressives comme le séchage [5, 108] ou l'utilisation de fixateur chimique (notamment le glutaraldéhyde) ont été proposées [109]. Mais ces traitements causent des altérations des échantillons et ne permettent donc pas de réaliser des observations sur du matériel dans son état natif. Des alternatives plus douces ont été développées. Par exemple, il est possible de piéger mécaniquement des cellules soit dans un gel d'agarose [110] soit sur une membrane poreuse [106, 111]. Ces deux techniques de piégeage impliquent des contraintes mécaniques sur la cellule piégée mais présentent l'avantage de ne pas ajouter de molécules supplémentaire au système (en tout cas dans le cas des membranes poreuses). Cependant, la membrane poreuse ne peut être utilisée que pour des cellules rondes comme les levures ou les bactéries de type *cocci*. Enfin, des méthodes basées sur les interactions électrostatiques ont été mises au point [56, 112]. Il s'agit de créer un film de PolyEthyleneImine (PEI) ou de Poly-L-Lysine (PL), chargé positivement, sur lequel les bactéries chargées négativement viennent se fixer. Ici, aucune contrainte mécanique n'est exercée sur la paroi des cellules, mais une molécule supplémentaire, potentiellement

contaminante, (PEI ou PL), est introduite dans le système. Un choix entre ces deux dernières techniques (membrane poreuse ou interactions électrostatiques) doit donc être fait en fonction des avantages et inconvénients (*cf.* Tableau 2) de chaque technique et aussi des objectifs poursuivis [98, 113].

Dans notre étude, nous avons utilisé l'immobilisation par contact prolongé, et l'immobilisation électrostatique puisque l'objectif est, entre autre, de déterminer les propriétés nanomécaniques de l'interface des bactéries du genre *Shewanella*. De plus, ces bactéries sont définitivement de forme bacillaire (*cf.* Figure 2) ce qui est incompatible avec la fixation dans un pore rond.

Tableau 2 : Avantages et inconvénients des différentes techniques de fixation des échantillons biologiques pour l'AFM.

Méthode	Avantages	Inconvénients	Références
Séchage	Simple, forte fixation	Déshydratation, dénaturation des interfaces	[5, 108, 114]
Filtre	Aucun ajout de molécules	Ne fonctionne que pour des cellules rondes Induit des contraintes mécaniques sur les cellules	[106, 111]
Agar	Support nutritif pour les cellules. Le moins agressif	Complexe à mettre en œuvre Contrainte mécanique	[110]
Glutaraldéhyde, colle	Simple et efficace	Dénaturation des interfaces	[109]
Monocouche de PEI ou poly-L-Lysine	Convient à toutes les bactéries et aux levures pour peu qu'elles soient chargées négativement Pas de contraintes mécaniques	Risque de contamination par le PEI ou la Poly-L-Lysine.	[56, 112, 115, 116]
Contact prolongé sur polystyrène	Pas de séchage, aucun ajout de molécules, pas de contraintes mécaniques	Nécessite au moins 14 h de contact, aléas dus au support, efficacité testé sur une seule souche	[35, 117]

2.4.3.2.2. Imagerie

Il existe plus de dix modes d'imagerie en AFM. Nous nous en tiendrons à décrire les deux modes principalement utilisés pour réaliser des images [98, 108] : le mode contact et le mode vibrant.

Dans le mode contact ou mode à force constante, les images sont enregistrées quand la pointe et l'échantillon sont en contact. Alors que la pointe balaye la surface de l'échantillon, une boucle de contrôle négatif ajuste la hauteur de la pointe (ou de l'échantillon suivant le matériel utilisé) pour maintenir une déflection du levier constante. Cette méthode fournit une image topographique calibrée dans les 3 dimensions de l'espace.

En mode vibrant ou tapping mode, le levier portant une pointe entre en vibration alors qu'il balaye la surface de l'échantillon. Comme la pointe n'entre en contact avec l'échantillon qu'à son minimum d'amplitude, les forces de cisaillement latérales induites par le balayage sont plus petites. Cette méthode peut être utile pour des échantillons biologiques qu'il est difficile de fixer suffisamment fort à une surface.

2.4.3.2.3. Spectroscopie de force

La microscopie à force atomique permet de mesurer localement (~10 nm^2) les forces d'interaction entre une pointe et une surface biologique. Les propriétés nanomécaniques de bactéries ou d'autres micro-organismes [118] (notamment des levures [119]) peuvent être déduites de la relation entre la force appliquée au levier et la profondeur d'indentation de la pointe dans l'échantillon souple.

Cependant, les interactions électrostatiques à longue portée peuvent conduire à des courbes de force non linéaire qui ressemblent fortement aux courbes de force enregistrée sur les bactéries [120]. Peu d'études font varier le pH ou la force ionique pour tenter de séparer les contributions électrostatiques de la souplesse de l'interface bactérienne [35, 115, 121, 122]. La difficulté soulevée ici est inhérente à la technique. La question est d'identifier sur les courbes force-distance le point de contact entre la surface bactérienne et la pointe, c'est à dire de différencier les forces de surface des forces correspondant aux déformations mécaniques du levier et/ou de la surface analysée. Pour contourner cette difficulté, nous avons travaillé à une force ionique élevée (0,1 M) diminuant considérablement la portée des interactions électrostatiques (~5 nm) et permettant ainsi de mesurer les propriétés nano-mécaniques via les courbes d'indentation. Le modèle le plus simple et le plus utilisé pour quantifier la portion non linéaire des courbes de force, pour les petites forces appliquées au levier, est le modèle de Hertz qui permet d'extraire un module élastique ou module d'Young, qui est de l'ordre du

kilo Pascal dans le cas des bactéries. Ce modèle a été largement utilisé pour des cellules épithéliales [123, 124], des plaquettes et des hématites [125, 126] ou des diatomées [127].
Ainsi la comparaison du module d'Young de bactéries, dans des environnements différents, devrait donner des indications sur la dynamique de l'interface des cellules soumises à des variations de conditions environnementales. Citons par exemple les mesures réalisées par Touhami *et al.*, [128] sur les levures du type *Saccharomyces cerevisiae* (*cf.* Figure 6). Lors de la multiplication des levures par bourgeonnement, la cellule fille laisse sur la cellule mère une cicatrice riche en chitine (le polysaccharide de l'exosquelette des crustacés). Cette zone est donc supposée plus rigide que le reste de la paroi de la levure. Dans ce contexte, des mesures de l'indentation en fonction de la force ont été réalisées sur le bourgeon et dans la région environnante. L'ajustement des courbes expérimentales avec le modèle de Hertz conduit aux valeurs de module d'Young suivantes : 6,1 +/- 2,4 MPa pour le bourgeon et 0,6 +/- 0,4 MPa pour la surface environnante. Cette expérience a été la première à démontrer, *in situ*, que le bourgeon est bien 10 fois plus dur, moins souple ou plus élastique que le reste de la paroi. Cette mesure est cohérente avec l'accumulation de chitine dans cette zone [129].

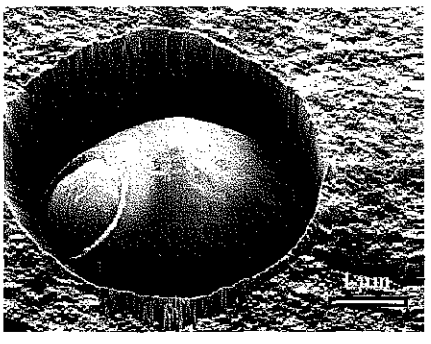

Figure 6 : Image AFM en 3 dimensions, en solution, montrant une cellule de *S. cerevisiae* seule dépassant d'un pore d'une membrane. La cellule présente un bourgeon qui se forme après le détachement des cellules filles [128]

De façon complémentaire, la constante de raideur des bactéries (K_b) peut être déterminée à partir de la portion linéaire des courbes force-distance (généralement observée pour des forces appliquées supérieures à 0,5 nN) en utilisant la relation suivante [130] :

$$k_b = -k_c \cdot \left(\frac{S}{S + k_c} \right)$$

où k_c est la constante de raideur du levier et S la pente mesurée sur la courbe force fonction de l'indentation. Cette équation considère 2 ressorts linéaires en série (le levier et la bactérie) possédant chacun leur constante de raideur. Des calculs théoriques montrent que cette déformation linéaire est en relation directe avec la pression de turgescence des cellules [57, 131].

Cette équation a surtout été appliquée à des bactéries. Les constantes de raideur rapportée dans la littérature varient de 0,01 à 0,5 N/m [56, 57]. Il est intéressant de constater ici l'importance du choix de la méthode d'immobilisation des cellules. Yao *et al.* en 2002 [57] ont mesuré une constante de raideur de 0,04 N/m sur une *Escherichia coli* immobilisée par des interactions électrostatiques (PEI) alors que la même bactérie fixée par du glutaraldéhyde à 2,5 % montre une constante de raideur de 0,15 N/m.

2.5. Réflexion sur la pertinence des expériences en laboratoire

Nous avons vu que la technique de préparation de l'échantillon est un point clé dans l'analyse des résultats. Ainsi, il est nécessaire de se poser la question de la pertinence de nos expériences en laboratoire, par rapport au système réel. Pour l'étude physico-chimique à l'interface solution-bactérie, chaque technique nécessite une étape de préparation de l'échantillon. Au final n'est-ce pas cette étape qui détermine, si ce n'est le phénomène mesuré, au moins, son intensité ? Quoiqu'il en soit, les progrès techniques tendent à limiter au maximum l'incidence de l'étape de préparation. Par exemple, pour la MET, la cryofixation fige instantanément (20 ms) l'échantillon dans sa dernière configuration. Dans le cas de l'AFM, nous travaillons maintenant en milieu liquide et grâce à des méthodes de fixation des bactéries peu agressives, sur des cellules vivantes. Pour la microélectrophorèse, les bactéries sont en solution et l'échantillon est renouvelé après chaque mesure de mobilité. Pembrey *et al.* [132] ont mené une étude exhaustive de l'impact des protocoles de préparation des échantillons pour l'étude des propriétés physico-chimiques de l'interface cellulaire. La vitesse de centrifugation, la solution de remise en suspension ont un impact démontré sur la mobilité électrophorétique, l'adhésion ou encore la viabilité des bactéries. Ce fait étant établi, la manipulation des micro-organismes demeure inévitable. En conséquence, une attention particulière doit être portée sur la description et le respect du protocole de préparation choisi.

2.6. Bilan du contexte scientifique

Cette analyse du contexte scientifique nous a permis de définir la majorité des concepts qui seront développés dans la suite de ce travail. Par exemple, les notions d'interface et d'hydrophobie ont été développées dans le but de préciser les notions que nous évoquons en employant ces mots. La définition de ces concepts fait débat et nous n'entendons pas imposer

ces choix, mais nous les exposons, afin de permettre une lecture non ambiguë de la suite du travail.

Parallèlement, le lecteur aura fait connaissance avec le genre bactérien *Shewanella* dont quatre représentants ont été le modèle choisis pour l'étude de la physico-chimie des interfaces bactériennes. Les ultrastructures de l'interface et le rôle de *Shewanella* spp. dans les processus de biominéralisation sont les principales raisons de ce choix.

Enfin, cette partie contexte scientifique, expose les techniques d'analyse utilisées dans ce mémoire pour la physico-chimie à l'interface bactérie-solution. Les avantages et inconvénients de chaque outil, ainsi que la nature du phénomène réellement mesuré, sont exposés pour permettre une lecture « en connaissance de cause » des articles scientifiques qui suivent. Il ne s'agit cependant pas d'une revue exhaustive des méthodes expérimentales permettant de sonder les interfaces bactériennes. Seul les techniques utilisées dans ce travail ont fait l'objet d'une description.

3. Quantification des propriétés nanomécaniques et électrohydrodynamiques des interfaces bactériennes

3.1. Structure de surface et propriétés nanomécaniques de *Shewanella putrefaciens* à 2 valeurs de pH (4-10) déterminées par microscopie à force atomique

La microscopie à force atomique permet de sonder *in situ,* en milieu liquide, les propriétés nanomécaniques des bactéries vivantes. Une des principales étapes limitantes de l'AFM est la phase d'adhésion des micro-organismes. Ceux-ci doivent être suffisamment fixés au support pour supporter les forces de cisaillement induites par le balayage de la pointe. Dans cette étude, les cellules de *Shewanella putrefaciens* CIP8040 ont naturellement adhéré à un support en polystyrène par contact prolongé (14h). Cette longue incubation garantit une adhésion suffisamment forte entre les cellules et le support sans que l'utilisation d'aucune molécule ajoutée ne puisse perturber l'interface des bactéries. Cependant, les bactéries qui ont été observées au cours de cette étude présentent une longueur moyenne supérieure à la longueur décrite classiquement pour des cellules de *S. putrefaciens* en phase stationnaire. La longue incubation dans un milieu carencé, plus proche des conditions environnementales qu'un milieu de culture riche, est un élément à prendre en compte pour expliquer l'allongement des cellules.

L'objectif était de déterminer si des variations de pH du milieu environnant induiraient une modification des propriétés nanomécaniques de l'interface de nos cellules. Pour ce faire, nous avons travaillé à 2 valeurs de pH (4 et 10) et réalisé les mesures de force sur les cellules incubées pendant 14 h à chacun des pH. Les courbes de force (*cf.* Figure 7), réalisées à la force ionique de 0,1 M pour s'affranchir au maximum des interactions électrostatiques, ont pour la première fois été décrites par une combinaison du modèle de Hertz, pour la partie non linéaire, et du modèle de Hook, pour la partie linéaire. Ainsi, le module d'Young et la constante de raideur des bactéries ont pu être quantifiées. Ces paramètres correspondent respectivement aux propriétés nanomécaniques des couches les plus externes de l'interface et à la pression de turgescence intracellulaire.

Nous avons montré qu'à pH 4 les interfaces sont moins souples (module d'Young et constante de raideur plus grands) qu'à pH 10. A pH 4, les structures de surface sont compactes et l'espace périplasmique réduit au minimum d'où une souplesse plus faible qu'à pH 10 où les polymères de surface sont plus lâches et l'espace périplasmique gonflé, en raison d'une augmentation des répulsions électrostatiques entre les chaînes et d'une augmentation de la perméabilité à l'eau.

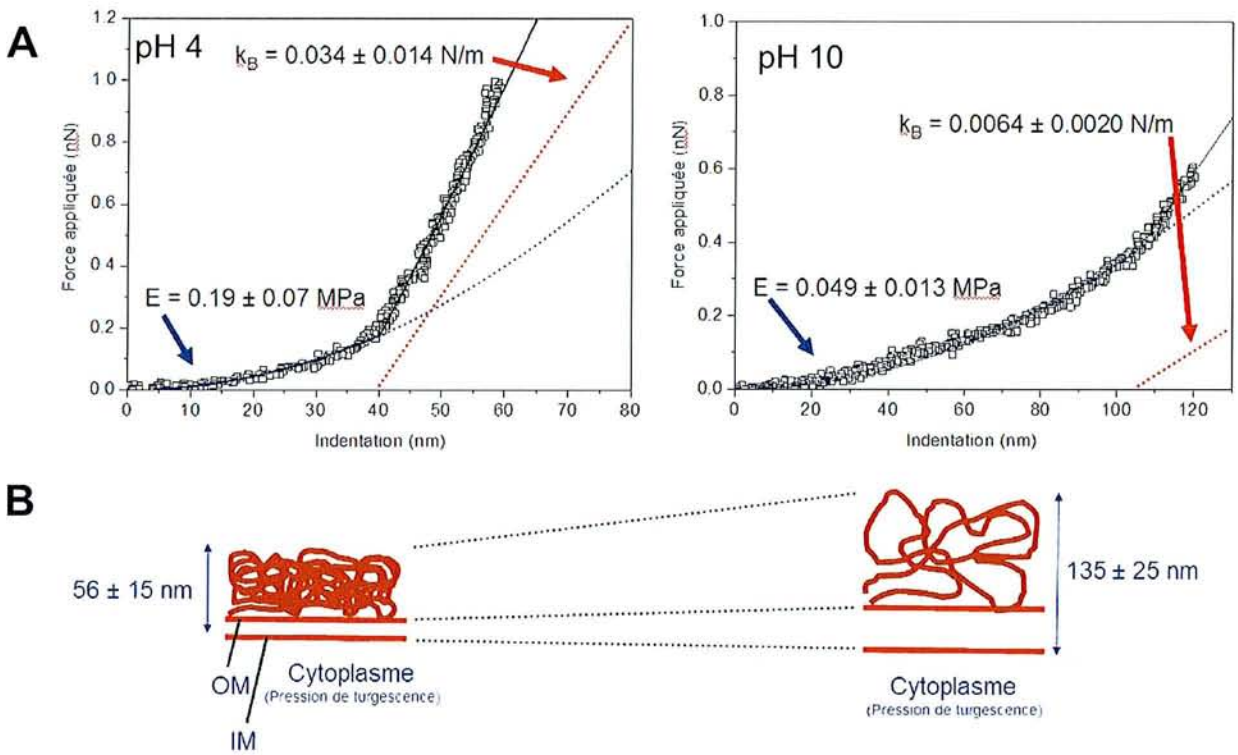

Figure 7 : A : les graphiques représentent la force appliquée par la pointe de l'AFM en fonction de l'indentation de celle-ci dans l'interface molle de la bactérie. Les courbes de force se décomposent en deux parties : une partie non linéaire caractérisée par le module d'Young (E) et une partie linéaire décrite par la constante de raideur de la bactérie (k_B). Ces deux paramètres sont plus grands à pH 4 qu'à pH 10. (bactérie plus dure à pH 4 qu'à pH 10)

B : schéma expliquant l'évolution de E et k_B entre pH 4 et pH 10. A pH 4, les structures de l'interface sont compactes et l'espace périplasmique réduit au minimum d'où une souplesse plus faible qu'à pH 10 où les polymères de surface sont plus lâches et le périplasme gonflé.

JOURNAL OF BACTERIOLOGY, June 2005, p. 3864–3868 Vol. 187, No. 11
0021-9193/05/$08.00+0 doi:10.1128/JB.187.11.3864–3868.2005

Surface Structure and Nanomechanical Properties of *Shewanella putrefaciens* Bacteria at Two pH values (4 and 10) Determined by Atomic Force Microscopy

Fabien Gaboriaud,* Sidney Bailet, Etienne Dague, and Frédéric Jorand

Laboratoire de Chimie Physique et Microbiologie pour l'Environnement, UMR 7564, CNRS, Université Henri Poincaré, Nancy 1, 405 rue de Vandœuvre, F-54600, Villers-lès-Nancy, France

Received 3 January 2005/Accepted 21 February 2005

The nanomechanical properties of gram-negative bacteria (*Shewanella putrefaciens*) were investigated in situ in aqueous solutions at two pH values, specifically, 4 and 10, by atomic force microscopy (AFM). For both pH values, the approach force curves exhibited subsequent nonlinear and linear regimens that were related to the progressive indentation of the AFM tip in the bacterial cell wall, including a priori polymeric fringe (nonlinear part), while the linear part was ascribed to compression of the plasma membrane. These results indicate the dynamic of surface ultrastructure in response to changes in pH, leading to variations in nanomechanical properties, such as the Young's modulus and the bacterial spring constant.

Bacterial surfaces are structurally complex, with several components constituting the bacterial cell envelope. In gram-negative bacteria, the envelope is made up of two lipid bilayer membranes: (i) the plasmic membrane, delimiting the inner part of the cell from the external one, and (ii) the outer membrane (OM), the most external membrane. Between these two layers, a thin and strong polymer, murein, or peptidoglycan layer is embedded in a concentrated gel-like matrix, the periplasmic space. The OM contains two types of lipids, lipopolysaccharide (LPS) and phospholipids, as well as a number of characteristic proteins. The LPS is composed of three parts: (i) the lipid A region that anchors the LPS to the OM; (ii) the distal, hydrophilic, O-antigen polysaccharide region that protrudes into the extracellular medium; and (iii) the core oligosaccharide region that connects the two (17). In addition, bacterial cell surfaces can also be studded or covered by extracellular polymeric substances (29) or some specific external structures (pili or fimbriae and flagella) (5).

As the outer surface of the OM directly interacts with the extracellular environment of the bacterial cell, characterizing such surfaces can provide crucial information for understanding processes such as bacterial adhesion, surface recognition, bio-mineralization, and others. As cell surface components are suspected of being very tenuous and sensitive to chemical treatment, cell surface ultrastructure components have been characterized by electron microscopy using a freeze substitution preparation. Such experiments have revealed new features of the cell surfaces, such as the external fringe that had not previously been observed using conventional methods (4). However, cell surfaces are also suspected of being sensitive to dehydration. For this reason, spatially resolved in situ direct observation of the organism in aqueous solutions would represent a significant advance, as a local characterization of the structural properties of bacterium-water interfaces lead to a generalized physicochemical understanding of bacterium-mediated mechanisms implied in many environmental processes.

Although atomic force microscopy (AFM) was originally introduced as a high-resolution imaging device, it can also be used to interact forces exerted on a cantilever in aqueous solutions. Many reviews about the theoretical and experimental backgrounds of such methods have been published and illustrate the numerous parameters that can be measured using force spectroscopy (e.g., references 9 and 12). The investigation of biological cells by AFM provides fundamental insights regarding long-range surface interactions and mechanical properties of cell surfaces from the interaction forces between the AFM probe (classical or modified tip, bacterial probe) and such surfaces (1, 3, 6, 8, 14, 16, 24, 26, 27, 30, 31).

Despite the numerous studies devoted to the microscopic quantification of force curves, the dynamic of the cell envelope in aqueous media is still difficult to elucidate. In this context, the above-described studies were aimed at describing the effects of pH on surface properties of *Shewanella putrefaciens*, probing in situ the AFM force curves on a nanometer scale. This model bacterium is a gram-negative facultative anaerobe and is considered to be one of the most efficient and versatile dissimilatory metal-reducing microorganisms (15). A great deal of research has focused on the ability of microorganisms like *Shewanella* to reductively transform iron oxyhydroxides (7, 11, 18, 21). However, few studies have been conducted on the physicochemical surface properties of *Shewanella* cells to help understand mechanisms at bacterium–aqueous-solution interfaces (7). Therefore, this paper compares force curves of *S. putrefaciens* at two pH values (4 and 10) through the natural adsorption of cells onto flat and noncoated inert polystyrene substrates. In order to closely preserve as much as possible the ultrastructures of the bacterial complex surfaces, the immobilization of bacteria was successfully carried out after the incubation stage under controlled physicochemical conditions to achieve bacterial adhesion. Yet, rod-shaped bacteria were im-

* Corresponding author. Mailing address: Laboratoire de Chimie Physique et Microbiologie pour l'Environnement, UMR 7564, CNRS, Université Henri Poincaré, Nancy 1, 405 rue de Vandœuvre, F-54600, Villers-lès-Nancy, France. Phone: 33 (0)3 83 68 52 39. Fax: 33 (0)3 83 27 54 44. E-mail: gaboriaud@lcpme.cnrs-nancy.fr.

mobilized on polymer-coated substrates that may promote structural rearrangements in the bacterial cell surface structure (25). However, the choice of such extreme pH values, of acidic versus basic media, was initially motivated to assess the repercussions of pH stress on bacterial surface properties (and not on physiological activity) usually addressed in macroscopic surface charge measurements, such as potentiometric titrations or electrophoretic mobility measurements. Nevertheless, the extrapolation of surface properties analyzed from immobilized bacteria to planktonic cells might be considered with caution.

The reference strain *Shewanella putrefaciens* CIP 8040 (Collection Institut Pasteur, Paris, France) corresponding to ATCC 80.71 was primarily isolated from the surface of tinted butter (28). Cells were aerobically grown on a solid medium (plate count agar; BioMérieux 51019) for a 48-h incubation period at 30°C. Nutritive broth (100 ml of Trypticase soy broth; BioMérieux 51072) was seeded with a 5-ml bacterial suspension (absorbance = 0.500 ± 0.025; λ = 600 nm). These precultures were stopped after 7 h, at the end of the middle of the exponential growth phase. Cultures were then grown out in 1.5-liter batch reactors initiated with 10 ml of the preculture at an optical density of 0.25 ± 0.10 at 600 nm. The 1-liter cultures were mixed at 150 rpm and 30 ± 0.5°C. The cells were harvested after 24 h of growth by centrifugation (10 min at 10,000 × *g*). Two washes were performed with KNO_3 solution (10^{-3} M, pH 7) by centrifugation at 10,000 × *g* for 10 min. The washed cell pellets were then dispersed in a solution at a given pH in KNO_3 (0.1 M) and incubated at 20 ± 2°C in a polystyrene dish (30-mm diameter, reference no. 306; Caubere Inc., France) overnight (14 h). Since bacterial adhesion increases as a function of time and regardless of a pH range between 3 and 11, the choice of 14 h was a good compromise for sufficient adhesion and a suitable time from a practical point of view. The aqueous phase was then removed and the dishes washed three times with KNO_3 solution by gently shaking the disk manually and by a distilled water trickle to detach weakly fixed bacteria.

Force curves were obtained at room temperature, using a commercial microscope (Thermomicroscope Explorer EcuPlus; Veeco Instruments). A single commercially available V-shaped silicon nitride tip (reference no. MLCT-EXMT-BF; Veeco Instruments) with a quoted probe curvature radius of ~50 nm (manufacturer specifications) and a measured spring constant of 0.01% ± 10% N/m (23) was used for all force measurements. Force measurements were taken in potassium nitrate solution at a fixed ionic strength of 0.1 M and at pH 4 or 10 at the rate of 0.1 $\mu m \cdot s^{-1}$. Raw cantilever deflection-piezo displacement curves were converted into force curves by using the cantilever spring constant and detector response (10). The zero relative piezo displacement was arbitrarily positioned to the lift-off from zero deflection on the approach curve. At least 100 curves recorded randomly from 10 bacteria were then averaged and standard deviations calculated.

The bacterial spring constant, k_B, was determined (i) either from the slope of the linear portion of the force-piezo displacement curves, using the formula (27, 31)

$$k_B = -k_c \frac{s}{(k_c + s)} \quad (1)$$

where k_c is the cantilever spring constant and s is the negative slope, or (ii) from indentation curves using equation 2. This equation describing the complete indentation curve combines the Hertzian model and Hooke's law to reproduce the nonlinear and linear force behaviors and gives the following relation between the loading force, F, and the indentation depth, δ,

$$F = \frac{2}{\pi} \frac{E}{(1 - \nu^2)} \tan(\alpha) \times \delta^2 + k_B\delta + A \quad (2)$$

where α is the cone opening angle, E is the elastic or Young's modulus, ν is Poisson's ratio, and A is a constant. Notice that the Hertzian model is widely used to describe the elastic response of biological cells indented by an AFM tip (19, 24).

The force measurements on *S. putrefaciens* cells at the two different pH values are shown in Fig. 1. In these curves, the loading force is plotted as a function of relative piezo displacements. This distance was set at zero, which theoretically corresponds to the contact point between tip and surface, at lift-off from zero deflection on the approach curve. This assumption implies negligible long-range surface forces. Under our experimental conditions, the high ionic strength (0.1 M) decreases commensurately the electrostatic contributions of surface charges. In fact, complementary electrophoresis experiments of bacterial suspensions under the two pH conditions employed here demonstrated low surface charges and no significant pH dependence (zeta potential < −20 mV). Moreover, the retraction curves showed no adhesion between tip and bacteria, indicating the absence of large fibrous polymers on the bacterial surfaces (not shown).

Thus, the force curves, recorded at different pH values (Fig. 1), essentially may correspond to nano-indentation of the AFM tips into bacterial envelopes. Independent of pH, such curves exhibit two common features, specifically, a nonlinear domain at low loading forces (<0.5 nN) and a practically linear domain at high loading forces (>0.5 nN). The increase in pH significantly changes the nanometric range of these two mechanical regimens, while the loading forces that correspond to the transition between the two regimens were similar for the two pH values: 0.58 nN (pH 4.0) and 0.54 nN (pH 10.0). This suggests that the mechanical transition between the two regimens is probably associated with the same structural compression features. To extract mechanical properties, the local spring constant of bacteria was determined from the slope of the linear portion of force curves using equation 1, yielding to bacterial spring constants of 0.05 N/m and 0.02 N/m for pH 4.0 and 10.0, respectively. These values are in the same order of magnitude as one reported in previous studies conducted with *Escherichia coli* strains (27) (k_b = 0.04 N/m) and close to the value obtained by Yao et al. (31), who examined *Pseudomonas aeruginosa* in growth medium (k_b = 0.02 N/m). Furthermore, Arnoldi et al. (2, 3) theoretically demonstrated that the spring constant of bacteria increases with its turgor pressure. The mechanical behavior of bacteria under high loading forces, typically 0.5 nN, could then be correlated with their turgor pressure from the spring constant. Therefore, the increase in the calculated bacterial spring constants at higher pHs suggests that the turgor pressure is about two times higher at pH 4 than at pH 10.

Notice that such measurement of the bacterial spring con-

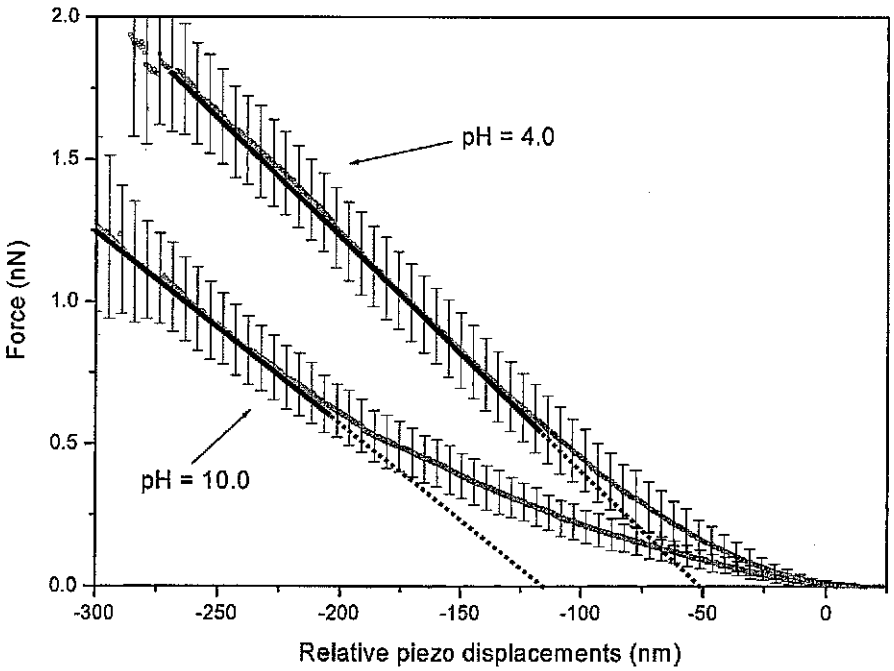

FIG. 1. Means and respective standard deviations of force curves at different pHs measured on the top of bacteria in aqueous electrolyte solution (KNO_3 = 0.1 M). The two dashed lines indicate linear behaviors that corresponded using equation 1 to bacterial spring constants of 0.05 N/m (pH 4) and 0.02 N/m (pH 10). The onset of the linear regimen corresponds to a loading force of 0.58 nN at a relative piezo displacement of −120 nm (−62 nm without cantilever deflection) for pH 4 and 0.54 nN at a distance of −190 nm (−136 nm without cantilever deflection) for pH 10. The zero piezo displacement was positioned to the lift-off from zero deflection on the approach curve.

stant considers the two mechanical regimens as two independent processes, and the eventual contribution of the nonlinear regimen to the linear part is not taken into account. In order to improve this description, force curves were converted into nano-indentation curves from the difference at constant force loading between respective piezo displacement forces measured on a stiff surface and on the deformable bacterial surface, (for details, see references 20 and 24). Figure 2a and b depict the loading force versus indentation depth of bacteria for the two pH values. These curves are fit very well with the combination of the Hertz model for the nonlinear part and a Hook's law spring. From these analyses, Young's modulus of the external layers of bacteria at the two pH values clearly showed the increase of stiffness by decreasing pH (0.21 MPa for pH 4 and 0.037 MPa for pH 10). Such a result indicates that the nonlinear regimen at pH 4 is about five times stiffer than at pH 10. Concerning the linear part, the bacterial spring constant demonstrated the same trend with regard to pH dependence as was previously determined with force curves using equation 1 but with values two times lower. This difference in the bacterial spring constant's values following the fitting procedure (equation 1 or 2) is fully in line with the obvious contribution of both mechanical regimens at a high loading force (up 0.5 nN).

Thus, such fits on the whole indentation curves allowed us to quantify the nanomechanical properties of the two regimens but also their ranges. In fact, the onset of the linear contribution to the loading force could be considered a specific distance in relation to the structural features of the bacterial envelope. These distances were estimated in Fig. 2 close to 60 nm (pH 4) and 155 nm (pH 10). Such a significant increase in the nanometric range by raising the pH was also clearly observed using the first approach (linear portion of force curves) (Fig. 1). In this case, the contribution of the cantilever deflection to the distance that corresponded to the piezo displacement has to be subtracted from values measured on force curves. Such calculation yielded to 62 nm (pH 4) and 136 nm (pH 10) (Fig. 1). Interestingly, both fitting approaches provided similar nanometric ranges for the transition between the two regimens at the two pH values, while the bacterial spring constants were largely overestimated using the slope of force curves (equation 1) mainly due to the added contribution of nonlinear behavior.

With respect to the structure of the surface layers of gram-negative bacteria, these two mechanical regimens could be correlated to the ultrastructure of the bacterial envelope. As previously demonstrated in the literature (2, 3), the linear regimen is induced by progressive compression of the plasmic membrane, maintained by bacterial turgor pressure. Concerning the nonlinear regimen, the mechanical deformation is thus associated to the progressive compression of the cell wall structure. Therefore, this interpretation indicates that the thickness of the cell wall increased from ~60 nm to ~140 nm and softened up as the pH rose from 4 to 10. It is important to point out that if we considered the nonnegligible contribution of the bacterial turgor pressure to the nonlinear regimen, the differences in thickness should be accentuated due to higher bacterial turgor pressure at pH 4 compared to that at pH 10. The constant transition loading force (~0.5 nN) observed for the two pH values is in favor of a negligible contribution

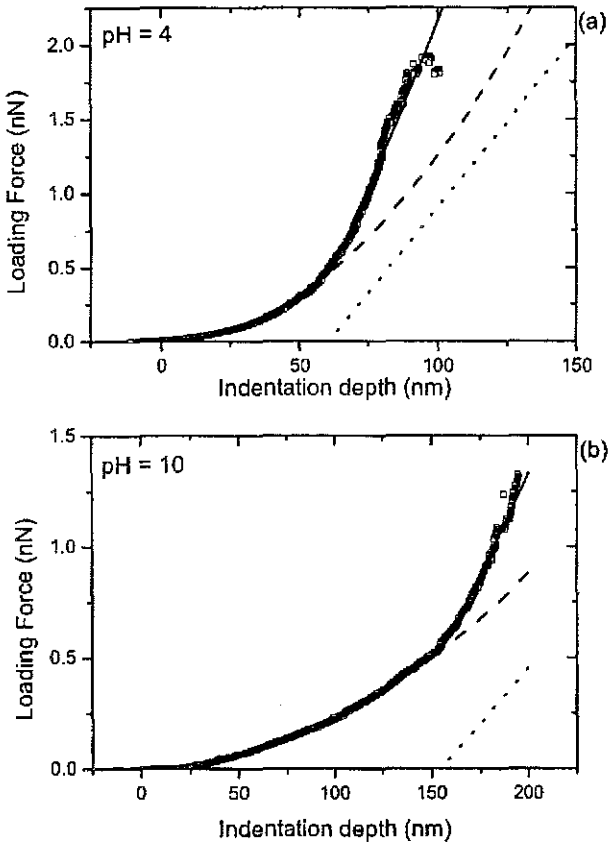

FIG. 2. Mean nano-identation curves obtained under the two pH conditions, pH 4 (a) and pH 10 (b), for *S. putrefaciens* cells at 0.1 M KNO_3. The curves were fitted by summing the contributions of the Hertz model (dashed line) and linear behavior with the bacterial spring constant (dotted line) to reproduce the complete indentation curves as the solid line (equation 2). Best fitting was achieved for an E of 0.21 MPa and a k_B of 0.022 N/m (a) and for an E of 0.037 MPa and a k_B of 0.01 N/m (b). The onset of the linear regimen (dotted line) corresponds to a loading force of 0.48 nN at an indentation of 60 nm for pH 4 and of 0.53 nN at an indentation of 155 nm for pH 10.

because, otherwise, such a value should be dependent on the pH also.

As the retraction curves did not present characteristic negative adhesion signatures of polymeric brush chains as observed previously (8, 22), a change of LPS conformations due to intermolecular repulsive electrostatic forces could not be related to the increase in thickness of the cell wall. In fact, previous investigations of several *Shewanella* species demonstrated the presence of polymeric fringe structures ranging from 20 to 130 nm in thickness depending on the species (13). Thus, the nonlinear behavior observed on force curves could be interpreted in terms of the presence of such a specific polymeric structure. In this case, the increase in the nanometric range was probably associated with the swelling of polymeric fringe. An alternative and/or complementary explanation could also be an increase of the periplasmic thickness. The relevant aspects of the evolution of the cell envelope in response to changes in pH are schematically illustrated in Fig. 3.

However, both proposed mechanisms to explain the increase in the thickness of the cell wall by raising pH should imply

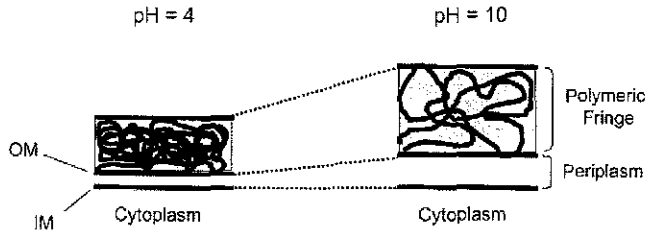

FIG. 3. Schematic view of the dynamic of the cell envelope in response to a change in pH from 4 to 10 (not drawn to scale). OM, outer membrane; IM, inner membrane.

water mobility either from (i) the external media to the polymeric fringe due to higher intermolecular repulsive forces (increasing void spaces) and/or (ii) the cytoplasmic to the periplasmic space caused by higher electrostatic repulsive forces between the inner part of the outer membrane and the outer part of the cytoplasmic membrane.

In summary, the results of this study suggest that AFM force curves can be used to probe the influence of environmental parameters, such as pH, on the mechanical surface properties of bacteria at a nanometric scale. The different mechanical regimens identified on average force curves demonstrated that the external layers of the bacteria contribute mainly to nonlinear forces and that the turgor pressure of the cytoplasm corresponds to linear forces.

We thank Guy Jeannesson and Christine Gérard for their tireless efforts to optimize physicochemical conditions to observe bacterial adhesion. We also thank Raz Jelinek and Laurent Michaud for their critical readings of the manuscript.

We are grateful to the CNRS for the financial support received from the research federation water-soil-earth (FR-633) grants and from PNIR-Biofilms. We also thank Henri Poincaré University (Nancy, France) for providing the BQR 2001 grant and the RIESE 2000 grant. Furthermore, we thank Jean-Claude Block and anonymous reviewers for critical review of the manuscript and helpful comments.

REFERENCES

1. **Ahimou, F., F. A. Denis, A. Touhami, and Y. F. Dufrêne.** 2002. Probing microbial cell surface charges by atomic force microscopy. Langmuir **18:** 9937–9941.
2. **Arnoldi, M., M. Fritz, E. Bäuerlein, M. Radmacher, E. Sackmann, and A. Boulbitch.** 2000. Bacterial turgor pressure can be measured by atomic force microscopy. Phys. Rev. E **62:**1034–1044.
3. **Arnoldi, M., C. M. Kacher, E. Bäuerlein, M. Radmacher, and M. Fritz.** 1998. Elastic properties of the cell wall of magnetospirillum gryphiswaldense investigated by atomic force microscopy. Appl. Phys. A **66:**S613–S617.
4. **Beveridge, T. J.** 1999. Structures of gram-negative cell walls and their derived membrane vesicles. J. Bacteriol. **181:**4725–4733.
5. **Beveridge, T. J., and L. L. Graham.** 1991. Surface layers of bacteria. Microbiol. Rev. **55:**684–705.
6. **Burks, G. A., S. B. Velegol, E. Paramonova, B. E. Lindenmuth, J. D. Feick, and B. E. Logan.** 2003. Macroscopic and nanoscale measurements of the adhesion of bacteria with varying outer layer surface composition. Langmuir **19:**2366–2371.
7. **Caccavo, F., Jr., P. C. Schamberger, K. Keiding, and P. H. Nielsen.** 1997. Role of hydrophobicity in adhesion of the dissimilatory Fe(III)-reducing bacterium *Shewanella alga* to amorphous Fe(III) oxide. Appl. Environ. Microbiol. **63:**3837–3843.
8. **Camesano, T. A., and B. E. Logan.** 2000. Probing bacterial electrosteric interactions using atomic force microscopy. Environ. Sci. Technol. **34:**3354–3362.
9. **Cappella, B., and G. Dietler.** 1999. Force-distance curves by atomic force microscopy. Surf. Sci. Rep. **34:**1–104.
10. **D'Costa, N. P., and H. H. Hoh.** 1995. Calibration of optical lever sensitivity for atomic force microscopy. Rev. Sci. Instrum. **66:**5096–5097.
11. **Fredrickson, J. K., J. M. Zachara, D. W. Kennedy, H. Dong, T. C. Onstott, N. W. Hinman, and S. M. Li.** 1998. Biogenic iron mineralization accompa-

nying the dissimilatory reduction of hydrous ferric oxide by a groundwater bacterium. Geochim. Cosmochim. Acta **62:**3239–3257.
12. **Janshoff, A., M. Neitzert, Y. Oberdorfer, and H. Fuchs.** 2000. Force spectroscopy of molecular systems-single molecule spectroscopy of polymers and biomolecules. Angew. Chem. Int. Ed. Engl. **39:**3212–3237.
13. **Korenevsky, A. A., E. Vinogradov, Y. Gorby, and T. J. Beveridge.** 2002. Characterization of the lipopolysaccharides and capsules of *Shewanella* spp. Appl. Environ. Microbiol. **68:**4653–4657.
14. **Li, X., and B. E. Logan.** 2004. Analysis of bacterial adhesion using a gradient force analysis method and colloid probe atomic force microscopy. Langmuir **20:**8817–8822.
15. **Lovley, D. R.** 1991. Dissimilatory iron(III) and manganese(IV) reduction. Microbiol. Rev. **55:**259–287.
16. **Lower, S. K., M. F. Hochella, and T. J. Beveridge.** 2001. Bacterial recognition of mineral surfaces: nanoscale interactions between *Shewanella* and α-FeOOH. Science **292:**1360–1363.
17. **Nikaido, H.** 1996. Outer membrane, p. 29–47. *In* F. C. Neidhardt (ed.), *Escherichia coli* and *Salmonella*: cellular and molecular biology, 2nd ed., vol 1. ASM Press, Washington D.C.
18. **Ona-Nguema, G., M. Abdelmoula, F. Jorand, O. Benali, A. Gehin, J. Block, and R. Genin Jean-Marie.** 2002. Iron(II,III) hydroxycarbonate green rust formation and stabilization from lepidocrocite bioreduction. Environ. Sci. Technol. **36:**16–20.
19. **Pelling, A. E., S. Sehati, E. B. Gralla, J. S. Valentine, and J. K. Gimzewski.** 2004. Local nanomechanical motion of the cell wall of Saccharomyces cerevisiae. Science **305:**1147–1150.
20. **Radmacher, M., M. Fritz, C. M. Kacher, J. P. Cleveland, and P. K. Hansma.** 1996. Measuring the viscoelastic properties of human platelets with the atomic force microscope. Biophys. J. **70:**556–567.
21. **Roden, E. E., and J. M. Zachara.** 1996. Microbial reduction of crystalline iron(III) oxides: influence of oxide surface area and potential for cell growth. Environ. Sci. Technol. **30:**1618–1628.
22. **Takano, H., J. R. Kenseth, S. S. Wong, J. C. O'Brien, and M. D. Porter.** 1999. Chemical and biochemical analysis using scanning force microscopy. Chem. Rev. **99:**2845–2890.
23. **Tortonese, M., and M. Kirk.** 1997. Characterization of application specific probes for SPM's. SPIE Proc. **3009:**53–58.
24. **Touhami, A., B. Nysten, and Y. F. Dufrêne.** 2003. Nanoscale mapping of the elasticity of microbial cells by atomic force microscopy. Langmuir **19:**4539–4543.
25. **Vadillo-Rodriguez, V., H. J. Busscher, W. Norde, J. de Vries, R. J. Dijkstra, I. Stokroos, and H. C. van der Mei.** 2004. Comparison of atomic force microscopy interaction forces between bacteria and silicon nitride substrata for three commonly used immobilization methods. Appl. Environ. Microbiol. **70:**5441–5446.
26. **Vadillo-Rodriguez, V., H. J. Busscher, W. Norde, J. de Vries, and H. C. van der Mei.** 2003. On relations between microscopic and macroscopic physicochemical properties of bacterial cell surfaces: an AFM study on Streptococcus mitis strains. Langmuir **19:**2372–2377.
27. **Velegol, S. B., and B. E. Logan.** 2002. Contributions of bacterial surface polymers, electrostatics, and cell elasticity to the shape of AFM force curves. Langmuir **18:**5256–5262.
28. **Venkateswaran, K., D. P. Moser, M. E. Dollhopf, D. P. Lies, D. A. Saffarini, B. J. MacGregor, D. B. Ringelberg, D. C. White, M. Nishijima, H. Sano, J. Burghardt, E. Stackebrandt, and K. H. Nealson.** 1999. Polyphasic taxonomy of the genus *Shewanella* and description of *Shewanella oneidensis* sp. nov. Int. J. Syst. Bacteriol. **49:**705–724.
29. **Wingenden, J., T. R. Neu, and H. C. Flemming (ed.).** 1999. Microbial extracellular polymeric substances. Springer-Verlag, New York, N.Y.
30. **Yao, X., M. Jericho, and T. Beveridge.** 1999. Thickness and elasticity of gram-negative murein sacculi measured by atomic force microscopy. J. Bacteriol. **181:**6865–6875.
31. **Yao, X., J. Walter, S. Burke, S. Stewart, M. H. Jericho, D. Pink, R. Hunter, and T. J. Beveridge.** 2002. Atomic force microscopy and theoretical considerations of surface properties and turgor pressures of bacteria. Colloids Surf. B **23:**213–230.

3.2. Exploration de la surface de *Shewanella* spp. par microélectrophorèse

Les forces électrostatiques influencent fortement les interactions bactérie-bactérie ou bactérie-support. De nombreuses études supposent l'interface eau-bactérie comme l'interface d'une particule dure. Expérimentalement, il apparaît immédiatement sur les courbes de mobilité électrophorétique en fonction de la force ionique, que cette approximation est fausse. A forte force ionique, la mobilité n'atteint pas un plateau asymptotique de zéro. Ce comportement traduit le caractère mou de l'interface de la bactérie. Ainsi, l'interprétation quantitative des mesures de mobilité, en terme de potentiel zéta, basée sur les théories de Smoluchowski ou Hückel [91], n'est pas envisageable. Dans cette première approche, nous avons utilisé un modèle où la particule dure centrale est sphérique, et le polymère portant les charges est homogène. Il s'agit du modèle qui était alors disponible. Depuis, les équations ont été dérivées pour des particules de forme cylindrique et un polymère hétérogène. Ces développements sont présentés dans la cinquième partie de ce travail. Les valeurs d'épaisseur du polymère à la surface des bactéries utilisées pour la modélisation ont été mesurées sur les clichés de MET.

Les mobilités des quatre souches de *Shewanella,* constituant le modèle de notre étude, ont été mesurées pour une gamme de pH de 2 à 12, à trois forces ioniques (0,1 M ; 0,01 M et 0,001 M) et dans une gamme de force ionique de 0,001 M à 0,3 M à pH 7. Nous avons retrouvé l'hétérogénéité de la souche BrY qui présente une répartition bimodale de ses mobilités pour des pH compris entre 4 et 10. Nous avons montré que CN32 qui ne présente aucun polymère détectable au MET [65] se déplace rapidement dans le champ électrique (densité de charge importante : $\rho 0$ = -40 mM et paramètre hydrodynamique petit $1/\lambda$ = 2 nm) ; par opposition à MR4 (*cf.* Tableau 3 et Figure 8) qui possède un polymère de 70 à 130 nm d'épaisseur et dont la mobilité est plus faible (densité de charge faible : ρ_0 = -10 mM et paramètre hydrodynamique important $1/\lambda$ = 3,5 nm).

La microélectrophorèse et l'application des théories développées pour les particules molles homogènes nous a permis de sonder de façon innovante l'interface eau-bactérie. Pour la première fois la densité de charge des polymères de surface et leur perméabilité à l'eau (paramètre hydrodynamique) ont été quantifiées.

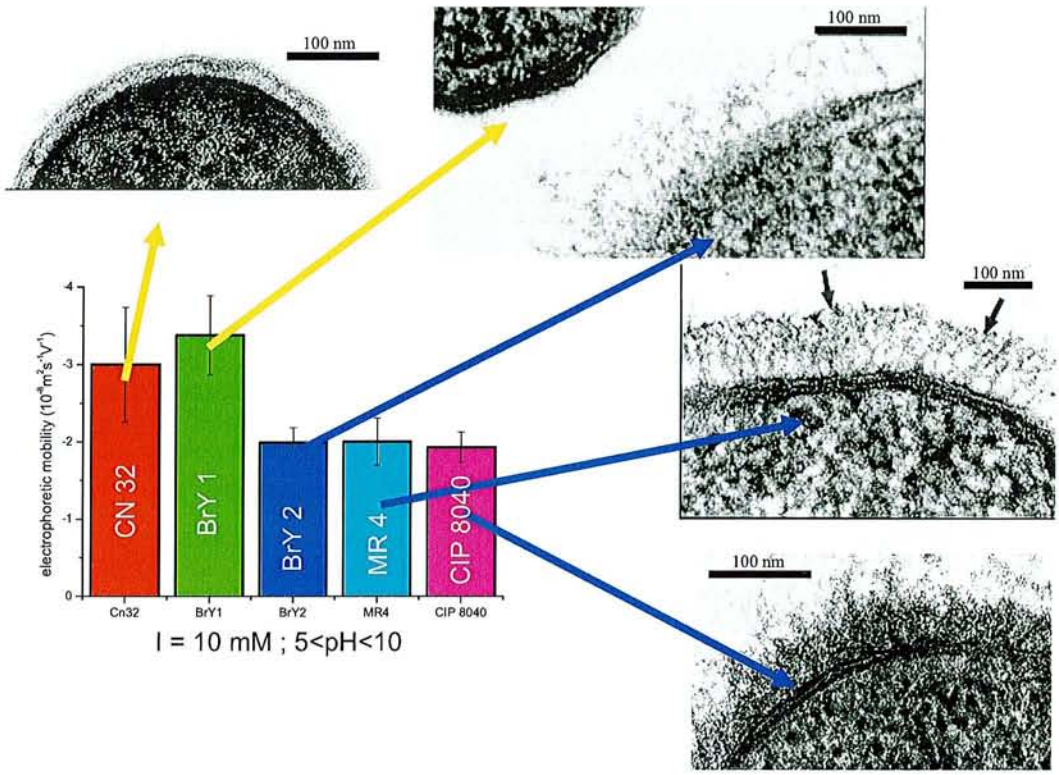

Figure 8 : Mobilité électrophorètique des quatre souches de *Shewanella* spp. pour un pH compris entre 5 et 10 à la force ionique de 0,01 M. Les souches sans polymère (CN32 et BrY1) présentent une mobilité plus grande que les souches avec polymère (MR4, CIP8040 et BrY2). NB : les résultats de la souche CIP 8040 sont extraits de [117]

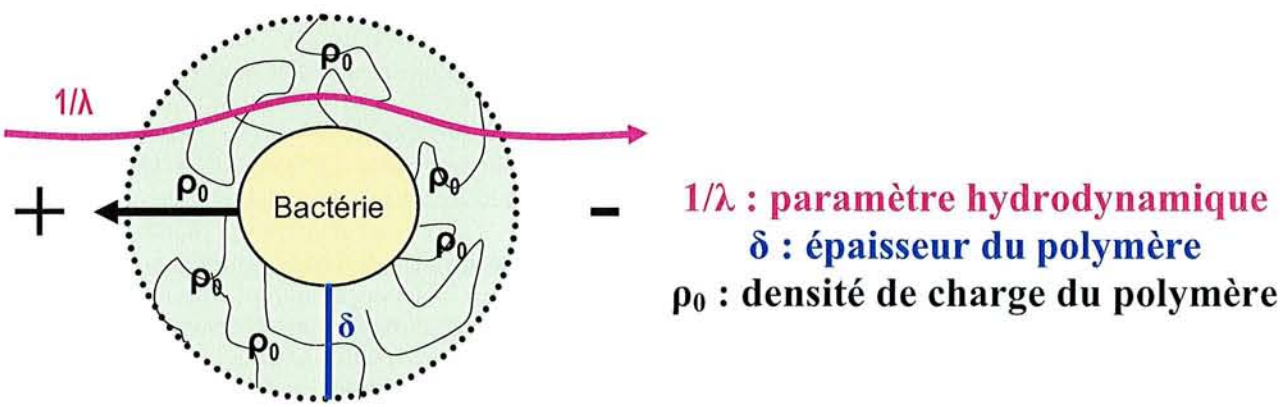

Figure 9 : Paramètres à prendre en compte pour la modélisation du déplacement d'une bactérie dans un champ électrique

Tableau 3 : Densité de charge et paramètre hydrodynamique pour les 4 souches de *Shewanella* spp.

Souche	Sous Population	ρ_0 (mM)	$1/\lambda$ (nm)	δ (nm)
CN32		- 40	2	5
BrY	BrY1	- 40	2,8	5
	BrY2	- 12	3,6	90
MR4		- 10	3,5	90
CIP8040		- 8	4	60

Probing Surface Structures of *Shewanella* spp. by Microelectrophoresis

Etienne Dague,* Jérôme Duval,[†‡§] Frédéric Jorand,* Fabien Thomas,[§] and Fabien Gaboriaud*
*Laboratoire de Chimie Physique et Microbiologie pour l'Environnement, UMR 7564, CNRS, UHP Nancy I, F-54600 Villers-lès-Nancy, France; [†]Department of Physical Chemistry and Colloid Science, Wageningen University, 6703 HB Wageningen, The Netherlands; [‡]CABE (Analytical and Biophysical Environmental Chemistry), University of Geneva, Science II, Geneva, Switzerland; and [§]Laboratoire Environnement et Minéralurgie, UMR 7569 CNRS-INPL, ENSG BP 40, F-54501 Vandoeuvre-lès-Nancy Cedex, France

ABSTRACT Long-range electrostatic forces substantially influence bacterial interactions and bacterial adhesion during the preliminary steps of biofilm formation. The strength of these forces depends strongly on the structure of the bacterium surfaces investigated. The latter may be addressed from appropriate analysis of electrophoretic mobility measurements. Due to the permeable character of the bacterium wall and/or surrounding polymer layer, bacteria may be regarded as paradigms of soft bioparticles. The electrophoretic motion of such particles in a direct-current electric field differs considerably from that of their rigid counterparts in the sense that electroosmotic flow takes place around and within the soft surface layer. Recent developments of electrokinetic theories for soft particles now render possible the evaluation of the softness degree (or equivalently the hydrodynamic permeability) from the raw electrokinetic data. In this article, the electrophoretic mobilities of three *Shewanella* strains (MR-4, CN32, and BrY) presenting various and well-characterized phenotypes of polymer fringe are reported over a wide range of pH and ionic strength conditions. The data are quantitatively analyzed on the basis of a rigorous numerical evaluation of the governing electrostatic and hydrodynamic equations for soft particles. It is clearly shown how the peculiar surface structures of the bacteria investigated are reflected in their electrohydrodynamic properties.

INTRODUCTION

Bacterial cell surface properties are central to understand the intricacies of interfacial phenomena in aqueous media such as bacterial adhesion, biomineralization, or biofilm formation. The assessment of bacterial properties at the molecular, microscopic, and macroscopic levels is far from being an easy task because of the plethora of polymer cell envelope structures that possibly exist and because of the intrinsic dynamic nature of these structures. In the past decade, a large set of data has been compiled using macroscopic methods so as to quantify the overall properties of bacterial suspensions. Such macroscopic approaches are based mostly on the quantitative estimation of i), the bacterial charge, as obtained from the characteristic isoelectric point (1,2) and ii), the hydrophobic character of bacterial strains from contact angle measurements or from the analysis of data related to the bacterial adhesion onto various substrates (3). Although such approaches have played their roles in the progress of our understanding of bacterial reactivity, several questions regarding the impacts of the structural, chemical, and biological heterogeneities on these overall (or, equivalently, averaged) characteristics remain open. The analysis of the physicochemical properties of the various polymeric-type structures beyond the outer membrane of gram-negative bacteria is a prospective and promising way to gain further insight into the processes underlying the bacterial reactivity.

The cell wall of a gram-negative bacterium exhibits an asymmetric outer membrane located above the periplasmic space containing a thin peptidoglycan layer and a gel-like matrix. Underneath the periplasmic space, the plasma membrane constitutes the last part of the gram-negative envelope that withstands the turgor pressure of the protoplast. Thus, the outer membrane is usually considered to be the outermost layer of the gram-negative cell wall. This asymmetric membrane consists of inner leaflet mostly composed of close-packed phospholipid chains whereas the outer leaflet contains the lipopolysaccharide (LPS) molecules. Other surface layer organizations above the bacterial cell wall (such as capsules, S-layers, or sheets) are frequently encountered (4). The three dimensionality of such specific structures may vary following the bacterial strain, as a result of the growth conditions or changes of the surrounding environment. Whereas the effects of those structures on the bacterial reactivity are now recognized, they still remain poorly understood and therefore require further attention.

Given the context sketched above, a breakthrough has recently been reached by assessing at a molecular scale the specific and nonspecific interactions of bacterial surfaces as a function of the chemical characteristics of the lipopolysaccharide layer (5,6). The data suggest that there is no correlation between the thickness of the LPS layer and the macroscopic adhesion propensity of the bacteria. This important result has been further confirmed and reported by other researchers (7,8). One of the major difficulties for analyzing the bacterial adhesion phenomena is to address and decouple the roles played by the microscopic and macroscopic physicochemical properties of the bacterial surface. Such apparent intricacy motivates further investigation on

Submitted June 8, 2005, and accepted for publication December 14, 2005.

Address reprint requests to Fabien Gaboriaud, Laboratoire de Chemie Physique et Microbiologie pour l'Environnement, 405 rue de Vandoeuvre, F-54600 Villers-lès Nancy, France. Tel.: 33-3-83-68-52-39; Fax: 33-3-83-27-54-44; E-mail: gaboriaud@lcpme.cnrs-nancy.fr.

0006-3495/06/04/2612/10 $2.00

doi: 10.1529/biophysj.105.068205

the structure and the dynamics of the bacterial interfaces in aqueous media.

Following the above considerations, the primary goal of this article is the analysis of the dependence of the electrophoretic mobility of various *Shewanella* strains (MR-4, CN32, BrY) on the characteristics of their respective polymer surface layers. The latter were described previously in the study of Korenevsky et al. (9) by freeze-substitution preparation for preserving the most delicate surface ultrastructure. Table 1 summarizes the results obtained by Korenevsky et al., which pertain to the external polymer features of the *Shewanella* bacteria used in our study. Basically, the cell surfaces of MR-4 revealed an extensive polymer fringe (from 70 to 130 nm) whereas those of CN32 were devoid of any fibrous or capsular materials. Unlike MR-4 and CN32 bacteria, cell population of the BrY strain exhibited an unequal expression of polymeric surface structures yielding very heterogeneous bacterial populations that presented characteristics of both the MR-4 and CN32 strains. Furthermore, *Shewanella* organisms are frequently encountered in aquatic habits, soils, and in the agri-food industry (10–12). In these different environments, *Shewanella* bacteria can form biofilms (12,13). There are classically depicted as one of the most efficient and versatile dissimilatory metal-reducing type of microogranism (14). Finally, they are also relevant within the fields of veterinary and medical bacteriology especially the *Shewanella putrefaciens* and *Shewanella algae* (15,16). However, few studies have so far been carried out on the analysis of the surface properties of *Shewanella* cells. Quantitative description of those properties at a microscopic level is the mandatory requirement for understanding the mechanisms at the bacterium/aqueous solution interface.

Having in mind the assessment of the physico-chemical properties of the *Shewanella* bacteria as a function of their respective and aforementioned surface structures, we report in this article their electrophoretic mobilities measured at various pH and ionic strength values. The data were interpreted on the basis of a theory for the electrokinetics of soft particles (1,17–20) so as to derive the bacterial softness and the volumic charge density of the permeable layer. Knowledge of these parameters is crucial in the understanding of the role played by the various gram-negative *Shewanella* strains in many environmental processes such as bioreduction of minerals in soils or in iron corroded surfaces, food industries, clinical specimens, and oil drilling (14,21–23).

TABLE 1 Nature and type of external polymeric surface structure for the *Shewanella* strains according to the study of Korenevsky et al. (9)*

Designation	Bacterial strain	Characteristics of cell surface structures
CN32	*S. putrefaciens*	Devoid of any fibrous material and not capsulated†
BrY^{FC}	*S. algae*	Heterogeneous populations of bacteria with and without capsular polysaccharides structures (from 60 to 90 nm)†
MR-4	*S. oneidensis*	Capsular polysaccharides structures (from 70 to 130 nm)†

*In addition, they demonstrated on the basis of proteinase K/sodium dodecyl sulphate-polyacrylamide gel electrophoresis that all these strains presented rough LPS (with core oligosaccharide and no O-side chain).
†From freeze-substitution electronic images (9).

MATERIALS AND METHODS

Bacterial cultures

S. algae BrY^{FC} (ATCC 51181), *S. oneidensis* MR-4, and *S. putrefaciens* CN32 (ATCC BAA-453) were kindly provided by Professor T. J. Beveridge (University of Guelph, Ontario, Canada). Bacterial strains were revived from a stock suspension at −80°C on a TSA medium (bioMérieux, Marcy l'Etoile, France) twice successively for 48 h at 30°C. Precultures were then prepared in 250 mL Erlenmeyer flasks containing 20 mL bacterial suspension (NaCl 0.7%; optical density: $OD_{600nm} = 0.5$) and 200 mL TSB (bioMérieux, 30 g/L) that were incubated for 14 h while shaking (300 rpm, 30°C). Cells were then harvested by centrifugation (10 min at $10,000 \times g$) and suspended in aqueous media (NaCl 0.7%, $OD_{600\,nm} = 2.0$). Cell suspensions (10 ml) were subsequently used to inoculate 750 mL TSB in a 1.5 L batch reactor (300 rpm, 30°C, 25 L/h air flux). Cells of the midexponential (5 h) and pseudostationary growth (24 h) phases were harvested by centrifugation (10 min at $10,000 \times g$), washed twice with appropriate potassium nitrate solutions, suspended in different ionic strength solutions (0.001, 0.01, and 0.1 mol/L of KNO_3) of bacterial concentration ranging from 5.10^6 to 1.10^7 cells/mL, and immediately used for microelectrophoresis experiments.

Electrophoretic mobility measurements

Electrophoretic mobility (EM) measurements were performed (Zetaphoremeter IV, CAD Instrumentations, Les Essarts le Roi, France) in a quartz suprasil cell at 24°C from the reflection of a laser beam by bacteria tracked with a charge-coupled device camera. By means of an image analysis software, recorded images were processed in real time to calculate the electrophoretic mobilities from the displacement (migration motion) of the bacteria subjected to a constant direct-current electric field (800 V/m). Different cycles were recorded to perform 100 measurements of the bacterial mobility at every pH and ionic strength values investigated. For each ionic strength, fresh cell suspensions prepared as described above were analyzed by adjusting the pH of the suspension with acid (HNO_3) or base solution (KOH).

Modeling the EM of a diffuse soft particle

The electrophoretic mobilities, measured as a function of the ionic strength, were quantitatively interpreted on the basis of the recent theory developed by Duval et al. (18–20) that accounts for the electrokinetic response of a soft particle without any restriction of size, charge, and Debye thickness. The theoretical approach is based on the rigorous numerical evaluations of the fundamental transport and electrostatic equations of a soft particle. This particle consists of an impermeable hard-core component of radius a, and a permeable polyelectrolyte layer of thickness δ (Fig. 1). In their interfacial modeling, Duval et al. introduced the possibility of inhomogeneous distribution for the polymer segments within the polymeric shell (Fig. 1). This was done by considering a diffuse interface where the properties of the soft ("fuzzy") layer gradually change from bulk polyelectrolyte to bulk electrolyte solution. The theoretical calculation of the electrophoretic mobility μ is done based on a consistent numerical evaluation of i), the electroosmotic velocity profile inside and outside the polymer fringe as governed by the Navier-Stokes equation, ii), the distribution of the local equilibrium electrostatic potential, as defined by the Poisson-Boltzmann equation (electrostatics) and, iii), the local variation of the electrochemical potential

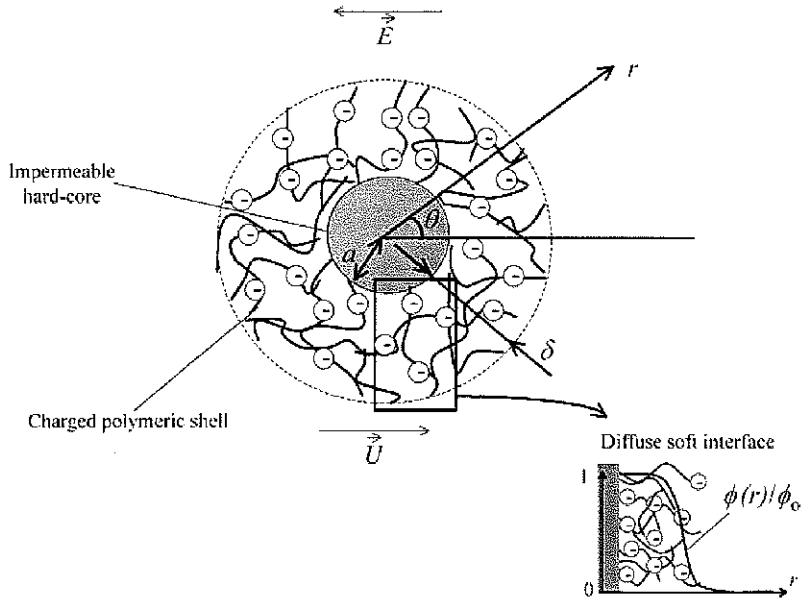

FIGURE 1 Schematic representation of a soft particle, composed of a hard core of radius a and a permeable charged polyelectrolyte layer of thickness δ, moving with a velocity $\vec{U}$ in an electrolyte subjected to direct-current electric field $\vec{E}$. The polar coordinates (r, θ) are indicated. The electrophoretic mobility μ is defined as the ratio U/E. For the sake of illustration, a scheme of a soft diffuse interface is given. Within the scope of such interfacial modeling, the volumic density of polymer segments, noted ϕ, decreases from the value ϕ_0 in the bulk polymer layer to zero in the bulk electrolyte medium. The mathematical function chosen for describing the interface is $\phi(r)/\phi_0 = (1/2)\{1 - \tanh((r - (a+\delta)/\alpha))\}$, where α denotes the typical decay length of the polymer density across the interface (18). For $\alpha = 0$, the model corresponds to that of a step function representation for the interface.

of the ionic species distributed in/around the particle due to polarization of the double layer by the externally applied field. Full details of the theory are available elsewhere (18–20). This theoretical approach for the electrokinetics of the so-called diffuse soft particles extends that originally developed by Ohshima (1), who derived various approximate analytical expressions for the mobility of a particle within restricted ranges of size, charge, and double layer thickness.

The bacteria investigated in our study may be assimilated to infinitely long cylinders with core radius a close to 500 nm whereas the thickness δ of the polymeric surface layer was estimated by electronic imagery (Table 1). For all bacterial strains examined within this article, the ratio surface layer thickness to core size indicates that the electrophoretic behavior of the various *Shewanella* strains is, at least for sufficiently large electrolyte concentrations (i.e., within the concentration range where the mobility hardly deviates from the high ionic strength plateau value), identical to that of a spherical particle with the dimensions a and δ for the bare and permeable components (24). Given these considerations, we derived the relevant electrostatic and hydrodynamic parameters of the various *Shewanella* strains on the basis of the numerical theory recently developed by Duval et al (20) for the electrophoresis of spherical, charged soft particles. Within the ionic strength range where plateau mobility is approximately reached (i.e., for electrolyte concentration higher than, let's say, 50 mM), all bacteria investigated satisfy the conditions derived by Ohshima (24) that underlie the assimilation of the electrophoretic mobility of a cylinder to that of an equivalent spherical particle.

From the numerical theory aforementioned, the experimental mobilities were fitted using two unknown parameters determined by least-square method: i), the permeability parameter, denoted as λ_0, the quantity $1/\lambda_0$ characterizing the typical flow penetration length within the soft polymeric layer, and ii), the volumic charge density ρ_0 of that layer. The computed results from the exact numerical theory reported in Duval et al. (18–20) were systematically compared with those obtained from the approximate analytical expression of Ohshima (1), written

$$\mu = \frac{\rho_0}{\eta\lambda_0^2} + \frac{\varepsilon}{\eta}\frac{\psi_0/\kappa_m + \psi^D/\lambda_0}{1/\kappa_m + 1/\lambda_0}, \quad (1)$$

where η and ε represent the dynamic viscosity and dielectric permittivity of water, respectively, and κ_m the reciprocal Debye thickness of the soft layer surrounding the bacterium. ψ_0 is the surface potential, i.e., the potential at the position corresponding to the location of the outer boundary of the surface layer, and ψ^D the Donnan potential. ψ^D is obtained from the balance in the bulk surface layer between charges stemming from the mobile ions and fixed ionogenic sites. κ_m, ψ_0, and ψ^D may be obtained from the following expressions (1):

$$\psi^D = \frac{RT}{F}\sinh^{-1}\left(\frac{\rho_0}{2Fc^\infty}\right) \quad (2)$$

$$\psi_0 = \psi^D - \frac{RT}{F}\tanh\left(\frac{F\psi^D}{2RT}\right) \quad (3)$$

$$\kappa_m = \kappa\left\{\cosh\left(\frac{F\psi^D}{RT}\right)\right\}^{1/2}, \quad (4)$$

with κ the classical reciprocal screening Debye length and c^∞ the bulk concentration (ionic strength) of the 1:1 electrolyte considered. Equations 1–4 are valid within the limits $\kappa a \gg 1$, $\kappa\delta \gg 1$, $\lambda_0\delta \gg 1$, and low Donnan potentials for which the polarization of the double layer by the applied electric field is negligible. For the cases where $\lambda_0\delta \approx 1$ or $\lambda_0\delta < 1$, Eq. 1 becomes (18,20):

$$\mu = \frac{\rho_0}{\eta\lambda_0^2}\frac{\cosh(\lambda_0\delta) - 1}{\cosh(\lambda_0\delta)} + \frac{\varepsilon}{\eta}\frac{\psi_0/\kappa_m + \psi^D/\lambda_0}{1/\kappa_m + 1/\lambda_0}. \quad (5)$$

RESULTS

EM distributions of single-strain bacterial population

The electrophoretic mobilities of single-strain bacterial population were measured in solutions of different ionic strength and pH values. The experimental setup used for that purpose allowed the recording of the mobilities of the individual cells to quantify the mobility distribution on a statistical basis. The goal was to differentiate presumably heterogeneous subpopulations in the microbial cultures, as done in a previous work (25). In a first set of experiments, the effect

of the bacterial growth time for the bacterial population (midexponential versus pseudostationary) on the EM distribution was examined for the different *Shewanella* strains. Fig. 2 illustrates the results of bacterial mobility for CN32 cells harvested after 5 and 24 h of growth in the midexponential and stationary phases, respectively. The typical pattern obtained for the mobility distribution indicates relatively monodisperse populations over the whole pH range investigated. No significant differences were observed for the EM during the growth phase (from midexponential to stationary phase). Standard deviations calculated from the electrophoregrams of Fig. 2 were in the $\pm 0.3.10^{-8}\,m^2V^{-1}s^{-1}$ range, which is very acceptable for biological systems. Similar Dirac-like EM distributions were obtained for the *S. oneidensis* MR-4 when varying the total ionic strength of the suspension in the range 1–300 mM (not shown). In contrast, *S. algae* BrY clearly exhibited different subpopulations, as illustrated in Fig. 3. The larger the charge carried by the bacteria, i.e., the larger the deviation of the pH as compared to the isoelectric point (~2), the easier the identification of the two subpopulations. From these distributions, mean values and standard deviations for the EM of the two respective subpopulations at different pH were calculated. In the following, those two subpopulations will be referred as BrY1 and BrY2.

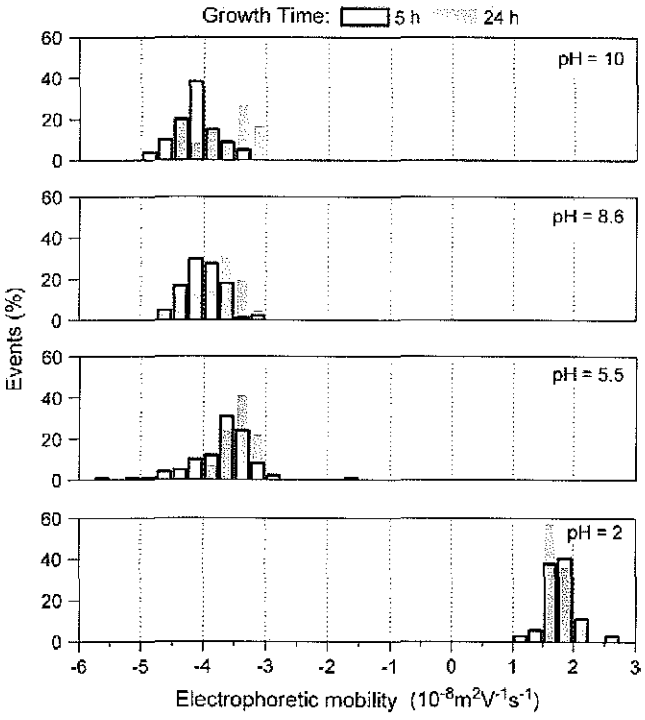

FIGURE 2 Distributions of the electrophoretic mobility measured for *S. putrefaciens* CN32 suspended in a 1 mM sodium nitrate solution at different pH values and two growth conditions before experimentation: extraction sampling 5 h for the midexponential phase and 24 h for the stationary phase.

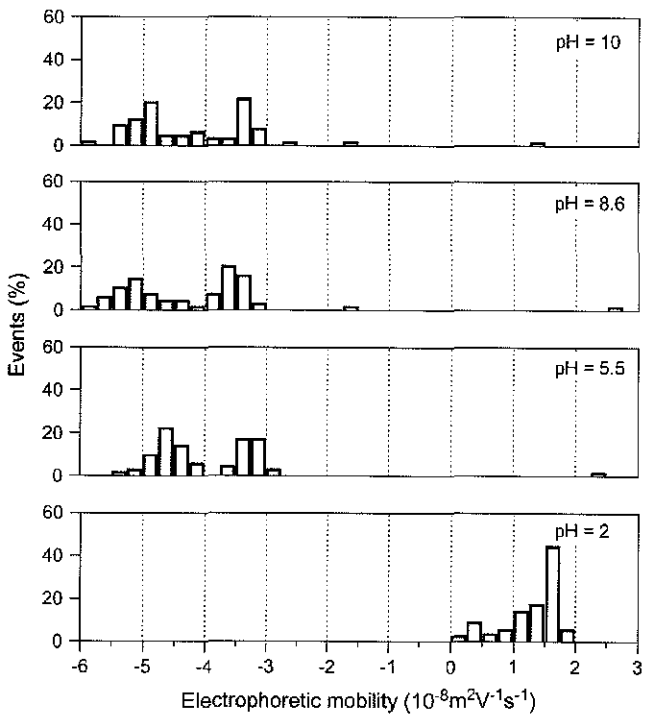

FIGURE 3 Distributions of the electrophoretic mobility measured for *S. algae* BrY suspended in a 1 mM sodium nitrate solution at different pH values.

EM of *Shewanella* spp.

The electrophoretic mobilities of the various *Shewanella* strains investigated are reported in Fig. 4 as a function of pH and ionic strength of the electrolyte solution. For all strains, the EM values are negative over a wide range of pH values, as found for most bacterial cells. Regardless of the ionic strength value and the bacterial strain, the EM significantly decreases (in absolute value) when decreasing the pH solution, whereas in the pH range 5–10, the EM levels off. This feature indicates that the ionogenic sites of the *Shewanella* species are either partly or entirely (see Discussion below) responsible for the overall electrokinetic charge carried by the bacteria via sorption/desorption of protons, or and that they are fully deprotonated for pH above 5. For all bacterial strains examined, the isoelectric point (iep), defined as the pH of zero mobility, is found to be located below 3.5 (Table 2). Slight deviations of the iep values were observed when varying the ionic strength, possibly as the result of any specific structuration of the bacterial surface (26) or specific adsorption of ions onto the pristine charged sites. *S. putrefaciens* CN32 shows the highest iep value (close to 3.2) whereas *S. oneidensis* MR4 the lowest one (<2). The iep of the other *Shewanella* species ranged between these two limits. The same trend was observed for the point of zero salt effect (pzse) that corresponds to the crossover between the mobility curves measured for different ionic strengths (Table 2). These two characteristic points are very close, which indicates that

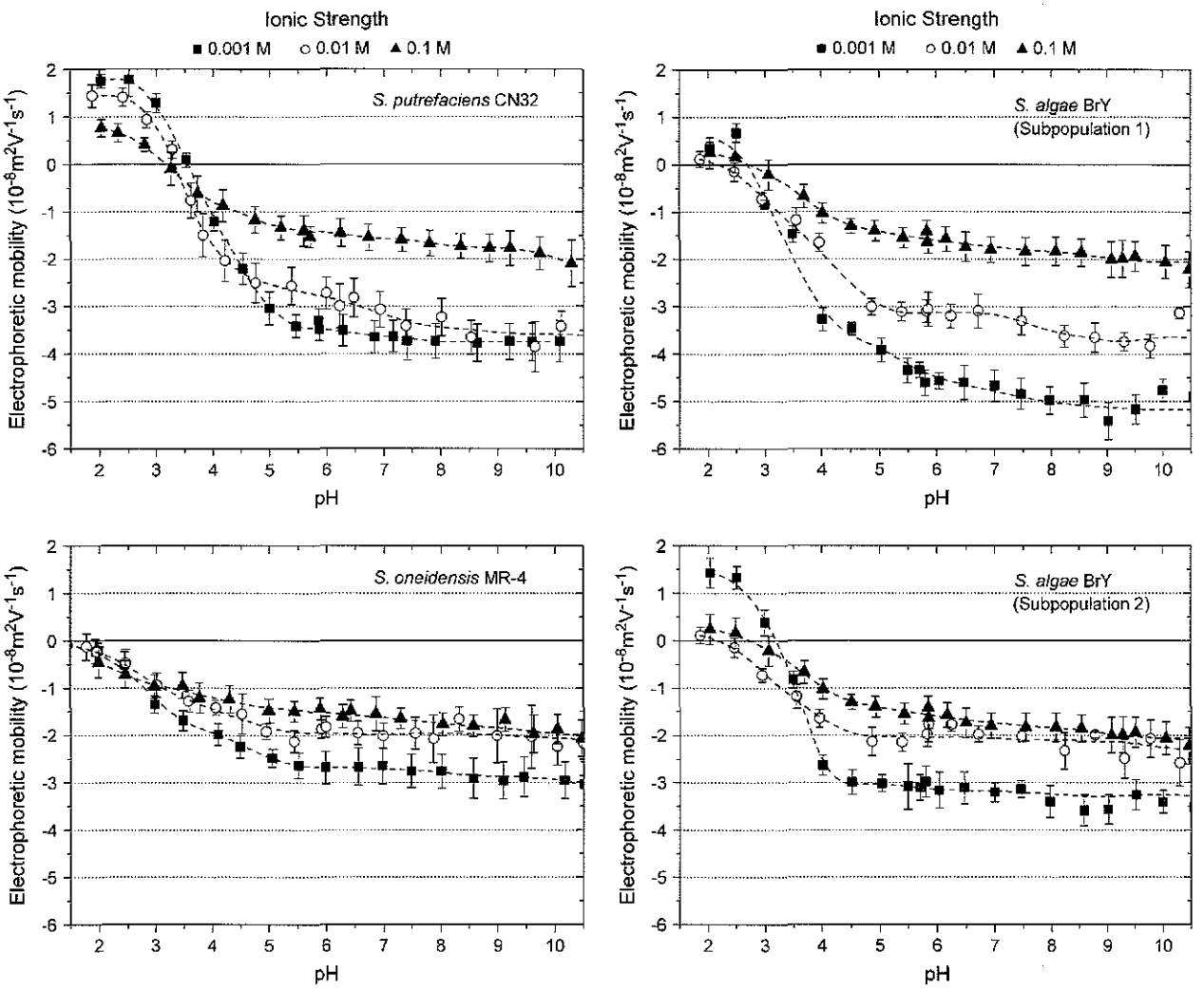

FIGURE 4 Electrophoretic mobility of the various *Shewanella* strains investigated in this study as a function of pH and ionic strength of the electrolytic solution.

specific ion adsorption is probably not predominant. However, intrinsic experimental error prevents from drawing a firm conclusion.

For all bacterial strains studied, the EM showed a dependence on ionic strength that is in agreement with the predictions expected from electrostatic double layer theory. When increasing the ionic strength, the EM decreases as the result of the screening of bacterial charge distributed throughout the wall and/or the polymer fringe. This feature is particularly marked in the pH range 5–10.

As intuitively expectedly, the nature of the bacteria investigated has also an influence on the magnitude of the EM. This is particularly clear from the mobility measurements carried out for sufficiently high ionic strength and pH values. In Fig. 5, comparison is made between the EM plateaus for the different bacterial strains as reached in the pH range 6–10 at a given electrolyte concentration (0.01 M). It appears that CN32 and BrY1 present higher EMs compared to those of BrY2 and MR-4. In the next section, the electrokinetic properties of the various bacterial strains, as reported in Figs. 2–5, are quantitatively analyzed to derive their electrohydrodynamic characteristics, which will be further discussed in relation with their surface structures.

Diffuse soft particle analysis of the EM

As a general rule, the EM of a soft particle differs from that of a hard (rigid) colloid in the sense that the EM reaches asymptotically a nonzero value for sufficiently high ionic

TABLE 2 Summary of the relevant electrokinetic characteristics of the *Shewanella* strains studied

	Iep			
Strain	0.001 M	0.01 M	0.1 M	Pzse
BrY	3.1	2.0	2.7	3.2–3.5
MR-4	<2	<2	<2	2.3–2.9
CN32	3.3	3.4	3.1	3.0–4.0

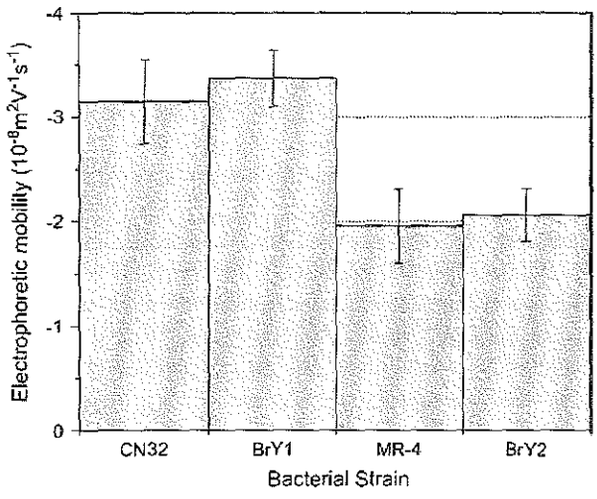

FIGURE 5 Comparison of the mobility plateaus reached at pH values from 5 to 10 for the various *Shewanella* strains and their respective populations. KNO_3 solution, ionic strength = 0.01 M.

strengths. This plateau is the specific signature of the presence of a soft, hydrodynamically permeable layer that surrounds the particle. From Eq. 5, one easily shows that in the high electrolyte concentration regime, the following relation

$$\mu \rightarrow \frac{\rho_0}{\eta\lambda_0^2}\frac{\cosh(\lambda_0\delta)-1}{\cosh(\lambda_0\delta)}$$
$$\text{when} \quad c^{\infty} \rightarrow \infty \,(\text{or equivalently} \, \kappa^{-1} \rightarrow 0) \qquad (6)$$

applies. Reported in Figs. 6 and 7 are the experimentally determined EMs of the different investigated strains for different ionic strength levels and for a neutral pH value. The value pH 7 was considered because at that particular pH, EMs reach a constant value with respect to the pH variation, as shown in Fig. 4. For a given electrolyte concentration, the mobilities are higher (in magnitude) within that range of pH values (between 5 and 10) so that the corresponding analysis of the electrohydrodynamic properties are more accurate and are influenced to a lesser extent by the inherent experimental error. For all bacterial strains, the EMs reach a nonzero constant value upon increase of the ionic strength, in line with expectation from electrokinetic theory for soft particles. The data were subjected to the analytical (and approximate) theory by Ohshima (Eqs. 1–4) and to the numerical approach (no approximations regarding the size and the charge of the particle) developed by Duval et al. (18–20). The results are given in Figs. 6 and 7 together with the experimental data. As suggested by the comparison of the mobility plateaus reported in Fig. 5, two different behaviors were observed regarding the *Shewanella* species.

For MR-4 and BrY2 (Fig. 6), the discrepancy between the experimental data (*solid circle*) and the results computed on the basis of the approximate expressions (*curves a*) increases significantly upon decrease of the ionic strength. This is due to the inaccuracy of Eqs. 1–4 to predict the EM at low ionic strength where i), the condition $\kappa\delta \gg 1$ is not respected (the thickness of the polymer fringe is $\delta \sim 100$ nm and the reciprocal Debye length is $\kappa^{-1} = 1$–10 nm in the concentration range 100–1 mM), and ii), the polarization of the electric double layer (not taken into account in Eqs. 1–4), which acts as a breaking (retarding) force for the migration of the particle, starts to play a significant role. In contrast, the

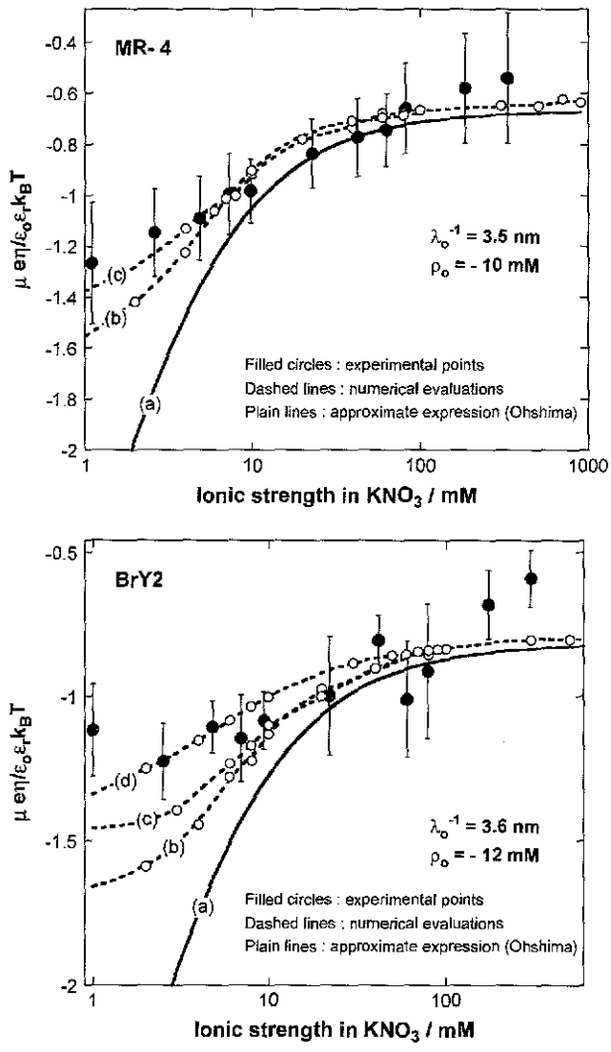

FIGURE 6 Electrophoretic mobilities (expressed in dimensionless form) as a function of ionic strength (●) of *S. oneidensis* strain MR-4 (*top panel*) and of the subpopulation BrY2 of *S. algae* (*bottom panel*). The plain lines (*curves a*) correspond to the best fit calculated from the approximate expressions derived by Ohshima (Eqs. 1–4) (1) whereas the dashed lines (*curves b* to *d*) represent the rigorous numerical evaluations on the basis of the theory developed by Duval et al. (18,19). Those different approaches were computed with $\lambda_0^{-1} = 3.5$ nm, $\rho_0 = -10$ mM for MR-4, and $\lambda_0^{-1} = 3.6$ nm, $\rho_0 = -12$ mM for BrY-2. Two different polymer shell thicknesses were considered in the numerical evaluations: $\delta = 60$ nm for curves *b*, and $\delta = 90$ nm for curves *c*. For BrY2, a diffuse interface representation of thickness $\alpha = 5$ nm (see Fig. 1) is considered (*curve d*) to reproduce the possibility of inhomogeneous distribution of charges in the polymeric shell. The dashed lines are guide to the eye for the points (○) theoretically calculated.

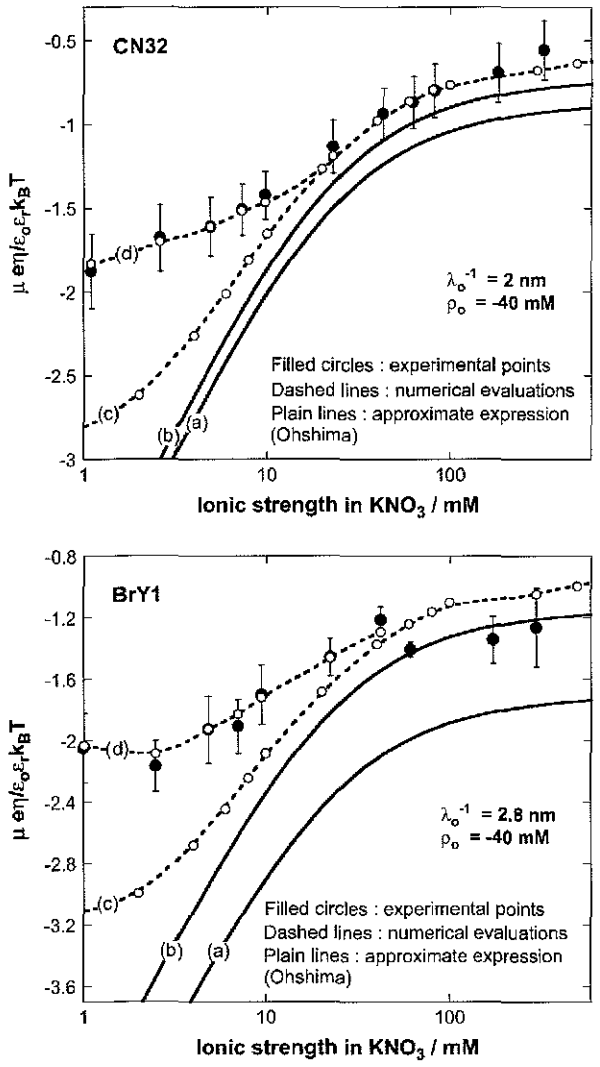

FIGURE 7 Electrophoretic mobilities as a function of ionic strength (●) of *S. putrefaciens* strain CN32 (*top panel*) and of the subpopulation BrY1 of *S. algae* (*bottom panel*). The plain lines correspond to the best fit calculated from the approximate expressions derived by Ohshima (Eqs. 1–5) (1) computed with $\lambda_0^{-1} = 2\,\text{nm}$, $\rho_0 = -40$ mM for CN32, and $\lambda_0^{-1} = 2.8\,\text{nm}$, $\rho_0 = -40$ mM for BrY1. The curves (*a*) do not consider the size of the polymeric shell (Eq. 1) whereas curves *b* takes into account the shell thickness $\delta = 5$ nm (Eq. 5). The dashed lines represent the rigorous numerical evaluations on the basis of the theory developed by Duval et al. (18,19) calculated with $\lambda_0^{-1} = 2\,\text{nm}$, $\delta = 5\,\text{nm}$ for CN32, and $\lambda_0^{-1} = 2.8\,\text{nm}$, $\delta = 5$ nm for BrY1. The curves (*c*) consider a fixed volumic charge density $\rho_0 = -40$ mM for CN32 and BrY1 whereas curves (*d*) were calculated after adjustment of the ρ_0 parameter with the electrolyte concentration (see text for further detail). The dashed lines are guide to the eye for the points (○) theoretically calculated.

mobilities calculated from the rigorous numerical evaluations of the key electrokinetic equations (*curves b*, *c*, and *d*) better reproduce the data over the whole range of electrolyte concentration. It is important to note that iterative adjustment (by least-square methodology) of the softness parameter λ_0 and the volumic charge density ρ_0 yielded the same results for those two parameters in all theoretical cases considered. This is so because the analytical theory by Ohshima (1) constitutes the high electrolyte concentration-limit of the rigorous theory and because the EM plateau value is depending on λ_0 and ρ_0 only (see the first term in the right-hand side of Eq. 1).

The aforementioned numerical theory (Fig. 6, *dashed lines*) allows for considering different thicknesses of the permeable polyelectrolyte layer (fringe) with or without a diffuse interface. In the case of MR-4 strain, the increase of shell thickness from 60 nm (Fig. 6, *top panel, curve b*) to 90 nm (*curve c*) improves the description of the experimental data. For the BrY2 strain (Fig. 6, *bottom*), such adjustment failed slightly to reproduce satisfactorily the data especially at low ionic strengths (*curves b* and *c*). To improve this description, a diffuse interface was considered to introduce the possibility of inhomogeneous distribution for the polymer segments within the polymeric shell, and interfacial step function modeling (see Fig. 1) was abandoned. A typical decay length α of 5 nm was used to reasonably fit the experimental data (Fig. 6, *bottom panel, curve d*). Because of the significant inaccuracy of the experimental data as compared to the differences in computed EM when considering or not a diffuse interface, no hard conclusion regarding the respective inhomogeneity of the polymer fringes of the MR-4 and BrY2 can be done. However, the values obtained for the softness parameter and the volumic charge density unambiguously indicate that MR-4 and BrY2 cells present a fairly similar and large hydrodynamic permeability (3.5 and 3.6 nm) and are weakly charged (−10 and −12 mM).

For CN32 and BrY1 (Fig. 7), the analytical expressions given by Eq. 1 (*curve a*) and Eq. 5 (*curve b*) are clearly inadequate to account for the data mainly because the high volumic charge density carried by the bacteria is responsible for large local electrostatic potentials where analytical treatment of the electrokinetic equations is no longer acceptable. In passing, it is noted that the EM plateaus reached at high electrolyte concentrations are better reproduced by Eq. 5, which takes into account the finite thickness δ of the polymer fringe (the approximation $\lambda_0\delta \gg 1$ clearly does not hold for CN32 and BrY1 bacteria). The value of $\delta = 5$ nm was chosen for the calculation on the basis of the known and reported dimension of the wall thickness of gram-negative stain bacteria (9,27). As already mentioned, the expression by Ohshima (1) is strictly valid within a given range of charge (or potential), polyelectrolyte shell thickness, and Debye length. The description of the experimental data on the basis of the electrokinetic theory for soft spherical particles (numerical evaluation) remains poor, especially at low ionic strength levels (*curve c*). Besides the assumption that consists in assimilating the mobility of an infinitely long cylinder to that of a spherical particle, which is certainly questionable at low ionic strength levels, another pitfall in the analysis is that the volumic charge density is taken constant over the whole range of electrolyte concentrations. However, it is well established that ionic strength may strongly modify the volumic charge density and that this modification is

intrinsically related to the magnitude of this charge. In other words, not only the chemistry (number and nature of ionogenic sites distributed throughout the bacterium wall) but also the electrostatics (magnitude of the charge and local electrostatic potential) mediate the intrinsic charge carried by the bacterium (28). Whereas for the weakly charged MR-4 and BrY2 bacterial strains the assumption of a constant ρ_0 when varying the electrolyte concentration seems reasonable, it clearly needs to be revisited for the highly charged CN32 and BrY1 strains. Consequently, the experimental EM for CN32 and BrY1 were fitted by considering adjustable ρ_0 at each ionic strength level (Fig. 7, *curves d*). The corresponding ρ_0 are given in Fig. 8 for the two types of cells. When lowering the ionic strength, the magnitude (in absolute value) of ρ_0 decreases in agreement with expectations from theory (28). In both cases, the softness parameters are significantly lower (2 and 2.8 nm) than that determined for the bacteria surrounded by a polymer fringe but is still characteristic of the presence of a permeable, soft layer, i.e., the bacterial wall itself.

DISCUSSION

Microelectrophoresis has been long used to evaluate the surface charge of colloidal particles from electrophoretic mobility measurements. Clearly, the theoretical concepts developed for the electrophoresis of rigid particles (Smoluchowski-Henry equations, e.g., (29)) are not valid for deriving the electrostatic and hydrodynamic properties of biological systems (1). As a major difference, the notion of ζ-potential is, for such soft systems, unambiguously physically irrelevant because it is impossible to locate a priori the position of the slip plane within the hydrodynamically permeable soft corona surrounding the particle.

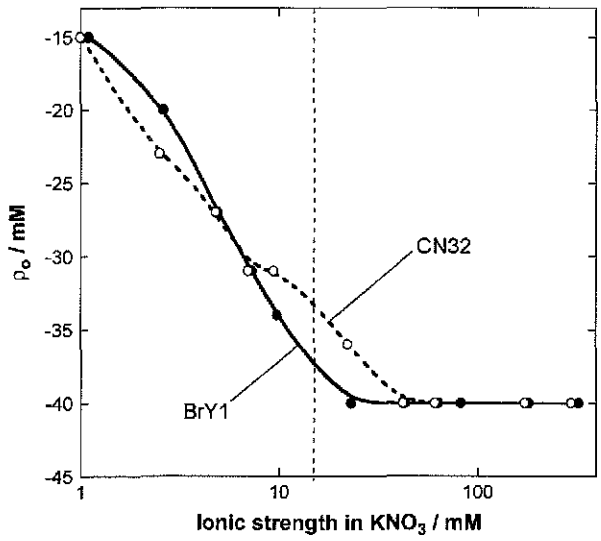

FIGURE 8 Plot of the volumic charge density ρ_0 used to fit the electrophoretic data pertaining to the BrY1 and CN32 cells (curves *d* of Fig. 7).

Fortunately, electrokinetic equations for soft particles have been derived and their recent numerical resolution allows the analysis of the electrophoretic migration of biological cells (30–35). However, the application of these models for bacterial cells is still sparse and difficult due, for example, to i), the possible heterogeneous character of microbial suspensions, and ii), the intricacy and diversity of surface ultrastructures of bacteria. In this study, the strains investigated have been chosen for their complementarities in terms of the presence or not of polymer fringe beyond the outer membrane (Table 1). Whereas the cell surfaces of CN32 are devoid of such surface appendage, those of MR-4 are covered by a polymeric shell. As far as the BrY strain is concerned, both phenotypes are present. These different and well-characterized bacterial phenotypes are very suitable for testing the interrelationship that exists between electrokinetic (i.e., electrophoretic) properties and bacterial surface structures.

As demonstrated in this article, the electrophoretic mobility distribution for a given microbial culture provides useful and key information related to its heterogeneous character. An illustrative example given here is the identification of two distinct subpopulations for the BrY strain, which is in line with previous observations of electronic micrographs (9) (Table 1). The two other strains investigated (CN32 and MR-4) depict a monodisperse pattern also consistent with electronic observations. Comparison of the electrophoretic mobility for the various *Shewanella* strains analyzed (particularly in the pH range 5–10, Fig. 5) indicates that the electrohydrodynamics of the bacteria is significantly influenced by the presence or not of a polymer fringe at the surface, the CN32 and BrY1 cells exhibiting larger mobility values than MR-4 and BrY2 cells. Since the presence of a polymer layer around the cell is intuitively expected to retard its migrative motion because of increasing electroosmotic drag (that is increasing friction forces), Fig. 5 suggests a priori that the first subpopulation of BrY strain (called BrY-1) is devoid of any polymeric appendage whereas the second one (BrY2) behaves as bacterial cells with polymer fringe. The presence or not of a fuzzy polymer layer around the bacterium has, apparently, also an impact on the iep values. Whereas the strain with polymer fringe (MR-4) exhibited values <2.5, the CN32 cells present an iep >3.1. Because of their heterogeneous character and since it is impossible to distinguish the BrY1 and BrY2 strains at low pH values, the effective iep for BrY lies in between the two aforementioned limits. As stated, the electrophoretic migration of a given bacterium is governed by a subtle balance between electrostatic processes, as the result of the presence of chemical groups within the cell wall or around the bacterium (9,26,36) and hydrodynamic processes.

To quantitatively identify the balance between these two contributions, approximate analytical and rigorous theoretical expressions were employed to analyze the electrophoretic mobility changes in response to ionic strength variation.

Regardless of the equations used, the permeability parameter (λ_0) and the volumic charge density (ρ_0) obtained from the fitting procedure are the same for all different theoretical approaches considered. Whereas Eqs. 1–4 are inadequate to account for the data at low ionic strengths, rigorous theory seems to provide a better description at such ionic strength level even if it should be kept in mind that the assimilation of the bacteria to spheres at low ionic strength levels may become questionable. Since there is so far no available numerical and rigorous theory for the electrophoresis of soft cylinders, we discuss the results within the framework of the spherical geometry theory, which provides the accurate electrohydrodynamic parameters λ_0 and ρ_0 (basically computed from the analysis of the mobility data measured at high ionic strengths).

The values for λ_0 and ρ_0 obtained for the various bacterial strains are collected in Table 3. As a general comment, cells without a polymer fringe (i.e., CN32 and BrY1) exhibit a rather large volumic charge density and a relatively low hydrodynamic permeability as compared to cells that present such a fringe (i.e., MR-4, BrY2). In other words, the bacterium wall is more rigid (i.e., less permeable) and more charged than the bacterial material constituting the soft polymeric structure around the cell wall. It is thereby added that although the electrophoretic migration of CN32 and BrY1 is obviously determined by the electrohydrodynamic properties of the cell wall, that of MR-4 or BrY2 is solely caused by the outer soft layer (~90 nm thickness) of the bacteria, the "slipping plane" (or the spatial zone of zero electroosmotic flow) being located well beyond the bacterial wall (we have $\lambda_0\delta \gg 1$). In other words, it is definitely correct to assign the λ_0 and ρ_0 values to the bacterial wall when referring to the analysis of the CN32 and BrY1 strains, and to the outer polymer fringe when dealing with the MR-4 and BrY2. Qualitatively, the respective electrostatic and hydrodynamic properties of the wall and polymer fringe of the—here studied—gram negative bacteria is in very good agreement with those obtained on bald and fibrillated oral streptococcal strains (28).

Going further in the analysis, it is interesting to compare the volumic charge density obtained in the case of CN32 strain with that derived from the potentiometric titration performed by Sokolov et al. (37) on the same strain. Whereas the comparison is rendered difficult by the necessity to know accurately the number of bacteria present in the titration cell for estimating an apparent volumic charge density ρ_0, the exercise unambiguously reveals the following finding: the volumic charge density obtained from the titration data at 0.1 M ionic strength is estimated from ~−0.2 to −15 M, which is about 1–2 orders of magnitude larger than the value obtained from the analysis of the electrophoretic mobility versus ionic strength curves. The significant discrepancy between the electrokinetic charge (as evaluated from electrophoresis) and the pristine charge (as measured by titration) has been for long observed for rigid colloids and very recently for soft bacteria (28). It principally originates from the accumulation of counterions in the bacterial cell wall as the result of electrostatic and specific adsorption processes. This leads to an effective charge, the electrokinetic charge, which is significantly lower than the pristine titrable charge. Results obtained in Duval et al. (28) for bald oral-streptococcal bacterial strain indicate that, depending on the pH and ionic strength conditions, the electrokinetic charge may represent only a few percent of the total charge measured by protolytic titration. This is well in qualitative agreement with the conclusions led out for the *Shewanella* CN32 bacteria of this study. Other reasons that possibly account for the difference between electrokinetic and titrable charges may be found by evoking the presence of metabolic processes of the bacteria that lead to a consumption of proton/hydroxide ions during the potentiometric titration without any protonation or deprotonation of the functional groups (proton pumping, exudation of organic acids. etc.). The occurrence of such processes has recently been emphasized by Claessens et al. (38).

Summarizing the preceding sections, the principal results of this study show the relationship that exists between the nature of the bacterium surface structure and its electrophoretic behavior. The presence of a polymer fringe confers the bacterium a relatively low electrokinetic charge density and a rather important hydrodynamic permeability. In the other situation, i.e., in the absence of any polymeric shell, the electrokinetic bacterial charge is largely increased due to ionization of functional groups located within the outer membrane and the permeable character significantly decreased.

TABLE 3 Summary of the volumic charge density (ρ_0) and the softness parameter (λ_0^{-1}) obtained from the best fitting procedure for the different strains investigated (Figs. 6 and 7)

Strain	Subpopulation	ρ_0 (mM)	λ_0^{-1} (nm)
CN32	–	−40	2
BrY	BrY1	−40	2.8
	BrY2	−12	3.6
MR-4	–	−10	3.5

The authors thank Yves Waldvogel (LEM, UMR 7569, Vandoeuvre-lès-Nancy, France) for help in electrophoresis experiments.

This study was supported by grants from CNRS (PNIR-Biofilms and Fédération Eau-Sol-Terre, Nancy) and by Henri Poincaré University of Nancy (special BQR grant).

REFERENCES

1. Ohshima, H. 1995. Electrophoretic mobility of soft particles. *Colloid Surf. A.-Physiochem. Eng. Asp.* 103:249–255.
2. Van Loosdrecht, M. C. M., J. Lyklema, W. Norde, G. Schraa, and A. J. B. Zehnder. 1987. Electrophoretic mobility and hydrophobicity as a measure to predict the initial steps of bacterial adhesion. *Appl. Environ. Microbiol.* 53:1898–1901.
3. Bos, R., H. C. van der Mei, and H. J. Busscher. 1999. Physico-chemistry of initial microbial adhesive interactions–its mechanisms and methods for study. *FEMS Microbiol. Rev.* 23:179–230.

4. Beveridge, T. J., and L. L. Graham. 1991. Surface layers of bacteria. *Microbiol. Rev.* 55:684–705.
5. Burks, G. A., S. B. Velegol, E. Paramonova, B. E. Lindenmuth, J. D. Feick, and B. E. Logan. 2003. Macroscopic and nanoscale measurements of the adhesion of bacteria with varying outer layer surface composition. *Langmuir.* 19:2366–2371.
6. Salerno, M. B., B. E. Logan, and D. Velegol. 2004. Importance of molecular details in predicting bacterial adhesion to hydrophobic surfaces. *Langmuir.* 20:10625–10629.
7. Vadillo-Rodriguez, V., H. J. Busscher, W. Norde, J. de Vries, and H. C. van der Mei. 2004. Relations between macroscopic and microscopic adhesion of *Streptococcus mitis* strains to surfaces. *An. Microbiol. (Rio J.).* 150:1015–1022.
8. Vadillo-Rodriguez, V., H. J. Busscher, W. Norde, J. de Vries, and H. C. van der Mei. 2003. On relations between microscopic and macroscopic physicochemical properties of bacterial cell surfaces: an AFM study on *Streptococcus mitis* strains. *Langmuir.* 19:2372–2377.
9. Korenevsky, A. A., E. Vinogradov, Y. Gorby, and T. J. Beveridge. 2002. Characterization of the lipopolysaccharides and capsules of *Shewanella* spp. *Appl. Environ. Microbiol.* 68:4653–4657.
10. Hjelm, M., L. R. Hilbert, P. Moller, and L. Gram. 2002. Comparison of adhesion of the food spoilage bacterium *Shewanella putrefaciens* to stainless steel and silver surfaces. *J. Appl. Microbiol.* 92:903–911.
11. Skjerdal, O. T., G. Lorentzen, L. Tryland, and J. D. Berg. 2004. New method for rapid and sensitive quantification of sulphide-producing bacteria in fish from artic and temperate waters. *Int. J. Food Microbiol.* 93:325–333.
12. Bagge, D., M. Hjelm, C. Johansen, I. Huber, and L. Gram. 2001. *Shewanella putrefaciens* adhesion and biofilm formation on food processing surfaces. *Appl. Environ. Microbiol.* 67:2319–2325.
13. Lies, D. P., M. E. Hernandez, A. Kappler, R. E. Mielke, J. A. Gralnick, and D. K. Newman. 2005. *Shewanella oneidensis* MR-1uses overlapping pathways for iron reduction at a distance and by direct contact under conditions relevant for biofilms. *Appl. Environ. Microbiol.* 71:4414–4426.
14. Lovley, D. R. 1991. Dissimilatory iron(III) and manganese(IV) reduction. *Microbiol. Rev.* 55:259–287.
15. Khashe, S., and J. M. Janda. 1998. Biochemical and pathogenic properties of *Shewanella alga* and *Shewanella putrefaciens*. *J. Clin. Microbiol.* 36:783–787.
16. Gram, L., and P. Dalgaard. 2002. Microbiological spoilage of fish and fish products. *Int. J. Food Microbiol.* 33:121–137.
17. Ohshima, H. 2002. Electrophoretic mobility of a charged spherical colloidal particle covered with an uncharged polymer layer. *Electrophoresis.* 23:1995–2000.
18. Duval, J. F. L. 2005. Electrokinetics of diffuse soft interfaces. 2. Analysis based on the nonlinear Poisson-Boltzmann equation. *Langmuir.* 21: 3247–3258.
19. Duval, J. F. L., and H. P. Van Leeuwen. 2004. Electrokinetics of diffuse soft interfaces. 1. Limit of low Donnan potentials. *Langmuir.* 20:10324–10336.
20. Duval, J. F. L., K. J. Wilkinson, H. P. Van Leeuwen, and J. Buffle. 2005. Humic substances are soft and permeable: evidence from their electrophoretic mobilities. *Environ. Sci. Technol.* 39:6435–6445.
21. Lower, S. K., M. F. Hochella, and T. J. Beveridge. 2001. Bacterial recognition of mineral surfaces: Nanoscale interactions between *Shewanella* and a-FeOOH. *Science.* 292:1360–1363.
22. Ona-Nguema, G., M. Abdelmoula, F. Jorand, O. Benali, A. Gehin, J.-C. Block, and J. M. R. Genin. 2002. Microbial reduction of lepidocrocite gamma-FeOOH by *Shewanella putrefaciens*: the formation of green rust. *Hyperfine Interact.* 139/140:231–237.
23. Das, A., and F. J. Caccavo. 2001. Adhesion of the dissimilatory Fe(III)-reducing bacterium *Shewanella alga* BrY to crystalline Fe(III) oxides. *Curr. Microbiol.* 42:151–154.
24. Ohshima, H. 2001. On the electrophoretic mobility of a cylindrical soft particle. *Colloid Polym. Sci.* 279:88–91.
25. van der Mei, H. C., and H. J. Busscher. 2001. Electrophoretic mobility distributions of single-strain microbial populations. *Appl. Environ. Microbiol.* 67:491–494.
26. Rijnaarts, H. H. M., W. Norde, J. Lyklema, and A. J. B. Zehnder. 1995. The isoelectric point of bacteria as an indicator for the presence of cell surface polymers that inhibit adhesion. *Colloid Surf. B.-Biointerfaces.* 4:191–197.
27. Beveridge, T. J. 1999. Structures of Gram-negative cell walls and their derived membrane vesicles. *J. Bacteriol.* 181:4725–4733.
28. Duval, J. F. L., H. J. Busscher, B. van de Belt-Gritter, H. C. van der Mei, and W. Norde. 2005. Electrodynamics of fibrillated and non fibrillated oral streptococcal strain from electrophoretic mobility and titration measurements: beyond the "classical soft particle approach". *Langmuir.* 21:11268–11282.
29. Hiemenz, P. C., and R. Rajagopalan. 1997. Principles of Colloid and Surface Chemistry. Marcel Dekker, New York.
30. Bos, R., H. C. van der Mei, and H. J. Busscher. 1998. Soft-particle analysis of the electrophoretic mobility of a fibrillated and non-fibrillated oral streptococcal strain: *Streptococcus salivarius*. *Biophys. Chem.* 74:251–255.
31. Hayashi, H., S. Tsuneda, A. Hirata, and H. Sasaki. 2001. Soft particle analysis of bacterial cells and its interpretation of cell adhesion behaviors in terms of DLVO theory. *Colloid Surf. B.-Biointerfaces.* 22:149–157.
32. Kiers, P. J. M., R. Bos, H. C. van der Mei, and H. J. Busscher. 2001. The electrophoretic softness of the surface of *Staphylococcus* epidermidis cells grown in a liquid medium and on a solid agar. *An. Microbiol. (Rio J.).* 147:757–762.
33. Makino, K., M. Ikekita, T. Kondo, S. Tanuma, and H. Ohshima. 1994. Change in electrophoretic mobility of HL-60RG cells by apoptosis. *Colloid Polym. Sci.* 272:487–492.
34. Morisaki, H., S. Nagai, H. Ohshima, E. Ikemoto, and K. Kogure. 1999. The effect of motility and cell-surface polymers on bacterial attachment. *Microbiology.* 145:2797–2802.
35. Takashima, S., and H. Morisaki. 1997. Surface characteristics of the microbial cell of *Pseudomonas syringae* and its relevance to cell attachment. *Colloid Surf. B.-Biointerfaces.* 9:205–212.
36. Caccavo, F., Jr., P. C. Schamberger, K. Keiding, and P. H. Nielsen. 1997. Role of hydrophobicity in adhesion of the dissimilatory Fe(III)-reducing bacterium *Shewanella alga* to amorphous Fe(III) oxide. *Appl. Environ. Microbiol.* 63:3837–3843.
37. Sokolov, I., D. S. Smith, G. S. Henderson, Y. A. Gorby, and F. G. Ferris. 2001. Cell surface electrochemical heterogeneity of the Fe(III)-reducing bacteria *Shewanella putrefaciens*. *Environ. Sci. Technol.* 35:341–347.
38. Claessens, J., T. Behrends, and P. Van Cappellen. 2004. What do acid-base titrations of live bacteria tell us? A preliminary assessment. *Aquat. Sci.* 66:19–26.

4. Etude multiéchelle de l'interface de *Shewanella*

Du microscopique au macroscopique :

couplage de l'approche locale (bactérie individuelle : AFM, MET)

et globale (population bactérienne : MATH, adhésion, mobilité électrophorétique)

La plupart des études accède aux propriétés physico-chimiques de l'interface des cellules par des mesures indirectes globales qualifiant par exemple i : le caractère donneur-accepteur d'électrons des cellules (tests d'adhésion des cellules à des solvants polaires et apolaires) [38], ii : la capacité d'adhésion des microorganismes à différents supports [17]. A ces différentes approches de caractérisation des propriétés de l'interface viennent s'ajouter la mesure de la charge utilisant dans la majorité des cas des concepts introduits pour des particules dites dures. Ces différentes approches expérimentales sont alors analysées au travers de modèles DLVO et/ou DLVO étendu, afin d'extraire des paramètres globaux thermodynamiques visant à décrire et prédire le comportement de ces cellules. Cette analyse, conduite depuis une dizaine d'années, a montré dans de nombreux cas son incapacité à décrire la réactivité de particules biologiques due en partie à la complexité et l'hétérogénéité de ces interfaces. Depuis quelques années, de nouvelles techniques microscopiques et spectroscopiques ont été développées et adaptées pour l'étude des systèmes biologiques. A cet égard, les microscopies à force atomique et électronique à transmission constituent des atouts essentiels pour décrire *in situ* à des échelles sub-microscopiques les propriétés ou la morphologie de l'interface eau-bactérie. Dans cet article, l'objectif est de relier les données locales aux approches plus macroscopiques pour aboutir aux mécanismes régissant la réactivité et la dynamique de ces bio-interfaces. Pour cela, les analyses en MET (*cf.* Figure 10), AFM [35] et microélectrophorèse [96] sont couplées à l'étude des propriétés d'adhésion au polystyrène et à l'octane de la souche de *S. putrefaciens* CIP8040 (*cf.* Figure 11) choisie pour cette étude multiéchelle. L'évolution des paramètres physico-chimiques est étudiée en fonction du pH et de la force ionique. La dynamique observée est mise en parallèle avec la capacité d'adhésion au polystyrène de CIP8040. A pH 4 et quelque soit la force ionique, les cellules présentent un plus fort pourcentage d'adhésion qu'à pH 7 ou 10 (*cf.* Figure 11 A). La spectroscopie de force nous montre qu'à pH 4, les bactéries sont plus rigides qu'à pH 10 (k_B respectivement de 0,01 N/m et 0,0022 N/m). La microélectrophorèse confirme que la densité de charge augmente avec le pH (ρ_0 = -6 mM à pH 4, ρ_0 = -9 mM à pH 10). Les mesures d'adhésion à l'octane (*cf.* Figure 11 B) (même si elles n'indiquent qu'une tendance), sont en accord avec la dynamique observée pour l'adhésion au polystyrène qui montre une chute de l'adhésion quand le pH augmente et/ou quand la force ionique diminue. Cette observation macroscopique s'explique par les évolutions des interactions électrostatiques, mais aussi par les évolutions nanomécaniques et hydrodynamiques mises en évidence, respectivement par AFM et microélectrophorèse.

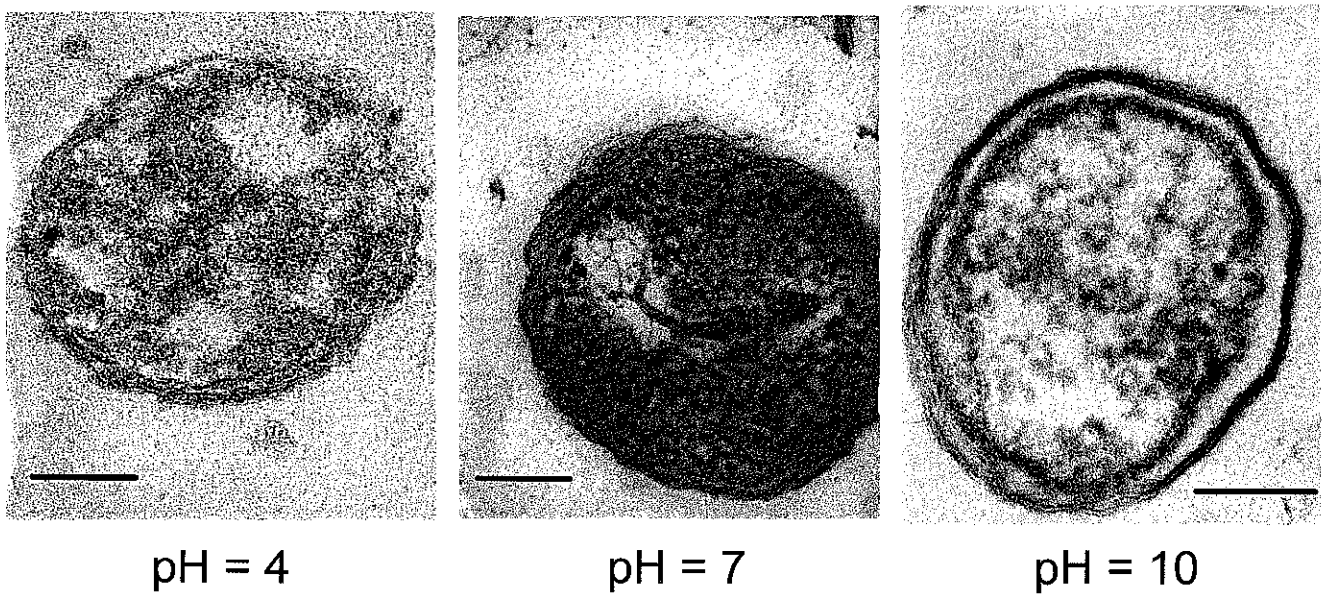

Figure 10 : Images caractéristiques de microscopie électronique à transmission de *Shewanella putrefaciens* conditionnées en milieu KNO_3 0,1M à pH 4, 7 et 10. La barre représente 100 nm.

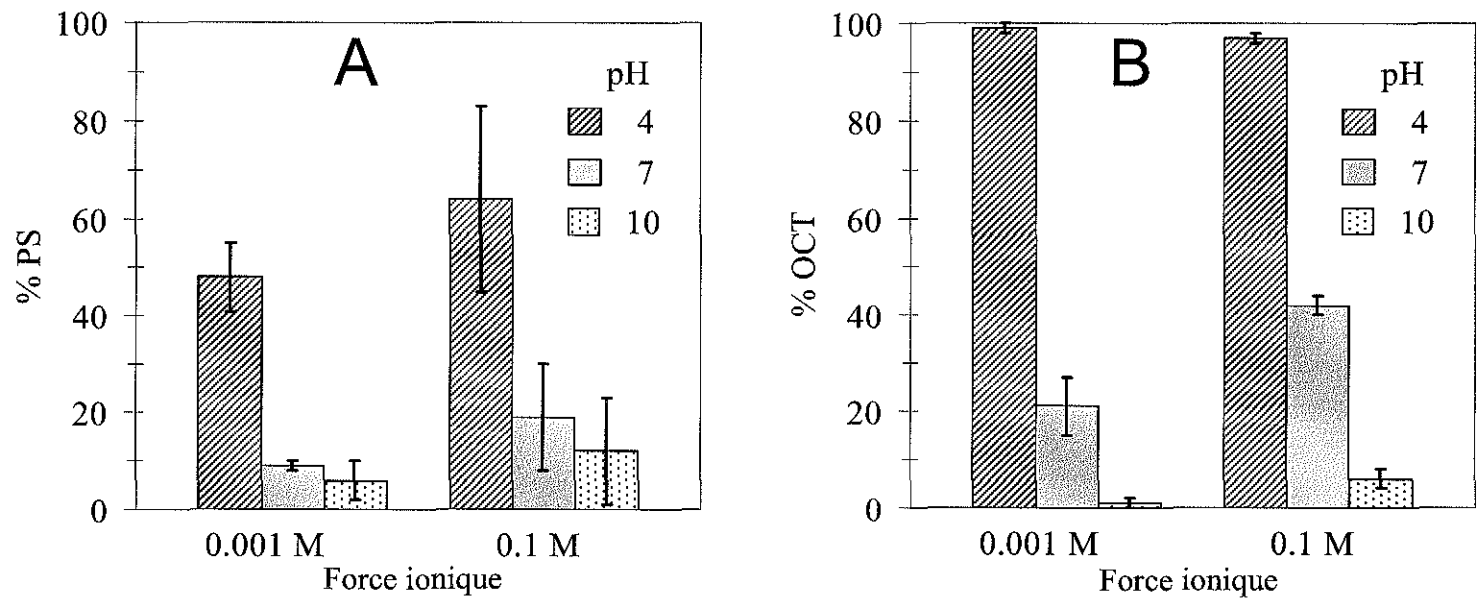

Figure 11 : A : Pourcentage de cellules adhérées au polystyrène en fonction de la force ionique et du pH du milieu. B : Influence du pH et de la force ionique sur le pourcentage de cellules adhérées aux gouttelettes d'octane générées lors du mélange.

Available online at www.sciencedirect.com
ScienceDirect
Colloids and Surfaces B: Biointerfaces 52 (2006) 108–116
COLLOIDS AND SURFACES B
www.elsevier.com/locate/colsurfb

Multiscale dynamics of the cell envelope of *Shewanella putrefaciens* as a response to pH change

Fabien Gaboriaud [a,*], Etienne Dague [a], Sidney Bailet [a], Frédéric Jorand [a], Jérôme Duval [b,c], Fabien Thomas [c]

[a] *Laboratoire de Chimie Physique et Microbiologie pour l'Environnement (UMR 7564), CNRS-University Nancy 1, 405 rue de Vandœuvre, F-54600 Villers-lès-Nancy, France*
[b] *CABE (Analytical and Biophysical Environmental Chemistry), University of Geneva, Science II, 30 Quai E, Ansermet, Switzerland*
[c] *Laboratoire Environnement et Minéralurgie (UMR 7569), CNRS-INPL, P.O. Box 40, F-54501 Vandoeuvre-lès-Nancy Cedex, France*

Received 23 April 2006; accepted 27 April 2006
Available online 7 May 2006

Abstract

The bacterial surface properties of gram-negative *Shewanella putrefaciens* were characterized by microbial adhesion to hydrocarbons (MATH), adhesion to polystyrene dishes, and electrophoresis at different values of pH and ionic strength. The bacterial adhesion to these two apolar substrates shows significant variations according to pH and ionic strength. Such behavior could be partly explained by electrostatic repulsions between bacteria and the solid or liquid interface. However, a similar trend was also observed at rather high ionic strength where electrostatic interactions are supposed to be screened. The nanomechanical properties at pH 4 and 10 and at high ionic strength were investigated by using atomic force microscopy (AFM). The indentation curves revealed the presence of a polymeric external layer that swells and softens up with increasing pH. This suggests a concomitant increase of the water permeability and so did of the hydrophilicity of the bacterial surface. Such evolution of the bacterial envelope in response to changes in pH brings new insight to the pH dependence in the bacterial adhesion tests. It especially demonstrates the necessity to consider the hydrophobic/hydrophilic surface properties of bacteria as not univocal for the various experimental conditions investigated.

Keywords: *Shewanella*; AFM; MATH; Adhesion; Electrophoretic mobilities; Soft particle theory

1. Introduction

Most of the physicochemical and biological processes in aqueous media that play a major role environment, industrial processes, or biomedical applications are governed by solid–liquid interfaces. A large body of data has been compiled in the past decades using mostly indirect techniques, such as potentiometric titration, water contact angle measurements in order to appreciate the acid–base and/or hydrophobic character of colloidal particles [1,2]. Such approaches have pointed out the overall reactivity of colloid particles at macroscopic scale but sometimes failed to provide a molecular-scale description of the relevant mechanisms. However, the recent developments of microscopic and spectroscopic methods offer the possibility to assess the microscopic and nanometric scales and therefore link these different types of experimental data.

Since its discovery in 1986, atomic force microscopy (AFM) has become an important tool for investigating in situ mineral surfaces as well as biological materials at sub-micrometric scale [3,4]. By imaging particles in aqueous solution, AFM can provide in situ real-time quantitative morphological information relative to the interaction forces resulting from surface forces and also probe nanomechanical properties. Force measurements are performed either by using the classical AFM pyramidal tip or the colloidal particle glued to AFM cantilever. In the colloidal probe method, particle-modified tips were used to evaluate in solution double-layer and London–van der Waals interaction forces between similar or dissimilar micrometric inorganic particles such as silica, titanium oxide, mica, hematite, alumina [5–7]. Recently, this technique was extended to colloidal probes coated

* Corresponding author. Tel.: +33 383685239; fax: +33 383275444.
E-mail address: gaboriaud@lcpme.cnrs-nancy.fr (F. Gaboriaud).

0927-7765/$ – see front matter © 2006 Elsevier B.V. All rights reserved.
doi:10.1016/j.colsurfb.2006.04.017

with microbial cells to quantify adhesion energies between cells and various substrates [8]. In the classical method using the Si_3N_4 pyramidal tip, the quantification of nanomechanical properties for deformable surfaces is gaining interest especially when dealing with biological specimens [9,10]. The main advantage of this mode is that the local tip–surface interactions allows for the mapping of the local properties in nanometric areas. In both modes, chemical modification of the probe was sometimes used to tune the nature of the interaction forces and identify areas with specific interactions such as hydrogen bonding or hydrophobic interactions [11]. These scientific and technological breakthroughs enable the probing of the local properties at a nanometric scale.

The AFM technique is gaining a growing interest in the investigations on bacteria, and a large number of studies were devoted to this topic. Recently, extensive efforts were carried out to correlate AFM approach and retraction data to macroscopic physicochemical properties such as bacterial adhesion, electrophoresis mobilities and water contact angles. Using nine strains of *Streptococcus mitis*, Vadillo-Rodriguez et al. [12] demonstrated that the nonlinear repulsive interaction observed upon approach curves is positively correlated with the initial deposition rates of bacteria to glass. It is important to note that the interpretation of these AFM results was based on the assumption of contact point between the AFM tip and the bacterial surface located at the beginning of constant compliance region. That is why; the theoretical analysis of the nonlinear region (which is supposed to correspond to the occurrence of surface forces) was interpreted using electrosteric models. In contrast, Li et al., recording interactions between colloid probe AFM and three strains of *Escherichia coli*, showed that the approach curves exhibit three different regions: (i) a noncontact phase hypothesized to arise primarily from interactions between the colloidal AFM tip and extracellular polymers on the bacterial surface, (ii) a contact phase interpreted as indentation of the AFM probe on the outer membrane of the cell, and (iii) a constant compliance region likely reflected in the contact of the colloid probe with the peptidoglycan layer. Moreover, macroscopic sticking coefficients for these three strains were positively correlated with the length of the former region (noncontact phase).

Despite these demonstrations of the evident relations between microscopic parameters inferred from AFM force curves and macroscopic properties, the structure and dynamics of the bacterial interface in aqueous media remains difficult to elucidate. For instance, what is the realistic interface of bacteria? How do lipopolysacharide chains contribute to electrosteric repulsion? Do the acid–base properties of bacterial membranes influence the bacterial reactivity and properties? The understanding of the local structure and reactivity of bacteria is an exciting challenge to constrain our macroscopic comprehension of bacterial surfaces.

Within that framework, cells of *Shewanella putrefaciens* were systematically investigated by microelectrophoresis, microbial adhesion to hydrocarbon droplets (MATH), bacterial adhesion to polystyrene dishes, local nanomechanical measurements by AFM, and transmission electronic experiments. The data produced by these different experimental approaches pertaining to different scales of observation were combined in order to expand the knowledge of the dynamics of solution-bacteria aqueous interfaces.

2. Materials and methods

2.1. Bacterial growth conditions

The bacterial strain *Shewanella putrefaciens* CIP 80.40^T (ATCC 80.71) was provided from Institut Pasteur (Paris, France). Cells from a stock suspension at −80 °C were pregrown in Trypcase Soy Broth (Biomerieux 51019) after two successive subcultures on solid medium at 30 °C. The preculture was stopped after 7 h at 30 °C and 10 ml ($(OD)_{600} = 0.25$) were mixed with 1 l of TSB in a batch reactor for 24 h at 30 °C. Bacteria were harvested by centrifugation (10 min, 10 000 × g, 20 °C) and washed two times in KNO_3 solution (10^{-3} M, pH 7). The washed cells were immediately resuspended in the desired pH and ionic strength KNO_3 solution for the different experimental assays. Bacterial suspensions were incubated for 14 h at 20 °C either in a polystyrene dish or in borosilicate flasks.

2.2. Microbial adhesion test to hydrocarbons (MATH)

The method described by Rosenberg et al. [13] was followed for the octane assay. After the 14 h incubation in glass flasks, 2.5 ml of the bacterial suspension ($(OD)_{600} = 0.3$) was mixed during 60 s of vortex with 1 ml of octane (Aldrich). The percentage of cells bound to the octane phase was calculated from the optical density measurements of the aqueous phase by:

$$\%\,\mathrm{OCT} = \left(1 - \frac{A}{A_0}\right) \times 100 \quad (1)$$

where A_0 is the optical density measured at 600 nm of the bacterial suspension before mixing and A is the optical density after mixing of the aqueous phase extracted with a Pasteur pipette.

2.3. Bacterial adhesion to polystyrene substrate

After 14 h of incubation in the PS dishes (306 Caubere Inc., France), the aqueous phase was eliminated and the dishes were washed by a distilled water jet to detach weakly fixed bacteria. The numeration of cells on PS dishes, in the initial bacterial suspensions and in the washing suspensions was carried out by specific coloration of cells with the fluorochrome 4′,6-diamidino-2-phenylindole (DAPI) (Aldrich 21.708-5). For the numeration of the adherent cells, DAPI solution (3 ml of 0.1 μg ml^{-1}) was added to washed PS dishes for 10 min of contact and washed three time with apyrogen water (B. Braun 66571E). For the numeration of free cells, cells in suspension were first fixed with formaldehyde (2% (v/v), Prolabo 20880.290) and then marked by DAPI (10% (v/v)). Dispersion agent (10% (v/v), Triton X 100, Prolabo 6032.28) was also added to enhance the dissociation of bacterial aggregates. After vortex homogenization, cells were collected by filtration over a dark 0.2 μm pore size membrane (Millipore GTBP04700) and rinsed once with 5 ml of apyrogen

water. Finally, the dishes and the dark membranes were dried and re-hydrated with buffered glycerine. In all cases numeration was obtained with an epifluorescence microscope (Leica) using a 1000 objective.

2.4. Electrokinetic measurements

After 14 h of incubation in borosilicate tubes, bacterial suspensions were diluted to obtain $(OD)_{600}$ in the range 0.02–0.03 with the corresponding KNO_3 solution at defined pH. The electrophoretic mobility of bacteria was measured using a Zetaphorometre IV (SEPHY-CAD Instrumentations). This apparatus is equipped with a quartz suprasil cell in which a constant field is generated by two palladium covered electrodes. The suspended particles are illuminated by laser reflection, their motion is recorded via an optical microscope mounted with a CCD camera, and their electrophoretic mobility is then calculated from the automatically recorded values of conductivity, voltage, and temperature.

2.5. Soft particle analysis of the electrophoretic mobility

The electrophoretic mobilities were fitted by using the approximate analytical expression [14]:

$$\mu = \frac{\rho_0}{\eta\lambda_0^2} + \frac{\varepsilon}{\eta}\frac{\psi_0/\kappa_m + \psi^D/\lambda_0}{1/\kappa_m + 1/\lambda_0} \quad (2)$$

where η and ε represent the dynamic viscosity and dielectric permittivity of water, respectively, ρ_0 the volumic charge density of the surface layer and κ_m the reciprocal Debye thickness of that layer. ψ_0 is the surface potential, that is the potential at the position corresponding to the location of the outer boundary of the surface layer and ψ^D the Donnan potential, as obtained from the balance in the bulk surface layer between charges stemming from the mobile ions and fixed ionogenic sites. κ_m, ψ_0 and ψ^D may be obtained from the following expressions [14]:

$$\psi^D = \frac{RT}{F}\sinh^{-1}\left(\frac{\rho_0}{2Fc^\infty}\right) \quad (3)$$

$$\psi_0 = \psi^D - \frac{RT}{F}\tanh\left(\frac{F\psi^D}{2RT}\right) \quad (4)$$

$$\kappa_m = \kappa\left\{\cosh\left(\frac{F\psi^D}{RT}\right)\right\}^{1/2} \quad (5)$$

with κ the classical reciprocal screening Debye length and c^∞ the bulk concentration of the 1:1 electrolyte considered. The first term in Eq. (2) corresponds to the plateau value for μ at high electrolyte concentrations where $\psi^D \to 0$ and $\psi_0 \to 0$. Eqs. (2)–(5) are valid within the limits $\kappa a \gg 1$, $\kappa\delta \gg 1$, $\lambda_0\delta \gg 1$ and low Donnan potentials for which the polarization of the double layer by the applied electric field is negligible. a and δ are the size of the particle core (impermeable) and the thickness of the surface layer (permeable), respectively. In the electrolyte concentration of interest (1–350 mM), the gram-negative bacteria may be assimilated to infinitely long cylinders (length around 3 μm as compared to $\kappa^{-1} \approx 0.5$–10 nm). Besides, as judged from AFM and TEM pictures, we have estimated $a \approx 500$ nm and $\delta \approx 60$ nm so that $\delta \ll a$. This ratio thickness surface layer to core size indicates a priori that the electrophoretic behavior of the *S. putrefaciens* CIP8040 is close to that of a spherical particle with the dimensions a and δ for the bare and permeable components [15]. Within the framework of that study, the approximate expressions ((2)–(5)) were systematically compared with the result obtained on the basis of the rigorous numerical theory developed by Duval et al. [16–18] which accounts for the mobility of a soft particle without any restriction of charge, size and double layer thickness.

2.6. Transmission electron microscopy

The cells incubated in borosilicate glass tubes were harvested by centrifugation and resuspended in KNO_3 solution with 10 ml of OsO_4 (1% in KNO_3 0.1 M) and then centrifuged and washed with KNO_3 0.1 M. The pellet was contacted with 1 ml of OsO_4 (1% in KNO_3 0.1 M) overnight, the pellet was then washed again and mixed with 0.5 ml of agar 2%. The conventional embedding for thin section, i.e. the osmium tetroxide protocol of Ryter and Kellenberger [19], was followed. Sections were imaged with a Zeiss E.M.95, 60 kV transmission electron microscope.

2.7. Atomic force microscopy

Force measurements were taken on the cells adhered onto PS dishes using a commercial microscope (Thermomicroscope Explorer Ecu+, Veeco instrument S.A.S). PS dishes were rapidly filled with the potassium nitrate solution after the 14 h incubation process and distilled water jet washing. Measurements were undertaken in high potassium nitrate concentration (0.1 mol l^{-1}) to minimize contribution of electrostatic interactions to force curves. A single V-shaped cantilever ($SiNi_3$, Veeco, Ref MLCT-EXMT-BF) with a measured spring constant of 0.01 N m^{-1} was used for all force measurements to avoid variations of force response due to different radii of curvature of AFM tips. Force curves were recorded on a number of different cells at scan rate of 0.1 μm s^{-1}. The raw curves were converted to force versus indentation curves based on the method described elsewhere. The nonlinear Hertzian behavior and linear Hooke's dependance observed on the loading force (F)–indentation depth (δ) curves were described by fitting curves with the following relation [20]:

$$F = \frac{2}{\pi}\frac{E}{(1-\gamma^2)}\tan(\alpha)\delta^2 + \frac{1}{2}[(k_B\delta + A) + |k_B\delta + A|] \quad (6)$$

where α is the cone opening angle set to 35°, γ the Poisson ratio assumed as 0.5, E the elastic or Young's modulus, k_B the bacterial spring constant and A a constant.

3. Results

3.1. Bacterial adhesion tests

These tests are among the most commonly used ones for the quantification of the hydrophilic/hydrophobic balance of bacterial surfaces, although it is well recognized that they are

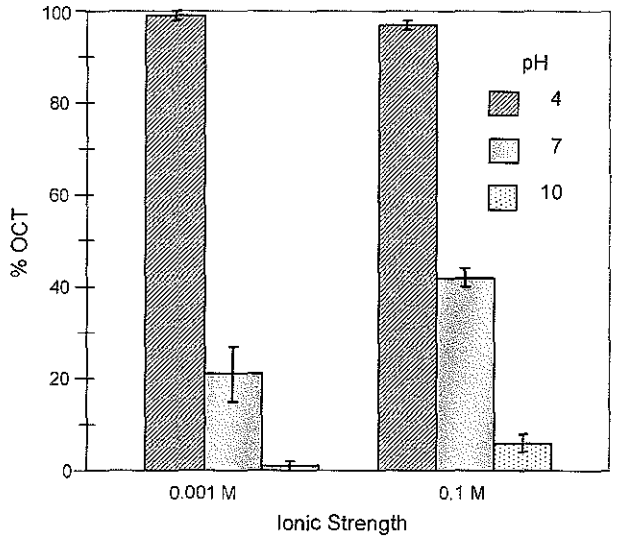

Fig. 1. Effect of pH and KNO_3 ionic strength on the percentage of cells trapped by the octane droplets.

only indicative of an overall reactivity, without any emphasis on the local contributions [1,21–23]. In the current study, the hydrophobicity of *S. putrefaciens* CIP8040 is analyzed through the adhesion tests at the hydrophobic surface of hydrocarbon droplets (MATH) and polystyrene (PS) dishes. Fig. 1 presents the percentage of cells trapped by the octane droplets, as a function of the pH and the ionic strength of the aqueous phase. Adhesion to octane was dramatically decreased when the suspension pH was increased from 4 to 10 regardless of the ionic strength. A moderate influence of the ionic strength was also observed, especially at pH 7 and 4, where the percentage of trapped cells increased with increasing ionic strength. The same trends were observed for bacterial adhesion on PS dishes (Fig. 2): increasing the pH and decreasing the ionic strength resulted in a decrease for the percentage of cells adhered to the polystyrene substrate. In passing, it should be noticed that the differences in proportion of adhered cells in MATH and PS tests (Figs. 1 and 2) depend on the nature of the tests. While cell adhesion on PS dishes results from the static adsorption of cells in one direction, i.e. the PS dish bottom, adhesion on octane droplets is favored by the large surface area of the droplets resulting from mechanical stirring. Another factor can be the formation of bacterial aggregates at pH 4 where the hydrophobicity is maximal, which tends to underestimate the amount of adhered cells on PS, whereas adhesion on octane droplets is not affected.

However, it can be assumed from these results that the hydrophilic/hydrophobic balance of *S. putrefaciens*, as revealed by these two bacterial adhesion tests, is controlled by a pH-dependent phenomenon.

3.2. Electrophoretic mobility (EM)

In the pH range 2–10, the EM of *S. putrefaciens* CIP8040 varied with the pH and the ionic strength, as illustrated in Fig. 3. Electrophoretic mobilities increased in magnitude upon increasing the pH, indicating a progressive dissociation of the acidic surface sites. Furthermore, the mobilities decreased with increasing ionic strength, due to screening of the surface charge by counterions. This feature is generic of ionic double layers and consistent with expectations based on the classical DLVO theory. The pH of zero mobility, the so-called isoelectric point, decreased from 2.6 to ~2.0 when increasing the ionic strength from 0.001 to 0.1 M. This shift indicates a specific affinity of the surface sites for anionic species from the background electrolyte. Further measurements are nevertheless required to identify clearly the nature of those species as well as the way they possibly interact with the ionogenic sites distributed throughout the bacterium surface. More intriguing is the weak EM variation observed in the pH range 4–10. At pH 4, the EM is close to its minimum value, which tends to suggest that the surface sites are almost fully dissociated at this point. This latter observation is not entirely in line with the strong effect of the pH on the adhesion tests, as previously presented (Figs. 1 and 2). The maximum adhesion

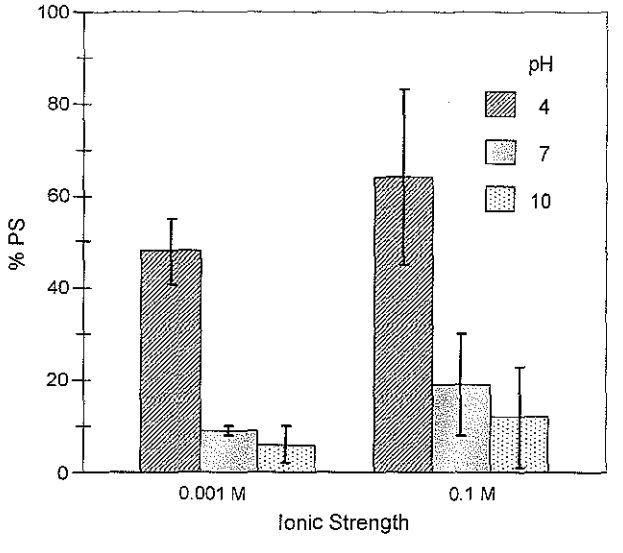

Fig. 2. Percentage of cells adhered on PS dishes as a function of pH and ionic strength (KNO_3).

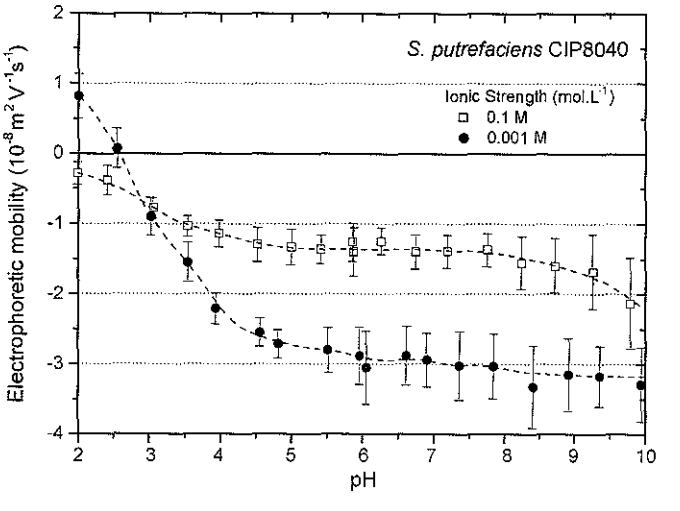

Fig. 3. Electrophoretic mobility of *S. putrefaciens* (CIP8040) at varying pH and ionic strength.

on hydrophobic interfaces is indeed expected to occur at the pH where the EM reaches a minimum value (in magnitude), that is where the acidic sites are fully protonated or equivalently, the bacterial adhesion to hydrophobic substrates is at its highest level. In the present case, such situation is met at pH 4 in Figs. 1 and 2 and at pH < 3 in Fig. 3.

3.3. Bacterial softness

It has been for long demonstrated that bacteria may be covered by polymeric layers that could be anchored to the outer membrane [24]. Such polymeric layer could confer the whole particle a "soft" character. Thus, the electrophoretic motion of such a soft particle in a dc electric field differs significantly from that of its bare counterpart. The approximate analytical theory originally developed by Ohshima accounts for such differences by including in the hydrodynamic modeling of the interface the possibility of flow penetration into the soft surface layer. This is done by introducing the so-called softness parameter, denoted as λ_0, the invert of which, λ_0^{-1}, has a length dimension and essentially characterizes the degree of flow penetration into the soft layer (permeability). Concretely, the presence of that soft layer manifests itself in a constant non-zero value reached by the EM for sufficiently high electrolyte concentrations [25]. This asymptotic plateau is the signature of soft interfaces and differentiates them from hard interfaces for which the electrokinetic response in concentrated electrolytes vanishes.

In the specific case of *S. putrefaciens* CIP8040, mobility measurements performed at various pH (4, 5.6, 7 and 10) as a function of electrolyte concentrations (Fig. 4) clearly point out the presence of the electrophoretic plateau aforementioned, such denoting a permeable character for the outer boundary layer surrounding the bacteria. On a quantitative level, an attempt was made to interpret the data by using the approximate analytical expression of Eqs. (2)–(5) [14]. In Fig. 4, we report the theoretical predictions derived on the basis of Eqs. (2)–(5) with $\lambda_0^{-1} \approx 4$ nm and $\rho_0 \approx -9$ to -6 mM, which values were obtained by means of a least square method to best fit the data. These necessarily approximate results (see range of validity for Eqs. (2)–(5) as mentioned in Section 2) are further compared with the mobilities calculated from the rigorous numerical evaluation of the fundamental electrokinetic equations for soft particles following a description of the interface largely discussed in [16–18]. As expected, analytical results deviate from the numerical ones upon decrease of the ionic strength due to a breakdown in the assumption of the approximate analytical expression Eqs. (2)–(5), namely resulting from a significant increase for the Donnan potential (ψ^D) and a decrease of the $\kappa\delta$ values.

However, both quantitative approaches yielded weak variations for the charge density of the soft layer ρ_0 upon changing pH between 4 and 10, which is consistent with the EM results from Fig. 3. Concerning the softness parameter, the value $\lambda_0^{-1} \approx 4$ nm extrapolated from the mobility data at the different pH values unambiguously indicates the presence of a surface layer with a fairly large permeability.

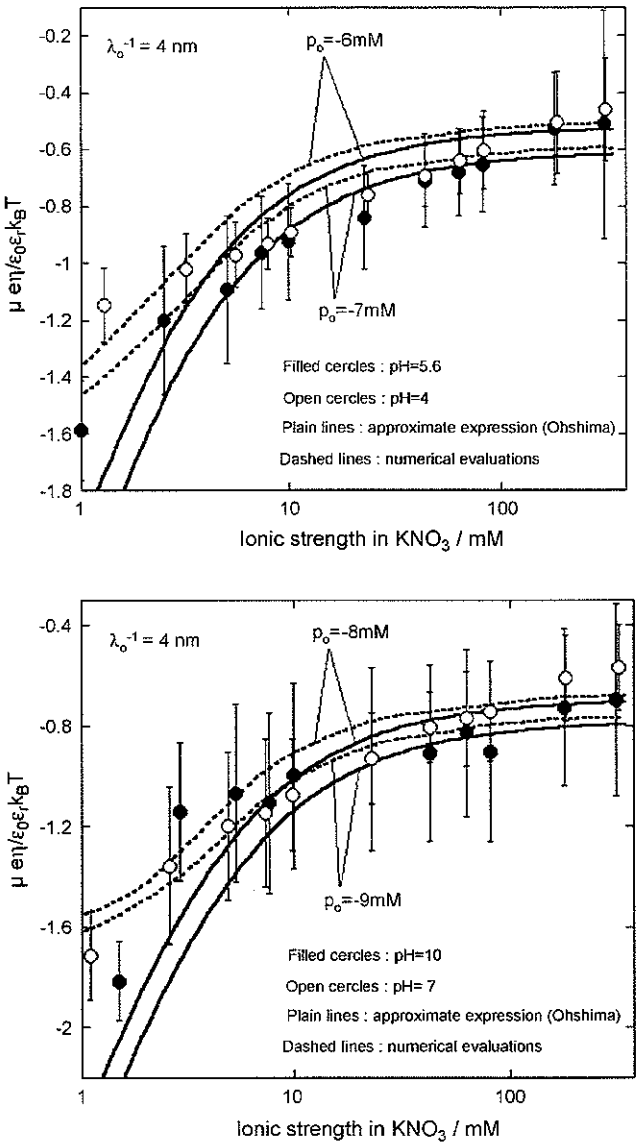

Fig. 4. Electrophoretic mobilities of *S. putrefaciens* as a function of ionic strength at different pH values: (top) 4 and 5.6; (bottom) 7 and 10. Plain lines are theoretical curves calculated via Eqs. (2)–(5) and dashed lines correspond to more rigorous numerical evaluations described elsewhere [16–18].

3.4. Micromorphology

Envelope profiles are representative of gram-negative bacteria with an outer membrane and a plasma membrane, cytoplasmic and periplasmic spaces (Fig. 5). As conventional embedding was carried out for sample preparation, ultrafine surface structures such as LPS layers or polymeric fringe [26] could not be distinguished on these micrographs. However, significant differences were observed between cells incubated at different pH values. The more singular feature concerned cells incubated at pH 10 which exhibit large periplasmic space as compared to those incubated at lower pH value. A first attempt gave mean distance for the periplasmic space measured on different micrographs of 50 ± 20 nm (from 15 separate bacteria). Such effect was specific to the basic media and not observed at pH 4. Therefore, this morphological dependence with pH indicates

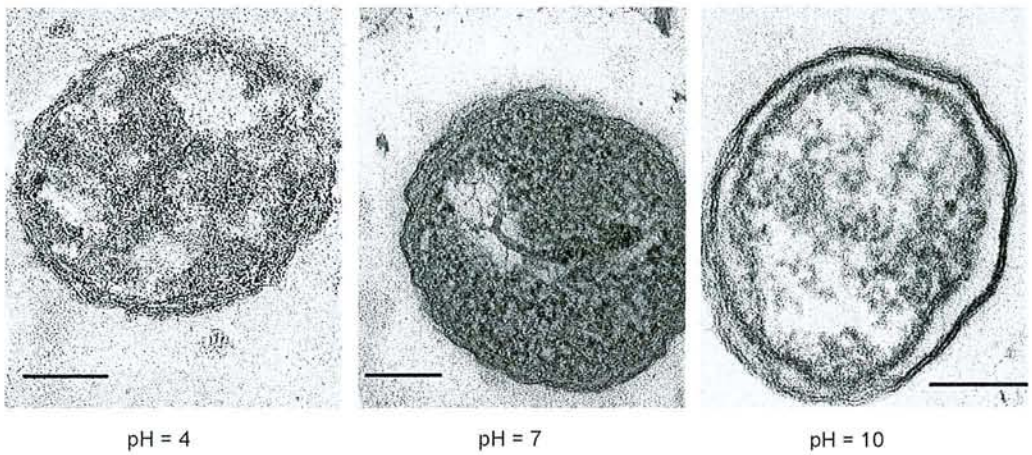

Fig. 5. Typical transmission electronic microscopic images of cells extracted from KNO_3 0.1 M as function of pH. Bar, 100 nm.

that such process is not osmotically driven, but may rather be controlled by the hydroxide concentrations. Notice that such method of preparation should be considered with great caution as the damage of bacterial envelope could be significant leading to experimental artefacts rather than observation of the real bacterial structure. Nonetheless, there is clear variation between micrographs coherent with the nanomechanical measurements carried out by AFM. Further observations by using freeze-substitution preparation to preserve the ultrafine surface structures may obviously provide additional insights on the dynamic of bacterial envelope in response to change in pH.

3.5. Nanomechanical measurements of bacterial envelope by AFM

Our previous attempt at measuring nanomechanical properties of *S. putrefaciens* cells was performed from the mean indentation curves obtained at the two pH values [20]. The analysis of these two mean curves at the two different pH values (4 and 10) reveals the occurrence of two mechanical regimes, respectively, nonlinear and linear. The mechanical quantification of these regimes was achieved by using Eq. (6) that combines the Hertzian model for the nonlinear part and Hook's law for the linear part. In the present study, indentation curves were ana-

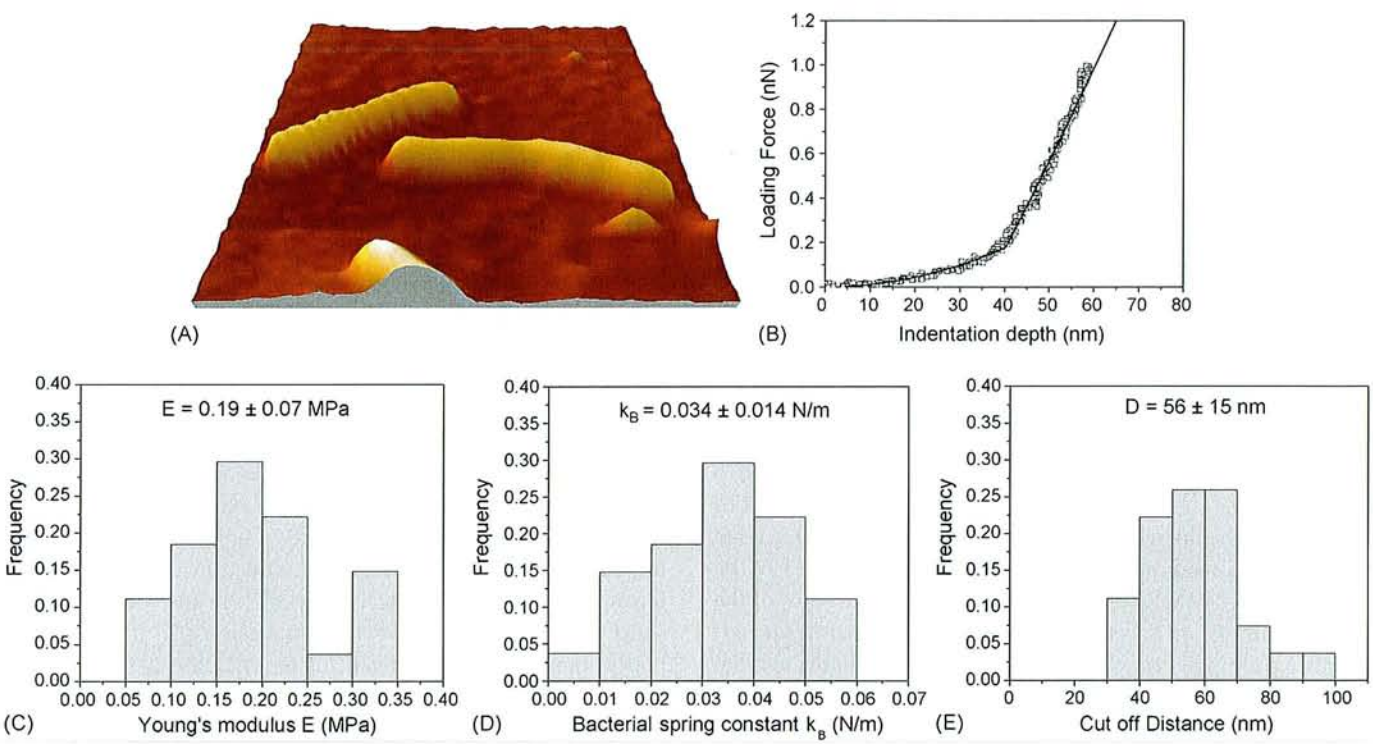

Fig. 6. Nanomechanical measurements of *S. putrefaciens* cells at pH 4 in concentrated electrolyte solution (KNO_3 0.1 M). (A) Typical AFM height image (image size, 10 μm × 10 μm, maximum height, 350 nm). (B) Typical force–indentation data fitted by using Eq. (6). (C) Frequency histogram of the Young's moduli. (D) Frequency histogram of the bacterial spring constant. (E) Frequency histogram of the distance that characterized the onset of the linear regime. $n = 45$.

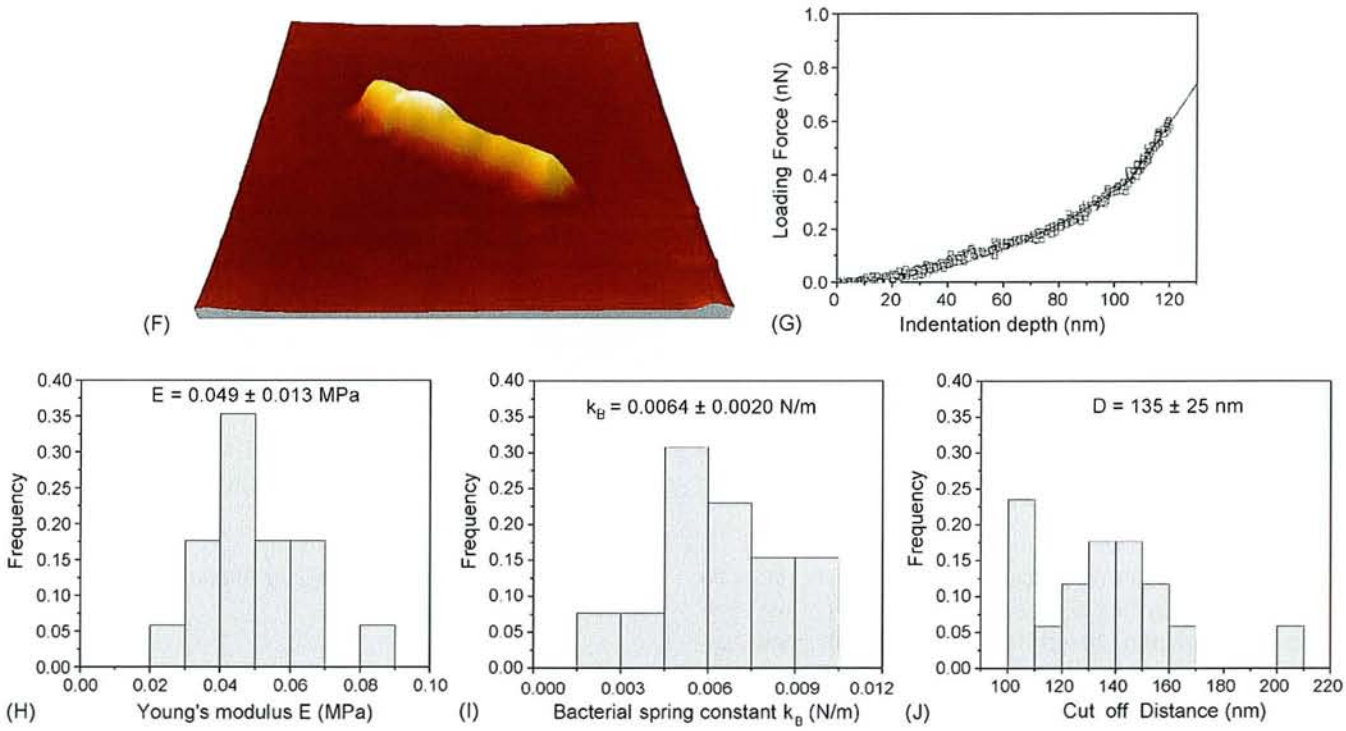

Fig. 7. Nanomechanical measurements of *S. putrefaciens* cells at pH 10 in concentrated electrolyte solution (KNO_3 0.1 M). (F) Typical AFM height image (image size, 10 μm × 10 μm, maximum height, 150 nm). (G) Typical force–indentation data fitted by using Eq. (6). (H) Frequency histogram of the Young's moduli. (I) Frequency histogram of the bacterial spring constant. (J) Frequency histogram of the distance that characterized the onset of the linear regime. $n = 45$.

lyzed separately to provide statistical information regarding the distribution of Young's modulus, bacterial spring constant and cut-off distance.

In typical AFM images of *S. putrefaciens* adsorbed onto polystyrene dishes (Fig. 6A, Fig. 7F), bacteria showed rod shape morphology. After these initial AFM scans of the surface, individual cells were selected for the measuring of force–distance curves. The force curves were then converted to nanoindentation curves and fitted by using Eq. (6). The experimental data are in satisfactory agreement with the theoretical prediction, as illustrated in Fig. 6B and Fig. 7G, which show representative curves for the two pH conditions, 4 and 10, respectively. From the fifteen curves taken for each pH condition, the Young's modulus, the bacterial spring constant and the cut-off distance were extracted on the basis of the corresponding fitted curves. Fig. 6 (C–E) and Fig. 7 (H–J) show the frequency histogram of the three aforementioned parameters for the pH 4 and 10, respectively. The distributions were found to be approximately Gaussian-like with a relatively narrow dispersion that enabled to demonstrate the significant variation of mechanical properties of the bacterial envelope in response to increase in pH. Indeed, the mean Young's modulus was found to decrease from 0.19 MPa (Fig. 6C) to 0.049 MPa (Fig. 7H) along with the increase of the mean cut-off distance from 56 nm (Fig. 6E) to 135 nm (Fig. 7J) by raising the pH from 4 to 10. This evolution indicates that the mechanical properties of external layers soften up with the increase of the thickness of these layers responsible of the non-linear behavior observed on indentation curves. As well, the bacterial spring constant significantly decreased from 0.034 N/m (Fig. 6D) to 0.0064 N/m (Fig. 7I). This linear contribution reproduced by Hook's law in Eq. (6) (second part of equation) begins at the cut-off distance and has been attributed to the progressive compression of the plasmic membrane in relation to the bacterial turgor pressure. In fact, the decrease of bacterial spring constant could be interpreted as the decrease of the turgor pressure.

4. Discussion

The bacterial adhesion tests pointed out the significant effects of pH on the observed results. At first sight, the decrease of bacterial adhesion by raising the pH may result from the increase of electrostatic repulsions between bacteria and PS dishes or between bacteria and octane droplets. In any case, such increase could be interpreted by a change in the surface charge of at least one of the two surfaces in interactions. Concerning the surface charge of hydrophobic surface, the apolar nature of the octane and polystyrene dishes would suggest the absence of a significant electrostatic potential at the surfaces. Nevertheless, experimental evidences [27–32] tend to show the opposite, and leads to assume physisorption of hydroxide ions onto a hydrophobic surfaces. This assumption was recently confirmed by Zangi and Engberts [33], who also attribute attraction of the hydroxide ion to the ordering of water molecules in the vicinity of the solid surface. Thus, the bacterial adhesion pH effects can be partly interpreted as the result of the increase of the negative surface charge on the hydrophobic substrates by raising pH. Actually, such explanation fails for experiments performed with high ionic strengths (0.1 M) that revealed the same behavior as those carried out in relatively low electrolyte concentration (Figs. 1 and 2). The electrostatic potential at such salt level is

expected to be negligible. Indeed, some complement force measurements carried out onto PS dishes at 0.1 M ionic strength corroborated the low magnitude and nanometric range of significant negative surface charge on the PS hydrophobic surfaces at this salt level (not shown). Concerning the bacterial surface charge, surface site speciation yields in most cases to negative surface charge mainly due to phosphate and carboxylic deprotonation. The *S. putrefaciens* (CIP 8040) electrokinetic curves illustrate such classical negative behavior observed for microorganisms (Fig. 3). In contrast, the mobilities of bacteria show no pronounced evolution between pH 4 and 10 and for the two studied ionic strengths. Therefore, the significant decrease of bacterial adhesion to hydrophobic substrates by increasing pH was not correlated to an increase of the surface charge of bacteria.

On the basis of this statement, the change in bacterial adhesion would be associated in part to variation of the hydrophobic/hydrophylic balance of the bacterial interfaces. A closer examination of the structure of the bacterial envelope at different pH revealed such dynamic behavior in response to the increase of the pH. The nanomechanical properties clearly demonstrates the increase of the softness of the most external layers with the increase of their thickness (from 56 to135 nm) by raising pH. In a recent paper [34], Korenevsky et al. describe polymeric fringes of various thicknesses (from 0 to 120 nm) among *Shewanella* cells. Therefore, it was suggested in our first attempt [20] that the nonlinear behavior observed for the force curves results from the indentation of such polymeric fringe whereas the occurrence of the linear behavior corresponds to the compression of the cytoplasm. However, the proposed mechanism suggests that the thickness of both the polymeric fringe and the periplasm increase with softness too. The thickness of the polymeric fringe could be estimated around the mean cut-off distance obtained from AFM results. As thick periplasm was observed on micrographs in acid medium (~6 nm), the nonlinear behavior could be predominantly associated to the indentation of the polymeric fringe. Therefore, the thickness of polymeric fringe at pH 4 could be estimated close to 50 nm which is consistent with the reported values [34]. For the basic media, the concomitant increase of the softness and of the range (135 nm) of the nonlinear behavior indicates the swelling of the polymeric fringe and the periplasm. Such feature agrees with the TEM observations that show the increase of the periplasm at pH 10 (Fig. 5). Thus, the swelling of the polymeric fringe could be estimated close to 35 nm that corresponded to the difference between the total nonlinear range measured on indentation curves (135 nm) and the periplasm thickness roughly determined from TEM images (50 nm). Therefore, the thickness of the polymeric fringe increases from 50 to 85 nm by raising the pH from 4 to 10. Interestingly, the softness parameter ($\lambda_0^{-1} \approx 4$ nm) deduced from the microelectrophoresis experiments also indicated the presence of a permeable surface layer typical of particle coated with polymeric layer. This result agrees with the presence of a polymeric fringe as observed for the studied strain. More intriguing is the constant value of the softness parameter obtained at different pH, which would indicate that the water flow within the polymeric fringe is not significantly affected by its thickness.

However, these results clearly demonstrate the dynamic of bacterial envelope in response to changes in pH. The increase of pH induces thickening and softening of both the periplasm and the polymeric layer. We can postulate that intermolecular forces are responsible for a repulsive behavior leading to the increase of void spaces into the polymeric fringe and between the cytoplasmic and the outer membranes. Therefore, such resulting repulsive forces probably increase the water permeability and obviously change the bacterial surface properties [20]. Following that reasoning, the increase of water permeability of the bacterial envelope by raising pH would result to a more hydrophylic bacteria at pH 10 than 4 due to the presence of water molecules close to the bacterial surfaces. This result is consistent with the significant decrease of the bacterial affinity for hydrophobic substrates Hydration of the cell envelope and electrostatic repulsions fully account for the lack in attachment of *Shewanella* to hydrophobic substrates at alkaline pH.

In summary, macroscopic bacterial adhesion tests and nanomechanical AFM measurements demonstrated significant variations with increasing pH. The increase of pH cancels the capacity of bacteria to adhere on hydrophobic substrates. The contribution of electrostatic forces seemed to be negligible as compared to that of the important mechanical and structural evolution of the bacterial envelope. Even if the bacterial mechanisms are still not elucidated, these results reveal some relations between macroscopic measurements and structural evolution of bacterial interfaces yielding probably different surface properties according to the pH, such as the water content of the cell envelope.

Acknowledgments

The authors thank G. Jeannesson and C. Gérard for their tireless efforts to optimize physico-chemical conditions to observe bacterial adhesion. This study was granted by CNRS (PNIR-Biofilms and Fédération Eau-Sol-Terre, Nancy) and by Henri Poincaré University of Nancy (special BQR grant). The authors wish to thank G. Villemin (LSE, Nancy) for electronic microscopy analyses and Y. Waldvogel (LEM) for help in electrophoresis experiments.

References

[1] R. Bos, H.C. van der Mei, H.J. Busscher, FEMS Microbiol. Rev. 23 (1999) 179.
[2] W. Stumm, Chemistry of the Solid–Water Interface, John Wiley & Sons, New York, 1992.
[3] Y.F. Dufrêne, J. Bacteriol. 184 (2002) 5205.
[4] H. Takano, J.R. Kenseth, S.S. Wong, J.C. O'Brien, M.D. Porter, Chem. Rev. 99 (1999) 2845.
[5] W.A. Ducker, T.J. Senden, R.M. Pashley, Nature 353 (1991) 239.
[6] C.M. Eggleston, G. Jordan, Geochim. Cosmochim. Acta 62 (1998) 1919.
[7] I. Larson, C.J. Drummond, D.Y.C. Chan, F. Grieser, Langmuir 13 (1997) 2109.
[8] S.K. Lower, M.F. Hochella, T.J. Beveridge, Science 292 (2001) 1360.
[9] A.E. Pelling, S. Sehati, E.B. Gralla, J.S. Valentine, J.K. Gimzewski, Science 305 (2004) 1147.
[10] Y.F. Dufrêne, Nat. Rev. Microbiol. 2 (2004) 451.
[11] F. Ahimou, F.A. Denis, A. Touhami, Y.F. Dufrêne, Langmuir 18 (2002) 9937.

[12] V. Vadillo-Rodriguez, H.J. Busscher, W. Norde, J. de Vries, H.C. van der Mei, Microbiology 150 (2004) 1015.
[13] M. Rosenberg, D. Gutnick, E. Rosenberg, FEMS Microbiol. Lett. 9 (1980) 29.
[14] H. Ohshima, Colloids Surf. A: Physicochem. Eng. Aspects 103 (1995) 249.
[15] H. Ohshima, Colloid Polym. Sci. 279 (2001) 88.
[16] J.F.L. Duval, K.J. Wilkinson, H.P. Van Leeuwen, J. Buffle, Environ. Sci. Technol. 39 (2005) 6435.
[17] J.F.L. Duval, H. Ohshima, Langmuir 22 (2006) 3533.
[18] E. Dague, J.F.L. Duval, F. Jorand, F. Thomas, F. Gaboriaud, Biophys. J. 90 (2006) 2612.
[19] A. Ryter, E. Kellenberger, J. Ultrastruct. Res. 2 (1958) 200.
[20] F. Gaboriaud, S. Bailet, E. Dague, F. Jorand, J. Bacteriol. 187 (2005) 3864.
[21] N. Mozes, F. Marchal, M.P. Hermesse, J.L. Van Haecht, L. Reuliaux, A.J. Leonard, P.G. Rouxhet, Biotechnol. Bioeng. 30 (1987) 439.
[22] N. Mozes, P.G. Rouxhet, J. Microbiol. Meth. 6 (1987) 99.
[23] M.N. Bellon-Fontaine, J. Rault, C.J. van Oss, Colloids Surf. B: Biointerf. 7 (1996) 47.
[24] T.J. Beveridge, L.L. Graham, Microbiol. Rev. 55 (1991) 684.
[25] H. Hayashi, S. Tsuneda, A. Hirata, H. Sasaki, Colloids Surf. B: Biointerf. 22 (2001) 149.
[26] T.J. Beveridge, J. Bacteriol. 181 (1999) 4725.
[27] R.M. Pashley, J. Phys. Chem. B 107 (2003) 1714.
[28] G.R. Burnett, R. Atkin, S. Hicks, J. Eastoe, Langmuir 20 (2004) 5673.
[29] P. Weidenhammer, H.J. Jacobasch, J. Colloid Interf. Sci. 180 (1996) 232.
[30] R. Zimmermann, S. Dukhin, C. Werner, J. Phys. Chem. B 105 (2001) 8544.
[31] L. Hermitte, F. Thomas, R. Bougaran, C. Martelet, J. Colloid Interf. Sci. 272 (2004) 82.
[32] H.J. Busscher, B. Belt-Gritter, H.C. van der Mei, Colloids Surf. B: Biointerf. 5 (1995) 111.
[33] R. Zangi, J.B.F.N. Engberts, J. Am. Chem. Soc. 127 (2005) 2272.
[34] A.A. Korenevsky, E. Vinogradov, Y. Gorby, T.J. Beveridge, App. Env. Microbiol. 68 (2002) 4653.

5. Relation entre les propriétés nanomécaniques et électrohydrodynamiques des bactéries

Dans cet article en préparation, nous avons envisagé de façon complémentaire les analyses réalisées en AFM et microélectrophorèse. Les interfaces de CN32 et MR4 ont été sondées par microélectrophorèse à différents pH et forces ioniques. La spectroscopie de force a été réalisée sur CN32 à 1 et 100 mM.

Pour analyser les résultats de mobilité électrophorétique en fonction de la force ionique, à différents pH, nous avons utilisé le dernier modèle développé, prenant en compte la géométrie cylindrique de la particule dure centrale (bactérie bacillaire) et le caractère diffus, c'est-à-dire hétérogène de l'interface bactérienne. Dans ce modèle, la densité des segments polymériques portant les charges diminue en s'éloignant de la particule centrale dure (*cf.* Figure 12). Cette nouvelle approche permet de modéliser de façon satisfaisante le comportement des cellules dans un champ électrique à faible force ionique. Cependant, l'approche développée au chapitre trois, consistant à moduler la densité de charge fonctionne également. Dans la réalité, les deux phénomènes coexistent certainement.

Les données sur la densité de charge ont permis de calculer la portée et la force des interactions électrostatiques entre un cylindre (bactérie) et une sphère (pointe AFM) (*cf.* Figure 13). Pour CN32, à 1mM, la portée calculée est de 40 nm et la force de 0,35 nN. C'est dans cette gamme de force et portée qu'il est impossible de corréler les courbes de force de CN32 à 1 mM avec un modèle de Hertz-Hook. En revanche, à 100 mM, le calcul nous indique que la force et la portée des interactions électrostatiques sont négligeables. Ainsi, en spectroscopie de force, seule l'indentation de la pointe dans l'interface de la bactérie est enregistrée.

L'évolution des courbes de force entre 1 et 100 mM (*cf.* Figure 14) traduit les effets de la pression osmotique. A 1mM, les cellules sont turgescentes, leur pression interne est très importante de sorte qu'un grand domaine linéaire est enregistré. En revanche, à 100 mM, la pression de turgescence est plus faible et les courbes de force montrent un grand domaine non linéaire modélisable par une loi de Hertz-Hook.

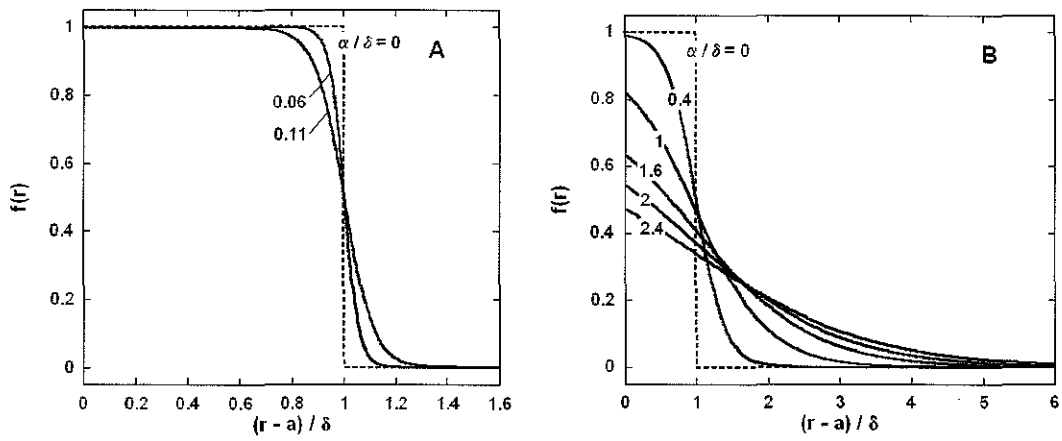

Figure 12 : f (r), est la fonction décrivant la distribution locale des segments polymériques contenus dans l'interface molle. Cette distribution est tracée en fonction de la distance par rapport à la surface de la particule centrale dure (r-a) rapportée à l'épaisseur de la couche souple (δ). Le trait pointillé (step function) représente le cas limite d'une interface homogène pour α/δ = 0. α représente la diminution de la densité de polymères au sein de l'interface. Les traits pleins montrent la solution pour les valeurs de α/δ indiquées à côté de la courbe. A: MR4 ; B: CN32.

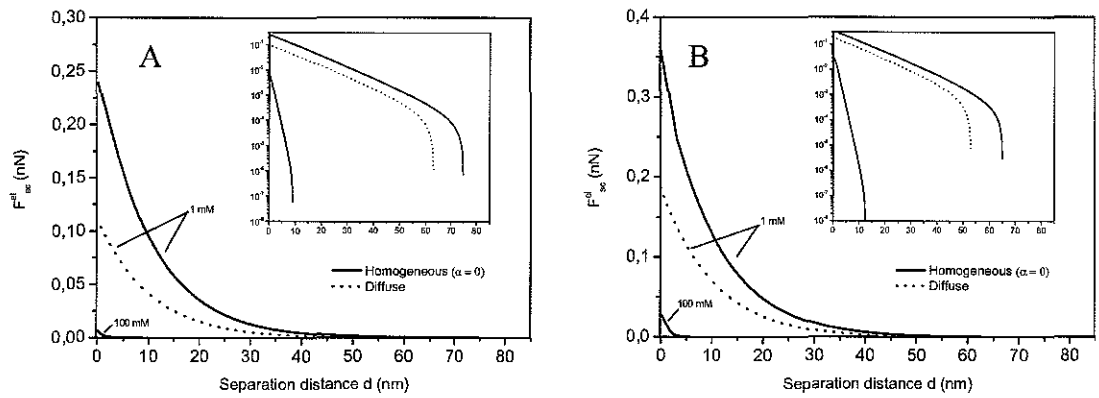

Figure 13 : Forces électrostatiques calculées en fonction de la distance de séparation entre la pointe AFM et la bactérie. A : *S. oneidensis* MR4 ; B : *S. putrefaciens* CN32.

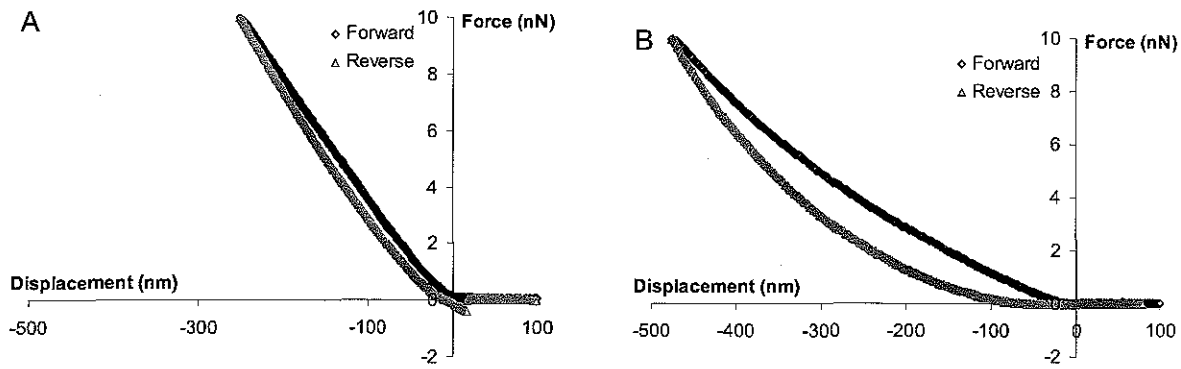

Figure 14 : Courbes de force brut typique de CN32 à 1 (A) et 100 mM (B).

ARTICLE EN PREPARATION

On the relationships between Nanomechanical Properties, Surface Forces and Electrohydrodynamic Characteristics of *Shewanella* spp. as probed by Force Spectroscopy and Microelectrophoresis

Etienne DAGUE [a], Jérôme DUVAL [b], Michelle L. GEE [c], James A. HOLDEN [d], Richard STRUGNELL [d], Fabien GABORIAUD [a]

[a] Laboratoire de Chimie Physique et Microbiologie pour l'Environnement (UMR 7564), CNRS-University Nancy 1, 405 rue de Vandœuvre, F-54600 Villers-lès-Nancy, France

[b] Laboratoire Environnement et Minéralurgie (UMR 7569), CNRS-INPL, P.O. Box 40, F-54501 Vandoeuvre-lès-Nancy Cedex, France

[c] School of Chemistry, University of Melbourne, Victoria 3010, Australia

[d] Department of Microbiology and Immunology, University of Melbourne, Victoria 3010, Australia

Abstract:

Keywords : *Shewanella*, Force Spectroscopy, Electrophoretic mobilities, Soft particle electrophoresis theory

1. INTRODUCTION:

The physicochemical characteristics of bacterial surfaces play an important role in the cell adhesion onto biological or mineral surfaces [1]. An understanding of the key interactions controlling these phenomena is particularly important to a wide variety of problems ranging from the biocorrosion of metals, the biofilm formation on orthopaedic implants to the biofouling of ship hulls in marine systems [2-4]. In all cases, the colonization of the different surfaces involves an initial bacterial attachment mediated by many physicochemical parameters such as the respective surface charge of the two interacted surfaces, the shear rates of the liquid, the surface free energy of the substrates and obviously the composition of the solution.

In the last decade, many attempts have been carried out to model the sticking coefficients of bacteria by using principally the DLVO theory and its extended version with acid-base Lewis contribution [5;6]. The theories so far proposed are based on traditional colloidal thermodynamic that has been developed for hard systems. Such important drawback is also limited by the experimental assessments of physicochemical characteristics for bacterial interfaces. The inherent softness and heterogeneity of the bacterial surfaces complicates significantly the physicochemical analysis of such interfaces by using the conventional methods mostly developed in the case of hard systems. A recent theory considering the softness and the diffuse character of biological system has been recently proposed to derive the volumic charge density, the hydrodynamic properties and the diffuse character of a permeable charged polymeric layer that coat an impermeable hard-core component [7]. Its application to microbial cells have been successfully performed for two strains of *Streptococcus salivarius* [8] and four strains of *Shewanella* species [9;10].

Alternatively, one of the questions that systematically comes back in these systems is: what is the "real" structure of the bacterial envelope and the resulting interface with the liquid medium. Some structural information has been extracted from transmission electron micrographs by using freeze-substitution preparation preserving the most delicate structures. While this technique is able to identify some specific bacterial ultrastructures such as capsule or thick lipopolysaccharide layers, it does not provide detailed information on surface properties of bacteria in native state. In contrast, by using an atomic force microscope (AFM) in its spectroscopy mode, the interactions between the AFM tip and the bacterial surface give novel information with nanometer resolution [11]. In particular, remarkable advances have been made in measuring nanomechanical properties in different conditions and assessing specific molecular recognition forces with functionalized tips [12]. However, the main drawback in the applications of force spectroscopy to the biological systems is the accurate determination of contact point that is required to differentiate surface forces from the mechanical deformation/indentation of both the cantilever and the cell. While this absolute contact point for non-deformable surfaces is positioned at the onset of the linear compliance, the possible contribution to non linear behaviour of compression and/or indentation of the soft biological systems complicate the interpretation of force curves.

In this study, the electrostatic, hydrodynamic and mechanical interfacial properties of a capsulated *Shewanella* strain (*S. oneidensis* MR-4) and a bald one (*S. putrefaciens* CN32) are derived from the combination of quantitative analyses of electrophoretic mobility and force measurements. Such breakthrough is partially due to the exact derivation of the interaction forces between the hard AFM probe and the soft rod-like bacteria (with or without a diffuse interface) on the basis of the electrostatic and hydrodynamic parameters extracted from soft particle analysis of electrophoretic mobilities.

2. EXPERIMENTAL SECTION:

2.1 Bacterial culture and preparation.

Shewanella putrefaciens CN32 (ATCC BAA-453) and *Shewanella oneidensis* MR-4 were kindly provided by Pr. T.J. Beveridge (University of Guelph, Ontario, Canada). Bacterial strains were revived from a stock suspension at -80 °C on a TSA medium (51044-Biomérieux, Marcy l'Etoile, France) twice successively for 48 hours at 30 °C to remove glycerol. Cultures were then prepared in 250 mL erlenmeyer flasks containing 20 mL bacterial suspension (NaCl 0.7 %, optical density: OD_{600nm} = 0.5) and 200 mL TSB (30g/L, 51019-BioMerieux) that were incubated for 14 hours while shaking (150 rpm, 30 °C). Cells were then harvested, in pseudo-stationary phase, by centrifugation (10 min, 10,000×g); washed twice with adequate KNO_3 solution (0.1 mol/L or 0.001M mol/L) and directly used for AFM experiments. For electrophoretic mobility measurements, that require a larger amount of cells, bacteria were grown in 750 mL batch reactor (300 rpm, 30 °C, 25 L/h air flux) during 24h and harvested in pseudo-stationary PHASE by centrifugation (10 min, 10,000×g) then washed twice in KNO_3 0,001 mol/L and resuspended to rich a concentration ranging from 5.10^6 cells/mL to 1.10^7 cells/mL.

2.2 Electrophoretic measurements.

Electrophoretic mobilities were measured by using a Zetaphoremeter IV (SEPHY-CAD instrumentations, Les Essarts le Roi, France) at room temperature. The bacterial suspensions were adjusted in pH and ionic strength and subsequently injected in the electrophoresis chamber which consists of a quartz suprasil cell that generated a constant electric field (800 V/m) between two palladium covered electrodes. The bacterial mobilities were calculated through the laser reflection by bacteria via an optical image recorded at different times by a CCD camera. Different cycles were performed to record at least 100 bacteria trajectories for each condition.

2.3 Force spectroscopy.

Force curves were obtained at room temperature, using an MFP-3D instrument (Asylum Research, Santa Barbara, USA). Silicon nitride cantilevers were purchased from Veeco (MLCT-EXMT-BF, Santa Barbara) and their spring constant calibrated using the thermal calibration method given an average value of 60 ± 5 pN/nm. All force experiments were made in potassium nitrate solution with an ionic strength of 1 or 100 mM at neutral pH . Cells were immobilized by physical adsorption on a polyethyleneimine (PEI)-coated glass slides as described elsewhere [13]. Glass slides were prepared freshly by incubation with PEI solution (0.2 %, 4 h), rigorously rinsed with Milli-Q water and dried in sterile condition. After being coated with PEI, a droplet of bacterial suspension (OD_{600nm} = 1) at the corresponding ionic strength was added to the slide during 1 h and subsequently rinsed before being used in AFM experiments. First of all, cells were imaged in soft contact mode to locate the bacterium. Force volume data were then collected to locate accurately the top of the cell using 10 × 10 grid at scan rate of 1 $\mu m\ s^{-1}$ and with 10 nN force trigger.

3. GOVERNING EQUATIONS

In this section, we present the theoretical formalisms used for the quantitative analyses of the AFM force curves and electrokinetic data measured for the MR4 and CN32 bacterial strains. Prior to this, we set the problem by describing the interphasial region between the aforementioned bacteria and their aqueous environment on the basis of the concept of diffuse soft interface as introduced in [7;14;15].

3.1. Parametrisation of the bacterial surface structures

From electronic micrographs (see [16]) and AFM images (not shown), MR4 and CN32 bacterial strains may be assimilated to rod-like bioparticles of length denoted as L_c. As mentioned previously, polymer surface structures are different following the strain. While the cells of CN32 are devoid of any detectable fibrous or capsular materials being essentially constituted of the classical gram-negative cell wall, those of MR-4 exhibit an extensive polymeric fringe with a thickness between 70 to 130 nm [16]. The presence of the cell wall and/or polymer-type layer at the periphery of the bacteria confers them a given hydrodynamic permeability, or said differently, a certain propensity for fluid flow penetration [7]. For that reason, bacteria are often regarded as paradigms of so-called soft particles [8;10]. As in previous analyses, we shall denote as a_c the radius of the rigid, ion-impermeable, cytoplasmic part of the bacterial cell -that part withstands the considerable inner Turgor pressure [17]- and δ the nominal thickness of the soft, ion-permeable layer located at the bacterial periphery (Figure 1). For MR-4, δ encompasses the cell wall and the capsular layer while for CN32 it corresponds only to the cell wall. However, one may show (see section 3) that the electro-hydrodynamic features of MR-4 are solely governed by the capsular layer of which the thickness largely exceeds the typical flow penetration length and the reciprocal screening Debye layer thickness for the range of electrolyte concentrations investigated within the framework of the current study [8;10].

For the sake of generality, the volume charge density ρ_{fix} carried by the soft layer is considered as heterogeneously distributed in space and thus position-dependent. The necessity for taking into account the anisotropic distribution of charges for environmental and biological particles has been extensively discussed in [18] and the reader is referred to that paper for further detail. Following the analyses on the electro-hydrodynamics of diffuse, heterogeneous soft particles [7], we adopt, for simplicity, a radial functionality for ρ_{fix} given by

$$\rho_{fix}(r)=\frac{1}{2}\omega\rho_o\left\{1-\tanh\left[\frac{r-(a+\delta)}{\alpha}\right]\right\} \qquad (1)$$

where r is the radial variable with the origin taken at the center of the particle. The parameter α has the dimension of a length and determines the degree of inhomogeneity for the charged polymer segment density distribution within the soft layer. Far from the particle, the charge density due to the fixed ionogenic sites distributed across the soft layer vanishes, which is in agreement with $\rho_{fix}(r\to\infty)=0$. The dimensionless parameter ω $(0<\omega\leq 1)$ in eq 1 is determined by the condition that imposes constancy for the total amount of charges upon variation of α and/or δ. ω is therefore given by the expression

$$\omega=\left[(a+\delta)^2-\delta^2\right]/\int_0^\infty\left\{1-\tanh\left[\frac{r-(a+\delta)}{\alpha}\right]\right\}r\,dr \qquad (2)$$

For a step function-like (or homogeneous) distribution of the charges within the soft layer, as classically adopted in the literature [19-23], we have $\omega\to 1$ and $\rho_{fix}(r)\equiv\rho_o$ with ρ_o the nominal space charge density.

3.2. Interaction forces between a hard spherical AFM probe and a soft rod-like particle

3.2.1. The electrostatic component

Consider an ion-impermeable (hard) spherical particle of uniform surface potential, denoted as ψ_s^o, and of radius a_s and a soft particle as described in §2.1. The particles are

immersed in a 1:1 electrolyte of bulk concentration c^{∞} and separated by a distance denoted as H (Figure 2, panel A). To compute the electrostatic interaction force between the AFM probe, assimilated to the hard particle, and the soft bacteria, we reason on the level of the Deryagin approximation [24]. This approximation allows the derivation of the electrical component of the Gibbs interaction energy between objects of non-planar symmetry from that per unit area of flat surfaces (Figure 2, panel B). This approach, which leads to the neglect of lateral interactions between surface elements of the interacting particles, is expected to work well for low κH and large particles. For the bacteria and ionic strength regime examined here, the latter condition is very well verified since $\kappa a_s >> 1$ and $\kappa a_c >> 1$ where κ is the reciprocal screening Debye length defined by

$$\kappa = \left(2F^2 c^{\infty} / \varepsilon_0 \varepsilon_r RT\right)^{1/2} \tag{3}$$

with F the Faraday constant, R the universal gas constant, T the absolute temperature and $\varepsilon_0 \varepsilon_r$ the dielectric permittivity of the electrolytic solution.

The electrical interaction energy (per unit surface area) between two parallel planar surfaces, denoted as U_{pp}, is obtained after integration of the disjoining pressure, Π_{pp}, according to

$$U_{pp}(H) = -\int_{\infty}^{H} \Pi_{pp}\left(H'\right) dH' \tag{4}$$

where H' is a dummy integration variable. Π_{pp} is the amount by which the normal component of the pressure tensor exceeds the outer pressure. It is defined by the sum of an osmotic and electrical (i.e. Maxwell stress) component, that is [25]

$$\Pi_{pp}(H) = 2c^{\infty} RT\left\{\cosh\left[y(H)\right] - 1\right\} - \frac{\varepsilon_0 \varepsilon_r}{2}\left(\frac{RT}{F}\right)^2 \left(\frac{\mathrm{d}y(H)}{\mathrm{d}x}\right)^2 \tag{5}$$

where y is the dimensionless potential defined by $y = F\psi / RT$ and x is the position in the direction perpendicular to the interfaces, as sketched in Figure 2 (panel B). Because of mechanical equilibrium of the interacting surfaces, Π_{pp} must be identical across the space region that corresponds to overlapping double layers. As such, for potential distribution exhibiting a minimum, one may evaluate Π_{pp} at the position $x = x_0$ that zeroths the Maxwell stress contribution. Rewriting eq 5 at $x = x_0$ defined by $\left(\mathrm{d}y(H)/\mathrm{d}x\right)_{x=x_0} = 0$, it comes

$$\Pi_{pp}(H) = 2c^{\infty} RT\left\{\cosh\left[y_{x=x_0}(H)\right] - 1\right\} \tag{6}$$

For the case of the interaction between similar surfaces (homointeraction), symmetry imposes that $x_0(H) = H/2$. For the more complex situation of hetero-interaction between surfaces with potentials (or charges) of the same sign, as examined here, x_0 is an implicit function of the separation distance. The H-dependence of x_0 is obtained after determination of the potential distributions $y(x)$ for every separation distance H. To that end, one needs to solve the non-linear Poisson-Boltzmann equation written

$$\frac{\mathrm{d}^2 y}{\mathrm{d}x^2} - \kappa^2 \sinh(y) = \frac{\rho_0 \omega}{4c^{\infty} F}\left\{1 - \tanh\left(\frac{x-\delta}{\alpha}\right)\right\} \tag{7}$$

where the right hand side corresponds to the spatial distribution of the polymer charge density expressed in planar symmetry with the coordinate system of Figure 2, panel B. The boundary

conditions associated to eq 7 reflect (i) the constancy of the surface potential for the AFM probe upon approach and (ii) the uncharged state of the surface that separates the cytoplasm from the surrounding polymeric layer (condition relative to the bacteria). Therefore, it comes

$$y(x=H)=F\psi_s^o/RT=y_s^o \tag{8}$$

and

$$(dy/dx)_{x=0}=0 \tag{9}$$

Equations 7-9 were solved for various H using an iterative finite differences scheme according to a globally convergent Newton-Raphson method [26]. Once the potential distribution determined, the position x_o, the corresponding (dimensionless) potential $y_{x=x_o}(H)$ and the disjoining pressure $\Pi_{pp}(H)$ (eq 6) could be evaluated. The searched electrostatic interaction energy U_{pp} was then estimated after numerical integration of the cubic spline interpolation of Π_{pp} (eq 4) with respect to H. The validity and accuracy of the numerical methodology was verified by comparing the results with those obtained within the framework of the Debye-Hückel approximation (low potentials) and homogeneous distribution for the fixed charge density across the soft surface layer of the bacteria $(\alpha \to 0)$. In that situation, one shows (Appendix 1) that U_{pp} may be written in the form

$$U_{pp}(H)\big|_{\alpha\to 0,y\le 1}=RTc^{\infty}\int_{\infty}^{H}\frac{1}{1-\Phi^2(H')}dH' \tag{10}$$

with

$$\Phi(H')=-\left[\tanh(\kappa H')+\frac{2y_s^oFc^{\infty}}{\rho_o\sinh(\kappa\delta)}\operatorname{sech}(\kappa H')\right] \tag{11}$$

The electrostatic interaction energy, denoted as U_{sc}, at a given separation distance H between the spherical and cylindrical particles depicted in Figure 2, may be obtained from U_{pp} via the Deryagin integration method. After calculation (Appendix 2), the result reads as

$$U_{sc}(H)=4a_c\int_0^{\pi/2}\int_0^{a_s}U_{pp}(\gamma(H,z,\theta))dzd\theta \tag{12}$$

where the coordinate system (z,θ) is depicted in Figure 2, panel A. γ represents the separation distance between surface elements taken on both particles and that face each other. On the basis of simple geometrical considerations (Appendix 2), one easily shows that γ is related to H, z and θ according to

$$\gamma(H,z,\theta)=H+a_c(1-\cos\theta)+a_s\left\{1-\left[1-\left(\frac{z}{a_s}\right)^2-\left(\frac{a_c}{a_s}\sin\theta\right)^2\right]^{1/2}\right\} \tag{13}$$

The two-dimensional integral as defined by eqs 12-13 was computed by standard numerical means [] from the cubic spline interpolation of U_{pp} with respect to H as obtained from the discretisized forms of eqs 4, 6-9. Finally, the electrostatic interaction force, F_{sc}^{el}, associated to U_{sc} is simply evaluated via

$$F_{sc}^{el}(H)=-\frac{dU_{sc}(H)}{dH} \tag{14}$$

3.2.2. The mechanical component

The indentation curves recorded for the bacterial surfaces by atomic force microscopy may be analysed on the basis of Hertzian mechanics theory and Hook formalism that account for the non-linear and linear components of the force versus indentation curves, respectively [27]. The punch load force, denoted as F^{load}, is then related to the indentation δ_{ind} via the relationship

$$F^{\text{load}} = \frac{4E\sqrt{a_s}}{3(1-\nu^2)}\delta_{\text{ind}}^{3/2} + \frac{1}{2}\left[\left(k_{\text{Bac}}\delta_{\text{ind}} + A\right) + \left|k_{\text{Bac}}\delta_{\text{ind}} + A\right|\right] \qquad (15)$$

where a_s is the radius of the spherical AFM tip, E is the elastic or Young's modulus, ν is the Poisson's ratio, k_{Bac} the bacterial spring constant and A is a constant. The bacterial spring constant k_{Bac} is determined either after analysis of the forces curves according to eq 15 or from the slope, s, of the linear portion of the force versus piezo displacement curves using [28;29]

$$k_{\text{Bac}} = -k_{\text{C}}\frac{s}{k_{\text{C}} + s} \qquad (16)$$

with k_{C} is the spring constant of the AFM cantilever. Overall, the mechanical parameters E and k_{B} were obtained from the fit of the experimental data using a least square optimisation method. The Poisson ratio ν was systematically assumed to be 0.5, as commonly adopted for bacterial surface ultrastructures assimilated to linear-elastic solids [12]. It is thereby stressed that the Hertzian mechanics formalism is strictly valid within the assumption that the material is homogenous, isotropic, semi-infinite and that it undergoes infinitely small strains. Whereas it is clear that the former assumption is incorrect for biological particles, as correctly recognized by Rosenbluth *et al* [30], it has been nonetheless thoroughly demonstrated that Hertzian mechanics is able to quantify differences in deformability between cell types in a simple and effective manner. This is the purpose of that study that focuses on (i) the respective nanomechanical properties of two bacterial strains with distinct phenotypes of surface structures and (ii) the relationship between those properties and the electrohydrodynamic bacterial features as determined by electrokinetics.

3.3. Electrokinetics of rod-like diffuse soft particles

The theory for the electrophoresis of diffuse (i.e. heterogeneous), soft, spherical particles has been discussed extensively elsewhere [7;29-35] and has already been successful in accounting the electro-hydrodynamics of various biocolloids [8-10;36] and environmental particles [37]. We extend here this formalism to the electrophoretic migration of a rod-like permeable particle under the action of an applied dc electric field. The analysis completes and improves that originally proposed by Ohshima who derived approximate analytical expressions for the electrophoretic mobility of a soft, homogeneous, cylindrical particle for sufficiently large ionic strengths at which polarization and relaxation of the electric double layer by the applied field may be neglected [38;39]. The theory reported here does not suffer from any restrictions on the bacterial charge, bacterial size and double layer thickness so that quantitative analysis of the electrokinetic data may be performed over a broad spectrum of experimental conditions (pH, ionic strength). As done in [7] for the case of diffuse soft spherical particles, the theoretical formalism takes into account the anisotropic distribution of the soft material surrounding the bacteria and particularly allows the evaluation of the underlying impact of such heterogeneity on the electrohydrodynamic properties of the bacteria. The necessity for evoking spatial dependence for the density of polymer segments within the soft surface layer has been discussed in detail in [7] and recently been pointed out by various spectroscopic studies, in

particular on microgel particles [40;41]. Also, de Kerchove *et al.* [42] underlined the shortcomings of the classical soft (homogeneous) particle analysis, as proposed by Ohshima [19-21] and others [22;23], for accounting the electrophoretic data of *Escherichia Coli* mutants by arguing the nonuniform distribution of charged groups along the lipopolysaccharides (LPS) as well as the patchlike repartition of the LPS in the bacterial periplasmic region.

3.3.1. Setting the problem

Unlike for soft, spherical particles, the electrophoretic mobility, denoted as μ, for a cylindrical particle depends on the direction of its long axis as compared to that of the applied electric field. As for hard cylinders, the mobility μ of a soft, cylindrical particle oriented at an arbitrary angle between its axis and an applied field, is averaged over a random distribution of orientations as follows [43]:

$$\mu = \frac{2}{3}\mu_{\perp} + \frac{1}{3}\mu_{\parallel} \tag{17}$$

where $\mu_{\perp}$ and $\mu_{\parallel}$ are the electrophoretic mobilities of the cylindrical particle with its axis perpendicular and parallel to the electric field, respectively. Below, the derivations of $\mu_{\perp}$ and $\mu_{\parallel}$ are given for an electrolyte composed of N types of mobile ionic species with valency z_i, of bulk concentrations c_i^{∞} and limiting ionic mobilities λ_i^{o} $(i = 1,...,N)$. We adopt the model of Debye-Bueche [44] in the framework of which the charged segments within the bacterial polymeric fringe are regarded as resistance centers of radius a_s that exert frictional forces on the liquid flowing in the charged layer. The corresponding friction coefficient is denoted as *k*. The hydrodynamic volume fraction of polymer segments, ϕ, is given by $\phi = 4n_s\pi a_s^3/3$ with n_s the polymer segment density.

The spatial distribution of the polymer segment density, n_s, is chosen dependent on *r* only (radial profile) and is written

$$n_s(r)/n_s^{o} = f(r) \tag{18}$$

where n_s^{o} is the nominal segment density of the layer with homogenously distributed chains and *f* is given by

$$f(r \to \infty) \to 0 \tag{19}$$

, which expresses the vanishing of the polymeric shell for $r \to \infty$. Using eq 18, the dependence of ϕ on *r* is simply given by $\phi(r)/\phi^{o} = f(r)$ with $\phi^{o} = 4n_s^{o}\pi a_s^3/3$. To obtain the distribution of *k*, the coefficient of friction exerted by the polymer segments on the flow, the Brinkman equation is employed [45]. It relates *k* to ϕ by considering the flux of fluid across the group of spheres of radius a_s as follows

$$k(r) = \eta\left\{\frac{a_s^2}{18}\left[3 + \frac{4}{\phi(r)} - 3\left(\frac{8}{\phi(r)} - 3\right)^{1/2}\right]\right\}^{-1} \tag{20}$$

with η the dynamic viscosity of water and the radial dependency of k and ϕ is explicitly written. From comparison with rigorous numerical calculations involving averaging over numerous initial stochastic configurations, eq 20 is shown to be valid for $\phi < 0.3$ [46]. For very low volume fractions ($\phi \to 0$), eq 20 reduces to Stokes' equation which predicts a linear dependence of k on ϕ, so that

$$k(r)/k_o = f(r) \tag{21}$$

with $k_o \left(=9\eta_w\phi_o/2a_s^2\right)$ the friction coefficient of the polymeric shell for a homogeneous distribution of segments. In the following, expression (21) will be used, which is justified for the usual water contents of soft charged layers commonly reported in the literature for bacteria. Assuming homogeneous distribution of the fixed ionogenic sites along a single polymer chain within the soft surface layer, the distribution function $f(r)$ then satisfies the relation

$$\rho_{fix}(r)/\rho_o = f(r) \tag{22}$$

with $\rho_{fix}(r)$ and ρ_o defined in eq 1. Within the framework of the current study, we shall consider for $f(r)$ the tanh-like function as given in eq 1. It is stressed however that the formalism below may be applied for any radial function f, either empirical, analytical or resulting from preliminary calculations based on theories that differ from their degree of sophistication. For a given system, rigorous evaluation of f requires beforehand exact knowledge of the interactions (polymer chains-solvent-ions) as well as identification of the nature of the chemical charges throughout the surface layer. Such analysis is extremely complex for biological systems and their analysis in terms of diffuse interfacial modelling is for that reason very useful and has the merit to reproduce -at least qualitatively- processes that lead to heterogeneity in the organisation of the polymer chains at the interface bacterium/electrolytic solution.

3.3.2. Fundamental equations for the derivation of $\mu_\perp$.

The standard set of electrokinetic equations governing the dynamics of a soft spherical particle with a discontinuous distribution of polymer chains has been extensively discussed in the literature [7;20;22;23;32;34]. Ohshima demonstrated that this set of fundamental electrokinetic equations can be expressed in terms of the liquid velocity, $\vec{u}(\vec{r})$, at the position $\vec{r}$ relative to the particle and the deviation $\delta\mu_i(\vec{r})$ of the electrochemical potential, $\mu_i(\vec{r})$, of the i-th ion species due to the applied electric field. The governing electrokinetic equations for cylindrical soft particles are similar than those for spherical geometry. Making explicit the dependence of the friction coefficient k on the position (as determined by eq 21), these equations are written for a diffuse interface as follows

$$\eta\nabla\times\nabla\times\vec{u}(\vec{r}) + \nabla p(\vec{r}) - \sum_{i=1}^{N}\delta\mu_i(\vec{r})\nabla c_i^{(0)}(r) + \rho_{el}^{(0)}(r)\nabla\psi^{(0)}(r) + \nabla\left(\rho_{el}^{(0)}(r)\delta\psi(\vec{r})\right) + k(r)\vec{u}(\vec{r}) = \vec{0} \tag{23}$$

$$i = 1,\ldots,N: \qquad \nabla.\left\{c_i^{(0)}(r)\vec{u}(\vec{r}) - \frac{1}{\lambda_i}c_i^{(0)}(r)\nabla\mu_i(\vec{r})\right\} = 0 \tag{24}$$

, where $p(\vec{r})$ is the pressure, $c_i(\vec{r}) = c_i^{(0)}(r) + \delta c_i(\vec{r})$ the local concentration of the i-th ionic species, $\rho_{el}(\vec{r}) = \rho_{el}^{(0)}(r) + \delta\rho_{el}(\vec{r})$ the charge density stemming from the mobile ions, and $\psi(\vec{r}) = \psi^{(0)}(r) + \delta\psi(\vec{r})$ the local electrostatic potential. The quantities indicated by the superscript (0) refer to those at equilibrium (i.e. in the absence of the electric field) and the

variables preceded by the symbol δ indicate small variations of the order E (i.e. linear in E). In eq 24, $\overline{\lambda_i}$ denotes the drag coefficient of ion i and is related to the limiting conductivity λ_i^o by the expression $\overline{\lambda_i} = |z_i| eF / \lambda_i^o$ with e the elementary charge. Equation (23) is the Navier-Stokes equation after linearization of the pertaining electrokinetic variables with respect to the applied field. Equation 24 results from the linearization of the combined equations expressing the velocity $\vec{v}_i(\vec{r})$ of an individual ion, as governed by diffusion and convection processes, and the continuity condition for that particular ion, i.e. $\nabla.\left(c_i(\vec{r})\vec{v}_i(\vec{r})\right) = 0$. In order to solve eq 23, it is convenient to take the curl so that the terms of the third, fourth and fifth orders in E vanish. The result reads as

$$\eta_w \nabla\times\nabla\times\nabla\times\vec{u}(\vec{r}) + \nabla\times\left\{k(r)\vec{u}(\vec{r})\right\} = \sum_{i=1}^{N} \nabla\delta\mu_i(\vec{r})\times\nabla c_i^{(0)}(r) \qquad (25)$$

On the basis of symmetry considerations, one may write the liquid velocity $\vec{u}(\vec{r})$ at the position r relative to the particle in the form [38;39]

$$\vec{u}(\vec{r}) = \left(-\frac{h(r)}{r} E\cos\theta, \frac{dh(r)}{dr} E\sin\theta, 0\right) \qquad (26)$$

where h is a radial function. Following the strategy adopted in [], the quantity $\delta\mu_i(\vec{r})$ is subsequently written

$$i = 1,...,N: \qquad \delta\mu_i(\vec{r}) = -z_i e\chi_i(r)(r)\vec{E}.\vec{e}_r = -z_i e\chi_i(r) E\cos\theta \qquad (27)$$

where the functions $\chi_i(r)$ are radial and $\vec{e}_r$ is the radial unit vector. Assuming that solvent-mediated (dispersive) forces may be neglected and that the different ionic species are point-like, the distribution of the electrolyte ions at equilibrium $c_i^{(0)}(\vec{r})$ obeys a Boltzmann statistics and the equilibrium potential $\psi^{(0)}(\vec{r})$ the Poisson-Boltzmann equation, both being function of the radial position only

$$\nabla^2\psi^{(0)}(r) = -\frac{1}{\varepsilon_o\varepsilon_r}\left\{\rho_{el}^{(0)}(r) + \rho_o f(r)\right\}, \qquad (28)$$

$$\rho_{el}^{(0)}(r) = F\sum_{i=1}^{N} z_i c_i^{(0)}(r) = F\sum_{i=1}^{N} z_i c_i^{\infty} \exp\left\{-z_i e\psi^{(0)}(r)/k_B T\right\} \qquad (29)$$

with k_B the Boltzmann constant. Substitution of the expressions (26), (27) and (29) for $\vec{u}(r)$, $\delta\mu_i(\vec{r})$ and $c_i^{(0)}(\vec{r})$, respectively in the differential equation (25) leads to

$$L_r\left\{L_r h(r)\right\} - \lambda_o^2\left[f(r)L_r h(r) - \frac{df(r)}{dr}\frac{dh(r)}{dr}\right]$$

$$= -\frac{F}{\eta}\frac{1}{r}\frac{dy(r)}{dr}\sum_i c_i^{\infty} z_i^2 \exp\left\{-z_i y(r)\right\}\chi_i(r) \qquad (30)$$

where L_r is the differential operator defined by

$$L_r \equiv \frac{d}{dr}\left\{\frac{1}{r}\frac{d}{dr}r\right\} = \frac{d^2}{dr^2} + \frac{1}{r}\frac{d}{dr} - \frac{1}{r^2}, \qquad (31)$$

and

$$\lambda_o = (k_o/\eta)^{1/2}, \qquad (32)$$

the nominal softness parameter of the permeable polymeric shell, that is for a uniform distribution of the segments. The quantity $1/\lambda_o$ has the dimension of a length and typically represents the characteristic penetration length of the flow within the soft structure. $y(r)\left(=e\psi^{(0)}(r)/k_BT\right)$ in eq 30 denotes the dimensionless equilibrium potential. The equation that determines $\chi_i(r)$ is obtained after combining eqs 24 and 27 . After some rearrangement, the result is read as follows [38;39]

$$i=1,...,N: \qquad L_r\chi_i(r)=\frac{dy}{dr}\left\{z_i\frac{d\chi_i(r)}{dr}-\frac{\overline{\lambda_i}}{e}\frac{h(r)}{r}\right\} \tag{33}$$

and the continuity condition $\nabla.\vec{u}(r)=0$ has been used.

3.3.3. Boundary conditions.

As a general comment, the boundaries associated to the governing electrokinetic equations written for a diffuse interface are substantially simpler than those considered for a sharp interface, as in []. The gradual transition from the polymeric shell to the electrolyte side avoids the necessity of introducing other boundaries than that between the hard and soft components of the particle (i.e. at $r=a$) and that pertaining to the far-field domain (i.e. for $r\to\infty$).

The slipping plane at which $\vec{u}=\vec{0}$ is located at the position $r=a$ so that, following Eq. (12),

$$h(r=a)=0 \tag{34}$$

and

$$\left.\frac{dh(r)}{dr}\right|_{r=a}=0 \tag{35}$$

The liquid velocity $\vec{u}(r)$ relative to the particle must comply the far field condition given by

$$\vec{u}(r\to\infty)\to-\vec{U}=(-U\cos\theta,U\sin\theta,0) \tag{36}$$

Using eq 26, eq 36 immediately yields

$$h(r\to\infty)\to\mu_\perp r+\Theta \tag{37}$$

where $\mu_\perp$ is the searched component of the electrophoretic mobility defined by eq 17 and Θ a constant. To determine the latter, one uses the fact that in the stationary state, the net force acting on the cylindrical particle must be zero. Let us consider a cylinder C of radius r sufficiently large to encompass the particle in such a way that the net electric charge within C is zero. Then, the only hydrodynamic force $\vec{\Im}_H$ needs to be considered and one may write

$$\vec{\Im}_H=\int_C\sigma^H.\vec{n}dS=\vec{0} \quad \text{as } r\to\infty \tag{38}$$

, where σ_H is the hydrodynamic stress, $\vec{n}$ the unit normal vector outward from the particle surface and the integration is carried over the surface of C. After calculation (Appendix 3), condition (38) is shown to be consistent with the asymptotic form $h(r\to\infty)$ that imposes $\Theta=0$. Consequently, we have

$$h(r\to\infty)\to\mu_\perp r+O\left(\frac{1}{r}\right) \tag{39}$$

which refines the boundary (37). One may easily show that eq 39 is verified when h satisfies the conditions

$$\left.\frac{d^2h(r)}{dr^2}\right|_{r\to\infty} = 0 \;;\; r^2\left.\frac{d\{h(r)/r\}}{dr}\right|_{r\to\infty} = 0 \qquad (40,41)$$

Equations (34, 35, 40, 41) are the boundaries associated with the differential eq 30 of the fourth order in h. The two boundary conditions verified by the functions φ_i are written

$$i = 1,...,N: \qquad \left.\frac{d\chi_i(r)}{dr}\right|_{r=a} = 0 \;\; ; \; \chi_i(r\to\infty)\to r \qquad (42,43)$$

Equation (42) results from combining the condition $\vec{u}(r).\vec{n}\big|_{r=a} = 0$ with that for the individual ionic flow velocity $\vec{v}_i$, i.e. $\vec{v}_i(r).\vec{n}\big|_{r=a} = 0$. Equation (43) is obtained after considering that far from the particle, perturbations of the local electric potential and local ion concentrations caused by the applied field become negligible. The boundaries pertaining to the (dimensionless) equilibrium potential distribution, y, express the bulk electroneutrality condition at large distances from the particle, i.e.

$$y(r\to\infty) = 0 \quad \text{(reference for the potentials)}, \qquad (44)$$

and the electrostatic conditions at the surface of the particle core, that is

$$\left.\frac{dy(r)}{dr}\right|_{r=a} = 0 \qquad (45)$$

The theoretical calculation of $\mu_\perp$ requires the consistent numerical evaluation of (a) the electroosmotic velocity profile $\vec{u}(\vec{r})$, or equivalently $h(r)$, as defined by eqs 30, 34, 35, 40, 41 (hydrodynamics), (b) the distribution of the local dimensionless equilibrium potential (electrostatics, eqs 28, 29, 44, 45) and (c) the radial functions $\chi_{i=1,...,N}(r)$ (eqs 33, 42, 43). After a suitable change of variables, the set of coupled electrokinetic equations may be transformed into a system of first-order differential equations with boundaries written in terms of explicit algebraic relations between the new variables. As for spherical geometry [37], this multidimensional root-problem can then be solved by numerical shooting from $r >> \kappa^{-1}$ to the position $r = 0$ using an adaptive stepsize Runge-Kutta method of the fifth-order implemented with a Newton-Raphson type scheme [26]. The potential was evaluated on the self-controlled nonuniform grid by cubic interpolation of the results obtained from the finite difference algorithm with a uniform step size.

The main assumptions of the above formalism are (a) the Reynolds numbers of the liquid flow inside and outside the charged, soft polymeric layer are small so that the liquid may be regarded as incompressible; (b) the electrophoretic velocity, $\vec{U}$, is proportional to the applied field, $\vec{E}$, which is correct for low E (in electrophoresis of the first kind, as considered here, terms in E of order higher than 1 may be neglected) and (c) the relative permittivities, ε_r, inside and outside the polymeric layer are the same or, equivalently, the water content within the soft layer is sufficiently large to neglect any spatial gradients in ε_r. These assumptions are in line with the conditions under which the electrophoretic experiments were carried out and in relationship to the nature of the bacterial surface that were investigated.

3.3.4. Fundamental equations for the derivation of $\mu_{\|}$.

When the cylinder is oriented parallel to $\vec{E}$, the components of the flow velocity $\vec{u}(r)$, according to the unit vectors describing the cylindrical coordinate system (r,θ,z), are simply given by:

$$\vec{u}(r)=\{0,0,u_z(r)\} \tag{46}$$

The Navier-Stokes equation that determines $u_z(r)$ is then written:

$$\frac{1}{r}\frac{\mathrm{d}}{\mathrm{d}r}\left(r\frac{\mathrm{d}u_z(r)}{\mathrm{d}r}\right)-\lambda_o^2 f(r)u_z(r)-\frac{EF}{\eta}\sum_i z_i c_i^{\infty}\exp\left(-z_i y(r)\right)=0 \tag{47}$$

where the function $f(r)$ is considered to be radial (as above) and the assumptions governing the validity of eq 47 are the same as those in the preceding section. $u_z(r)$ is limited by the boundaries:

$$u_z(r\to a)=0\,;\; u_z(r\to\infty)=-\mu_{\|}E \tag{48,49}$$

Computation of the hydrodynamic flow profile, $u_z(r)$, as determined by eqs 47-49 and accurate evaluation of the associated $\mu_{\|}$ may be performed using classical finite-differences schemes or equivalently a numerical algorithm very similar to that employed for the evaluation of $\mu_{\perp}$.

4. RESULTS AND DISCUSSION

4.1. Soft particle analysis of the electrophoretic mobilities.

To address the electrophoretic behaviour of soft particle, some information about the external structure of the bacterial envelope are required to quantitatively examine the electrophoretic mobility of bacteria. The two *Shewanella* strains investigated present different well-characterized phenotypes of polymer fringe. The cell surfaces of CN32 are constituted of the classical cell wall of gram-negative, i.e. the outer membrane above the periplasmic space that is underneath the plasma membrane, without any fibrous or capsular materials whereas those of MR-4 exhibit an extensive polymer fringe (from 70 to 130 nm) above the bacterial cell wall. Our previous attempt at quantifying the electrophoretic characteristics of various *Shewanella* strains has demonstrated the capabilities of soft particle analysis to differentiate both the electrokinetic charge density and the hydrodynamic permeability [10]. These analyses have been carried out on the basis of numerical evaluation developed by Duval et al. for the electrophoresis of spherical, charged soft particles. In particular, the theoretical calculations have been performed by considering spherical particle and homogeneous distribution for the friction coefficient and the space charge density. As judged by the recent paper [7] pointing out the effects of inhomogeneity of the interface on the electrophoretic motion, i.e. the diffuse character of the polyelectrolyte layer, the possibility of diffuse interface for *Shewanella* cells is considered in this article. The effect of the geometry is also considered by solving for the first time the equations involved in the electrophoretic migration of a rod-like permeable particle with an homogeneous or diffuse (heterogeneous) interface.

4.1.1 The homogeneous case.

The quantitative examinations of the electrophoretic mobilities for the two *Shewanella* strains are reported in as a function of ionic strength and for a neutral pH value (Figure 3). The homogeneous case that corresponds to a step function representation of the interface (Figure 1) has been firstly computed to evaluate the effects of the geometry (spherical versus rod

geometry) on the calculations of mobilites. The least mean square evaluations of the two unknown parameters that are the permeability character (λ_0) and the volumic charge density (ρ_0) yield slightly the same values as obtained previously by considering a cylinder equivalent to a spherical particle [10]. In the case of MR-4 cells, the best fit calculated on the basis of rod-like geometry (Figure 3, panel A, doted line) gave the same volumic charge density (ρ_0 = -10 mM) and hydrodynamic permeability (λ_0^{-1} = 3.5 nm) as the spherical assumption (see ref [10]). By the same manner, this numerical evaluation for CN32 (Figure 3, panel B, doted line) yielded the same value for the hydrodynamic permeability (λ_0^{-1} = 2 nm) and reasonably the same value for volumic charge density, i.e. ρ_0 = -40 and -35 mM for the spherical and rod-like geometry, respectively. However, the spherical assumption initially assumed in our previous work [10] was a reasonable approximation to derive the electrohydrodynamic properties.

As observed previously for the spherical case, the discrepancy between experimental data and the results computed on the basis of numerical evaluation considering a soft rod-like particle increases upon decrease of ionic strength especially for CN32 (Figure 3, panel B). This is mainly due to the assumptions assimilating the polyelectrolyte layer as homogeneous and/or with a volumic charge density constant over the whole range of electrolyte concentrations. It is well established that the ionic strength strongly modifies the magnitude of the volumic charge density but also the diffuse character of the interface. As demonstrated by the recent theoretical work of Duval and Ohshima [7], the mobility of diffuse soft interfaces results of a subtle balance between the electrical force and electroosmotic drag. Unfortunately, modelling the electrophoretic data on the basis of the diffuse soft theory may be achieved by varying not only λ_0 and ρ_0 but also α that determines the degree of inhomogeneity of the polyelectrolyte distribution. However, the uniqueness of the solution of such fitting procedure is not physically realistic and thus requires simplifying the system. In fact, we can reasonably describe the two extreme configurations as i) the homogeneous case by varying the volumic charge density with $\alpha = 0$ and ii) the heterogeneous one by adjusting the diffuse character of interface through α with a constant volumic charge density (value taken from the best fit with $\alpha = 0$).

At first, the homogeneous case is considered and the experimental data that deviates from the aformentionned calculation were fitted by considering adjustable ρ_0 to reproduce the data at low ionic strength (Figure 3, dashed lines). As expected, the magnitude of the volumic charge density decreases when lowering the ionic strength. Whereas the strain with polymer fringe (MR-4) exhibits slight change in ρ_0 from -10 to -7 mM, the CN32 cells present a rather large variation from -35 to -15 mM. According to the classical double layer theory, the range and the magnitude of electrostatic potential decrease when increasing the ionic strength. This process due to the screening of surface charge favors to the acid-base (protolytic) reactions and leads to the increase of the concomitant increase of the pristine charge. Assuming the bacterial mobility is governing by electrostatic screening effects, the decrease of volumic charge density at low ionic strength is in agreement with the double layer statement.

Interestingly, the ionic strength values at which the doted lines start to deviate from the experimental data are significantly different according to the strain. Indeed, the homogeneous description (α=0, step like function) with a constant volumic charge describes reasonably the whole set of data for MR-4 cells above 8 mM ionic strength. In contrast, such assumption already fails from 50-60 mM for the CN32. However, the experimental data were fitted by considering adjustable ρ_0 at each ionic strength. Another interpretation of the discrepancies at low ionic strength could be performed by taking into account the increase of the diffuse (heterogeneous) character when decreasing ionic strength.

4.1.2 The diffuse (heterogeneous) case.

Analysis of the electrophoretic mobilities on the basis of soft diffuse theory described in section 3.3 is reported in Figure 4 and 5 for MR-4 and CN32, respectively. In this case, the effects of pH are also presented to illustrate our purpose. In all figures, the doted lines correspond to the previous homogeneous case ($\alpha/\delta = 0$) while the plain lines were computed upon tuning a single adjustable parameter α. The increase of the dimensionless parameter α/δ corresponds to a more pronounced diffuse character.

As a general comment, the electrophoretic mobilities at different pH could not be reproduced over the entire range of ionic strength using an homogeneous approach with constant volumic charge (Figs 4 and 5, doted lines). As observed for the neutral pH, this observation is much more pronounced for the CN32 cells as compared to the MR-4 behaviour. This effect results in Figs 4 and 5 by different critical concentrations c_c^{∞} corresponding to the ionic strength value at which the homogeneous assumption (doted lines) starts to fail. These values are reported in Table 1. The increase of the pH induces the increase of the critical concentrations because of the raise of the diffuse character and/or the volumic charge density. The experimental values below these critical concentrations were fitted by adjusting α, the diffuse parameter. This trend is then quantified through the dimensionless parameter α/δ that demonstrated higher values for basic media than acid one for the two types of strains and a more pronounced diffuse character for CN32 compared to MR-4 behaviour. For the sake of illustration, some profiles f(r) characteristic of the two type of strains are given in Figure 6 as a function of α/δ. It appears clearly that the local distribution of the polymer segment density within the soft layer stated by this function is wider for CN32 than MR-4. This effect could be connected to the potentially swelling process of the bacterial interface as the ionic strength decreases and/or the pH increases. Indeed, the electrostatic contribution to osmotic pressure at different ionic strength for the three studied pH have been calculated on the basis of the homogeneous case, $\alpha/\delta = 0$ (Figure 7). The critical concentrations inferred from Figs 3-4 (Table 1) are reported in Figure 7 to extract the critical values of the electrostatic contribution to the osmotic pressure. While these values are very similar at different pH for MR-4 (Figure 7, panel A), significant differences are observed for CN32 between the acid behaviour and the other pH values. It is important to point out that the graphical determination of the critical concentration is not trivial because of the experimental error of the data and their discrete values. However, polyelectrolyte polymers are well known to change their three dimensional structures as a function of ionic strength. Whether it be the swelling or shrinking processes, the structural response of the polymer is a subtle balance between different contributions to the osmotic pressure. Beside the elastic and the polymer-solvent mixing contributions that we could consider in our case as similar regardless the conditions, the comparison of the electrostatic contributions in relation to the critical concentration is a good indicator of the presence or not of a swelling/shrinking process. Indeed, the similar values of pressure observed for MR-4 indicate that below these critical concentrations, swelling processes may occur to counter balance the electrostatic interactions between the polymer chains. In contrast, the critical pressures calculated for CN32 were different and significantly higher than those ones for MR-4. It seems likely that the homogeneous assumption is not physically realistic even at high strengths for CN32 because the important charge density can imply the interface to swell and thus the heterogeneous character is already pronounced at high strengths. To summarize, it is obvious that the discrimination between the two aforementioned assumptions, i.e. changes in volumic charge density and/or heterogeneous character, could not be completely achieved with the available data and theory.

4.2. Theoretical electrostatic interaction forces between the AFM tip and bacteria

One major problem in force measurements for deformable surfaces as bacteria is the accurate determination of the contact point between the AFM tip and the cell surface. Such value is required to differentiate surface forces from the mechanical deformation of the cell and/or the cantilever. On the basis of the electrohydrodynamic characteristics described above and on the theoretical development presented in section 3.2.1, we attempted for the first time to calculate the effective electrostatic interactions between a soft interface and the hard tip. As recently pointed out by Gaboriaud and Dufrêne [12], the interpretations of force data for microbial cells in the literature considered the electrostatic component on the basis of linearized or non-linearized Poisson-Bolztmann equations involving two hard surfaces. In any case, the soft and even less the diffuse characters of the bacterial surface were considered. The theoretical interpretations of the electrophoretic data allowed addressing the two reasonable physical situations and their electrostatic characteristics in order to calculate the electrostatic interaction forces between the AFM tip and the bacteria. As described previously, a homogeneous or heterogeneous (diffuse) interface could be considered for the bacteria. Reported in Figure 8 are the theoretical electrostatic interactions for the two strains at a low (1 mM) and high (100 mM) salt levels as a function of the separate distance between the tip and the cell. Expectedly, the calculation performed at high salt level (c^{∞} = 100 mM) for the two type of strains leaded to weak electrostatic interactions that could not be probed by using AFM spectroscopy. This result is very important because it justifies the approaches developed in the literature at such salt level which claimed the specific measurement of mechanical properties without significant contribution of the electrostatic interactions [9;27]. In contrast, the electrostatic components at low salt level (c^{∞} = 1 mM) are much more significant. The comparison between the homogeneous and diffuse assumptions revealed the higher contribution for the homogeneous case due in most part to the shift of the separation distance between the tip and the cell surface. From the AFM point of view, the cell surface starts when the tip meets the first molecular structure even if this structure is diffuse. While the charge density of the heterogeneous case (ρ_0 = - 35 mM) for CN32 (Figure 8, panel B) was two times higher than the charge observed for the homogeneous case (ρ_0 = - 15 mM), the resulting electrostatic interaction forces are largely diminished due to the diffuse distribution of the interface that shifts the most external part of the bacterial interface to lower electrostatic potential. The same trend was observed for MR-4 (Figure 8, panel A). However, the electrostatic potential distributions are strongly dependant to the thickness of the permeable polyelectrolyte layer. Indeed, Duval and Ohshima [7] clearly demonstrated for thick layers ($\kappa\delta \gg 1$ and $\alpha \ll \delta$), which corresponds to the MR-4 situation, that the potential distribution basically matches the segment density profile, f(r). In contrast, if the thickness is in the same order of magnitude of the κ^{-1} distance as for CN32, the potential distribution determined by the Poisson-Boltzmann equation is largely affected by non-linear coupling between ρ_{fix} (Eq. 22) and ρ_{el} (Eq. 29).

4.3. Force measurements between the AFM tip and bacterial surface.

Figure 9 shows the force curve for CN32 at 1 mM (panel A) and 100 mM (panel B). The force is plotted as a function of the relative piezo displacement arbitrarily positioned to the lift-off from zero force on the approach curve. This assumption for the contact point is accurate at high salt level (100 mM) as the electrostatic contribution is negligible (Figure 8, panel B) while for the low salt level (1 mM), the contribution on electrostatic interactions has to be take into account as it will be discussed later in the manuscript.

At 1 mM, force curves exhibited a wide linear domain and a weak hysteresis between the forward and reverse curves (Figure 9, panel C). In contrast, the curves recorded at 100 mM showed a broad non linear domain and an important hysteresis. It appears clearly that cells at

low salt level are significantly stiffer than cells at high salt level as the force increased more rapidly. In addition, such stiffness is consistent with hysteresis trend as the viscoelastic properties are dependant of the difference between the forward and reverse curves. Roughly speaking, a stiff object do not present any hysteresis while the object is softer more the hysteresis is important.

The nanomechanical properties have been extracted from the analysis of force curves by using two different approaches depending on the salt level. At 1 mM, the presence of electrostatic interactions prevents the direct quantification of nanomechanical properties from the indentation curves. To take into account all the interactions (electrostatic and mechanical), the local spring constant of bacteria was determined systematically at low salt level from the slope of the linear portion of force curve (Figure 10, top panel) using Eq. 16. The X-data of force curves (force as a function of displacement) were then shifted by adding the abscissa intercept point of the linear fit (negative value). This procedure is based on our previous analysis and theoretical calculation that demonstrated the linear behaviour of force curve is related to the turgor pressure of the cell. Thus, such shift locates the zero displacement (contact point) just above the cytoplasmic region, in other words when the tip touch the inner membrane. Finally, the 5 nm thickness was also adding to the X-data of force curves to position the contact point between the AFM tip and the cell at the surface of the thin polyelectrolyte polymer layer. As discussed previously, this value of 5 nm considers the interface as homogeneous in a first attempt. Figure 10 shows a typical force curve shifted from these two values revealing non linear surface force forces. The previous calculations of electrostatic interaction between the AFM tip and the bacteria described in section 4.2. are compared with the experimental data in the bottom panel of Figure 10 for the two aforementioned assumptions, homogeneous (solid line) or diffuse (dotted line). Surprisingly, the theoretical electrostatic interactions are of the same order of magnitude as the experimental ones. It is important to point out that no fitting procedure has been made to adjust the theoretical calculations which were computed only on the basis of the electrokinetic characteristics. Therefore, such agreement between the theory and the experimental data demonstrates the potentiality to combine the microelectrophoresis with soft analysis calculations to quantify the electrostatic interactions involved in AFM force curves. In addition, the bottom panel of Figure 10 shows that the negative displacement range between 0 and -30 is not well described by the linear fit. This is probably consistent with the diffuse assumption because our previous electrokinetic calculation mentioned that the polyelectrolyte polymer layer in this condition could swell to an extent of 11.5 nm (2.3α) as calculated from the diffuse parameter (α = 5 nm) leading to a thickness for the cell wall close to 16.5 nm which is very close to the non linear behaviour observed in such negative domain. Therefore, the diffuse assumption could be one of the explanations for this discrepancy. At 100 mM, the nanomechanical properties could be directly quantified from the indentation curve as no significant electrostatic interactions are expected. Figure 11 illustrates one of these analyses by combining the Hertz model for the non-linear behaviour and a Hooke's law for the linear one (Eq. 15). As mentioned previously, the non-linear domains as reproduced by the Hertz fit were very important and reached the half part of the bacteria (200 nm). This effect demonstrated the significant impact of ionic strength on the turgor pressure of the cell.

Notice that some experiments have been carried out by changing the salt level *in situ* on the same sample from 1 mM to 100 mM. The same area have been probed to analyse the best the same bacteria. The same trend was observed that is to say the nanomechanical and viscoelastic properties significantly decreased upon the increase of ionic strength. All the relevant mechanical parameters are reported in Table 2.

Table 1: Critical concentrations c_c^{∞} deduced from the deviation of the homogeneous doted lines to the experimental data (Figs 4 and 5).

	MR-4		CN32	
pH	c_c^{∞} (mM)	Π_{el} (N m^{-2} /2RTV)	c_c^{∞} (mM)	Π_{el} (N m^{-2} /2RTV)
4	2 ± 1	0.042	15 ± 5	0.05
7	4 ± 2	0.042	15 ± 5	0.10
10	15 ± 5	0.042	70 ± 10	0.14

Table 2: Relevant parameters extracted from the analysis of force and/ or indentation curves for CN32 strain (n=50).

	Ionic strength	
	1 mM	100mM
Force hysteresis area (m.N)	227 ± 92	398 ± 111
E (kPa)	ND	38 ± 12
K_{Bact} (N/m)	0.122 ± 0.026	0.015 ± 0.001

Figure Captions:

Figure 1: Schematic representation of the cross section a cylindrical bacteria considered as a soft particle, composed of a hard-core of radius a_c and a permeable charged polyelectrolyte layer of thickness δ, moving with a velocity $\vec{U}$ in an electrolyte subjected to a dc electric field $\vec{E}$. The polar coordinates (r,θ) are indicated. The electrophoretic mobility μ is defined as the ratio U/E. For the sake of illustration, a scheme of a soft diffuse interface is given.

Figure 2: Schematic diagrams representing the interactions between a hard spherical AFM tip and a soft rod-like bacteria. (A) Schema of the potential interactions and the characteristic distances involved in the interactions. (B) Geometrical representation of Derjaguin approximation in the cylindrical-sphere interactions.

Figure 3: Experimental (filled circles) and theoretical (doted lines) electrophoretic mobilities (expressed in dimensionless form) at neutral pH of (A) *S. oneidensis* strain MR4 and (B) *S. putrefaciens* CN32. All the theoretical calculations correspond to the homogeneous description of the permeable polyelectrolyte layer (α=0). Those different approaches were computed with λ_0^{-1}=3.5 nm for MR-4 and λ_0^{-1}=2.0 nm for CN32.

Figure 4: *S. oneidensis* MR4 electrophoretic mobilities (expressed in dimensionless form) as a function of ionic strength (filled circles) for three different pH. (A: pH 4, B: pH 7, C: pH 10). The dotted lines represent the numerical evaluation with λ^{-1} = 3.5 nm, δ = 90 nm and with different ρ_0 following the pH (A: ρ_0 = -8 mM, B: ρ_0 = -10 mM, C: ρ_0 = -17 mM) for increasing α/δ values (A: 0 to 0.05, B: 0 to 0.06, C: 0 to 0.11) to adequately consider the diffuse character of the soft layer expressed at low ionic strength. Under c_c^{∞}, the critical ionic strength, the heterogeneity of the polymer must be considered to adequately fit the experimental data.

Figure 5: *S. putrefaciens* CN32 electrophoretic mobilities (expressed in dimensionless form) as a function of ionic strength (filled circles) for three different pH. (A: pH 4, B: pH 7, C: pH 10). The dotted lines represent the numerical evaluation developed with λ^{-1} = 2 nm, δ = 5 nm and with different ρ_0 following the pH (A: ρ_0 = -25 mM, B: ρ_0 = -35 mM, C: ρ_0 = -70 mM), for increasing α/δ values (A: 0 to 1.4, B: 0 to 1.0, C: 0 to 2.4) to adequately consider the diffuse character of the soft layer expressed at low ionic strength. Under c_c^{∞}, the critical ionic strength, the heterogeneity of the polymer must be considered to adequately fit the experimental data.

Figure 6: f (r), the local distribution of the polymer segment density within the soft surface layer, is plotted as a function of the distance from the hard core surface (r-a) normalized to the thickness of the soft layer (δ). The dotted line (step function) represents the limit case of a homogeneous soft layer for α/δ equal to 0. α denoted the typical decay length of the polymer density across the interface. The solid lines give the solution for the α/δ values indicated next to the curve. A: MR4 ; B: CN32.

Figure 7: Osmotic pressure within the polymer as a function of the ionic strength. No swelling is observed under the critical pressure $\Pi_{el,c}$. The critical pressure is reached for a given ionic strength named critical concentration c_c^{∞} Figure 6A gives the osmotic pressure profile of MR4 and figure 6B for CN32. Note that the pH the c_c^{∞} deduce from an unique $\Pi_{el,c}$ are in the same range than the c_c^{∞} shown on figure 3 and 4.

Figure 8: Theoretical electrostatic interaction forces between the AFM tip and the two type of strains. The data were computed for MR-4 (A) in the case of homogeneous assumption (plain lines, $\alpha/\delta = 0$) for $c^{\infty} = 100$ mM with $\rho_0 = -10$ mM or $c^{\infty} = 1$ mM with $\rho_0 = -7$ mM; in the case of heterogeneous calculation (dotted line) for $c^{\infty} = 1$ mM with $\rho_0 = -10$ mM and $\alpha/\delta = 0.06$; for CN32 (B) in the case of homogeneous assumption (plain lines, $\alpha/\delta = 0$) for $c^{\infty} = 100$ mM with $\rho_0 = -35$ mM or $c^{\infty} = 1$ mM with $\rho_0 = -15$ mM; in the case of heterogeneous calculation (dotted line) for $c^{\infty} = 1$ mM with $\rho_0 = -35$ mM and $\alpha/\delta = 1$.

Figure 9: Typical force curves of *S. putrefaciens* CN32 in neutral pH at different potassium nitrate concentrations (A) 1 mM and (B) 100 mM. The panel (C) represents the difference between the forward and reverse curves at the two salt conditions.

Figure 10: Theoretical interpretation of the forward force curve for *S. putrefaciens* CN32 at low salt level (1 mM). The top panel shows the solid line (Equation 16) that reproduces the linear behaviour of force curve due to turgor pressure of the cell and the bottom panel magnifies the contact region to compare the experimental data with the electrostatic interaction forces computed in section 4.2 (Figure 8, panel B) by using an homogeneous assumption (solid line) or heterogeneous one (dotted line). The raw force curve was shifted by the X intercept point of the linear fit and the assumed thickness of the cell wall ($\delta = 5$ nm), see text for explanation.

Figure 11: Theoretical interpretation of the indentation curve for *S. putrefaciens* CN32 at high level (100 mM). The experimental data were fitted by summing the Hertz model (dashed line) and linear behaviour (dotted line) using Eq. (15) to reproduce the complete curve as solid line. In this typical force curve, best fitting was achieved for an E of 40 kPa and a k_{Bac} of 0.0175 N/m.

Figure 1

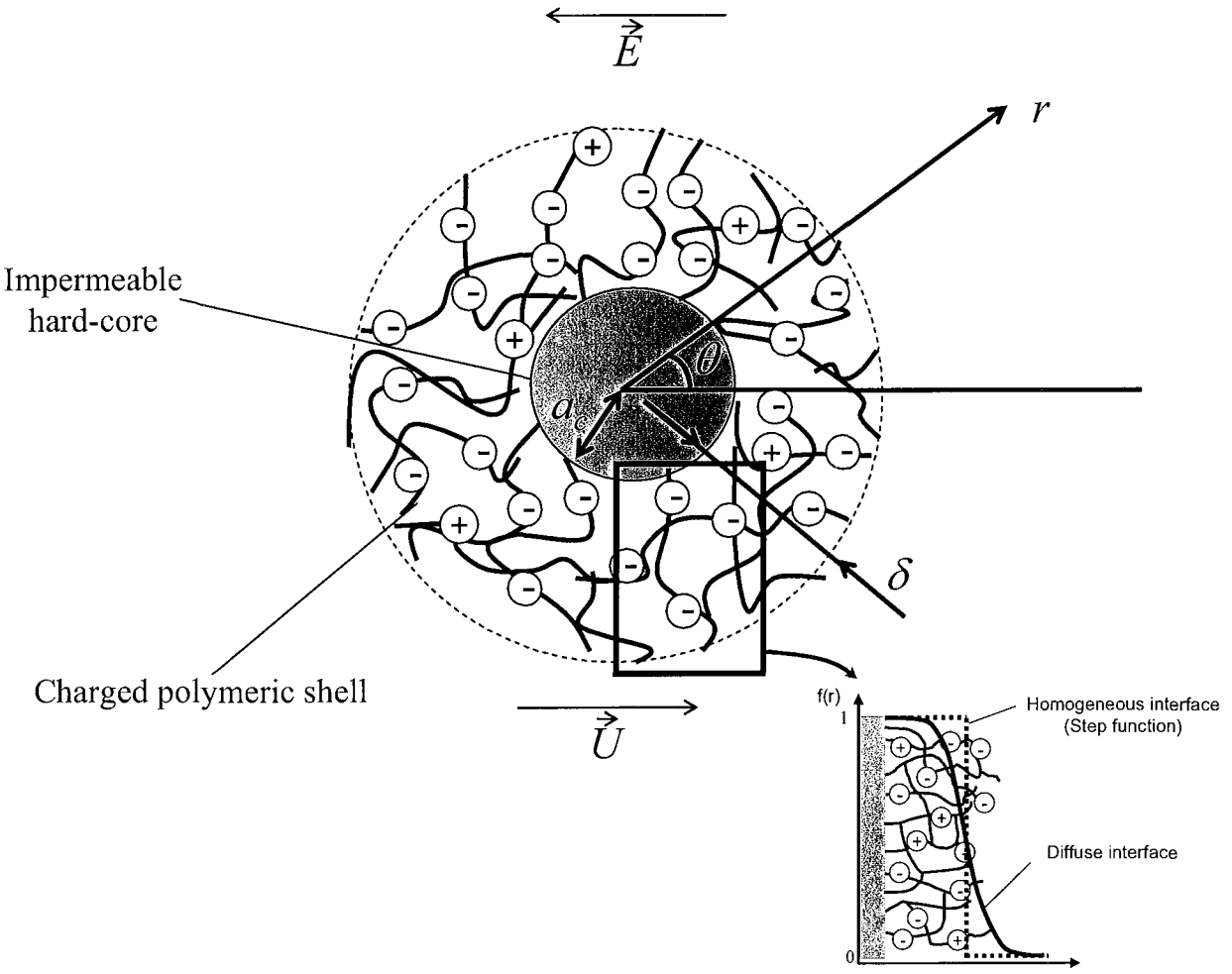
$\vec{E}$
r
Impermeable
hard-core
θ
a_c
δ
Charged polymeric shell
$\vec{U}$
f(r)
1
0
Homogeneous interface
(Step function)
Diffuse interface

Figure 2

(A)

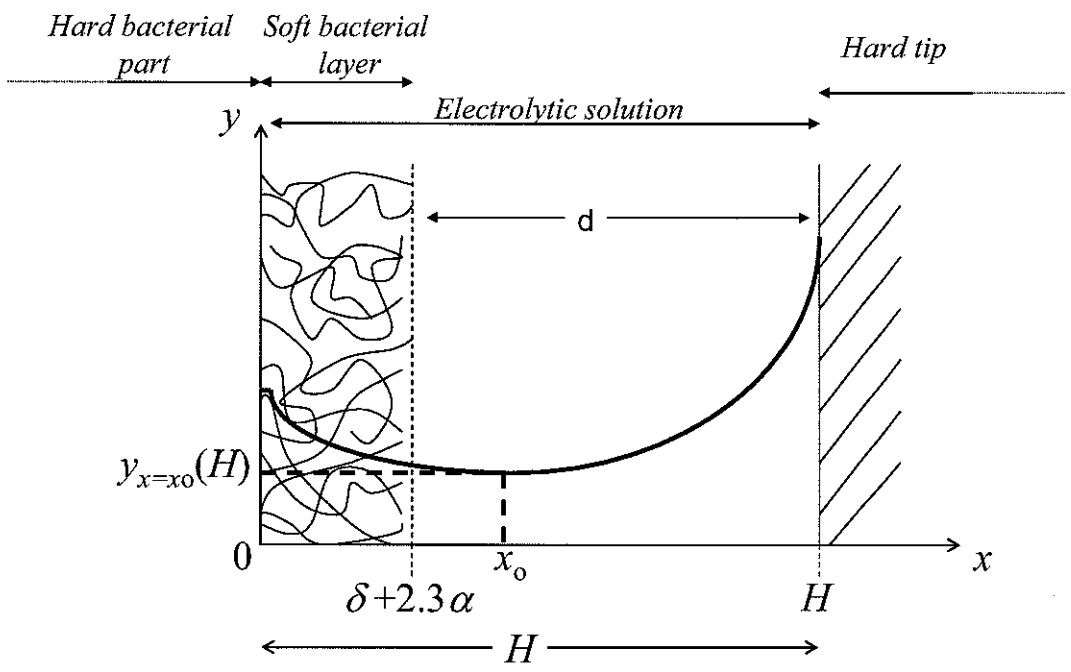

(B)

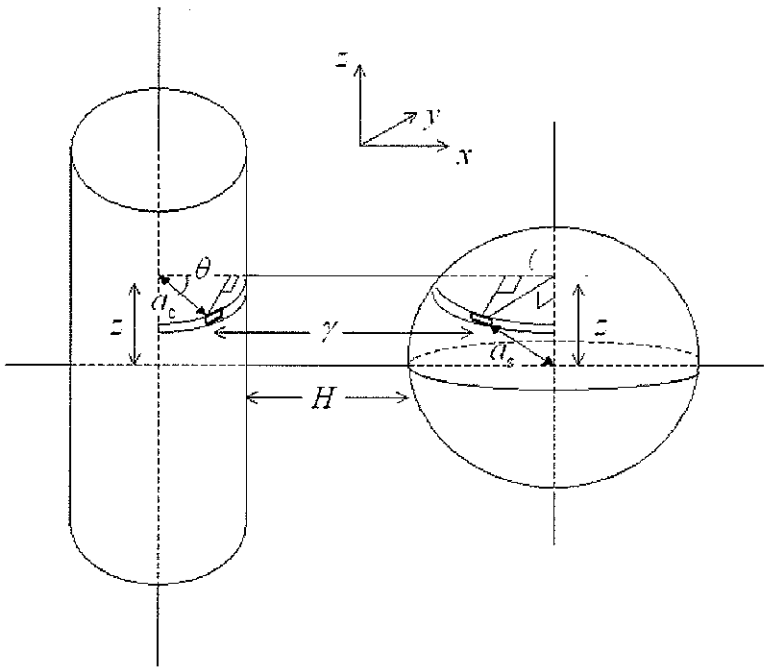

Figure 2

Figure 3

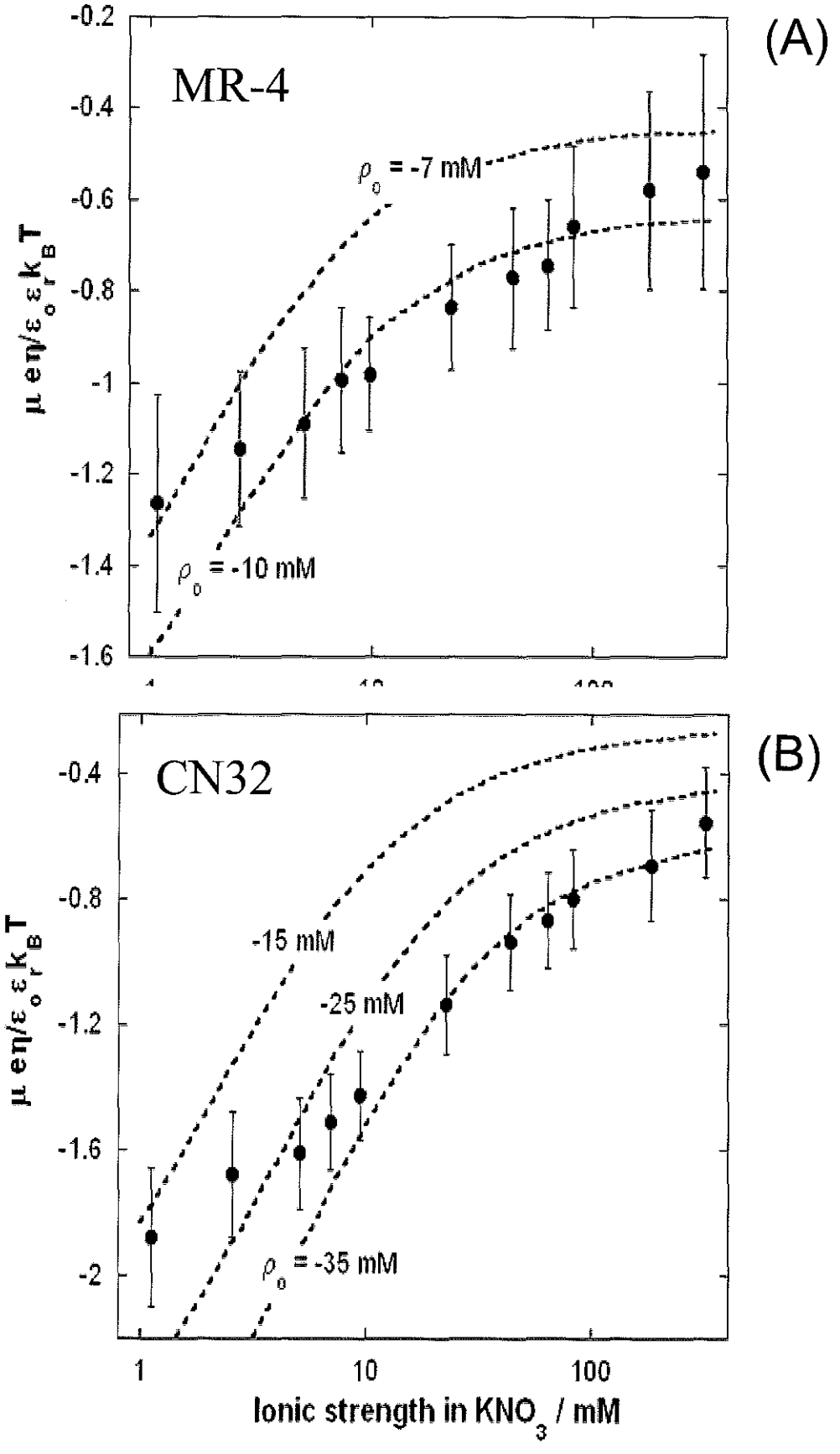
(A)
MR-4
ρ_0 = -7 mM
ρ_0 = -10 mM
-0.2
-0.4
-0.6
-0.8
-1
-1.2
-1.4
-1.6
μ e$\eta/\varepsilon_o \varepsilon_r k_B T$
(B)
CN32
-15 mM
-25 mM
ρ_0 = -35 mM
-0.4
-0.8
-1.2
-1.6
-2
1
10
100
Ionic strength in KNO_3 / mM

Figure 4 MR-4

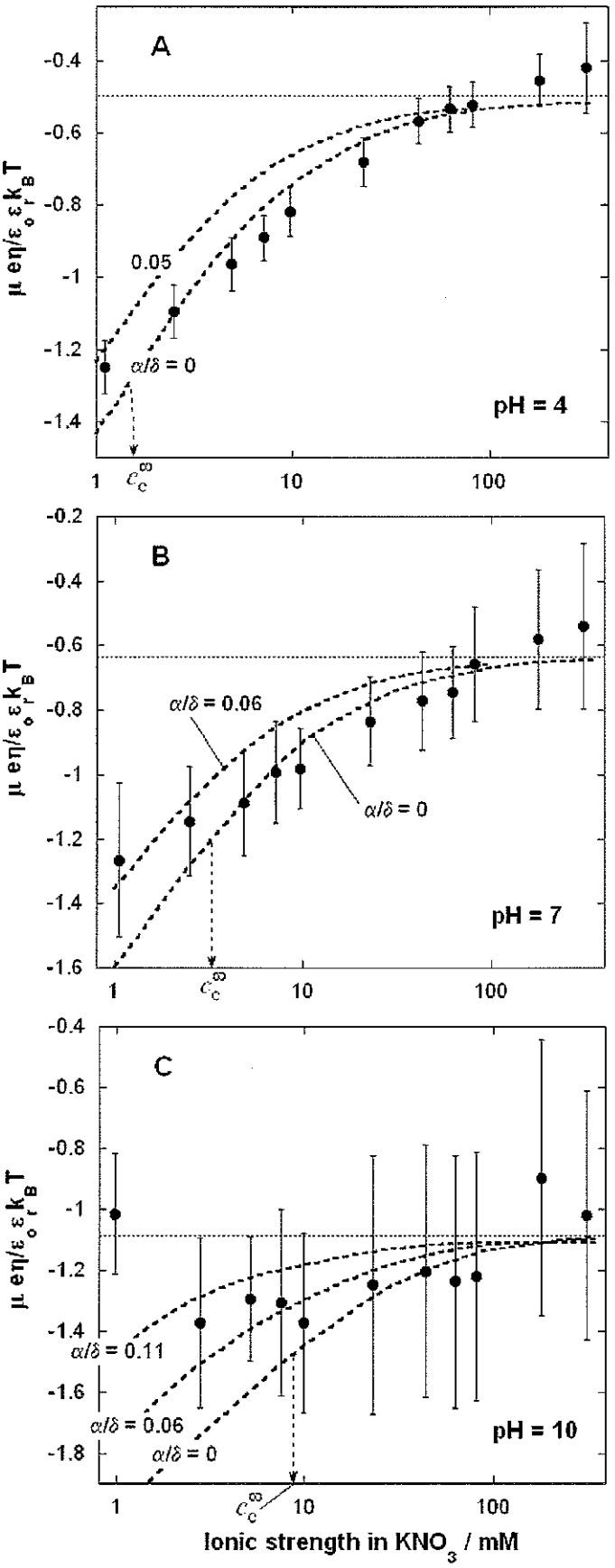
A
B
C
pH = 4
pH = 7
pH = 10
0.05
α/δ = 0
α/δ = 0.06
α/δ = 0.11
c_c^∞
μ eη/ε$_o$ε$_r$k$_B$T
Ionic strength in KNO$_3$ / mM

Figure 5 CN32

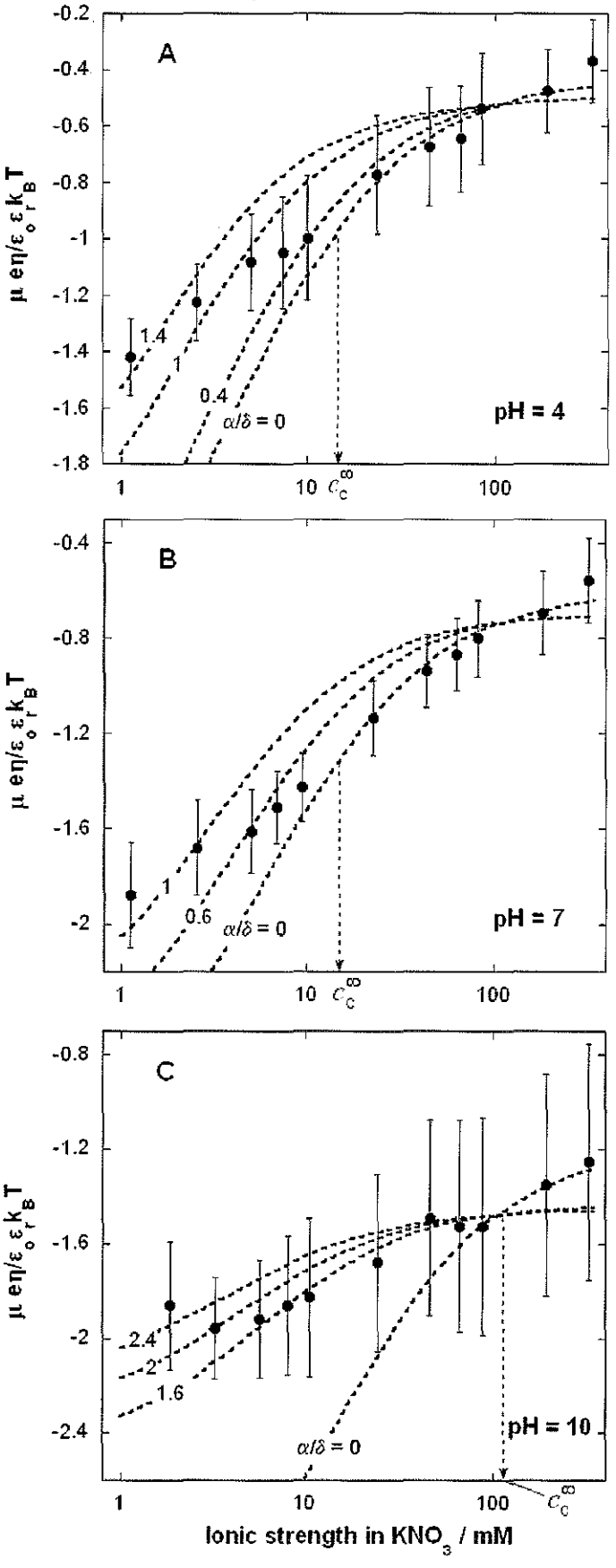

Figure 6

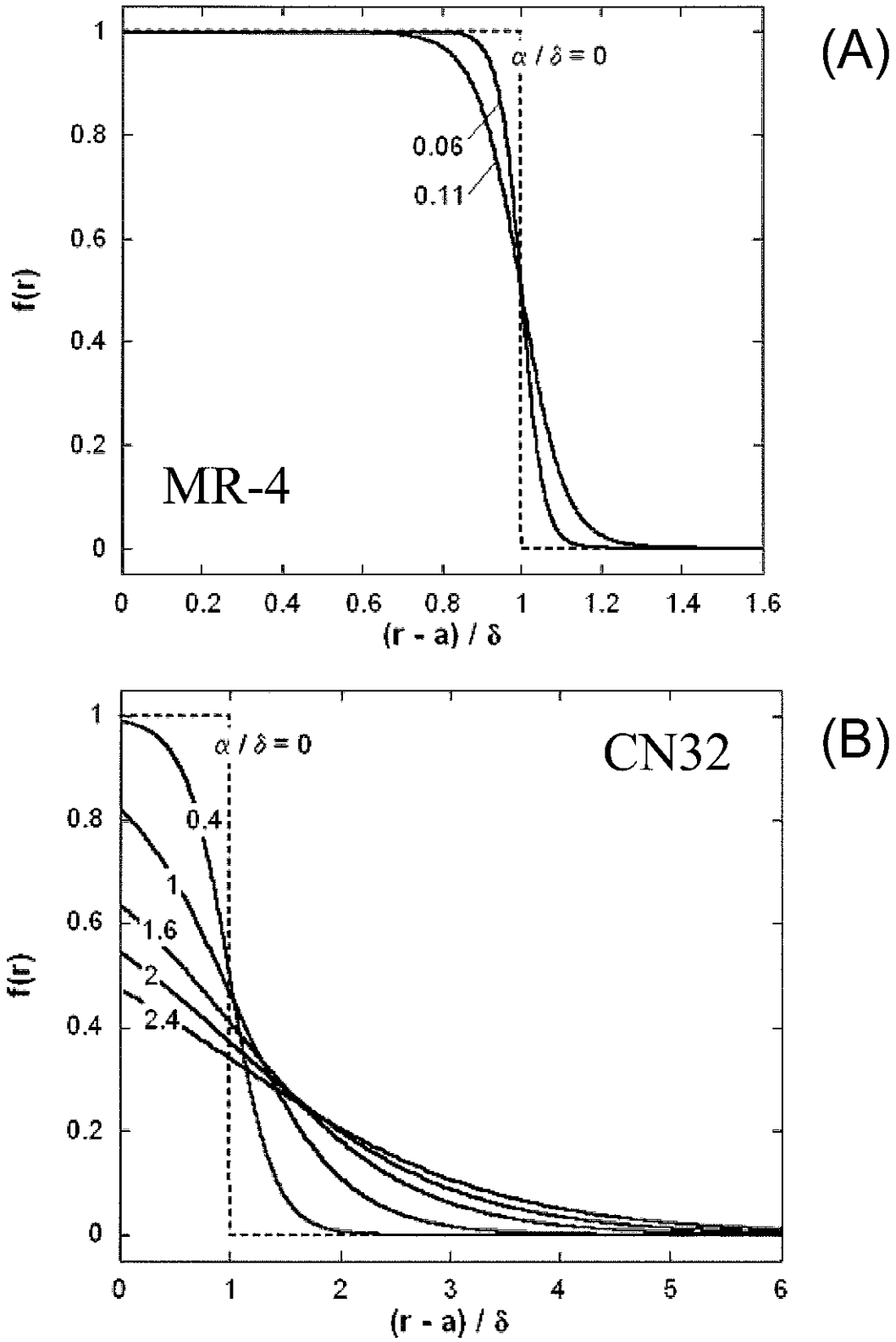

Figure 7

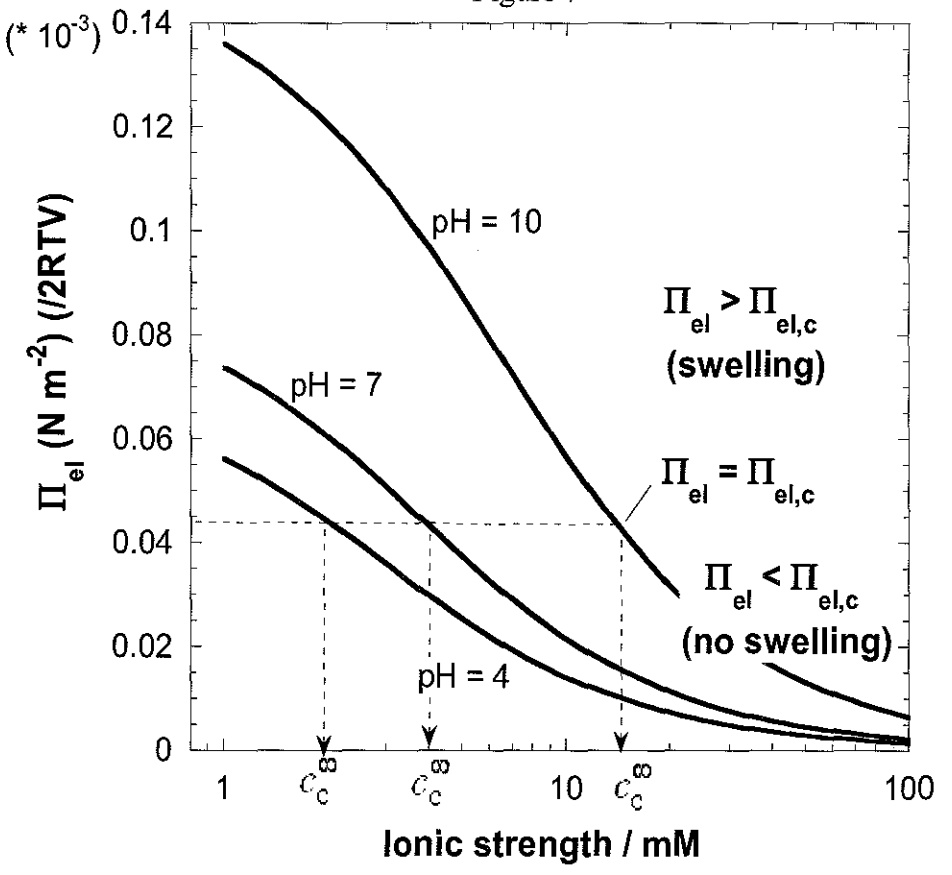
(* 10-3)
0.14
0.12
0.1
0.08
0.06
0.04
0.02
0
Πel (N m-2) (/2RTV)
pH = 10
pH = 7
pH = 4
Πel > Πel,c
(swelling)
Πel = Πel,c
Πel < Πel,c
(no swelling)
1
10
100
Ionic strength / mM

(A)

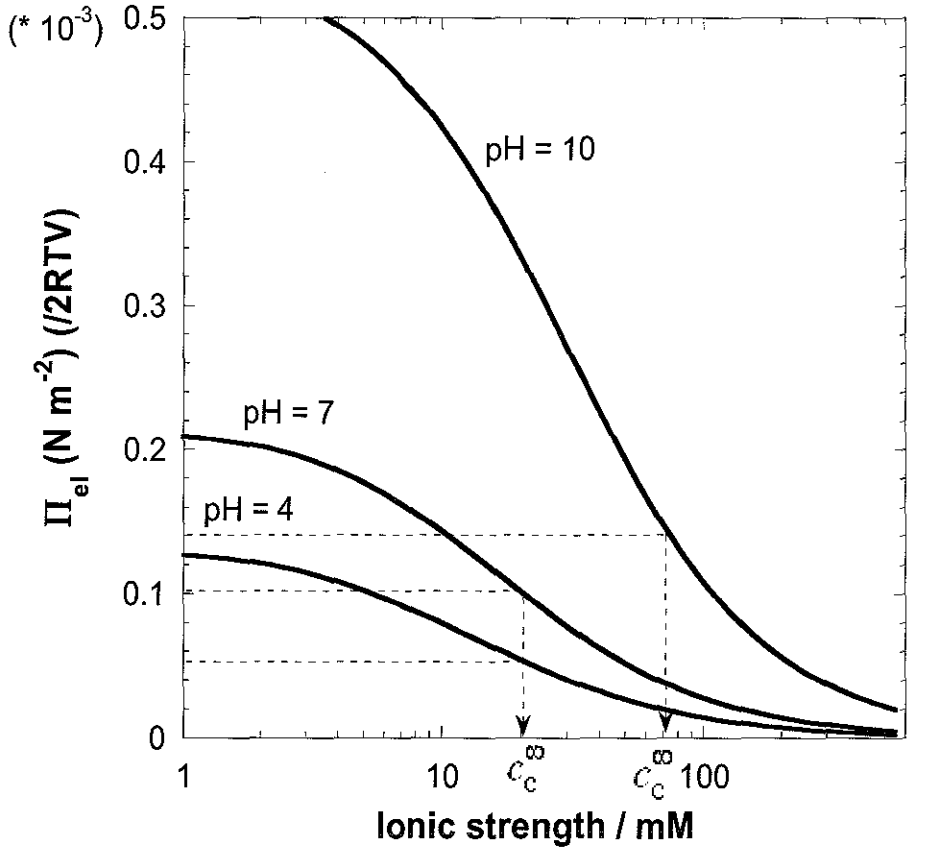
(* 10-3)
0.5
0.4
0.3
0.2
0.1
0
Πel (N m-2) (/2RTV)
pH = 10
pH = 7
pH = 4
1
10
100
Ionic strength / mM

(B)

Figure 8

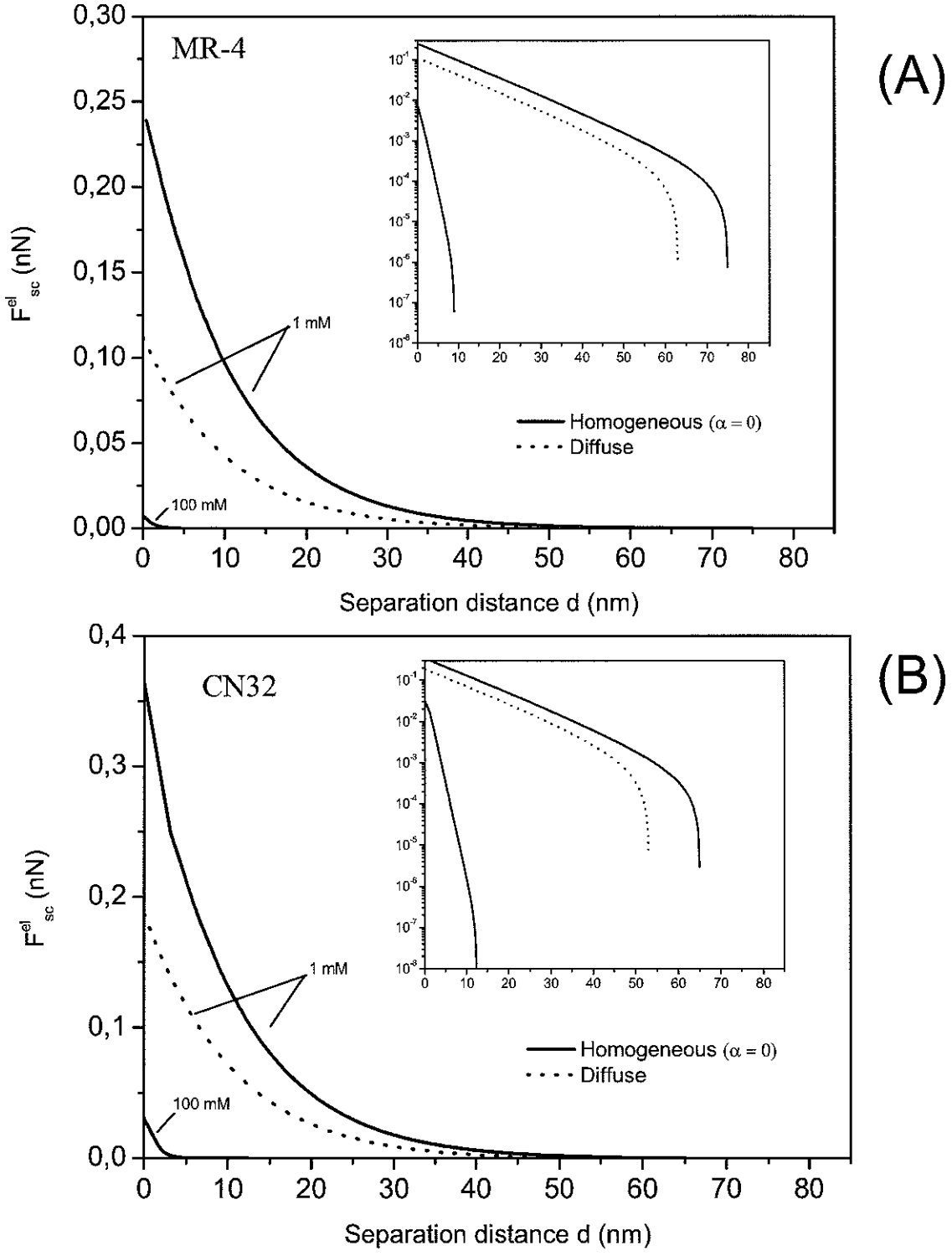
(A)
MR-4
F^{el}_{sc} (nN)
1 mM
100 mM
Homogeneous (α = 0)
Diffuse
Separation distance d (nm)
(B)
CN32
F^{el}_{sc} (nN)
1 mM
100 mM
Homogeneous (α = 0)
Diffuse
Separation distance d (nm)

Figure 9

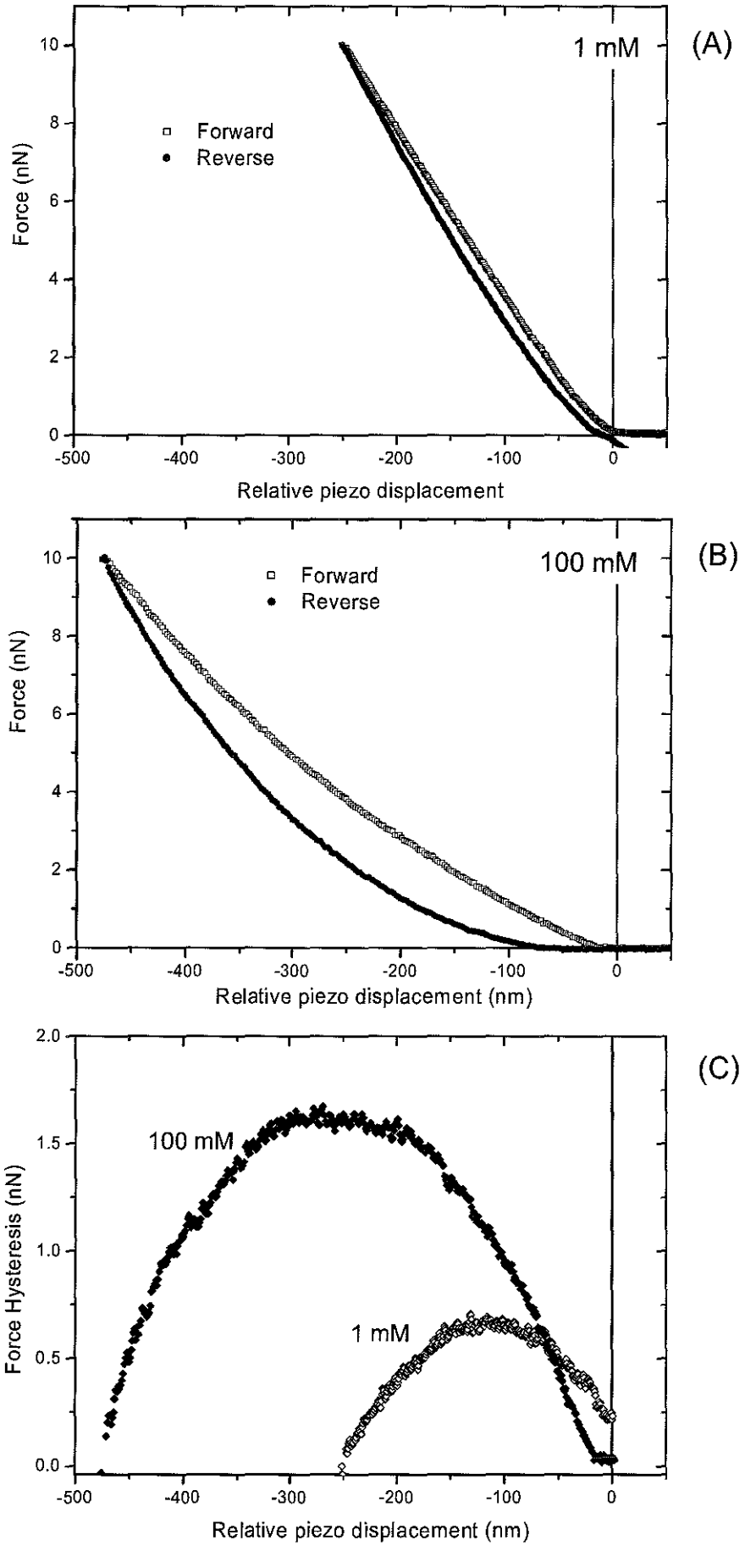
1 mM
(A)
Forward
Reverse
Force (nN)
Relative piezo displacement
100 mM
(B)
Forward
Reverse
Force (nN)
Relative piezo displacement (nm)
(C)
100 mM
1 mM
Force Hysteresis (nN)
Relative piezo displacement (nm)

Figure 10

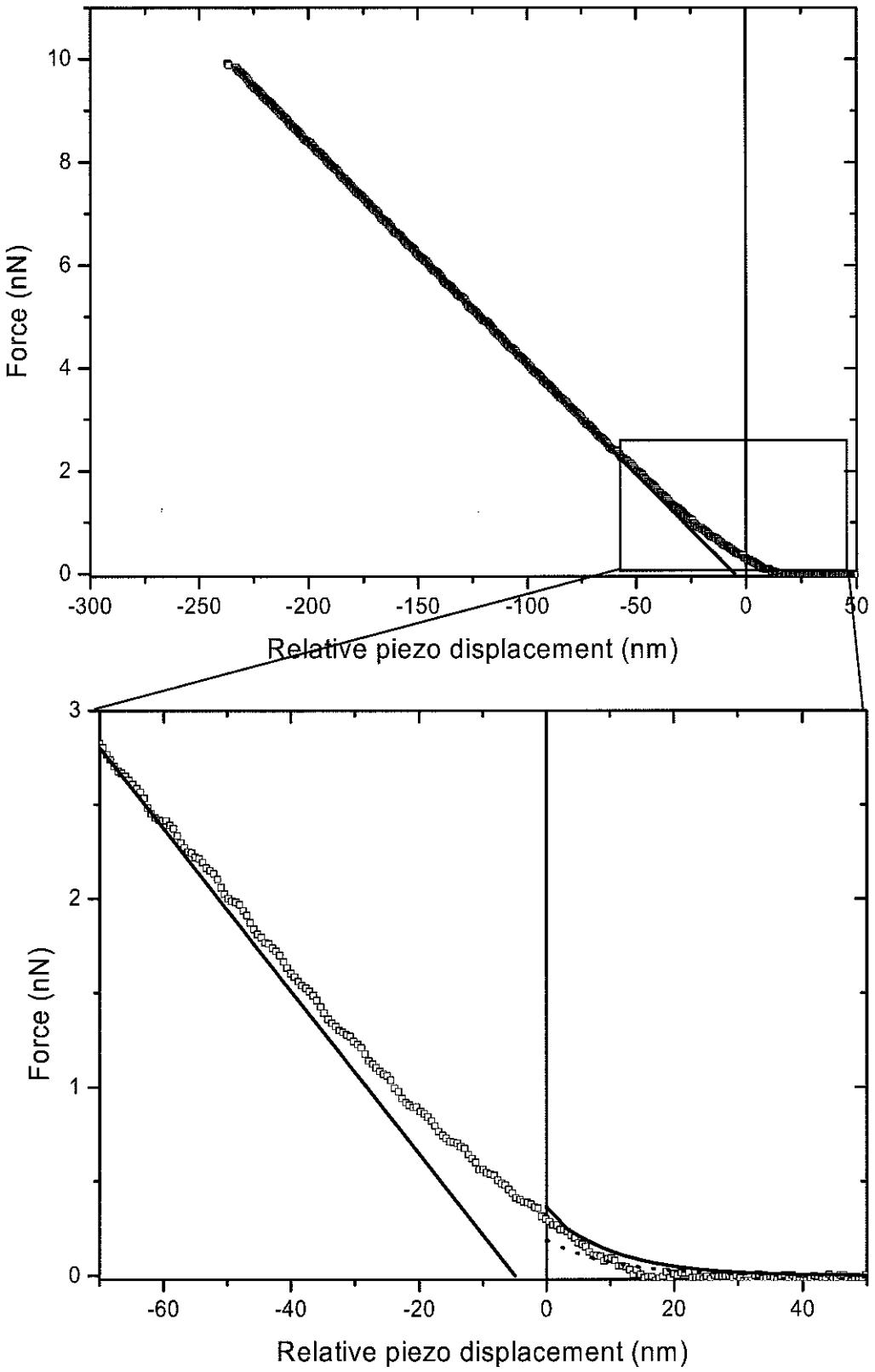
Force (nN)
Relative piezo displacement (nm)
Force (nN)
Relative piezo displacement (nm)

Figure 11

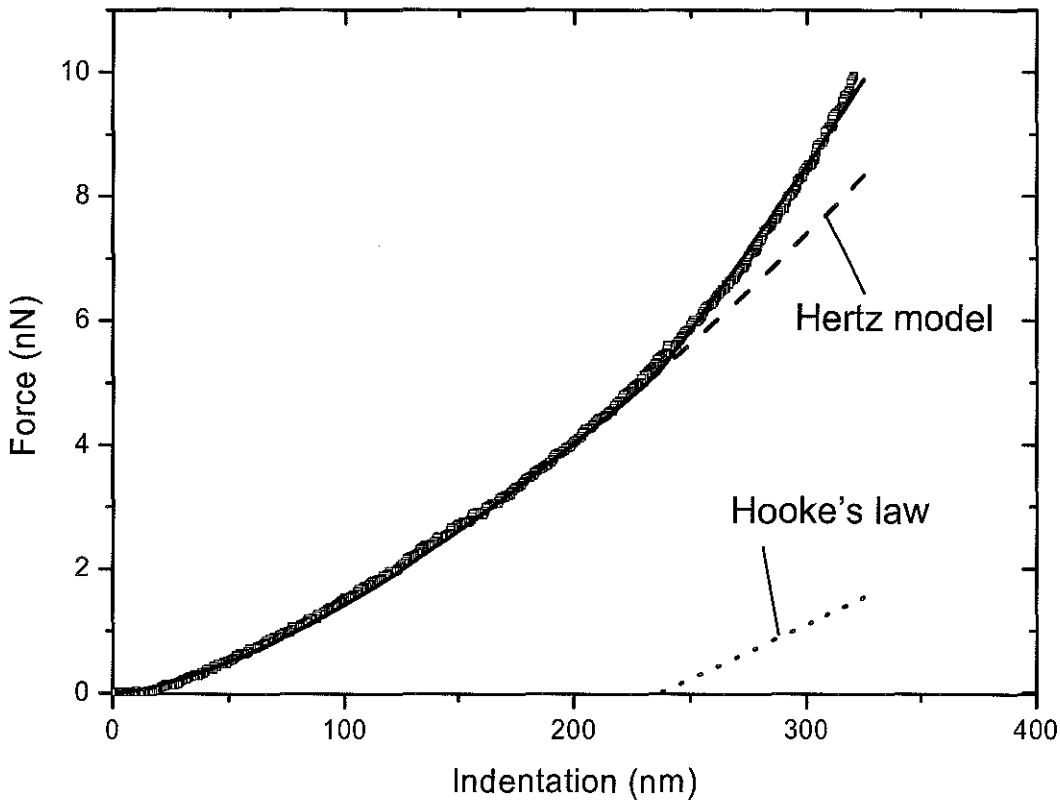
Force (nN)
Indentation (nm)
Hertz model
Hooke's law
0
2
4
6
8
10
0
100
200
300
400

Appendix 1.

The general solution of the linearized Poisson-Boltzmann equation (7) may be written in the form

$$y(x) = A\cosh(\kappa x) + B\sinh(\kappa x) + \frac{\cosh(\kappa x)}{\kappa}\int_0^x g(x)\sinh(\kappa x)\,dx + \frac{\sinh(\kappa x)}{\kappa}\int_0^x g(x)\cosh(\kappa x)\,dx \quad \text{(A1)}$$

where A and B are integration constants and g the function defined by

$$g(x) = \frac{\rho_o \omega}{4c^\infty F}\left\{1 - \tanh\left(\frac{x-\delta}{\alpha}\right)\right\} \quad \text{(A2)}$$

The boundary conditions expressed by eqs 8 and 9 yield

$$A = \frac{y_s^o}{\cosh(\kappa H)} - \frac{1}{\kappa}\int_0^H g(x)\sinh(\kappa x)\,dx + \frac{\tanh(\kappa H)}{\kappa}\int_0^H g(x)\cosh(\kappa x)\,dx \quad \text{(A3)}$$

and

$$B = 0 \quad \text{(A4)}$$

Using (A1), one easily shows that the position $x_o \neq 0$ $(\delta < x_o < H)$, defined by $dy/dx\big|_{x=x_o} = 0$, is the solution of the transcendental integral equation written

$$\tanh(\kappa x_o) = \frac{\int_0^{x_o} g(x)\cosh(\kappa x)\,dx}{\kappa A + \int_0^{x_o} g(x)\sinh(\kappa x)\,dx} \quad \text{(A5)}$$

In the case of homogenous distribution of the charges throughout the soft surface layer of thickness δ, we have $\omega = 1$, $g(x) = \frac{\rho_o}{2c^\infty F}$ for $0 < x < \delta$ and $g(x) = 0$ for $\delta < x < H$. The various integral terms in eqs (A3) and (A5) may be analytically computed. After some arrangement, one obtains

$$y(x)\big|_{\alpha\to 0} = \frac{\cosh(\kappa x)}{\cosh(\kappa H)}\left(y_s^o + \frac{\rho_o}{2c^\infty F}\sinh(\kappa H)\sinh(\kappa\delta)\right) - \frac{\rho_o}{2c^\infty F}\sinh(\kappa x)\sinh(\kappa\delta) \quad \text{(A6)}$$

and the H-dependence of x_o is explicitly given by

$$\tanh(\kappa x_o)\big|_{\alpha\to 0} = 1/\left[\tanh(\kappa H) + \frac{2y_s^o F c^\infty}{\rho_o \sinh(\kappa\delta)}\operatorname{sech}(\kappa H)\right] = -1/\Phi(H) \quad \text{(A7)}$$

where Φ is defined by eq 11.

The potential $y(x = x_o)\big|_{\alpha\to 0}$ may then be expressed as follows

$$y(x = x_o)\big|_{\alpha\to 0} = -\frac{\rho_o}{2Fc^\infty}\sinh(\kappa\delta)\sinh(\kappa x_o)\left(1 - \coth^2(\kappa x_o)\right) \quad \text{(A8)}$$

Using the relationship $\sinh(\kappa x_o) = \tanh(\kappa x_o)/\left(1 - \tanh^2(\kappa x_o)\right)^{1/2}$, the combination of (A7) and (A8) leads to

$$y(x=x_o)\big|_{\alpha\to 0} = \frac{1}{\left(-1+\coth^2(\kappa x_o)\right)^{1/2}} \tag{A9}$$

For sufficiently small potentials consistent with a Debye-Huckel treatment, linearization of eq 6 provides

$$\Pi_{pp}(H) = RTc^{\infty}\left\{y_{x=x_o}(H)\right\}^2 \tag{A10}$$

Combination of (A8), (A9), (A10) and eq 4 yields the expressions given by eqs 10-11.

Appendix 2.

As shown in Figure 2B, the differential surface element chosen on the cylindrical particle and the corresponding surface element projected on the sphere have the same facing area of $a_c \mathrm{d}z\mathrm{d}\theta$ with θ and z as indicated in Figure 2B. Within the framework of Derjagin's approach, the electrostatic component of the Gibbs interaction energy between those surface elements is given by $U_{pp}(\gamma)a_c \mathrm{d}z\mathrm{d}\theta$ with γ the separation distance between the surface elements aforementioned and U_{pp} as defined by eq 4. On the basis of simple geometric considerations, one easily shows the following relationship

$$\gamma(H,z,\theta) = H + a_c - a_c\cos\theta + a_s - \ell \tag{A11}$$

with ℓ as specified in Figure 2B and given by

$$\ell = \left(a_s{}^2 - z^2 - (a_s\sin\theta)^2\right)^{1/2} \tag{A12}$$

Combining eqs A11 and A12 yields eq 13 in the text. The electrostatic component of the Gibbs interaction energy between the cylinder and the sphere, denoted as U_{sc}, is then given by eq 12 where the prefactor 4 stems from the axisymmetry of the integration range in the θ-direction. Since the radii of the cylinder and the sphere are not too much different in our study, integration over the pertaining ranges of θ and z should be done following the conditions $\ell \in [0, a_s]$ and $a_s{}^2 - z^2 - (a_s\sin\theta)^2 > 0$. Any coordinates (θ, z) that do not match those conditions physically correspond to situations where the surface element on the cylinder does not have a projected counterpart on the sphere or that the latter is situated in the region of the sphere that does not face the cylinder (and thus does not contribute to U_{sc}).

Appendix 3.

In the spatial domain where the local polymer segment density distribution f (eqs 1 and 22) is zero, eq 30 reduces to

$$L_r\left\{L_r h(r)\right\} = G(r), \quad r > r^* \tag{A13}$$

with G given by

$$G(r) = -\frac{F}{\eta}\frac{1}{r}\frac{\mathrm{d}y(r)}{\mathrm{d}r}\sum_i c_i^{\infty} z_i{}^2 \exp\left\{-z_i y(r)\right\}\chi_i(r) \tag{A14}$$

and r^* is the radial position that marks the "boundary" between the outer edge of the polymeric fringe surrounding the bacteria and the electrolytic solution. At $r = a + \delta + 2.3\alpha$, the polymer segment density is about 1 % of that reached at the position $r = a$ and the value $\delta + 2.3\alpha$ thus provides a good estimation of r^*. First integration of eq A13 provides

$$L_r h(r) = \frac{r}{2}\int_{\infty}^{r} G(r)\mathrm{d}r - \frac{1}{2r}\int_{\infty}^{r} r^2 G(r)\mathrm{d}r + \frac{C_1}{2}r + \frac{C_2}{r}, \quad r > r^* \tag{A15}$$

with $C_{1,2}$ constants. Second integration of eq A13 yields

$$h(r)=\frac{r^3}{16}\int_{\infty}^{r}G(r)\mathrm{d}r-\frac{1}{16r}\int_{\infty}^{r}r^4G(r)\mathrm{d}r-\frac{r\ln r}{4}\int_{\infty}^{r}r^2G(r)\mathrm{d}r+\frac{r}{4}\int_{\infty}^{r}r^2\ln rG(r)\mathrm{d}r+$$
$$\frac{C_1}{16}r^3+\frac{C_2}{2}\left(r\ln r-\frac{r}{2}\right)+\frac{C_3}{2}r+\frac{C_4}{r},\quad r>r^* \tag{A16}$$

with $C_{3,4}$ constants. The hydrodynamic force $\vec{\Im}_{\mathrm{H}}$, as defined by eq 38, is given by

$$\vec{\Im}_{\mathrm{H}}=Lr\int_{0}^{2\pi}\left(\sigma_{rr}^{\mathrm{H}}\cos\theta-\sigma_{r\theta}^{\mathrm{H}}\sin\theta\right)\mathrm{d}\theta\frac{\vec{E}}{\left\|\vec{E}\right\|} \tag{A17}$$

where σ_{rr}^{H} and $\sigma_{r\theta}^{\mathrm{H}}$ are the radial and tangential components of the hydrodynamic stress tensor and p the pressure . In cylindrical geometry, σ_{rr}^{H} and $\sigma_{r\theta}^{\mathrm{H}}$ are given by

$$\sigma_{rr}^{\mathrm{H}}=-p+2\eta\frac{\partial u_r}{\partial r} \tag{A18}$$

and

$$\sigma_{r\theta}^{\mathrm{H}}=\eta\left[r\frac{\partial\left(u_\theta/r\right)}{\partial r}+\frac{1}{r}\frac{\partial u_r}{\partial\theta}\right], \tag{A19}$$

respectively. Substituting for u_r and u_θ the expressions of the radial and azimutal components of the vector field $\vec{u}$ defined by eq 26, one infers

$$\sigma_{rr}^{\mathrm{H}}=-p+2\eta E\cos\theta\left(-\frac{1}{r}\frac{\mathrm{d}h(r)}{\mathrm{d}r}+\frac{h(r)}{r^2}\right) \tag{A20}$$

$$\sigma_{r\theta}^{\mathrm{H}}=\eta E\sin\theta\left(\frac{\mathrm{d}^2h(r)}{\mathrm{d}r^2}-\frac{1}{r}\frac{\mathrm{d}h(r)}{\mathrm{d}r}+\frac{h(r)}{r^2}\right), \tag{A21}$$

In the far field domain $r>>r^*$, there is not net electrical charge, that is $\rho_{\mathrm{el}}^{(0)}(r\to\infty)=0$ and $c_{\mathrm{i}=1,\ldots,\mathrm{N}}^{(0)}(r\to\infty)=c_{\mathrm{i}}^{\infty}$ where $\rho_{\mathrm{el}}^{(0)}$ and $c_{\mathrm{i}=1,\ldots,\mathrm{N}}^{(0)}$ are the equilibrium space charge densities due to the mobile ionic species and ionic concentrations, respectively. From eq 23, one thus derives

$$\nabla p(\vec{r})=-\eta\nabla\times\nabla\times\vec{u}(\vec{r}),\quad r>r^* \tag{A22}$$

After some rearrangement, the right hand side of eq A22 is written

$$\nabla\times\nabla\times\vec{u}(\vec{r})=\left(\frac{L_rh(r)}{r}E\cos\theta,-\frac{\mathrm{d}}{\mathrm{d}r}\left(L_rh(r)\right)E\sin\theta,0\right) \tag{A23}$$

so that integration of eq A22 at fixed r gives

$$p=\eta r\frac{\mathrm{d}}{\mathrm{d}r}\left(L_rh(r)\right)E\cos\theta+p_{\mathrm{o}},\quad r>r^* \tag{A24}$$

with p_{o} the pressure far from the particle. The quantities σ_{rr}^{H} and $\sigma_{r\theta}^{\mathrm{H}}$ (eqs A20 and A21) can be rewritten in term of the asymptotic developments of $L_rh(r)$ and $h(r)$ given in eqs A15 and A16, respectively. The results read as follows

$$\sigma_{rr}^{\mathrm{H}}=-p_{\mathrm{o}}+\eta E\cos\theta\left(\frac{4C_4}{r^3}-\frac{3C_1}{4}r\right),\quad r>r^* \tag{A25}$$

$$\sigma_{r\theta}^{\mathrm{H}}=\eta E\sin\theta\left(\frac{4C_4}{r^3}+\frac{C_1}{4}r\right),\quad r>r^* \tag{A26}$$

so that $\vec{\Im}_H$ (eq A17) is finally given by

$$\vec{\Im}_H = -C_1 L r^2 \pi \vec{E}, \quad r > r^* \tag{A27}$$

The condition $\vec{\Im}_H(r \to \infty) = 0$ imposes that $C_1 = 0$, which is in line with the far field behavior for h that is written $h(r \to \infty) \to \mu_\perp r + \Theta$. The latter expression further leads to $C_2 = 0$, $\Theta = 0$ and $C_3 = 2\mu_\perp$. As a result we have

$$h(r \to \infty) \to \mu_\perp r + \frac{C_4}{r} \tag{A28}$$

which is eq (39) in the main text.

REFERENCES

1. Bryers, J. D. *Biofilms II*, Wiley-Liss ed.; New York, 2000.
2. Hall-Stoodley, L.; Costerton, J. W.; Stoodley, P. *Nature Reviews Microbiology* **2004**, *2*, 95.
3. Ramey, B. E.; Koutsoudis, M.; von Bodman, S. B.; Fuqua, C. *Current Opinion in Microbiology* **2004**, *7*, 602.
4. Lloyd, J. R.; Lovley, D. R.; Machesky, M. L. *Advances in Applied Microbiology* **2002**, *53*, 85.
5. van Oss, C. J.; Chaudhury, M. K.; Good, R. J. *Chem.Rev.* **1988**, *88*, 927.
6. Strevett, K. A.; Chen, G. *Research in microbiology* **2003**, *154*, 329.
7. Duval, J. F. L.; Ohshima, H. *Langmuir* **2006**, *22*, 3533.
8. Duval, J. F. L.; Busscher, H. J.; van de Belt-Gritter, B.; van der Mei, H. C.; Norde, W. *Langmuir* **2005**, *21*, 11268.
9. Gaboriaud, F.; Dague, E.; Bailet, S.; Jorand, F.; Duval, J.; Thomas, F. *Colloids Surf.B: Biointerfaces* **2006**, *50*, 123.
10. Dague, E.; Duval, J.; Jorand, F.; Thomas, F.; Gaboriaud, F. *Biophys.J.* **2006**, *90*, 2612.
11. Butt, H. J.; Cappella, B.; Kappl, M. *Surf.Sci.Reports* **2005**, *59*, 1.
12. Gaboriaud, F.; Dufrêne, Y. F. *Colloids Surf.B: Biointerfaces* **2006**, *In press*.
13. Burks, G. A.; Velegol, S. B.; Paramonova, E.; Lindenmuth, B. E.; Feick, J. D.; Logan, B. E. *Langmuir* **2003**, *19*, 2366.
14. Duval, J. F. L.; Van Leeuwen, H. P. *Langmuir* **2004**, *20*, 10324.
15. Duval, J. F. L. *Langmuir* **2005**, *21*, 3247.
16. Korenevsky, A. A.; Vinogradov, E.; Gorby, Y.; Beveridge, T. J. *App.Env.Microbiol.* **2002**, *68*, 4653.
17. Arnoldi, M.; Fritz, M.; Bäuerlein, E.; Radmacher, M.; Sackmann, E.; Boulbitch, A. *Phys.Rev.E* **2000**, *62*, 1034.
18. Duval J. F. L. 2006.
19. Ohshima, H. *J.Colloid Interface Sci.* **1994**, *163*, 474.
20. Ohshima, H. *Advances in Colloid and Interface Science* **1995**, *62*, 189.
21. Ohshima, H. *Colloid & Polymer Science* **2005**, *283*, 819.
22. Lopez-Garcia, J. J.; Grosse, C.; Horno, J. *J.Colloid Interface Sci.* **2003**, *265*, 327.
23. Lopez-Garcia, J. J.; Grosse, C.; Horno, J. *J.Colloid Interface Sci.* **2003**, *265*, 341.
24. Derjaguin, B. V. *Kolloid-z* **1934**, *69*, 155.
25. Lyklema J. *Fundamental of interfaces and colloid science: Particulate colloids*; 2005; Chapter 3.
26. Press, W. H.; Teukolsky, S. A.; Vetterling, W. T.; Flannerty, B. P. *Numerical recipes in fortran, the art of scientific computing*, 2nd ed.Cambridge University Press: New York, 1986.
27. Gaboriaud, F.; Bailet, S.; Dague, E.; Jorand, F. *J.Bacteriol.* **2005**, *187*, 3864.
28. Ducker, W. A.; Xu, Z.; Israelachvili, J. *Langmuir* **1994**, *10* , 3279.
29. Velegol, S. B.; Logan, B. E. *Langmuir* **2002**, *18*, 5256.
30. Rosenbluth, M. J.; Lam, W. A.; Fletcher, D. A. *Biophys.J.* **2006**, *90*, 2994.
31. Ohshima, H. *Colloids Surf.A: Physicochem.Eng.Aspects* **1995**, *103*, 249.
32. Hill, R. J.; Saville, D. A.; Russel, W. B. *J.Colloid Interface Sci.* **2003**, *258*, 56.
33. Hill, R. J.; Saville, D. A.; Russel, W. B. *J.Colloid Interface Sci.* **2003**, *263*, 478.
34. Hill, R. J.; Saville, D. A. *Colloids Surf.A: Physicochem.Eng.Aspects* **2005**, *267*, 31.
35. Hill, R. J. *Phys.Rev.E* **2004**, *70*, 051406-051406-16.
36. Duval, J. F. L.; Wilkinson, K. J.; Van Leeuwen, H. P.; Buffle, J. *Environ.Sci.Technol.* **2005**, *39*, 6435.

37. Duval, J. F. L.; Slaveykova, V. I.; Hosse, M.; Buffle, J.; Wilkinson, K. J. *Biomacromolecules* **2006**, *In press*.
38. Ohshima, H. *Colloid Polym.Sci.* **2001**, *279*, 88.
39. Ohshima, H. *J.Colloid Interface Sci.* **2003**, *258*, 252.
40. Fernandez-Nieves, A.; de las Nieves, F. J.; Fernandez-Barbero, A. *J.Chem.Phys.* **2004**, *120*, 374.
41. Masson, T. G.; Lin, M. Y. *Phys.Rev.E* **2005**, *71*, 040801-040801-4.
42. de Kerchove, A. J.; Elimelech, M. *Langmuir* **2005**, *21*, 6462.
43. De Keizer, A.; Van Der Drift, W. P. J. T.; Overbeek, J. T. *Biophys.Chem.* **1975**, *3*, 107.
44. Debye, P.; Bueche, A. M. *J.Chem.Phys.* **1948**, *16*, 573.
45. Brinkman, H. C. *Research* **1949**, *2*, 190.
46. Sangani, A. S.; Yao, C. *Physics of Fluids* **1988**, *31*, 2435.

6. Discussion générale, perspectives et conclusions

La physico-chimie à l'interface bactérie-eau est un domaine en évolution depuis au moins 20 ans. Certaines techniques ont montré leur limite (mesure de l'hydrophobie), d'autres sont apparues (AFM par exemple) avec comme attrait constant de mieux comprendre les phénomènes qui régissent l'adhésion des micro-organismes [17, 133]. Dans cette partie, nous discuterons d'abord les principaux résultats présentés dans ce mémoire. *Shewanella* ayant aussi été choisie en raison de sa capacité à réduire le Fe (III) en absence d'oxygène, nous aborderons ensuite les conséquences possibles des propriétés interfaciales bactérie-solution aqueuse sur la biominéralisation. Enfin nous évoquerons, en guise de perspectives, l'utilisation des acquis de ce travail sur d'autres systèmes biologiques, afin de répondre à des problématiques différentes.

6.1. Discussion autour des principaux acquis

Dans ce travail, nous avons abordé, de façon innovante, la question des propriétés nanomécaniques, des forces de surface et des caractéristiques hydrodynamiques des bactéries. La spectroscopie de force, appliquée aux bactéries est récente. En effet, l'analyse en spectroscopie de force a mis en évidence une modification des propriétés interfaciales des bactéries en réponse à des variations de pH ou de force ionique. Parallèlement, nous avons montré que ces variations des conditions physico-chimiques du milieu entraînent des modifications des capacités d'adhésion des cellules.

Alors qu'il est généralement admis que les interactions électrostatiques [134] jouent un rôle majeur dans les phénomènes d'adhésion, peu de travaux [135-137] consacrés à la mesure du potentiel de « surface » des bactéries considèrent l'interface molle que les micro-organismes présentent avec leur milieu environnant. La théorie décrivant le comportement d'une particule molle dans un champ électrique a été initiée à partir de 1994-1995 [91, 93] par Ohshima. Les développements théoriques réalisés au cours des dix dernières années ont progressivement éliminé les approximations liées à la modélisation. Les premiers modèles assimilaient les interfaces bactériennes à une surface plane recouverte d'une couche de polymères chargés [91]. Dans un deuxième temps, la bactérie a été considérée comme une sphère dure, portant les charges, recouverte d'une couche de polymères souples mais non chargés. Dans la troisième partie de ce mémoire, nous avons contribué à faire progresser ce modèle en considérant un polymère portant les charges. Cependant la géométrie de la particule dure restait sphérique et donc en désaccord avec la forme bacillaire (cylindrique) des

bactéries du genre *Shewanella*. Dans la cinquième partie de ce travail, les équations décrivant la mobilité d'une particule cylindrique recouverte d'un polymère chargé sont pour la première fois exposées. De plus, le caractère diffus, ou hétérogène, de l'interface est pris en compte *via* le paramètre d'hétérogénéité (α) qui décrit la diminution de la densité des segments polymériques, à mesure que l'on s'éloigne de la surface de la particule dure. Cette analyse permet de mesurer, à partir des données de microélectrophorèse, la densité de charge dans l'interface molle (ρ_0), le caractère plus ou moins diffus de l'interface (α), la souplesse hydrodynamique de la couche molle (λ) et enfin, si ce paramètre n'est pas disponible par ailleurs, l'épaisseur de l'interface souple (δ). Ainsi, MR4 possède un polymère dont la densité de charges est faible (-10 mM) avec une grande souplesse hydrodynamique (3,5 nm). Pour cette souche, le caractère hétérogène est beaucoup moins marqué que pour la souche CN32. En effet, pour CN32 (densité de charge = -35 mM à forte force ionique et souplesse hydrodynamique faible = 2 nm), il est indispensable de considérer soit l'évolution de la densité de charge, soit la modification du caractère diffus de l'interface, quand la force ionique varie. Ces deux hypothèses sont pertinentes et permettent de modéliser les résultats expérimentaux. Soit l'interface est considérée comme homogène, quel que soit la force ionique, et alors seule la densité de charge de l'interface va diminuer avec la force ionique ; soit c'est la densité de charge qui est constante et c'est alors l'hétérogénéité de l'interface qui augmente quand la force ionique diminue. Dans la réalité les deux phénomènes ont probablement lieu concomitamment. Il n'est malheureusement pas possible, dans l'immédiat, de discerner la part de chacune des deux hypothèses.

Les résultats obtenus en spectroscopie de force montrent que les courbes de force de CN32 à 1 mM ne s'accordent pas, pour des indentations faibles, au modèle de Hertz proposé au chapitre trois. Ceci est sans doute dû à la contribution des interactions électrostatiques pointe-bactérie. Celles-ci ont été calculées dans le chapitre cinq selon une approche cylindre mou homogène ou hétérogène (bactérie) - sphère dure (pointe AFM). Ce calcul tient compte des caractéristiques électrocinétiques, c'est-à-dire de la densité de charge, et indirectement de la souplesse hydrodynamique et du caractère diffus des polymères, contrairement aux approches classiques plan-plan de DLVO linéarisé [138] pour des sphères dures. Ici, aucune approximation de tailles ou de charges n'est réalisée. L'interprétation des courbes de force à faible force ionique se nourrit des résultats obtenus en électrocinétique. Pour CN32 1 mM, les calculs permettent de reproduire les données expérimentales et ainsi différencier les forces de surface des propriétés nanomécaniques. De plus, ces résultats montrent que l'approche

hétérogène est probablement la plus pertinente. En revanche, à 100 mM, le calcul montre que les interactions électrostatiques sont négligeables. Les propriétés nanomécaniques sont ainsi directement quantifiables par une loi de Hertz-Hook avec un grand domaine non linéaire correspondant à l'indentation de la pointe dans l'interface molle. La différence de propriété mécanique à 1 et 100 mM est due à la variation de pression osmotique du milieu. A 1 mM, la bactérie est turgescente, d'où un domaine linéaire étendue, alors qu'à 100 mM, le domaine non linéaire est majoritaire, traduisant une diminution de la pression de turgescence de la cellule.

Les épaisseurs des structures sondées en spectroscopie de force et électrocinétique ne sont pas du même ordre de grandeur. En effet, alors que la spectroscopie de force détermine les propriétés interfaciales sur des domaines de la centaine de nanomètres, les caractéristiques électrocinétiques vont, elles, être dépendantes d'une zone beaucoup plus petite (environ 30 nm). Les deux approches ne mesurent donc pas des phénomènes aux mêmes échelles et les caractéristiques électrocinétiques ne sont en relation qu'avec le début des courbes de force. Ces deux approches présentent donc une synergie pour la description des premiers nanomètres puis sont complémentaires car la spectroscopie de force permet d'accéder aux propriétés nanomécaniques des cellules pendant que l'électrocinétique permet de quantifier l'électrohydrodynamique des couches les plus externes.

Grâce à la connaissance des propriétés nanomécaniques et électrohydrodynamiques de l'interface de CN32, MR4 et CIP 8040 nous pouvons proposer une explication de leur capacité d'adhésion au polystyrène (*cf.* Figure 15 et annexe 3) : CN32 ne possède aucune frange polymérique mais une densité de charge de l'interface importante (en tout cas, à forte force ionique). En revanche MR4 possède une épaisse frange polymérique, peu chargée, souple du point de vue hydrodynamique. Aussi, alors que la surface du polystyrène est chargée positivement [139] (*cf.* annexe 1), CN32 présente un fort pourcentage d'adhésion au polystyrène tandis que MR4 adhère très peu, quelles que soient les conditions de pH et de force ionique. Dans le cas de CN32, la force ionique et le pH ont une forte influence sur sa capacité d'adhésion, or nous avons montré que ces deux paramètres (pH et force ionique) induisent des modifications de l'hétérogénéité de l'interface ainsi que de ses caractéristiques nanomécaniques. La diminution de la force ionique induit une augmentation importante du caractère diffus de l'interface dans le cas de CN32, mais pas pour MR4 (*cf.* Figure 12). Parallèlement, l'observation montre que l'adhésion de CN32 est très modifiée par les variations de force ionique alors que ces mêmes variations n'ont pas ou peu d'influence sur

MR4. L'augmentation de pH induit, chez CIP8040, à une force ionique de 100 mM, une augmentation de la souplesse nanomécanique (*cf.* Figure 7) et sur cette même souche l'adhésion diminue avec l'augmentation du pH (*cf.* Figure 11). Sur CN32, l'augmentation de la force ionique induit aussi une augmentation de la souplesse nanomécanique (*cf.* Figure 14) qui se traduit cette fois par une meilleure adhésion (*cf.* annexe 3). La densité de charge et l'hydrodynamique semblent donc prépondérants pour prévoir les capacités d'adhésion d'un microorganisme.

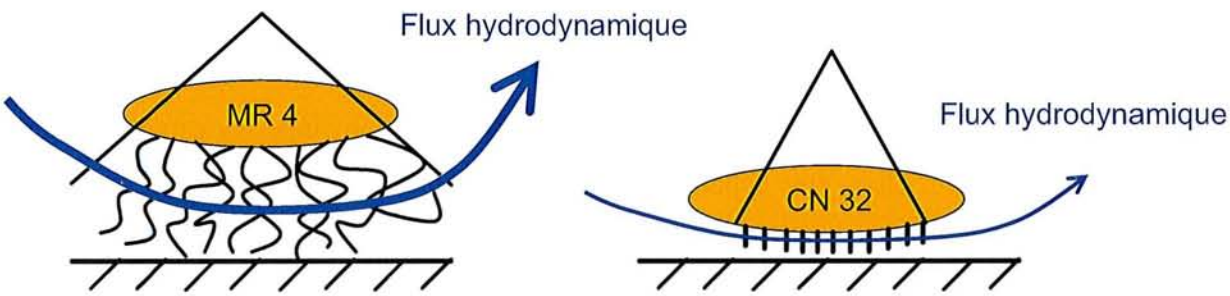

Figure 15 : Explication du comportement adhésif de CN32 et MR4 sur la base de leurs propriétés nanomécaniques et électrohydrodynamiques.

Cette explication mérite d'être confortée par l'étude d'autres modèles bactériens et d'autres systèmes biologiques. Par exemple, on pourrait envisager de travailler sur des mutants d'une des souches dont les polymères plus ou moins longs serait la seule différence. Ce type d'approche a d'ailleurs, été tenté sur *E. coli* K12 [56, 140, 141]. Des mutants présentant des longueurs de LPS variables sont commercialement disponibles. Trois souches différentes ont été fixées, successivement, sur un cantilever d'AFM à l'aide de glutaraldéhyde [140, 142]. Cette technique de fixation est très efficace, mais le glutaraldéhyde crée des ponts entre protéines, entre acides aminés du peptidoglycane [143] ce qui modifie l'état de l'échantillon. Cette réserve étant faite, Razatos *et al.*, démontrent que les cellules avec un LPS complet sont attirées par une surface de verre alors que les souches mutantes avec un LPS tronqué sont repoussées, ce qui va dans le sens de notre hypothèse. Cependant, une autre étude, utilisant les mêmes souches mais une technique de fixation des cellules moins agressive [56], c'est-à-dire fixation via les interactions électrostatiques entre une bactérie chargée négativement et une surface recouverte de PEI, conclut qu'aucune différence entre les courbes de force *versus* indentation n'existe entre des souches d'*E. Coli* K12 avec différentes longueurs de LPS. En revanche, ils mettent en évidence que le glutaraldéhyde rend les cellules plus dures, mais l'effet semble être aussi intense pour les différents mutants. Ainsi l'utilisation de mutants ne

résout pas toutes les difficultés. Dans cet exemple, le choix du système biologique est élégant ; pour autant, aucune conclusion sur les propriétés nanomécaniques des cellules n'a pu être obtenue. Dans ce contexte, une autre approche pour obtenir les souches mutantes pourrait être envisagée. Certaines souches présentent des pourcentages d'adhésion à l'octane (ou à un autre hydrocarbure) très élevé. Les cellules non adhérentes au solvant, présentes dans la phase liquide, peuvent être recultivées. Cette manœuvre, répétée plusieurs fois, conduit à l'obtention de mutants semi adhérents puis totalement non adhérents [69]. La caractérisation des propriétés physico-chimiques (souplesse nanomécanique et hydrodynamique, capacité d'adhésion à une surface, ultrastructure de l'interface, composition élémentaire par XPS) de l'interface de mutants ainsi obtenus serait sans doute très instructive.

6.2. Perspectives liées aux propriétés interfaciales des cellules en biominéralisation

La littérature [48, 144, 145] et des essais préliminaires ont montré qu'en absence d'oxygène, les quatre souches constituant notre modèle sont capables d'utiliser la lépidocrocite (γ-FeOOH) comme accepteur final d'électrons lors de la respiration. Le Fe(II) peut alors cristalliser soit en magnétite, soit en rouille verte. Les conditions qui déterminent l'obtention de l'un ou de l'autre de ces deux minéraux ont été étudiées par Zegeye [47]. Les mécanismes d'échanges d'électrons entre la bactérie et l'oxyde de fer, au cours des processus de bioréduction, ne sont pourtant pas totalement élucidés. Selon un mécanisme connu, des navettes à électrons (de type quinone) assurent le transfert des électrons [146] ; alors que d'autres auteurs montrent qu'un contact entre l'oxyde de fer et la bactérie est nécessaire pour que le transfert d'électrons puisse avoir lieu [147, 148]. Dans la situation « contact », le transfert d'électrons est sans doute influencé par les propriétés de l'interface solution aqueuse-bactérie. Notre hypothèse, basée sur ce mécanisme, présume alors que la vitesse de bioréduction sera influencée par les propriétés interfaciales des bactéries. Ainsi la vitesse de réduction de MR4 (frange polymérique 70 à 130 nm) devrait être différente de celle CN32 (aucun polymère visible). Malheureusement, deux essais de réduction de la lépidocrocite (γ-FeOOH) ont montré des résultats opposés (dans un cas réduction plus rapide avec la souche CN32, dans l'autre réduction plus rapide avec la souche MR4). Les paramètres variables entre les deux essais étaient la taille de l'inoculum bactérien ou la « qualité » de la lépidocrocite utilisée. Le nombre de cellules a été contrôlé par comptage après marquage par le fluorochrome DAPI et s'avère être sensiblement identique. En revanche, aucune certitude ne peut être dégagée pour la lépidocrocite. La diffraction des rayons X identifie dans les deux cas

γ-FeOOH, mais cette technique ne donne pas d'informations sur l'hétérogénéité de l'échantillon en terme de taille, de surface spécifique, de charge de surface ou sur la répartition des faces cristallines des particules. Des travaux sur la goethite [149] ont montré que des modes de synthèses différents et contrôlés conduisent à des minéraux aux propriétés physico-chimiques différentes pour les paramètres précédemment cités. Malheureusement, des expériences menées au LCPME [46] suggèrent que les cinétiques de bioréduction de la goethite (l'oxyhydroxyde ferrique thermodynamiquement le plus stable [150]) sont très lentes. Ainsi il sera nécessaire de contrôler les synthèses de la lépidocrocite afin de pouvoir répéter les essais de bioréduction avec CN32 et MR4.

Dans un deuxième temps, il pourrait être envisagé de suivre *in situ* le processus de bioréduction grâce à des expériences en AFM. L'énergie d'interaction entre les cellules et la lépidocrocite pourrait aussi être déterminée grâce à la spectroscopie de force. Il s'agit de perspectives ouvertes par ce travail. En effet, l'interface solution aqueuse - *Shewanella* a maintenant été décrite. Il reste à contrôler les synthèses de lépidocrocite, puis à s'interroger sur les interactions physico-chimiques entre ce minéral et les bactéries du genre *Shewanella.*

6.3. Applications et perspectives liées à l'utilisation de la démarche expérimentale sur d'autres modèles biologiques

Le genre *Shewanella* a été choisi comme modèle de cette étude pour la diversité des structures de l'interface disponible, et, sa capacité à réduire le fer. D'une part, ce modèle nous a permis d'avancer dans le domaine de la bioadhésion et de mieux comprendre les phénomènes physico-chimiques qui régissent la première étape de formation des biofilms. D'autre part, nous venons d'en discuter, l'interface de *Shewanella* intéresse plus particulièrement les biominéralogistes. Cependant, la démarche expérimentale développée sur ce modèle, pour ces deux applications (bioadhésion et biominéralisation) est extensible à d'autres domaines. Ainsi, la méthodologie mise au point sur *Shewanella* a-t-elle été utilisée pour étudier d'autres systèmes biologiques au cours de collaborations internes ou externes au laboratoire. Les thématiques abordées au cours de ces travaux ont été différentes de celles liées à l'adhésion des micro-organismes ou à la biominéralisation.

Les travaux en collaboration avec G. Lindsey et R. Karreman de l'université de Cap Town en Afrique du Sud ont porté sur la levure *Saccharomyces cerevisiae* et sa protéine de choc thermique Hsp12 (*cf.* article en annexe 2). Cette levure présente une interface d'environ 10 nm d'épaisseur principalement composée de polysaccharides (β1,3 glucan) et de protéines.

Des travaux antérieurs montrent que la protéine Hsp 12 confère à *S. cerevisiae* une certaine résistance à la pression [151] et à la dessiccation-réhydratation [152]. A partir de ces constats, il a été postulé que la protéine Hsp 12 joue le rôle d'assouplissant de la paroi de cette levure. Dans l'étude menée en collaboration, nous avons travaillé sur une souche mutante ΔHsp12 (déletée pour le gène de la protéine Hsp12) et sur la souche sauvage (W). Les mesures de spectroscopie de force, en milieu liquide sur des levures vivantes, prouvent que les cellules ΔHsp12 sont plus rigides que les cellules de la souche sauvage (constante de raideur respectivement : 72 +/- 3 mN/m et 17 +/- 5 mN/m). L'analyse des mobilités électrophorétiques confirme cette différence entre la souche mutée ΔHsp12 et la souche sauvage : la souplesse hydrodynamique (λ^{-1}) de la souche sauvage est de 3 nm mais seulement de 2,3 nm pour la souche mutante. La combinaison de ces deux techniques a permis de confirmer, *in situ*, le rôle d'assouplissant de la protéine Hsp12 jusque là mis en évidence par des méthodes *ex situ* [153].

Enfin, dans le cadre d'une collaboration avec Raphaël Duval et Marion Grare du groupe d'étude des vecteurs supramoléculaires des médicaments (UMR 7565), nous avons tenté de mettre en évidence l'impact de molécules à visée antiseptique sur les propriétés d'interface de *Pseudomonas aeruginosa.* Cette bactérie est retrouvée dans 11 % des cas d'infections nosocomiales [154], préoccupation de santé publique majeure du fait de leur forte morbidité. Cette situation est liée à un mésusage des antibiotiques mais aussi à une capacité d'innovation vraie, trop faible dans le domaine des stratégies antibactériennes. Dans ce contexte, une molécule nouvelle, le calixarène CX1 [155], a été évaluée en terme d'efficacité antibactérienne et de toxicité (*via* l'index de sélectivité). Les premières expériences en spectroscopie de force montrent que l'interface de *P. aeruginosa* est plus dure quand il a été cultivé en présence du CX1. Ce travail préliminaire ouvre des perspectives intéressantes de recherche. S'il est démontré que le CX1 agit sur la membrane bactérienne, il faudra alors chercher la molécule ciblée. Une fois celle-ci identifiée, il pourra être envisagée de mesurer l'énergie d'interaction entre un levier greffé avec du CX1 et la molécule ciblée. D'autre part, des expériences en temps réel pourrait être menée pour tenter d'observer l'action du CX1 sur la morphologie des cellules. Des essais préliminaires semblent montrer un impact du CX1 sur la structure de l'enveloppe de *P. aeruginosa* (*cf.* Figure 16). Ainsi il serait intéressant de comparer une image AFM des bactéries avant l'ajout de CX1, puis 15 min, 30 min, 1h après

l'ajout d'une certaine dose de CX1. La même expérience avec différentes doses de CX1 permettraient peut être de mettre en évidence une relation dose-effet.

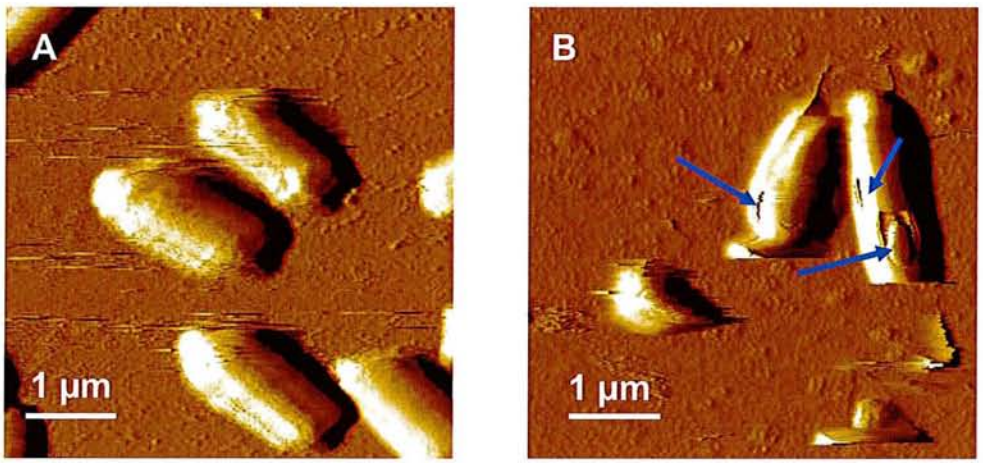

Figure 16 : image AFM (mode contact, milieu liquide) en déflection de *Pseudomonas aeruginosa*. A : bactéries non traitées ; B : bactéries cultivées en présence de 32 µg de CX1 par mL. Les flèches indiquent des possibles détériorations de la membrane bactérienne.

6.4. Conclusion

La physico-chimie des interfaces bactérie-solution aqueuse évolue avec les méthodes d'étude. Dans cette thèse, nous avons développé une démarche expérimentale innovante, permettant de sonder *in situ*, l'interface des bactéries avec le milieu qui les entoure. La combinaison d'approches complémentaires comme l'AFM et l'analyse de la mobilité des bactéries dans un champ électrique selon la théorie des particules molles, fournit de nouveaux éléments de compréhension des phénomènes d'adhésion. Les propriétés nanomécaniques et électrohydrodynamiques sont des facteurs à prendre en compte pour tenter de prévoir la capacité d'adhésion d'un microorganisme. De plus, nous avons montré que les propriétés des structures interfaciales ne sont pas figées mais évoluent en fonction du pH et de la force ionique (*cf.* Figure 17).

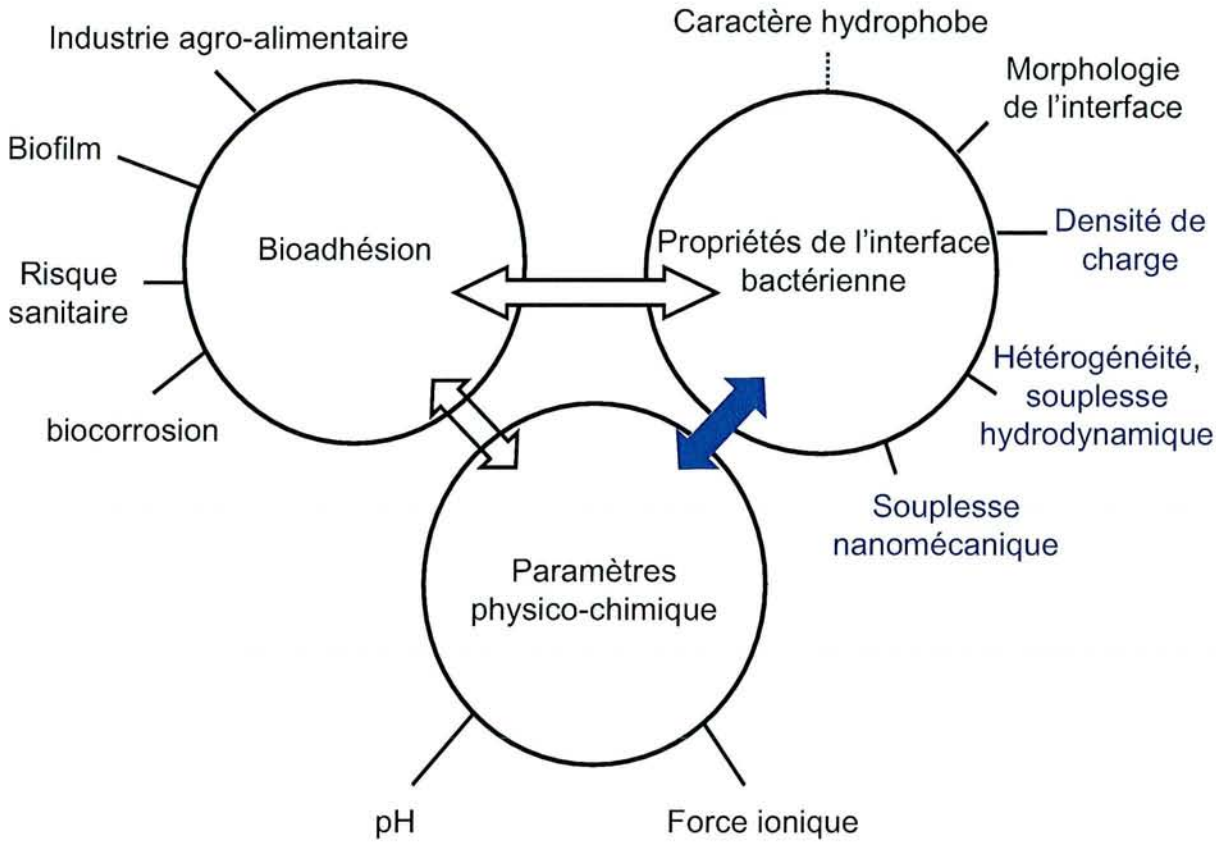

Figure 17 : Schéma illustrant les liens entre la bioadhésion, les propriétés d'interface et les paramètres physico-chimiques. Nous avons introduit les concepts de densité de charge, d'hétérogénéité et de souplesse hydrodynamique et nanomécanique comme des propriétés interfaciales à considérer pour expliquer les phénomènes de bioadhésion. De plus, nous avons montré l'influence du pH et de la force ionique sur les propriétés de l'interface bactérienne (flèche pleine)

Le modèle de notre étude, quatre bactéries du genre *Shewanella*, a été choisi pour la diversité de l'interface eau-cellule rencontrée entre les souches. Cette diversité nous a permis de comparer une souche (MR4) présentant une frange polymérique importante (environ 120 nm d'épaisseur) avec une souche dépourvue de polymères visibles au MET (CN32). Dans le cas de la souche BrY, nous avons été capables de différencier les deux sous-populations, sur la base de la mobilité électrophorétique des deux phénotypes. Cela nous a poussé à mieux comprendre les paramètres qui gouvernent le déplacement d'une bactérie (particule molle) dans un champ électrique et à utiliser les théories développées par Ohshima et Duval. Parallèlement nous avons développé les approches par spectroscopie de force pour quantifier les propriétés nanomécanqiues des bactéries. La combinaison synergique de ces deux approches nous a permis de proposer une explication des capacités d'adhésion au polystyrène, à différents pH et forces ioniques, de CN32 et MR 4. De plus ces bactéries sont capables de réduire le Fe(III) solide et ont à ce titre une certaine importance dans le cycle biogéochimique

du fer. La connaissance acquise au cours de cette thèse sur l'interface *Shewanella*-solution pourra être mise à profit dans le domaine de la biominéralisation.

Enfin, le phénomène de bioadhésion est le fil conducteur de cette thèse. La réactivité de l'interface solution aqueuse-bactérie conditionne l'étape d'adhésion d'une bactérie planctonique à un support, annonciatrice du développement d'un biofilm. De nombreux secteurs industriels sont concernés par la question des biofilms : station d'épuration des eaux usées urbaines, tous systèmes de refroidissement à eau, fabrication de microprocesseurs. La bioadhésion est aussi un problème de santé public. Par exemple, l'adhésion de bactéries sur des prothèses, puis leur développement, constituent la première cause d'échec de la pause de ces implants et conduit presque inévitablement au retrait de la prothèse.

Ainsi, les recherches fondamentales sur la physico-chimie des interfaces bactérie-solution aqueuse, présentées dans cette thèse, ont amené des avancées méthodologiques permettant d'améliorer la compréhension du phénomène de bioadhésion.

7. Références bibliographiques

1 Block, J. C. (1996) Diversité microbiologique des réseaux de distribution d'eau potable. Bull. Soc. Fr. Microbiol. **11**, 7-10

2 Block, J. C. and Appenzeller, B. M. R. (2001) Biofilms et distribution d'eau potable. Bull. Soc. Fr. Microbiol. **16**, 7-12

3 Montanaro, L., Campoccia, D., Rizzi, S., Donati, M. E., Breschi, L., Prati, C. and Arciola, C. R. (2004) Evaluation of bacterial adhesion of *Streptococcus mutans* on dental restorative materials. Biomaterials **25**, 4457-4463

4 Rosenberg, M., Judes, H. and Weiss, E. (1983) Cell surface hydrophobicity of dental plaque microorganisms in situ. Infection and immunity **42**, 831-834

5 Alakomi, H. L., Paananen, A., Suihko, M. L., Helander, I. M. and Saarela, M. (2006) Weakening effect of cell permeabilizers on Gram-negative bacteria causing biodeterioration. Appl. Environ. Microbiol. **72**, 4695-4703

6 Monier, J. M. and Lindow, S. E. (2004) Frequency, size and localization of bacterial aggregates on bean leaf surfaces. Appl. Environ. Microbiol. **70**, 346-355

7 Morris, C. E., Monier, J. M. and Jacques, M. A. (1997) Methods for observing microbial biofilms directly on leaf surfaces and recovering them for isolation of culturable microorganisms. Appl. Environ. Microbiol. **63**, 1570-1576

8 Gales, G., Libert, M. F., Sellier, R., Cournac, L., Chapon, V. and Heulin, T. (2004) Molecular hydrogen from water radiolysis as an energy source for bacterial growth in a basin containing irradiating waste. FEMS Microbiol. Lett. **240**, 155-162

9 Gottenbos, B., Henny, C., Van der Mei, H. C. and Busscher, H. J. (2000) Initial adhesion and surface growth of *Staphylococcus epidermidis* and *Pseudomonas aeruginosa* on biomedical polymers. J. Biomed. Mat. Res. **50**, 208-214

10 Ong, Y.-L., Razatos, A., Georgiou, G. and Sharma, M. M. (1999) Adhesion forces between *E. coli* and biomaterial surfaces. Langmuir **15**, 2719-2725

11 Gristina, A. G. (1987) Biomaterial-centered infection : microbial adhesion *versus* tissue integration. Science **237**, 1588-1595

12 Tang, H., Wang, A., Liang, X., Cao, T., Salley, S. O., McAllister Iii, J. P. and Ng, K. Y. S. (2006) Effect of surface proteins on *Staphylococcus Epidermidis* adhesion and colonization on silicone. Colloids and Surfaces B: Biointerfaces **51**, 16-24

13 Lewin, R. (1984) Microbial adhesion is a sticky problem. Science **224**, 375-377

14 Touhami, A., Jericho, M. H., Boyd, J. M. and Beveridge, T. J. (2006) Nano-scale characterization and determination of adhesion forces of *Pseudomonas aeruginosa* pili using atomic force microscopy. J. Bacteriol. **188**, 370-377

15 Beveridge, T. J. (1999) Structures of Gram-negative cell walls and their derived membrane vesicles. J. Bacteriol. **181**, 4725-4733

16 Mozes, N. and Rouxhet, P. G. (1987) Methods for measuring hydrophobicity of microorganisms. J. Microbiol. Methods **6**, 99-112

17 Bos, R., Van der Mei, H. C. and Busscher, H. J. (1999) Physico-chemistry of initial microbial adhesive interactions - its mechanisms and methods for study. FEMS Microbiol. Rev. **23**, 179-229

18 Caccavo, F. J., Schamberger, P. C., Keiding, K. and Nielsen, P. H. (1997) Role of hydrophobicity in adhesion of the dissimilatory Fe(III)-reducing bacterium *Shewanella alga* to amorphous Fe(III) oxide. Appl. Environ. Microbiol. **63**, 3837-3843

19 Hsu, B. M. and Huang, C. (2002) Influence of ionic strength and pH on hydrophobicity and zeta potential of *Giardia* and *Cryptosporidium*. Colloids Surfaces A: Physicochem. Eng. Asp. **201**, 201-206

20 Van Loosdrecht, M. C. M., Lyklema, J., Norde, W., Schraa, G. and Zehnder, A. J. B. (1987) The role of bacterial cell wall hydrophobicity in adhesion. Appl. Environ. Microbiol. **53**, 1893-1897

21 Van der Mei, H. C., Weerkamp, A. H. and Busscher, H. J. (1987) A comparison of various methods to determine hydrophobic properties of streptococcal cell surfaces. J. Microbiol. Methods **6**, 277-287

22 Van Oss, C. J. (1995) Hydrophobicity of biosurfaces - origin, quantitative determination and interaction energies. Colloids and Surfaces B: Biointerfaces **5**, 91-100

23 Dai, X., Boll, J., Hayes, M. E. and Aston, D. E. (2004) Adhesion of *Cryptosporidium parvum* and *Giardia lamblia* to solid surfaces : the role of surface charge and hydrophobicity. Colloids and Surfaces B: Biointerfaces **34**, 254-263

24 Harkes, G., Feijen, J. and Dankert, J. (1991) Adhesion of *Escherichia coli* on to a series of poly(methacrylates) differing in charge and hydrophobicity. Biomaterials **12**, 853-860

25 Claessens, J., van Lith, Y., Laverman, A. M. and Van Cappellen, P. (2006) Acid-base activity of live bacteria: Implications for quantifying cell wall charge. Geochimica et Cosmochimica Acta **70**, 267-276

26 Rijnaarts, H. H. M., Norde, W., Bouwer, E. J., Lyklema, J. and Zehnder, A. J. B. (1995) Reversibility and mechanism of bacterial adhesion. Colloids and Surfaces B: Biointerfaces **4**, 5-22

27 Van der Mei, H. C., Vries, J. and Busscher, H. J. (2000) X-ray photoelectron spectroscopy for the study of microbial cell surfaces. Surface science reports **39**, 1-24

28 Van der Mei, H. C., Léonard, A. J., Weerkamp, A. H., Rouxhet, P. G. and Busscher, H. J. (1988) Surface properties of *Streptococcus salivarius* HB and non fibrillar mutants : measurement of zeta potential and elemental composition with X-ray photoelectron spectroscopy. J. Bacteriol. **170**, 2462-2466

29 Yelloji Rao, M. K., Somasundaran, P., Schilling, K. M. and Carson, R. (1995) Electrokinetic properties of *Streptococcus sanguis* and *Actinomyces naeslundii*. Colloids and Surfaces B: Biointerfaces **4**, 87-95

30 Rouxhet, P. G., Mozes, N., Dengis, P. B., Dufrêne, Y. F., Gerin, P. A. and Genet, M. J. (1994) Application of X-ray photoelectron spectroscopy to microorganisms. Colloids and Surfaces B: Biointerfaces **2**, 347-369

31 An, Y. H. and Friedman, R. J. (1998) Concise review of mechanisms of bacterial adhesion to biomaterial surfaces. J. Biomed. Mater. Res. **43**, 338-348

32 Baikun, L. and Logan, B. E. (2004) Bacterial adhesion to glass and metal-oxides surfaces. Colloids and Surf. B: Biointerfaces **36**, 81-90

33 Stenström, T. A. (1989) Bacterial hydrophobicity, an overall parameter for the measurement of adhesion to soil particles. Appl. Environ. Microbiol. **55**, 142-147

34 Rosenberg, M., Gutnick, D. and Rosenberg, E. (1980) Adherence of bacteria to hydrocarbons : a simple method for measuring cell-surface hydrophobicity. FEMS Microbiol. Lett. **9**, 29-33

35 Gaboriaud, F., Bailet, S., Dague, E. and Jorand, F. (2005) Surface structure and nanomechanical properties of *Shewanella putrefaciens* bacteria at two pH values (4 and 10) determined by Atomic force microscopy. J. Bacteriol. **187**, 3864-3868

36 Van der Mei, H. C., Bos, R. and Busscher, H. J. (1998) A reference to microbial cell surface hdrophobicity based on contact angle. Colloids and Surfaces B: Biointerfaces **11**, 213-221

37 Guellil, A., Block, J. C. and Urbain, V. (1998) Adaptation of the microbial adhesion to hydrocarbon test (math) for measuring activated sludge hydrophobicity. Wat. Sci. Technol. **37**, 359-362

38 Bellon-Fontaine, M. N., Rault, J. and van Oss, C. J. (1996) Microbial adhesion to solvents: a novel method to determine the electron-donor/electron-acceptor or Lewis acid-base properties of microbial cells. Colloids and surfaces B: Biointerfaces **7**, 47-63

39 Busscher, H. J., Van de Belt-Grotter, B. and Van der Mei, H. C. (1995) Implications of microbial adhesion to hydrocarbons for evaluating cell surface hydrophobicity 1. zeta potentials of hydrocarbon droplets. Colloids and Surfaces B: Biointerfaces **5**, 111-116

40 Van der Mei, H. C., Van de Belt-Grotter, B. and Busscher, H. J. (1995) Implications of microbial adhesion to hydrocarbons for evaluating cell surface hydrophobicity 2. adhseion mechanisms. Colloids and Surfaces B: Biointerfaces **5**, 117-126

41 Mozes, N., Marchal, F., Hermesse, M. P., Van Haecht, J. L., Reuliaux, L., Leonard, A. J. and Rouxhet, P. G. (1987) Immobilization of microorganisms by adhesion: interplay of electrostatic and nonelectrostatic interactions. Biotechnol. Bioeng. **30**, 439-450

42 Van Merode, A. E. J., Van der Mei, H. C., Busscher, H. J. and Krom, B. P. (2006) Influence of culture heterogeneity in cell surface charge on adhesion and biofilm formation by *Enterococcus faecalis*. J. Bacteriol. **188**, 2421-2426

43 Lytle, D., Frietch, C. and Covert, T. (2004) Electrophoretic mobility of *Mycobacterium avium* complex organisms. Appl. Environ. Microbiol. **70**, 5667-5671

44 Ahimou, F., Denis, F. A., Touhami, A. and Dufrene, Y. F. (2002) Probing microbial cell surface charges by atomic force microscopy. Langmuir **18**, 9937-9941

45 Ona-Nguema, G., Abdelmoula, M., Jorand, F., Benali, O., Gehin, A., Block, J. C. and Genin, J. M. (2002) Iron(II,III) hydroxycarbonate green rust formation and stabilization from lepidocrocite bioreduction. Environ. Sci. Technol. **36**, 16-20

46 Ona-Nguema, G. (2003) Biogènèse d'hydroxysels mixtes Fe(II-III) de type rouille verte en culture de *Shewanella putrefaciens*. In LCPME, UMR 7564, Thèse de doctorat, Université Henri Poincaré Nancy I, Nancy, France

47 Zegeye, A. (2006) Formation et stabilité des hydroxysels Fe(II-III) de type rouille verte en cultures bactériennes. In LCPME, UMR 7564, Thèse de doctorat, Université Henri Poincaré Nancy I, Nancy, France

48 Amitabha, D. and Caccavo, F., Jr (2001) Adhesion of the dissimilatory Fe(III)-reducing bacterium *Shewanella alga* BrY to crystalline Fe(III) oxides. Curr. microbiol. **42**, 151-154

49 Hjelm, M., Hilbert, L. R., Moller, P. and Gram, L. (2002) Comparison of adhesion of the food spoilage bacterium *Shewanella putrefaciens* to stainless steel and silver surfaces. J. Appl. Microbiol. **92**, 903-911

50 Bagge, D., Hjelm, M., Johansen, C., Huber, I. and Gram, L. (2001) *Shewanella putrefaciens* adhesion and biofilm formation on food processing surfaces. Appl. Environ. Microbiol. **76**, 2319-2325

51 Abboud, R., Popa, R., Souza-Egipsy, V., Giometti, C. S., Tollaksen, S., Mosher, J. J., Findlay, R. H. and Nealson, K. H. (2005) Low temperature growth of *Shewanella oneidensis* MR-1. Appl. Environ. Microbiol. **71**, 811-816

52 Khashe, S. and Janda, M. (1998) Biochemical and pathogenic properties of *Shewanella alga* and *Shewanella putrefaciens*. J. Clinical Microbiol. **36**, 783-787

53 Beveridge, T. J. and Davies, J. A. (1983) Cellular response of *Bacillus subtilis* and *Escherichia coli* to the gram stain. J. Bacteriol. **156**, 846-858

54 Prescott, L. M., Harley, J. P. and Klein, D. A. (2003) Microbiology

55 Cowan, S. W., Schirmer, T., Rummel, G., Steiert, M., Ghosh, R., Pauptit, R. A., Jansonius, J. N. and Rosenbusch, J. P. (1992) Crystal structures explain fonctional properties of two *E. coli* porins. Nature **358**, 727-733

56 Burks, G. A., Velegol, D., Paramonova, E., Lindenmuth, B. E., Feick, J. D. and Logan, B. E. (2003) Macroscopic and nanoscale measurements of the adhesion of bacteria with varying outer surface composition. Langmuir **19**, 2366-2371

57 Yao, X., Walter, J., Burke, S., Stewart, S., Jericho, M. H., Pink, D., Hunter, R. and Beveridge, T. J. (2002) Atomic force microscopy and theoretical considerations of surface properties and turgor pressures of bacteria. Colloids and Surfaces B: Biointerfaces **23**, 213-230

58 Beveridge, T. J. (1981) Ultrastructure, chemistry and function of the bacterial cell wall. Int. Rev. Cytol. **72**, 229-317

59 DeBeer, D., Srinivasab, R. and Stewart, P. S. (1994) Direct measurement of chlorine penetration into biofilms during disinfection. Appl. Environ. Microbiol. **60**, 4339-4344

60 Filloux, A. and Vallet, I. (2003) Biofilm: set-up and organization of a bacterial community. Med. Sci. **19**, 77-83

61 Venkateswaran, K., Moser, D. P., Dollhopf, M. E., Lies, D. P., Saffarini, D. A., Mac Gregor, B. J., Ringelberg, D. B., White, D. C., Nishijima, M., Sano, H., Burghardt, J., Stackebrandt, E. and Nealson, K. H. (1999) Polyphasic taxonomy of the genus *Shewanella* and description of *Shewanella oneidensis* sp. nov. International Journal of Systematic Bacteriology **49**, 705-724

62 Nealson, K. H. and Myers, C. R. (1992) Microbial reduction of manganese and iron new approches to carbon cycling. Appl. Environ. Microbiol. **58**, 439-443

63 DiChristina, T. J. and Delong, E. F. (1993) Design and application of rRNA targeted oligonucleotide probes for the dissimilatory iron and manganese reducing bacterium *Shewanella putrefaciens*. Appl. Environ. Microbiol. **59**, 4152-4160

64 Myers, C. R. and Nealson, K. H. (1988) Bacterial manganese reduction and growth with manganese oxide as sole electron acceptor. Science **240**, 1319-1321

65 Korenevsky, A., Vinogradov, E., Gorby, Y. and Beveridge, T. J. (2002) Characterization of the lipopolysaccharides and capsules of *Shewanella* spp. Appl. Environ. Microbiol. **68**, 4653-4657

66 Cowan, M. M., Van der Mei, H. C., Rouxhet, P. G. and Busscher, H. J. (1992) Physicochemical and structural investigation of the surfaces of some anaerobic subgingival bacteria. Appl. Environ. Microbiol. **58**, 1326-1334

67 Bruinsma, G. M., van der Mei, H. C. and Busscher, H. J. (2001) Bacterial adhesion to surface hydrophilic and hydrophobic contact lenses. Biomaterials **22**, 3217-3224

68 Rouxhet, P. G. and Mozes, N. (1987) Methods for measuring hydrophobicity of microorganisms. J. Microbiol. Methods **6**, 99-112

69 Rosenberg, M. (1991) Basic and applied aspects of microbial adhesion at the hydrocarbon : water interference. Critical Rev. Microbiol. **18**, 159-173

70 Vadillo-Rodriguez, V., Busscher, H. J., Van der Mei, H. C., Vries, J. and Norde, W. (2004) Role of lactobacillus cell surface hydrophobicity as probed by AFM in adhesion to surfaces at low and high ionic strength. Colloids and Surfaces B: Biointerfaces **41**, 33-41

71 Rosenberg, M. (2006) Microbial adhesion to hydrocarbons: twenty-five years of doing MATH. FEMS Microbiol. Lett. **262**, 129-134

72 Hemery, G., Chevalier, S., Bellon-Fontaine, M. N., Haras, D. and Orange, N. (2006) Growth temperature and OprF porin affect cell surface physicochemical properties and adhesive cacpacities of *Pseudomonas fluorescens* MF37. J. Ind. Microbiol. Biotechnol. **On line first**

73 Briandet, R., Meylheuc, T., Maher, C. and Bellon-Fontaine, M. N. (1999) *Listeria monocytogenes* Scott A: cell surface charge, hydrophobicity, and electron donor and acceptor characteristics under different environmental growth conditions. Appl. Environ. Microbiol. **65**, 5328-5333

74 Ahimou, F., M., P., Jacques, P., P., T. and Rouxhet, P. G. (2001) Influence of electrical properties on the evaluation of the surface hydrophobicity of *Bacillus subtilis*. J. Microbiol. Methods **45**, 119-126

75 Takashima, S. and Morisaki, H. (1997) Surface characteristics of the micobial cell of *Pseudomonas syringae* and its relevance to cell attachment. Colloids and Surfaces B: Biointerfaces **9**, 205-212

76 Hayachi, H., Tsuneda, S., Hirata, A. and Sasaki, H. (2001) Soft particle analysis of bacterial cells and its interpretation of cell adhesion behaviors in terms of DLVO theory. Colloids and Surfaces B: Biointerfaces **22**, 149-157

77 Lytle, D. A., Johnson, C. H. and Rice, E. W. (2002) A systematic comparison of the electrokinetic properties of environmentally important microorganisms in water. Colloids and Surfaces B: Biointerfaces **24**, 91-101

78 Van Loosdrecht, M. C. M., Lyklema, J., Norde, W., Schraa, G. and Zehnder, A. J. B. (1987) Electrophoretic mobility and hydrophobicity as a mesure to predict the initial steps of bacterial adhesion. Appl. Environ. Microbiol. **53**, 1898-1901

79 Rijnaarts, H. H. M., Norde, W., Lyklema, J. and Zehnder, A. J. B. (1995) The isoelectric point of bacteria as an indicator for the presence of cell surface polymers that inhibit adhesion. Colloids and Surfaces B: Biointerfaces **4**, 191-197

80 Sokolov, I., Smith, D. S., Henderson, G. S., Gorby, Y. A. and Ferris, F. G. (2001) Cell surface electrochemical heterogeneity of the Fe(III)-reducing bacteria *Shewanella putrefaciens*. Environ. Sci. Technol. **35**, 341-347

81 Claessens, J., Behrends, T. and Van Cappellen, P. (2004) What do acid-base titrations of live bacteria tell us ? A preliminary asessement. Aquat. Sci. **66**, 19-26

82 Haas, J. R. (2004) Effects of cultivation conditions on acid-base titration properties of *Shewanella putrefaciens*. Chemical Geology **209**, 67-81

83 Daughney, C. J. and Fein, J. B. (1998) The effect of Ionic strength on the adsorption of H+, Cd2+, Pb2+, and Cu2+by *Bacillus subtilis* and *Bacillus licheniformis*: a surface complexation model. J. Coll. Interface Sci. **198**, 53-77

84 Fein, J. B., Daughney, C. J., Yee, N. and Davis, T. A. (1997) A chemical equilibrium model for metal adsorption onto bacterial surfaces. Geochimica et Cosmochimica Acta **61**, 3319-3328

85 Duval, J. F. L., Bussher, H. J., Van de Belt-Gritter, B., Van der Mei, H. C. and Norde, W. (2005) Analysis of the interfacial properties of fibrillated and nonfibrillated oral streptococcal strains from electrophoretic mobility and titration measurements : evidence for the shortcomings of the "classical soft-particle approach". Langmuir **21**, 11268-11282

86 Hong, Y. and Brown, D. G. (2006) Cell surface acid-base properties of *Escherichia coli* and *Bacillus brevis* and variation as a function of growth phase, nitrogen source and C:N ratio. Colloids and Surfaces B: Biointerfaces **50**, 112-119

87 Fein, J. B., Boily, J.-F., Yee, N., Gorman-Lewis, D. and Turner, B. F. (2005) Potentiometric titrations of *Bacillus subtilis* cells to low pH and a comparison of modeling approaches. Geochimica et Cosmochimica Acta **69**, 1123-1132

88 Schar-Zammaretti, P., Dillmann, M.-L., D'Amico, N., Affolter, M. and Ubbink, J. (2005) Influence of termentation medium composition on physicochemical surface properties of *Lactobacillus acidophilus*. Appl. Environ. Microbiol. **71**, 8165-8173

89 Duval, J. F. L. and Ohshima, H. (2006) Electrophoresis of diffuse soft particles. Langmuir **22**, 3533-3546

90 Duval, J. F. L. (2005) Electrokinetics of diffuse soft interfaces. 2. Analysis based on the nonlinear Poisson-Boltzmann equation. Langmuir **21**, 3247-3258

91 Ohshima, H. (1995) Electrophoretic mobility of soft particles. Colloids and Surfaces A: Physicochem. Eng. Asp. **103**, 249-255

92 Ohshima, H. (2002) Electrophoretic mobility of a charged spherical colloidal particle covered with an uncharged polymer layer. Electrophoresis **23**, 1993-2000

93 Ohshima, H. (1994) Electrophoretic mobility of soft particles. J. colloid and interface Sci. **163**, 474-483

94 Duval, J. F. and Van Leeuwen, H. P. (2004) Electrokinetics of diffuse soft interfaces. 1. limit of low donnan potentials. Langmuir **20**, 10324-10336

95 Yezek, L. P., Duval, J. F. L. and vanLeeuwen, H. P. (2005) Electrokinetics of diffuse soft interfaces. III. Interpretation of data on the polyacrylamide/water interface. Langmuir **21**, 6220-6227

96 Dague, E., Duval, J., Jorand, F., Thomas, F. and Gaboriaud, F. (2006) Probing surface structures of *Shewanella* spp. by microelectrophoresis. Biophys. J. **90**, 2612-2621

97 Edelmann, L. (2002) Freeze-dried and resin-embedded biological materials is well suited for ultrastructure research. Journal of Microscopy **207**, 5-26

98 Ubbink, J. and Schar-Zammaretti, P. (2005) Probing bacterial interactions: integrated approaches combining atomic force microscopy, electron microscopy and biophysical techniques. Micron **36**, 293-320

99 Hunter, R. and Beveridge, T. J. (2005) High-resolution visualization of *Pseudomonas aeruginosa* PAO1 Biofilms by freeze-substitution transmission electron microscopy. J. Bacteriol. **187**, 7619-7630

100 Matias, V. R. F. and Beveridge, T. J. (2006) Native cell wall organization shown by cryo-electron microscopy confirms the existence of a periplasmic space in *Staphylococcus aureus*. J. Bacteriol. **188**, 1011-1021

101 Zuber, B., Haenni, M., Ribeiro, T., Minnig, K., Lopes, F., Moreillon, P. and Dubochet, J. (2006) Granular layer in the periplasmic space of gram-positive bacteria and fine structures of *Enterococcus gallinarum* and *Streptococcus gordonii* septa revealed by cryo-electron microscopy of vitreous sections. J. Bacteriol. **188**, 6652-6660

102 Graham, L. L. and Beveridge, T. (1990) Effect of chemical fixatives on accurate preservation of *Escherichia coli* and *Bacillus subtilis* structure in cells prepared by freeze-substitution. J. Bacteriol. **172**, 2150-2159

103 Graham, L. L., Harris, R., Villiger, W. and Beveridge, T. J. (1991) Freeze-substitution of Gram negative eubacteria : general cell morphology and enveloppe profiles. J. Bacteriol. **173**, 1623-1633

104 Binnig, G. and Quate, C. F. (1986) Atomic force microscope. Phys. rev. letters. **56**, 930-933

105 Hansma, P. K., Elings, V. B., Marti, O. and Bracker, C. E. (1988) Scanning tunneling microscopoy and atomic force microscopy : application to biology and technology. Science **247**, 209-216

106 Dufrêne, Y. F. (2002) Atomic force microscopy, a powerful tool in microbiology. J. Bacteriol. **184**, 5205-5213

107 Dufrêne, Y. F. (2004) Using nanotechniques to explore microbial surfaces. Nature Reviews **2**, 451-460

108 Bolshakova, A. V., Kiselyova, O. I., Filonov, A. S., Frolova, O. Y., Lyubchenko, Y. L. and Yaminsky, I. V. (2001) Comparative studies of bacteria with an atomic force microscope operating in different modes. Ultramicroscopy **86**, 121-128

109 Bowen, W. R., Lovitt, R. W. and Wright, C. J. (2001) Atomic force microscopy study of the adhesion of *Saccharomyces cerevisiae*. J. colloid and interface Sci. **237**, 54-61

110 Doktycz, M. J., Sulliban, C. J., Hoyt, P. R., Pelletier, D. A., Wu, S. and Allison, D. P. (2003) AFM imaging of bacteria immobilized on gelatin coated mica surfaces. Ultramicroscopy **97**, 209-216

111 Dupres, V., Menozzi, F. D., Locht, C., Clare, B. H., Abbott, N. L., Cuenot, S., Bompard, C., Raze, D. and Dufrêne, Y. F. (2005) Nanoscale mapping and functional analysis of individual adhesins on living bacteria. Nature methods **2**, 515-520

112 Schaer-Zammaretti, P. and Ubbink, J. (2003) Imaging of lactic acid bacteria with AFM-elasticity and adhesion maps and their relationship to biological and structural data. Ultramicroscopy **97**, 199-208

113 Vadillo-Rodriguez, V., Busscher, H. J., Norde, W., De Vries, J., Dijkstra, R. J. B., Stokroos, I. and Van der Mei, H. C. (2004) Comparison of atomic force microscopy interaction forces between bacteria and silicon nitride substrata for the three commonly used immobilization methods. Appl. Environ. Microbiol. **70**, 5441-5446

114 Whitehead, K. A., Rogers, D., Colligon, J., Wright, C. and Verran, J. (2006) Use of the atomic force microscope to determine the effect of substratum surface topography on the ease of bacterial removal. Colloids and Surfaces B: Biointerfaces **51**, 44-53

115 Camesano, T. A. and Logan, B. E. (2000) Probing bacterial electrosteric interactions using atomic force microscopy. Environ. Sci. Technol. **34**, 3354-3362

116 Vadillo-Rodriguez, V., Busscher, H. J., Norde, W., Vries, J. and Van der Mei, H. C. (2004) Relations between macroscopic and microscopic adhesion of *Streptococcus mitis* strains to surfaces. Micriobiol. **150**, 1015-1022

117 Gaboriaud, F., Dague, E., Bailet, S., Duval, J. F., Jorand, F. and Thomas, F. (2006) Multiscale study of the dynamic of bacterial envelope at solide-water interfaces: application to *Shewanella putrefaciens* strains. Colloids and Surfaces B: Biointerfaces **50**, 123-131

118 Dufrêne, Y. F. (2001) Application of atomic force microscopy to microbial surfaces: from reconstituted cell surface layers to living cells. Micron **32**, 153-165

119 Dufrêne, Y. F., Boonaert, C. J. P., van der Mei, H. C., Busscher, H. J. and Rouxhet, P. G. (2001) Probing molecular interactions and mechanical properties of microbial cell surfaces by atomic force microscopy. Ultramicroscopy **86**, 113-120

120 Heinz, W. F. and Hoh, J. H. (1999) Relative surface charge density mapping with the atomic force microscope. Biophys. J. **76**, 528-538

121 Abu-Lail, N. I. and Camesano, T. A. (2006) The effect of solvent polarity on the molecular surface properties and adhesion of *Escherichia coli*. Colloids and Surfaces B: Biointerfaces **51**

122 Abu-Nail, N. I. and Camesano, T. A. (2006) Specific and nonspecific interaction forces between *Esherichia coli* and silicon nitride, determind by Poisson statistical analysis. Langmuir **In Press**

123 Hoh, J. H. and Schonenberger, C. A. (1994) Surface morphology and mechanical properties of MDCK monolayers by atomic force microscopy. J. Cell Sci. **107**, 1105-1114

124 Radmacher, M. (2002) Measuring the elastic properties of living cells by the atomic force microscope. Methods Cell Biol. **68**, 67-90

125 Radmacher, M., Fritz, M., Kacher, C. M., Cleveland, J. P. and Hansma, P. K. (1996) Measuring the viscoelastic properties of human platelets with the atomic force microscope. Biophys. J. **70**, 556-567

126 Bremmell, K. E., Evans, A. and Prestidge, C. A. (2006) Deformation and nano-rheology of red blood cells: An AFM investigation. Colloids and Surfaces B: Biointerfaces **50**, 43-48

127 Rotsch, C., Braet, F., Wisse, E. and Radmacher, M. (1997) AFM imaging and elasticity measurements on living rat liver macrophages. Cell. Biol. Int. **21**, 685-696

128 Touhami, A., Nysten, B. and Dufrêne, Y. F. (2003) Nanoscale mapping of the elasticity of microbial cells by atomic force microscopy. Langmuir **19**, 4539

129 Roberts, R. L., Bowers, B., Slater, M. L. and Carib, E. (1983) Chitin synthesis and localization in cell division cycle mutants of *Saccahromyces cerevisiae*. Mol. Cell Biol. **3**, 922-030

130 Ducker, W. A., Xu, Z. and Israelachvili, J. N. (1994) Measurments of hydrophobic and DLVO forces in bubble surface interactions in aqueous solutions. Langmuir **10**, 3279-3289

131 Arnoldi, M., Bäuerlein, E., Radmacher, M., Sackmann, E. and Boulbitch, A. (2000) Bacterial turgor pressure can be measured by atomic force microscopy. Phys. Rev. E. **62**, 1034-1044

132 Pembrey, R. S., Marshall, K. C. and Schneider, R. P. (1999) Cell surface analysis techniques : what do cell preparation protocols do to cell surface properties. Appl. Environ. Microbiol. **65**, 2877

133 Van Loosdrecht, M. C. M., Lyklema, J., Norde, W. and Zehnder, A. J. B. (1989) Bacterial adhesion : a physicochemical problem. Microbial ecology **17**, 1-15

134 Van Loosdrecht, M. C. M., Norde, W. and Zehnder, A. J. B. (1990) Physical chemical description of bacterial adhesion. J. Biomaterials Applications **5**, 91-106

135 Bos, R., van der Mei, H. C. and Bussher, H. J. (1998) Soft particle analysis of the electrophoretic mobility of a fibrillated and non-fibrillated oral streptococcal strain: *Streptococcus salivarius*. Biophys. Chem. **74**, 251-255

136 Tsuneda, S., Jung, J., Hayachi, H., Aikawa, H., Hirata, A. and Sasaki, H. (2003) Influence of extracellular polymers on electrokinetic properties of heterotrophic bacterial cells examined by soft particle electrophoresis theory. Colloids and Surfaces B: Biointerfaces **29**, 181-188

137 Rodriguez, V. V., Busscher, H. J., Norde, W. and van der Mei, H. C. (2002) Softness of the bacterial cell wall of *Streptococcus mitis* as probed by microelectrophoresis. Electrophoresis **23**, 2007-2001

138 Gaboriaud, F. and Dufrêne, Y. F. Atomic force microscopy of microbial cells: application to nanomechanical properties, surface forces and molecular recognition forces. Colloids and Surfaces B: Biointerfaces **In Press**

139 Gaboriaud, F., Bailet, S., Dague, E. and Jorand, F. A local nanomechanical AFM investigation of polystyrene surface properties incubated with *Shewanella putrefaciens*. Microscopy and Microanalysis **In Press**

140 Razatos, A., Ong, Y.-L., Sharma, M. M. and Georgiou, G. (1998) Molecular determinants of bacterial adhesion monitored by atomic force microscopy. PNAS **95**, 11059-11064

141 Razatos, A. (2001) Application of atomic force microscopy to study initial events of bacterial adhesion. Methods enzymol. **337**, 276-285

142 Razatos, A., Ong, Y. L., Boulay, F., Elbert, D. L., Hubbell, J. A., Sharma, M. M. and Georgiou, G. (2000) Force measurements between bacteria and poly(ethylene glycol)-coated surfaces. Langmuir **16**, 9155-9158

143 Hopwood, D. (1972) Theorytical and pratical aspects of glutaraldehyde fixation. Histochemistry Journal **4**, 267-303

144 Caccavo, F., Jr, Ramsing, N. and Costerton, J. (1996) Morphological and metabolic responses to starvation by the dissimilatory metal-reducing bacterium *Shewanella alga* BrY. Appl. Environ. Microbiol. **62**, 4678-4682

145 Turick, C. E., Caccavo, F. J. and Tisa, L. S. (2003) Electron transfer from *Shewanella algae* BrY to hydrous ferric oxide is mediated by cell-associated melanin. FEMS Microbiol. Lett. **220**, 99-104

146 Rosso, K. M., Zachara, J. M., Fredrickson, J. K., Gorby, Y. A. and Smith, S. A. (2003) Nonlocal bacterial electron transfer to hematite surfaces. Geochimica et Cosmochimica Acta **67**, 1081-1087

147 Nevin, K. P. and Lovley, D. R. (2000) Lack of production of electron-shuttling compounds or solubilization of Fe(III) during reduction of insoluble Fe(III) oxide by *Geobacter metallireducens*. Appl. Environ. Microbiol. **66**, 2248-2251

148 Reguera, G., McCarthy, K. D., Metha, T., Nicoll, J. S., Tuominen, M. T. and Lovley, D. R. (2005) Extracellular electron transfer via microbial nanowires. Nature **435**, 1098-1101

149 Gaboriaud, F. and Ehrhardt, J.-J. (2003) Effects of different crystal faces on the surface charge of colloidal goethite ([alpha]-FeOOH) particles: an experimental and modeling study. Geochimica et Cosmochimica Acta **67**, 967-983

150 Cornell, R. M. and Schertmann, U. (1996) The iron oxides: structure, properties, reactions, occurences and uses. VCH

151 Motshwene, P., Karreman, R., Kgari, G., Brandt, W. and Lindsey, G. (2004) LEA (late embryonic abundant)-like protein Hsp12 (heat-shock protein 12) is present in the cell wall and enhances the barotolerance of the yeast *Saccharomyces cerevisiae*. Biochemical Journal **377**, 769-774

152 Sales, K., Brandt, W., Rumbak, E. and Lindsey, G. (2000) The LEA-like protein HSP 12 in *Saccharomyces cerevisiae* has a plasma membrane location and protects membranes against desiccation and ethanol-induced stress. Biochimica et Biophysica Acta (BBA) - Biomembranes **1463**, 267-278

153 Karreman, R. J. and Lindsey, G. G. (2005) A rapid method to determine the stress status of *Saccharomyces cerevisiae* by monitoring the expression of a Hsp12: green fluorescent protein (GFP) construct under the control of the Hsp12 promoter. J. Biomol. Screen. **10**, 253-259

154 Raisin, G. (2001) Enquête de prévalence des infections nosocomiales 2001. www.invs.sante.fr/surveillance/raisin **publiés le 28/10/2003**

155 Mourer, M., Duval, R. E., Finance, C. and Regnouf-de-Vains, J.-B. (2006) Functional organisation and gain of activity: the case of the antibacterial tetra-para-guanidinoethyl-calix[4]arene. Bioorganic & Medicinal Chemistry Letters **16**, 2960-2963

Annexe 1

A local nanomechanical AFM investigation of polystyrene surface properties incubated with *Shewanella putrefaciens* cells.

Fabien Gaboriaud, Sidney Bailet, Etienne Dague, and Frédéric Jorand*

Laboratoire de Chimie Physique et Microbiologie pour l'Environnement, UMR 7564, CNRS, Université Henri Poincaré-Nancy 1, 405 rue de Vandœuvre, F-54600, Villers-lès-Nancy, France

Abstract: The surface properties of polystyrene dishes (PS) incubated for 14 h with gram-negative cells (*Shewanella putrefaciens*) were investigated with the Atomic Force Microscopy (AFM) in aqueous solutions at two pH values (4 and 10). The AFM images and force curves revealed the presence of polymeric layer adsorbed onto PS surfaces in acid media. In contrast, no evolution was observed in the case of basic media.

Key words: AFM, Force spectroscopy, *Shewanella putrefaciens*, bacterial adhesion

INTRODUCTION

Microbial adhesion is the first fundamental step to colonize surfaces which allow bacteria to grow as biofilm, a form of life for microbes in aqueous environments in natural and manmade ecosystems (Bryers, 2000). The control and prevention of such surface colonization is probably one of the most important challenges for the current decades. The understanding of fundamental mechanisms yielding to microbial attachment should provide the biological and/or physicochemical key parameters to anticipate biofilm formation especially concerning pathogenesis of infectious diseases. However, extensive research in this framework provides reasonable evidence that initial adhesion yielding bacterial attachment may be described in terms of specific and/or non-specific interactions between bacteria and the target surface (Bellon-Fontaine, et al., 1996; Bos, et al., 1999; Vadillo-Rodriguez, et al., 2003). Non-specific interactions governed by long range surface forces have been primarily described by the Derjaguin-Landau-Verwey-Overbeek (DLVO) theory. This model accounts for electrostatic and van der Waals forces and in the extended version the acid base interactions. Even though, the DLVO approach is often not sufficient to explain bacterial events, due in part to complexities and heterogeneities of biological surfaces. Indeed, the nature of these components is extremely diverse, consisting of protein, carbohydrate or lipid heteropolymers (Beveridge & Graham, 1991; Graham, et al., 1991). Briefly, two types of structure can be considered: components anchored in the outer membrane/murein-protein-layer and those not anchored. The former typically consists of lipopolysaccharids (LPS) for Gram negative bacteria or lipoteichoic acids for Gram positive bacteria. The latter type concerns a less well defined group of polymers regrouped under the term EPS for extra-cellular polymeric substances (Wingenden & Neu, 1999). This describes closely (e.g. capsular polymers) or loosely bound EPS, or soluble EPS not displaying any specific contact. This definition includes products of cellular lysis and hydrolysis of macromolecules. Involvement of EPS in biofilm dynamic and structure has been well documented (Bryers, 2000; Wingenden & Neu, 1999). For instance, EPS substances may contribute both strengthen adhesion to the substratum and lead to cell-cell attachment (Bryers, 2000). However, the bacterial production of such extracellular polymeric substances may thus change significantly surface properties of colonized substratum to favor bacterial adhesion (Van der Aa & Dufrene, 2002).

The present paper investigates the surface properties of polystyrene dishes beforehand incubate with bacterial suspension with two significant different pH values (4 and 10). To this end, local force curves were recorded onto PS substrata by using *in situ* atomic force microscopy (AFM). This study began from the statement that bacterial density adsorbed onto PS substrate for acid media is significantly higher than basic one (Gaboriaud, et al., 2005). In previous study, local nanomechanical properties of the external layers of bacteria demonstrated the concomitant change of the turgor pressure of the cell and the polymeric thickness of the outermost layers of cell wall. This lead to the conclusion that bacterial surface properties in response to pH change significantly vary with the structural and mechanical modifications of bacterial ultrastructures of the

envelope (Gaboriaud, et al., 2006). However, the present work study the contribution of EPS substances to this mechanism as previously investigated by Van der Aa and Dufrêne (Van der Aa & Dufrene, 2002).

MATERIAL AND METHODS

Bacterial culture.

Gram-negative bacterial strain (Shewanella putrefaciens CIP 8040-ATCC 80.71, Collection Institut Pasteur, Paris, France) was aerobically cultured at 30°C on a solid medium (Plate Count Agar, Biomérieux 51019) for 48 h. This culture was used to inoculate a second culture in nutritive broth media (100 ml, Trypcase Soy Broth, Biomérieux 51072) for 7h. Then, ultimate culture was carried out in 1.5 L batch reactor at 30 °C for 24 h. Bacteria were harvested by centrifugation, washed twice with potassium nitrate solution (10^{-3} M), and suspended at a given pH (HNO_3 or KOH) in KNO_3 (0.1 M).

Bacterial adhesion to PS dishes.

PS dishes (30 mm diameter, Caubere Inc, Ref 306, France) were subsequently washed with concentrated nitric acid (1 M), ethanol, rinsed with demineralized water and finally dried over a Bunsen burner. Bacterial suspension (pH 4 or 10, KNO_3 0.1 M) was incubated in a PS dish for 14 h. This incubation period corresponds to optimize time for the achievement of the adsorption of bacteria at the two pH conditions. The aqueous phase was then removed, the dishes washed by a distilled water trickle to detach weakly fixed bacteria and immediately filled with acid or basic potassium nitrate solutions for AFM experiments. Abiotic control PS samples were prepared by using the same aforementioned protocol but incubated PS dish for 14 h. with only acidic, basic or neutral potassium nitrate solutions.

Atomic force microscopy. AFM imaging and force-distance measurements were obtained with a commercial microscope (Thermomicroscope Explorer EcuPlus, Veeco instruments). All measurements were performed with the same silicon nitride cantilever (Red MLCT-EXMT-BF, Veeco Instruments) with a quoted probe curvature radius of ~50 nm. This microlever had a spring constant of 0.01 ± 10% N/m according to the measurement on a cantilever of known force constant (Tortonese & Kirk, 1997). All experiments were conducted in potassium nitrate solution at a fixed ionic strength (0.1 M) for the two pH values, 4 and 10. AFM height images were collected in solution using a 100 x 100 µm piezoelectric scanner with a scan size range from 10 to 50 µm. AFM images were processed with the Scanning Probe Image Processor program (SPIP Version 2.3208, Image Metrology, Denmark). The slope of raw images was corrected by a least mean square of degree 1 fitted to the entire image and then subtracting this fitted plane from each height value. The average and standard deviations of root mean square roughness (RMS) were calculated for at least ten images. Deflection-piezo displacement curves were recorded at rate of 0.1 µm/s. To check both the linearity of our experimental device up to 200 nm of cantilever deformation and the eventual contamination of the AFM tip, force curves were recorded before and after each sample on clean glass slides. Raw curves (photodiode signal vs relative piezo displacement) were converted into force vs relative piezo displacement by using the photodetector sensivity and the cantilever spring constant. At least 100 force curves were recorded randomly on two replicates and then averaged and standard deviations calculated.

RESULTS AND DISCUSSION

Figure 1 shows representative AFM images of PS surfaces incubated 14 hours with abiotic potassium nitride solution, as the control sample (pH 4, A) or with bacterial suspension at pH 4 (B-C) and pH 10 (D-E). PS surface features in contact with bacterial suspension demonstrated significant differences in response to changes in pH. In fact, PS dishes incubated at pH 10 gave rise to AFM images (D-E) that presented RMS roughness that was very similar to the value obtained for the abiotic control PS samples (Table 1). In contrast, PS bacterial-incubated at pH 4 exhibited (B-C) significant higher RMS value compared to its respective control (Figure 1A). Obviously, such effects are apparent on AFM images but the difference in maximum height used to contrast images complicated the comparison of AFM images. That is why, z-profiles are presented in to illustrate such roughness differences.

To complement these observations, local force measurements were carried out onto PS surfaces. The abiotic control PS samples, which provided reference data, behaved as stiff surfaces. Indeed, force curves () showed wide range of linear compliance which result of the elastic deformation of the AFM cantilever onto non-deformable PS surface. In the case of non-deformable surface in interactions with the AFM tip, the slope of the curves in the constant compliance region corresponds to the spring constant of the AFM cantilever (k= 0.01 N/m, table 1, control samples). This specific case of stiff sample regarding the AFM cantilever allows to arbitrarily positioned the zero relative piezo displacement to the onset of linear compliance. This characteristic value corresponds to the contact between the AFM tip and the PS surfaces. Thus, the potential presence of surface forces translates into negative (attractive) or positive (repulsive) forces in the positive regions of relative piezo displacements.

Indeed, force curves measured on the abiotic control PS samples at pH 4 and 10 depicted the occurrence of attractive and repulsive forces in acid and basic media, respectively (). Such attractive and repulsive forces measured at pH 4 and 10 respectively, can be attributed to electrostatic forces between the AFM tip, which becomes

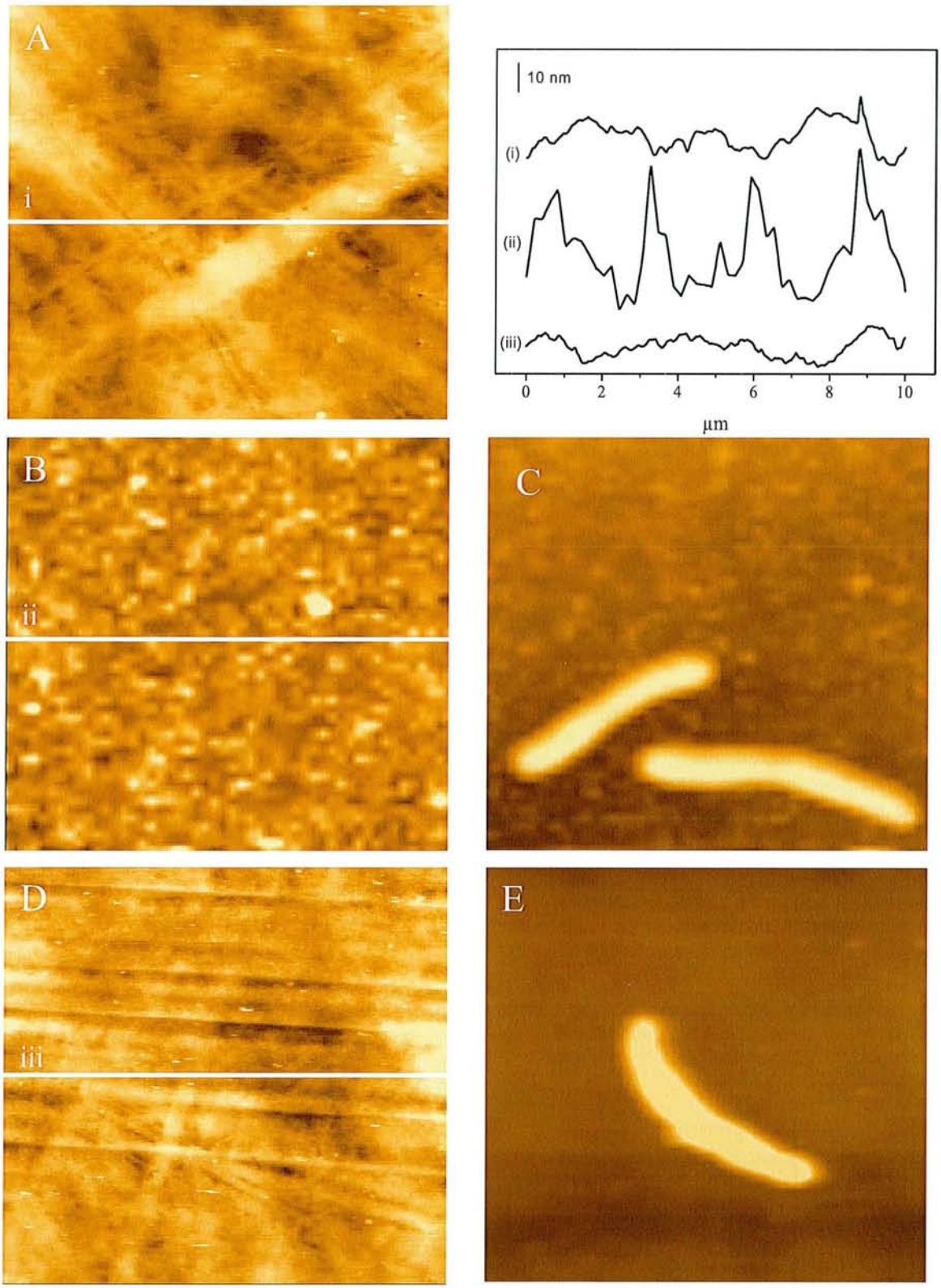

Figure 1. Typical AFM images recorded in electrolyte solution (KNO_3 0.1 mol L^{-1}) of polystyrene dishes after 14 hours of incubation stage: (A) abiotic control sample at pH 4; (B-C) incubated with *S. putrefaciens* bacterial suspension at pH 4 and (D-E)) incubated with *S. putrefaciens* bacterial suspension at pH 10. The Maximum height of the different AFM images are respectively A: 26 nm, B: 100 nm, C: 500 nm, D: 23 nm, E: 200 nm. The z-profiles describe height distributions along the lines shown within AFM images.

more and more negatively charged as the pH increases (Ducker, et al., 1991) and the polystyrene surface which appears to express acido-basic properties (positive at pH 4 and negative at pH 10). But the attractive forces observed at pH 4 may also correspond to van der Waals forces. However, these two force curves recorded on the abiotic control samples give a reference to observe changes in PS surface properties in response to bacterial incubation.

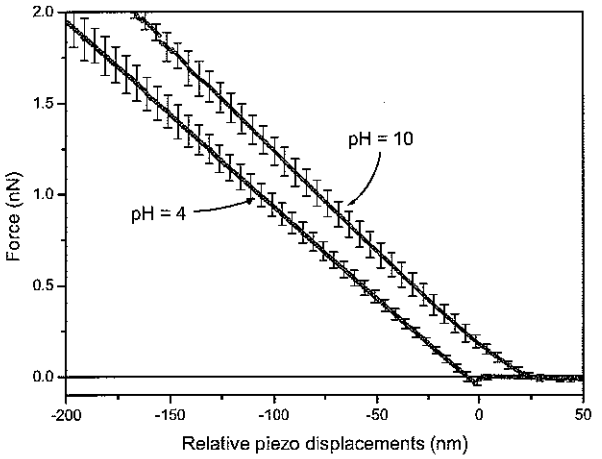

Figure 2. Average and respective standard deviation of deflection curves recorded at different pH on the abiotic control PS samples.

The analysis of force curves recorded on PS surfaces incubated with *S. putrefaciens* bacterial suspension at pH 10 (A-substrate) and pH 4 (B-substrates [1] and [2]) corroborated the previous observations on AFM images. Indeed, surface properties of PS dishes incubated in basic media did not significantly changed compared to the control sample while different nanomechanical behaviour (from the control sample) was observed for sample incubated in acid media. In fact, two types of force curves were observed for acid media, named as substrate-[1] and substrate-[2]. Both exhibited a wide linear range in the negative relative piezo displacement domain with slopes significantly lower than the control stiff surface (Table 1).

Table 1. Root mean square roughness and slope of force curves in the constant compliance region measured on the abiotic control PS samples and the PS incubated with *Shewanella putrefaciens* suspension.

		RMS Roughness (nm)	Slope ($N.m^{-1}$)
pH 10	Control	3.5 (± 1)[a]	-0.011 (± 0.001)[e]
	Substrate	4.5 (± 1)[b]	-0.010 (± 0.001)[e]
pH 4	Control	3.8 (± 1)[c]	-0.010 (± 0.001)[f]
	Substrate [1]	14 (± 1)[d]	-0.008 (± 0.001)[f]
	Substrate [2]		-0.008 (± 0.001)[f]

[a] Representative AFM images not shown but similar to Fig. 1A, [b] Representative AFM images in Fig. 1D-E, [c] Representative AFM images in Fig. 1A, [d] Representative AFM images Fig. 1B-C. [e] Force curves in Fig. 3A, [f] Force curves in Fig. 3B.

Such features translate into the contribution of an elastic deformation of substrate suggesting the presence of polymeric coating adsorbed on PS dishes. The surface forces also evolve from attractive to repulsive interactions that confirm the significant change of surface properties of PS substrates. This modification of PS dishes incubated with bacterial suspension at pH 4 was consistent with AFM images suggesting the presence of a rough substrate in this condition.

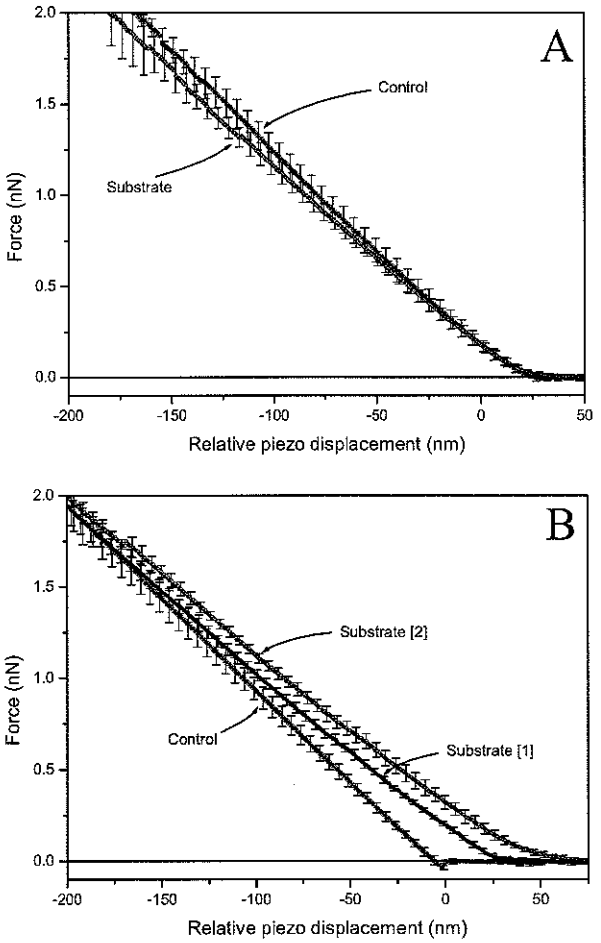

Figure3. Average and respective standard deviation of force curves for (i) the controls corresponding to curves of Fig. 2and (ii) the substrates that corresponded to PS dishes incubated with *S. putrefaciens* suspension (ionic strength of 0.1 M, 14 hours). Two pH conditions were tested: (A) pH = 10 and (B) pH = 4.

Retraction curves provided further insights on the type of interaction between the tip and the morphological nature of PS substrates. Figure 4 shows typical single raw curves obtained on the abiotic control (Fig. 4a) and bacterial-incubated (Fig. 4b) PS samples. Retraction curves recorded on the control PS sample revealed single adhesion signature characteristic of two relatively flat surfaces in interaction. In contrast, curves corresponding to the bacterial-incubated sample in acid media demonstrated multiple adhesions. However, this feature indicates that the polymer adsorbed, previously suggested, behave as elongated polymer structure.

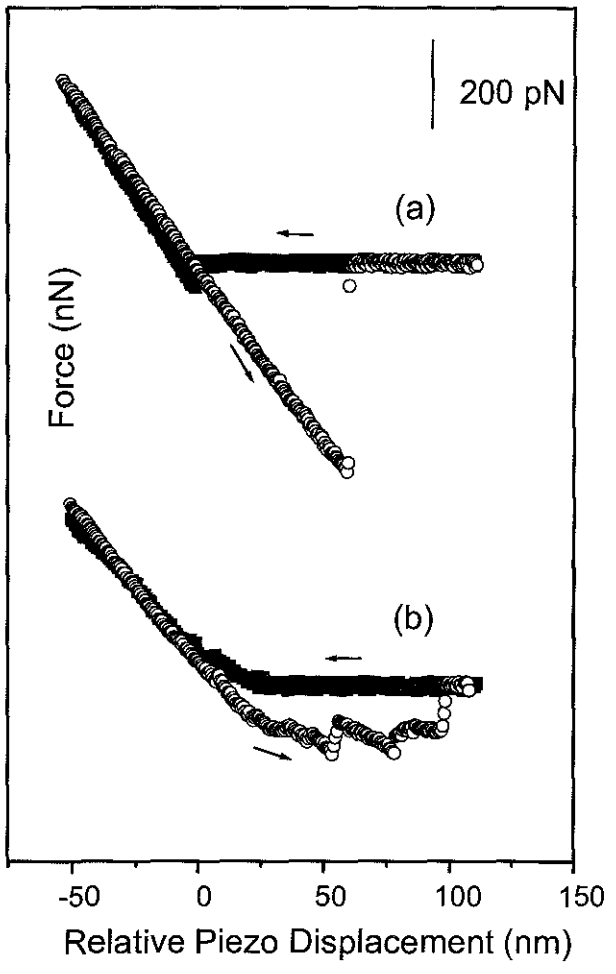

Figure 4. Representative single approach and retraction curves measured at pH 4 on (a) the abiotic control PS sample and on (b) the corresponding substrate of PS dishe incubated with bacterial suspension.

In summary, the substrate in contact with bacterial suspensions showed, as a function of pH, the presence or not of polymers. These polymers adsorbed on the polystyrene surface at pH 4 may result from EPS or cell lysis by-product during the incubation step. Complement experiments by using epi-fluorescence microscopy with "live-dead" test demonstrated that the membrane integrity of bacteria was effectively affected in acid media and not in basic one. In contrast, the numeration of cell did not shown significant differences between these two pH conditions. Therefore, we can conclude that the membrane lysis could be partly responsible of the presence of an extracellular polymer layer in acid solution. However, it is usually proposed that biofilms are initiated from the initial adsorption of organic matter on the surface to enhance the fixation of bacteria (Bryers, 2000). These results demonstrated the capability of AFM to resolve the nanomechanical evolution of PS surfaces incubated at two pH values. The next challenge would be to resolve kinetically the bacterial adhesion versus polymer adsorption.

REFERENCES

Bellon-Fontaine, M.N., Rault, J. & van Oss, C.J. (1996). Microbial adhesion to solvents: a novel method to determine the electron-donor/electron-acceptor or Lewis acid-base properties of microbial cells. Colloids and surfaces B: Biointerfaces **7**, 47-63.

Beveridge, T.J. & Graham, L.L. (1991). Surface layers of bacteria. Microbiological reviews **55**, 684-705.

Bos, R., van der Mei, H.C. & Busscher, H.J. (1999). Physico-chemistry of initial microbial adhesive interactions - its mechanisms and methods for study. FEMS Microbiology Reviews **23**(2), 179-229.

Bryers, J.D. (2000). Biofilms II. New York.

Ducker, W.A., Senden, T.J. & Pashley, R.M. (1991). Direct measurement of colloidal forces using an atomic force microscope. Nature **353**, 239-141.

Gaboriaud, F., Bailet, S., Dague, E. & Jorand, F. (2005). Surface structure and nanomechanical properties of *Shewanella putrefaciens* bacteria at two pH values (4 and 10) determined by Atomic force microscopy. J. Bact. **187**(11), 3864-3868.

Gaboriaud, F., Dague, E., Bailet, S., Duval, J.F., Jorand, F. & Thomas, F. (2006). Multiscale study of the dynamic of bacterial envelope at solide-water interfaces: application to *Shewanella putrefaciens* strains. Colloids and Surfaces B: Biointerfaces **50**, 123-131.

Graham, L.L., Harris, R., Villiger, W. & Beveridge, T.J. (1991). Freeze-substitution of Gram negative eubacteria : general cell morphology and enveloppe profiles. J. Bact. **173**(5), 1623-1633.

Tortonese, M. & Kirk, M. (1997). Characterization of application specific probes for SPM's. Micromachinig and Imaging **SPIE Proc.**(3009), 53-58.

Vadillo-Rodriguez, V., Busscher, H.J., Norde, W., de Vries, J. & van der Mei, H.C. (2003). On relations between microscopic and macroscopic physicochemical properties of bacterial cell surfaces: an AFM study on *Streptococcus mitis* strains. Langmuir **19**(6), 2372-2377.

Van der Aa, B.C. & Dufrene, Y.F. (2002). *In situ* characterisation of bacterial extracellular polymeric substances by AFM. Colloids and Surfaces B: Biointerfaces **23**, 173-182.

Wingenden, J. & Neu, T.R. (1999). Microbial ectracellular polymeric substances Flemming (Ed.), H.C. **New York springer verlag**.

Acknowledgments: The authors thank G. Jeannesson and C. Gérard for their tireless efforts to optimize physico-chemical conditions to observe bacterial adhesion. This study was granted by CNRS (PNIR-Biofilms and Fédération Eau-Sol-Terre, Nancy) and by Henri Poincaré University of Nancy (special BQR grant).

Annexe 2

Available online at www.sciencedirect.com
ScienceDirect
Biochimica et Biophysica Acta 1774 (2007) 131–137
Biochimica et Biophysica Acta
BBA
www.elsevier.com/locate/bbapap

The stress response protein Hsp12p increases the flexibility of the yeast *Saccharomyces cerevisiae* cell wall

Robert J. Karreman [a], Etienne Dague [b], Fabien Gaboriaud [b], Fabienne Quilès [b], Jerome F.L. Duval [c], George G. Lindsey [a,*]

[a] *Department of Molecular and Cellular Biology, University of Cape Town, Private Bag, Rondebosch, 7701, South Africa*
[b] *Laboratory of Physical Chemistry and Microbiology for the Environment, Nancy-University, CNRS, 405 rue de Vandoeuvre, F-54600 Villers-lès-Nancy, France*
[c] *Laboratory Environment and Mineral Processing, Nancy-University, CNRS, P.O. Box 40, F-4501, Vandoeuvre-lès-Nancy, Cedex, France*

Received 4 August 2006; received in revised form 3 October 2006; accepted 19 October 2006
Available online 27 October 2006

Abstract

The yeast *S. cerevisiae* cell wall comprising a 10 nm thick layer of polysaccharides, predominantly β(1,3)-glucan and proteins, is the interface between the cell and the neighbouring environment. As such it is not a static entity but rather one that is dynamically remodelled in response to changes in the environmental conditions. We have recently proposed from studies using yeast cells lacking the gene encoding Hsp12p (*Δhsp12* yeast) and from incorporation of Hsp12p into agarose, used as a model system for the β-glucan layer of the cell wall, that the hydrophilic stress response cell wall protein Hsp12p acts as a cell wall plasticizer. In this report we have used force spectroscopy to confirm that *Δhsp12* yeast are indeed less flexible than the wild type strain. The spring constant of the cell wall of *Δhsp12* yeast, k_{cw} was determined to be 72±3 mN m^{-1} as compared to 17±5 mN m^{-1} obtained for the wild type strain. A similar result was found on the basis of a quantitative analysis of the electrophoretic mobilities measured for the two yeast strains. Those indicated that the hydrodynamic permeability quantified through the softness parameter of the external layer of *Δhsp12* cells was smaller than the one of wild type cells. We proposed from surface infrared spectroscopy measurements that yeast compensate for the lack of Hsp12p by reducing the carbohydrate/proteins ratio of the cell wall or increasing the cell wall chitin content.

Keywords: *Saccharomyces cerevisiae*; Cell wall flexibility; Force spectroscopy; Infrared spectroscopy; Electrophoresis; Soft particle analysis; AFM

1. Introduction

Hsp12p is a small (12 kDa) hydrophilic stress response protein in the yeast *Saccharomyces cerevisiae*, the mRNA for which has been shown to be up-regulated by a variety of stresses including increased temperature, osmotic strength, salt concentration, by growth in lipid media as well as after perturbation of the cell wall [1–3]. Originally identified as a Late Embryogenic Abundant (LEA)-like protein [4], we initially showed that Hsp12p was present in the yeast cell close to the plasma membrane and was able to protect an artificial liposome membrane system against desiccation and subsequent rehydration, and ethanol-induced stress [5]. We subsequently demonstrated that Hsp12p is also present in the cell wall, where we have proposed that it acts as a plasticizer [6]. Evidence for this is that the cell size of a yeast cell lacking the *HSP12* gene (*Δhsp12* strain), when compared with the wild type strain, was less responsive to changes in external osmolality but that the cells were more prone to bursting after a rapid decease in the barometric pressure. Since these results only correlated the presence of Hsp12p with changes in cell behaviour, we purified Hsp12p and incorporated the purified protein into agarose, used as a model system to represent the β-glucan layer of the cell wall [7]. Whereas incorporation of solutes such as salts and osmolytes known to induce Hsp12 expression reduced the flexibility of the agarose, i.e. increased the resistance to deformation, incorporation of Hsp12p resulted in increased flexibility being observed. Simultaneous incorporation of solutes

Abbreviations: AFM, atomic force microscopy; HSP, heat shock protein; LEA, late embryogenic abundant; YEPD, yeast extract peptone dextrose; PEI, polyethyleneimine; ATR, Attenuated Total Reflection; FTIR, Fourier Transform infrared; DTGS, deuterated triglycine sulphate

* Corresponding author. Tel.: +27 21 650 2406; fax: +27 21 689 7573.
E-mail address: lindsey@science.uct.ac.za (G.G. Lindsey).

1570-9639/$ - see front matter © 2006 Elsevier B.V. All rights reserved.
doi:10.1016/j.bbapap.2006.10.009

together with Hsp12p resulted in intermediate flexibilities depending on their relative concentrations.

In recent years, Atomic Force Microscopy (AFM) has become an important tool to quantify the interaction forces and physical properties of microbial surfaces [8]. In particular, force spectroscopy has been developed for investigating native cell surfaces with piconewton sensitivity and nanometer lateral resolution, providing novel information on the nanomechanical properties of cell walls [9–11] and on the forces and localisation of molecular recognition events [12,13]. In addition, the recent numerical resolution of the governing electrokinetic equations for diffuse soft particles has allowed the rigorous determination of the key electrostatic and hydrodynamic parameters that determine the electrophoretic migration of biological cells subjected to a DC electric field [14–16]. Basically, this analysis makes it possible to estimate the volumic charge density and the softness parameter of microbial surfaces. Information on the spatial heterogeneity of cell wall polymers may also be obtained. During the past decade, infrared spectroscopy has essentially only been used to identify yeasts [17] with a few studies investigating the chemical and structural properties of dried yeasts [18,19]. It is possible, however, to record infrared spectra in aqueous suspension using the Attenuated Total Reflection (ATR) mode. This allows one to gain chemical information regarding the peripheral layers of the yeast cells to a depth of approximately 1 μm in a physiological environment.

In this report we have combined force spectroscopy and soft particle analysis of the electrophoretic measurements to quantify the nanomechanical and the electrohydrodynamic properties of two different yeast strains. We demonstrated that the presence of the stress response protein Hsp12p resulted in a more flexible cell, thereby confirming our hypothesis that Hsp12p acts a cell wall plasticizer in the yeast *S. cerevisiae*.

2. Materials and methods

2.1. Yeast strains and growth conditions

The yeast strains used (gifts from Dr. P. Meacock at the Department of Genetics, University of Leicester, Leicester, UK) were the haploid segregants from the diploid strain 842 (a/α, ade2-1/ade2-1, trp1-1/trp1-1, leu2-3/leu2-112, his3-11/his3-15, ura3/ura3, canr1-100/CAN) [20]. Growth media and growth conditions were as described previously [6].

2.2. Force spectroscopy by AFM

Yeast cells in YEPD growth medium were washed into 1 mM KNO_3 pH 6.5 and the concentration adjusted to a cell density of 0.06 at 600 nm. Glass microscope slides (Menzer GmBH, Braunschweig, Germany) 38×26 mm were washed overnight in 70% nitric acid before being rinsed with distilled water. The slide was then covered with 0.2% (w/v) solution of polyethyleneimine (PEI, Sigma Chemical Co.) in water and left at 20 °C for 4 h after which it was washed with distilled water. The washed slide was covered with 2 ml of the yeast cell suspension and then left for a further 1 h at 20 °C before excess yeast was removed by gently rinsing the slide with 1 mM KNO_3 pH 6.5. The slide was covered with 1 mM KNO_3 pH 6.5 and subsequently examined by AFM. In parallel, the procedure was optimized by using an Olympus BX51 phase contrast microscope at 100× magnification to ensure an even yeast cell coating had been obtained.

All AFM measurements were performed in aqueous solution (1 mM KNO_3 pH 6.5) at room temperature using a commercial microscope (Thermomicroscope Explorer EcuPlus, Veeco Instruments). Samples were initially imaged at low resolution to identify individual cells on the PEI-coated glass plate. Force curves were measured between a single silicon nitride tip (k_c=0.03 N/m, MLCT-EXMT-BF, Veeco Instruments) and the cell surface. A single force measurement was performed on an individual cell to avoid potential hysteresis. A minimum of 5 individual cells from 2 separate yeast cultures were used for such measurements. The raw deflection–piezo displacement curves were converted into force curves by using the sensitivity of the photodetector and the spring constant of the cantilever. The zero relative piezo displacement of each curve was arbitrarily positioned to the lift-off from zero force on the approach curve. For each sample, force curves and standard deviations were calculated (n=5).

2.3. Microelectrophoresis and soft particle analysis

Electrophoretic mobility measurements were performed using a Zetaphoremeter IV (SEPHY-CAD Instrumentations) equipped with laser illumination and video interface via a CCD camera and image software analysis. Measurements were carried out in a quartz suprasil cell at 25 °C by recording at least fifty measurements of cell mobility for each condition. The mobilities of fresh cell suspensions in 1 mM KNO_3 pH 6.5, prepared as described for AFM measurements, were recorded at various ionic strengths ranging from 1 mM to 30 mM KNO_3 pH 6.5. The relationship between electrophoretic mobility and ionic strength was analysed following the theoretical formalism described recently [14]. Briefly, the electrokinetic response of the investigated yeast is assimilated to that of a soft particle that is composed of an impermeable hard-core component covered with a permeable polyelectrolyte layer [14]. The rigorous numerical evaluation of the electrophoretic mobilities without any restriction on the particle size, particle charge and Debye layer thickness allows the derivation of the relevant interfacial electrostatic and hydrodynamic parameters. The spherical yeast cells studied were modelled as soft spherical entities of core radius a close to 1.5 μm and a cell wall thickness δ of about 100 nm. The experimental data were fitted using the method of least mean squares to determine the softness parameter (λ_0) and the volumic charge density (ρ_0)of the cell wall.

2.4. Infrared spectroscopy

Attenuated Total Reflectance Fourier Transform infrared (ATR-FTIR) spectra of yeast suspensions in MilliQ water were measured between 4000 cm^{-1} and 600 cm^{-1} on a Perkin Elmer 2000 spectrometer equipped with a KBr beam splitter and a deuterated triglycine sulphate (DTGS) thermal detector. The ATR accessory consists of a horizontal diamond crystal prism (ASI, 9 internal reflections or bounces on the upper surface, angle of incidence: 45°, penetration depth at 1500 and 1000 cm^{-1}: 1 and 1.5 μm, respectively). The spectral resolution was 4 cm^{-1} and the total accumulation time approximately 4 min. Irradiance through the empty cell was about 20% of the full signal without the ATR accessory. ATR spectra of the sample were plotted using an absorbance scale corresponding to $\log(R_{reference}/R_{sample})$ where the reference spectrum was the spectrum of water. The contribution of water vapour and carbon dioxide was removed using the H_2O/CO_2 procedure of the Spectrum 5.0.1 software. The ATR spectra are not strictly proportional to the absorption coefficients at each wavenumber since no further correction has been applied [21]. In practice, measurements required approximately 100 μl of the yeast cell suspension applied to the horizontal surface of the diamond prism.

3. Results

3.1. Nanomechanical measurements by AFM

The main difficulty with AFM of biological samples is the prerequisite immobilization of the sample onto a support to allow imaging in solution and subsequent force analysis. Another requirement is to preserve, as much as possible, the viability and the delicate surface ultrastructure of the cell. The two main approaches that have been used to fulfil these two conditions are either mechanical trapping [10,22] or physical

adsorption onto either a hydrophobic substrate or a surface coated with a positive macromolecule such as poly-L-lysine or polyethyleneimine (PEI) [23–25]. PEI-coated glass slides were chosen for the current study, as this allows the concomitant recording of the force curves of the soft cell together with the reference force curve of the stiff PEI-coated glass slide.

Light microscopic examination of the PEI-coated glass slide prepared for AFM showed the presence of individual yeast cells over the entire slide (not shown). The yeast cells were not closely packed but present at a density commensurate with easy location of individual cells. Force measurements were therefore unaffected by the presence of adjacent cells which might prevent lateral deformation brought about by indentation due to the application of force. The yeast cells remained viable throughout the AFM procedure, since subsequent overnight incubation of the slide at 30 °C in 20 ml YEPD growth medium resulted in substantial yeast growth (not shown). No differences in viability were observed between the wild type and the *Δhsp12* strains.

Sections 50×50 μm of the PEI-coated slide were scanned using AFM to locate individual cells, which were then scanned at higher resolution. We initially used 100 mM KNO_3 as the incubation medium for yeast cell adherence to the PEI-coated slide, the use of this salt concentration aimed to reduce electrostatic interactions. Although cells were visible under light microscopy after such treatment, no cells were located upon scanning the slide using AFM. We considered this to be due to the cells being displaced by the AFM probe due to poor adhesion brought about by the low surface charge of yeast cells, as demonstrated by their electrophoretic behaviour (see later). Accordingly 1 mM KNO_3 was used as the incubation medium for yeast cell adherence. Since electrostatic interactions and deformation of soft cells both result in non linear behaviour especially at low loading, the mechanical contribution of the non linear domain was not interpreted [10,11] Fortunately, the linear behaviour of the force curve corresponds to the mechanical deformation of the cell wall and the spring constant of the cell wall, k_{cw}, could be calculated using the equation:

$$k_{cw} = -k_c \cdot \left(\frac{S}{S + k_c}\right)$$

where k_c represents the spring constant of the cantilever and S the slope of the linear domain of the force curve.

Yeast cells bound to the PEI-coated slide in 1 mM KNO_3 were observed to be spherical with diameters ranging between 2.5 μm and 6 μm. A typical AFM scanned image of a yeast cell is shown in Fig. 1. Regions of individual cells of similar size were identified as potential sites for measurement of the force curves. Regions with bud scars were not selected since these regions have been reported to exhibit increased rigidity due to the presence of chitin [10].

In contrast with the stiff behaviour displayed by the glass surface, the force curves recorded for the two yeast strains exhibited soft behaviour with a non linear component at low loading forces and a quasi-linear domain at high loading forces (Fig. 2). The nanomechanical properties of 2.5 μm diameter

Fig. 1. Typical AFM height image (12×12 μm; Z-Range: 3 μm) of a *S. cerevisiae* wild type cell recorded in aqueous solution (1 mM KNO_3, pH 6.5).

cells of the two strains were significantly different, the *Δhsp12* strain appearing stiffer (k_{cw}=72±3 mN m^{-1}) than the wild type strain (k_{cw}=17±5 mN m^{-1}). Interestingly, the size of the cell affected the nanomechanical properties of the cell, as the spring constant of the cell walls of 4.5 μm diameter *Δhsp12* cells was significantly lower (k_{cw}=19±2 mN m^{-1}). Using agarose as a model system for the yeast cell wall, we demonstrated that the flexibility of agarose decreased upon incorporation of osmolytes such as mannitol [7]. We therefore investigated the effect of mannitol on the spring constant of the cell wall, k_{cw}, of wild type yeast by incubating the PEI-coated glass slide containing these yeasts in 0.8 M mannitol for 10 min before determining the force curves. We found that the spring constant in the presence of mannitol increased 8-fold to 141±1 mN m^{-1} (Fig. 2).

3.2. Soft particle analysis

The electrophoretic mobility of a particle in an electric field depends on the ionic strength of the environment as well as on the softness of the particle. Yeast cells may be regarded as soft particles since they are surrounded by hydrodynamically permeable cell walls, where electro-osmotic flow may occur. The electrophoretic mobility of a rigid particle tends to zero at high ionic strength whereas that of soft particles, such as biological cells, exhibits a non-zero asymptotic electrophoretic mobility. This feature is the characteristic signature of the presence of a hydrodynamically permeable layer surrounding the particle. For soft particles, the classical equations originally derived by Smoluchowski and Henry are inappropriate since they refer to rigid particles exclusively. Instead, the complex electro-hydrodynamic properties of a soft particle, that ultimately govern its electrophoretic migration, should be computed *ab initio* from the governing Navier–Stokes and Poisson–Boltzmann equations with the appropriate boundary conditions [14]. This view is supported by the fact that zeta-potential, classically adopted within the framework of the electrokinetics of hard materials, is irrelevant when dealing with soft matter. This is because there is *a priori* no unambiguous way to locate the slip plane within the charged permeable layer that confers the softness to the particle investigated.

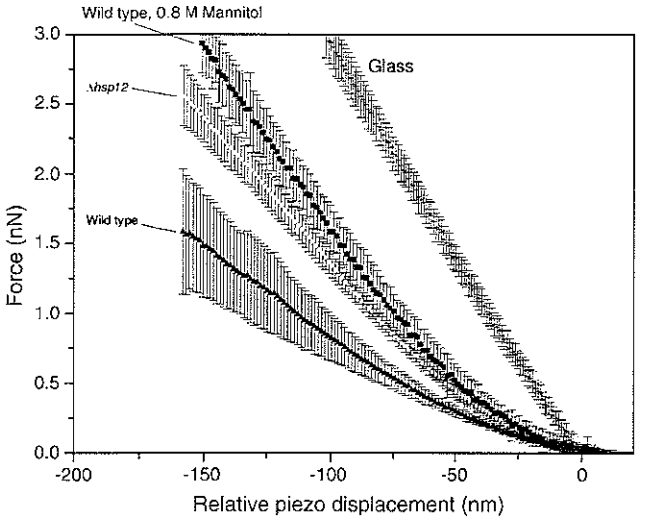

Fig. 2. Mean and respective standard deviations ($n=5$) of force curves measured on the top of 2.5 μm diameter cells of the two different yeast strains (wild type and *Δhsp12*) in aqueous electrolyte solution (1 mM KNO_3, pH 6.5) and the wild type strain in the presence of electrolyte solution containing 0.8 M mannitol. The force curve obtained on the glass surface is also shown for comparative purposes.

The experimentally determined electrophoretic mobilities of the wild type and the *Δhsp12* yeast strains at different ionic strengths and at neutral pH value are shown in Fig. 3. The electrophoretic mobilities of both strains reached a non-zero constant value upon increasing the ionic strength, as expected from the theoretical considerations of soft particle behaviour. We used a recent numerical method that describes the electrophoretic behaviour of soft particles. This method has already been used successfully in determining the electrohydrodynamic behaviour of other soft systems such as bacteria and humic substances [15,26]. The analysis allows the determination of the softness parameter (λ_0) and the volumic charge density (ρ_0) of the soft layer for both strains of yeast. The quantity $1/\lambda_0$ has a length dimension and characterises the typical penetration length of the flow within the charged polyelectrolytic layer surrounding the cell.

In agreement with both the literature and the AFM image, the cells were modelled as spherical particles with a hard core of radius 1.5 μm coated with a polyelectrolyte permeable layer 100 nm thick. The resulting best fit calculations are shown in Fig. 3 as plain lines. While the volumic charge densities were similar for the two strains, the hydrodynamic permeability was significantly higher for the wild type strain ($1/\lambda_0=3\pm0.3$ nm) compared with the *Δhsp12* strain ($1/\lambda_0=2.3\pm0.2$ nm). This result suggested that the external layer of the *Δhsp12* cells is more compact, more rigid and less flexible than the corresponding layer of wild type cells.

3.3. Infrared spectroscopy

Since the yeast cells were between 2.5 μm and 6 μm diameter, infrared spectroscopy using the ATR devices only detected spectral features associated with the peripheral layers of the cells which contacted the diamond crystal. The 1800 cm^{-1} to 800 cm^{-1} region of the ATR-FTIR spectra of the two yeast strains is shown in Fig. 4 with the spectral assignments summarised in Table 1. The spectra were normalised with respect to the amide II band centred at 1540 cm^{-1}, representative of only the protein-like compounds since neutral polysaccharides have no vibrational bands in the 1800–1500 cm^{-1} region of the infrared spectrum. The inset in Fig. 4 depicts the difference spectrum in the 1300 cm^{-1} to 900 cm^{-1} region.

The spectra of the yeast strains displayed bands at similar wavenumbers, indicating similar chemical compounds, although significant different absorbance values were observed at specific wavenumbers. Particularly, the region above 1500 cm^{-1} showed the same features, and we have assumed that the cell wall protein

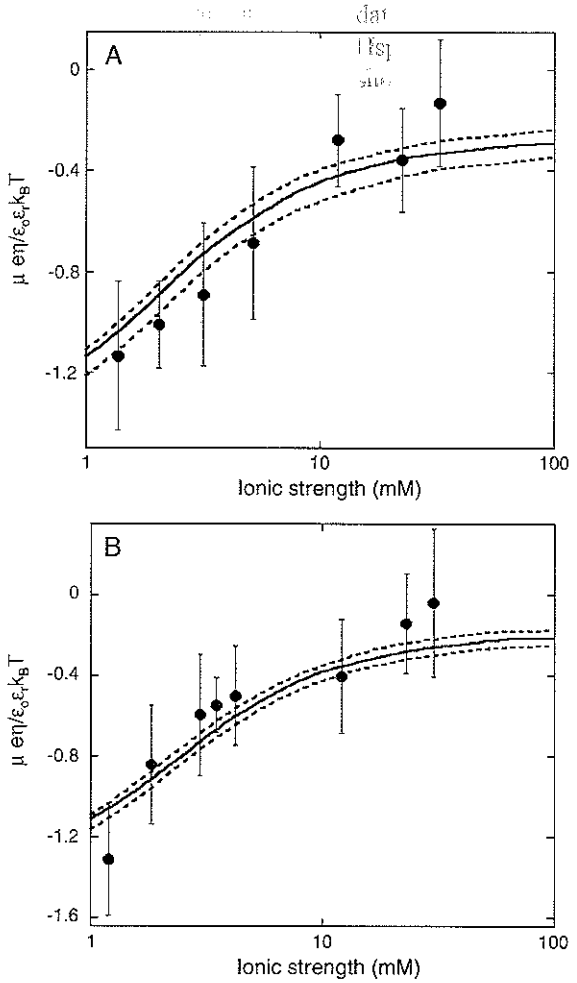

Fig. 3. Dimensionless electrophoretic mobilities as a function of ionic strength (KNO_3, pH 6.5) for the wild type strain (A) and the *Δhsp12* strain (B). The quantities e, η, $\varepsilon_0\varepsilon_r$, k_B and T denote the elementary charge, the dynamic viscosity of water, the dielectric permittivity of water, the Boltzmann constant and the absolute temperature, respectively. Experimental data (filled circles) were fitted numerically (plain and dashed lines) using the adjustable parameters, $1/\lambda_0$ characterising the typical flow penetration (nm) within the soft polymeric layer, and ρ_0, the volumic charge density of that layer. Model parameters: (A) $1/\lambda_0=3$ nm (plain curve); $1/\lambda_0=3$ nm±10% (dashed curves); $\rho_0=-6$ mM (B) $1/\lambda_0=2.3$ nm (plain curve); $1/\lambda_0=2.3$ nm±10% (dashed curves); $\rho_0=-7$ mM. The thickness of the permeable polyelectrolyte layer (δ) was taken to be 100 nm with a core radius of the cell of approximately 1.5 μm.

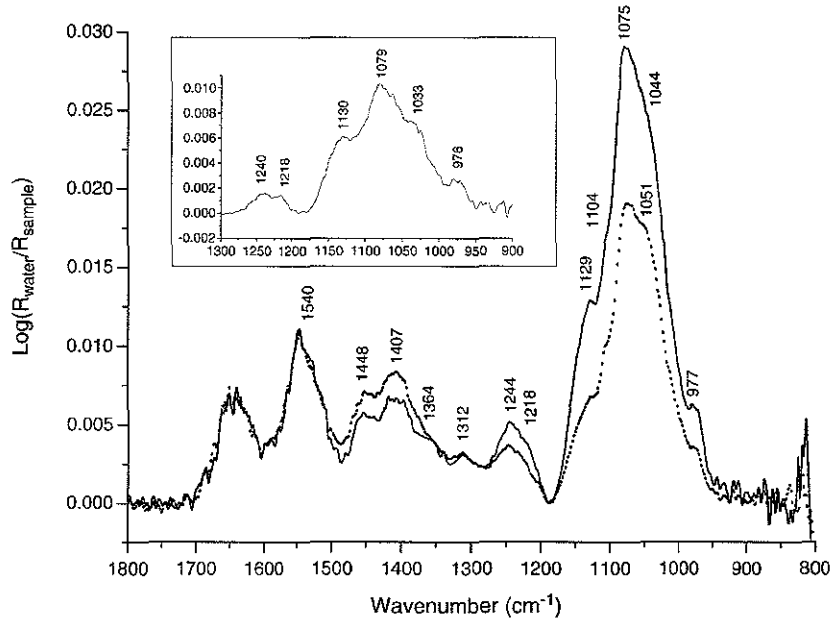

Fig. 4. ATR-FTIR spectra of wild type strain (solid line) and *Δhsp12* strain (broken line) yeasts in water. The spectra were normalised with respect to the amide II band at 1540 cm^{-1}. The insert depicts the 1300–900 cm^{-1} region of the difference spectrum (wild type spectrum — *Δhsp12* spectrum).

composition of the two yeast strains was the same. The amide III band at 1244 cm^{-1} was overlapped by the antisymmetric stretching of phosphate groups at 1218 cm^{-1}, which were assigned to phosphate groups linked to polysaccharides present in the cell wall. The presence of polysaccharides was principally established from the absorption between 1200 cm^{-1} and 950 cm^{-1}, characteristic of β(1,3)-glucans and mannans (Table 1), the principal polysaccharide constituents of the cell wall [27]. Unfortunately, the strong absorption of water below 900 cm^{-1} prevented resolution of the anomeric region which would have yielded additional information on the glycosidic linkages.

The spectra of the two yeast strains, especially that of the 1300 cm^{-1} to 950 cm^{-1} region, showed that the relative quantities of polysaccharides and phosphodiesters present in the two strains were quite different, with an increased polysaccharide:protein ratio observed for the wild type strain. The spectrum resulting from the difference between the normalised spectra (Fig. 4 inset) showed no signal above 1500 cm^{-1} characteristic of proteins but showed increased values between 1150 and 950 cm^{-1} characteristic of the presence of both β(1,3)-glucans and mannans. This was confirmed by inspection of the 1270 cm^{-1} to 1200 cm^{-1} region of the spectrum. The band at 1240 cm^{-1}, assigned to β(1,3)-glucans and the band at 1218 cm^{-1}, assigned to phosphate groups (probably from phosphopeptidomannans) also showed that the quantity of these compounds was higher in the wild type strain.

Table 1
Assignments [18,19,37] of infrared vibrational bands of the 1800–900 cm^{-1} region of the ATR-FTIR spectrum of yeast cells in aqueous suspension (Key: ν: stretching, δ: bending)

Wavenumber (cm^{-1})	Assignment
1644	Amide I (νC=O, δN-H, νC-N); δH2O (possible residual band arising from non perfect compensation for water)
1540	Amide II band (νC-N, δC-NH)
1448	δCH_2
1407	δCH
1312	β glucans
1244	Amide III (δCN-H, νC-N, νC=O);
1240	β glucans
1218	P=O stretching in phosphate esters
1200–950	C–O–C, C–O, C–C stretchings, CH_2 (sugars); PO_2, C–O–P and P–O–P stretchings (weak intensity)
1129; 1051; 977	Mannans
1104; 1075	β(1,3)-glucans

4. Discussion

In this report, we have used complementary physicochemical techniques to assess the nanomechanical and hydrodynamic properties of the *S. cerevisiae* cell wall in relation to the vibrational features of peripheral layers of the cell. Few studies have reported the mechanical measurement of yeast cells [10,28]. Smith et al. [28] determined the average surface modulus of the yeast cell and found this value to be almost 10^3 times greater than those determined in this study. The two studies are not comparable, however, since not only was a different yeast strain used but also the mechanical measurements were performed by compressing the whole cell rather than a localised area of the cell wall. Although Touhami et al. [10] also investigated the nanomechanical properties of *S. cerevisiae* cells using force spectroscopy, the direct comparison of force measurements is always risky as the force data are strongly dependant on the experimental configuration (cantilever spring constant, tip geometry, cell preparation). In addition, we used the laboratory strain W303, which would correspond to a conventional bottom fermenting yeast, whilst Touhami et al. used the

industrial strain MUCL38475, a top fermenting yeast, presumably with different ploidy [10]. Despite this, the average Young's modulus reported by Touhami et al. by using a Hertz model (E=0.6 MPa) corresponds to a spring constant close to 42 mN m^{-1}, which is of the same order of magnitude as those reported in our study.

To the best of our knowledge, this is the first study that has investigated the impact of a single protein on the mechanical properties and chemical composition of the cell wall. We have shown that the hydrophilic stress response protein Hsp12p affected the flexibility, texture and polysaccharide content of the yeast cell wall. Cells lacking Hsp12p were found to be significantly less flexible than wild type cells, requiring approximately four times more force to deform to the same extent cells containing this protein. These data confirmed earlier work from which we deduced that Hsp12p might act as a cell wall plasticiser [6]. This had showed that wild type cells increased or decreased in size more markedly than cells lacking Hsp12p when decreasing or increasing the osmolality of the environment. Moreover, wild type cells were less prone to breakage after a rapid change in the barometric pressure and were more prone to abrasion-mediated damage than *Δhsp12* cells. This latter behaviour is typical of plastics, where rigid polymers are more abrasion-resistant than flexible polymers synthesised from the same monomeric units [29].

Hsp12p was also shown to affect the flexibility of the cell wall by calculation of the softness parameter, determined from the ionic-strength dependence of the electrophoretic mobilities of the wild type and the *Δhsp12* cells. These data suggested that the effect of Hsp12p was not only to decrease the rigidity of the yeast the cell wall but also to increase its permeability. Although we attributed the more marked change in size of wild type than *Δhsp12* cells when decreasing or increasing the osmolality of the environment to changes in cell wall flexibility alone, it is possible that some component of this change was brought about by an altered rate of water ingress or egress respectively. This is currently under investigation. Infrared spectroscopy suggested that yeast responded to deletion of the *HSP12* gene by reducing the content of β-glucans, mannans and phosphopeptidomannans in the cell wall. Yeast mutants lacking glucan synthase activity have been shown to have also a compensatory increase in the cell wall chitin content [36]. The lowered amount of glucan in the cell wall of *Δhsp12* cells might also have resulted in a similar increase in the chitin content. This would result in these cells having less flexible cell walls since the bud scar, a region of the cell wall comprised mainly of chitin, has been shown to be stiffer than the surrounding cell wall [10].

This trend is also consistent with previous results obtained in an *in vitro* system [7] that demonstrated the plasticizer effect of Hsp12p protein. Indeed, incorporation of Hsp12p into the polysaccharide agarose, used as a model system to represent the β-glucan polysaccharide layer of the yeast cell wall, resulted in a concentration-dependent increase in the flexibility of the agarose gel. In contrast, inclusion of osmolytes such as mannitol in the agarose matrix resulted in a concentration-dependent decrease in the flexibility of the agarose gel strength; as in our study. Therefore, the agarose system appeared to be a useful model to investigate changes in cell wall flexibility.

Microarray studies have shown that *HSP12* is up-regulated by both the cell integrity pathway and the general stress response pathway [30,31]. In the case of the latter pathway, we have demonstrated that this results in the presence of an increased Hsp12p concentration [4]. The cell integrity pathway is a Mitogen Activated Protein (MAP) kinase pathway in yeast, which responds to stresses which directly affect cell wall assembly and integrity (for a review, see [32]). Targets for this pathway include proteins involved in cell cycle regulation [33], cell wall biosynthesis [34], cell wall assembly [35] and stress responses; this includes Hsp12p [30]. The general stress response pathway, also a MAP kinase pathway, is up-regulated by a variety of factors including increased osmolality. Exposure of yeast cells to the osmolyte mannitol, to simulate osmotic stress, resulted in an approximate 8-fold decrease in cell wall flexibility as measured by force measurements. We would postulate that yeast cells sense the changed cell wall flexibility, possibly via the cell integrity pathway and the resultant increased Hsp12p synthesis is designed to counter the changed flexibility of the cell wall. The mechanism by which Hsp12p is inserted into the cell wall remains unclear, however, since there are no obvious sequence motifs in Hsp12p which might direct this protein to this locus.

Acknowledgements

RJK and GGL would like to acknowledge the support of the National Research Foundation of South Africa and the University of Cape Town Research Fund. FG also thanks the CNRS programs (PNIR-Biofilm and ACI ECCO) for partial support of this work.

References

[1] R.L. Stone, V. Matarese, B.B. Magee, P.T. Magee, D.A. Bemlohr, Cloning, sequencing and chromosomal assignment of a gene from *Saccharomyces cerevisiae* which is negatively regulated by glucose and positively by lipids, Gene 96 (1990) 171–176.

[2] J.C.S. Varela, U.M. Praekelt, P.A. Meacock, R.J. Planta, W.H. Mager, The *Saccharomyces cerevisiae HSP12* gene is activated by the high-osmolarity glycerol pathway and negatively regulated by protein kinase A, Mol. Cell Biol. 15 (1995) 6232–6245.

[3] R. Garcia, C. Bermejo, C. Grau, R. Perez, J.M. Rodriguez-Pena, J. Francois, C. Nombela, J. Arroyo, The global transcriptional response to transient cell wall damage in *Saccharomyces cerevisiae* and its regulation by the cell, J. Biol. Chem. 279 (2004) 15183–15195.

[4] L. Mtwisha, W.F. Brandt, S. McCready, G.G. Lindsey, HSP12 is a LEA-like protein in *Saccharomyces cerevisiae*, Plant Mol. Biol. 37 (1998) 513–521.

[5] K. Sales, W.F. Brandt, E. Rumbak, G.G. Lindsey, The LEA-like protein HSP12 in *Saccharomyces cerevisiae* has a plasma membrane location and protects membranes against desiccation and ethanol-induced stress, Biochim. Biophys. Acta 1463 (2000) 267–278.

[6] P. Motshwene, R. Karreman, G. Kgari, W. Brandt, G. Lindsey, LEA (late embryonic abundant)-like protein Hsp12p (heat-shock protein 12) is present in the cell wall and enhances the barotolerance of the yeast *Saccharomyces cerevisiae*, Biochem. J. 377 (2004) 769–774.

[7] R.J. Karreman, W.F. Brandt, G.G. Lindsey, The yeast *Saccharomyces cerevisiae* stress response protein Hsp12p decreases the gel strength of

agarose used as a model system for the β-glucan layer of the cell wall, Carbohydr. Polym. 60 (2005) 193–198.
[8] F. Gaboriaud, Y.F. Dufrêne, Atomic force microscopy of microbial cells: application to nanomechanical properties, surface forces and molecular recognition forces, Colloids Surf., B Biointerfaces 54 (2006) 1–10.
[9] W.F. Heinz, J.H. Hoh, Spatially resolved force spectroscopy of biological surfaces using the atomic force microscope, Trends Biotech. 17 (1999) 143–150.
[10] A. Touhami, B. Nysten, Y.F. Dufrêne, Nanoscale mapping of the elasticity of microbial cells by atomic force microscopy, Langmuir 19 (2003) 4539–4543.
[11] F. Gaboriaud, S. Bailet, E. Dague, F. Jorand, Surface structure and nanomechanical properties of *Shewanella putrefaciens* bacteria at two pH values (4 and 10) determined by Atomic force microscopy, J. Bacteriol. 187 (2005) 3864–3868.
[12] P. Hinterdorfer, Y.F. Dufrêne, Detection and localization of single molecular recognition events using atomic force microscopy, Nat. Methods 3 (2006) 347–355.
[13] A. Touhami, B. Hoffmann, A. Vasella, F.A. Denis, Y.F. Dufrene, Aggregation of yeast cells: direct measurement of discrete lectin-carbohydrate interactions, Microbiology 149 (2003) 2873–2878.
[14] J.F.L. Duval, H. Ohshima, Electrophoresis of diffuse soft particles, Langmuir 22 (2006) 3533–3546.
[15] E. Dague, J. Duval, F. Jorand, F. Thomas, F. Gaboriaud, Probing surface structures of *Shewanella* spp. by microelectrophoresis, Biophys. J. 90 (2006) 2612–2621.
[16] J.F.L. Duval, H.J. Bussher, B. van de Belt-Gritter, H.C. van der Mei, W. Norde, Analysis of the interfacial properties of fibrillated and nonfibrillated oral streptococcal strains from electrophoretic mobility and titration measurements: evidence for the shortcomings of the "classical soft-particle approach", Langmuir 21 (2005) 11268–11282.
[17] M. Wenning, H. Seiler, S. Scherer, Fourier-Transform Infrared microspectrometry, a novel and rapid tool for identification of yeasts, Appl. Environ. Microbiol. 68 (2002) 4717–4721.
[18] A.J. Michell, G. Scurfield, An assessment of infrared spectra as indicators of fungal cell wall composition, Aust. J. Biol. Sci. 23 (1970) 345–360.
[19] K. Bahmed, F. Quilès, R. Bonaly, J. Coulon, Fluorescence and infrared spectroscopic study of cell walls from *Candida*, *Khyveromyces*, *Rodotorula* and *Schizosaccharomyces* yeasts in relation with their chemical composition, Macromolecules 4 (2003) 1763–1772.
[20] U.M. Praekelt, P.A. Meacock, *HSP12*, a new small heat shock gene of *Saccharomyces cerevisiae*: analysis of structure, regulation and function, Mol. Gen. Genet. 223 (1990) 97–106.
[21] F.M. Mirabella Jr., N.J. Harrick, Internal reflection spectroscopy: review and supplement, Harrick Scientific Corporation, New York, USA, 1985.
[22] Y.F. Dufrêne, Application of atomic force microscopy to microbial surfaces: from reconstituted cell surface layers to living cells, Micron 32 (2001) 153–165.
[23] G.A. Burks, D. Velegol, E. Paramonova, B.E. Lindenmuth, J.D. Feick, B.E. Logan, Macroscopic and nanoscale measurements of the adhesion of bacteria with varying outer surface composition, Langmuir 19 (2003) 2366–2371.
[24] T.A. Camesano, B.E. Logan, Probing bacterial electrosteric interactions using atomic force microscopy, Environ. Sci. Technol. 34 (2000) 3354–3362.
[25] V. Vadillo-Rodriguez, H.J. Busscher, W. Norde, J. de Vries, R.J.B. Dijkstra, I. Stokroos, H.C. van der Mei, Comparison of atomic force microscopy interaction forces between bacteria and silicon nitride substrata for the three commonly used immobilization methods, Appl. Environ. Microbiol. 70 (2004) 5441–5446.
[26] J.F.L. Duval, K.J. Wilkinson, H.P. van Leeuwen, J. Buffle, Humic substances are soft and permeable: evidence from their electrophoretic mobilities, Environ. Sci. Technol. 39 (2005) 6435–6445.
[27] F.M. Klis, P. Mol, K. Hellingwerf, S. Brul, Dynamics of cell wall structure in *Saccharomyces cerevisiae*, FEMS Microbiol. Rev. 26 (2002) 239–256.
[28] A.E. Smith, Z.B. Zhang, C.R. Thomas, K.E. Moxham, A.P.J. Middelberg, Proc. Natl. Acad. Sci. 97 (2000) 9871–9874.
[29] J.K. Lancaster, Abrasive wear of polymers, Wear 14 (1969) 223–239.
[30] R. Garcia, C. Bermejo, C. Grau, R. Perez, J.M. Rodriguez-Pena, J. Francois, C. Nombela, J. Arroyo, The global transcriptional response to transient cell wall damage in *Saccharomyces cerevisiae* and its regulation by the cell integrity signalling pathway, J. Biol. Chem. 279 (2004) 15183–15195.
[31] H.C. Causton, B. Ren, S.S. Koh, C.T. Harbison, E. Kanin, E.G. Jennings, T.I. Lee, H.L. True, E.S. Lander, R.A. Young, Remodeling of yeast genome expression in response to environmental changes, Mol. Biol. Cell 12 (2001) 323–337.
[32] D.E. Levin, Cell wall integrity signalling in *Saccharomyces cerevisiae*, Microbiol. Mol. Biol. Rev. 69 (2005) 262–291.
[33] J. Ogas, B.J. Andrews, I. Herskowitz, Transcriptional activation of CLN1, CLN2, and a putative new G1 cyclin (HCS26) by SWI4, a positive regulator of G1-specific transcription, Cell 66 (1991) 1015–1026.
[34] J.C. Igual, A.L. Johnson, L.H. Johnston, Coordinated regulation of gene expression by the cell cycle transcription factor SW1 and the protein kinase C MAP kinase pathway for yeast cell integrity, EMBO J. 15 (1996) 5001–5013.
[35] U.S. Jung, D.E. Levin, Genome-wide analysis of gene expression regulated by the yeast cell wall integrity pathway, Mol. Microbiol. 34 (1999) 1049–1057.
[36] A.F. Ram, J.C. Kapteyn, R.C. Montijn, L.H. Caro, J.E. Douwes, W. Baginsky, P. Mazur, H. van den Ende, F.M. Klis, Loss of the plasma membrane-bound protein Gas1p in *Saccharomyces cerevisiae* results in the release of beta1,3-glucan into the medium and induces a compensation mechanism to ensure cell wall integrity, J. Bacteriol. 180 (1998) 1418–1424.
[37] A. Galichet, G.D. Sockalingum, A. Belarbi, M. Manfait, FTIR spectroscopic analysis of *Saccharomyces cerevisiae* cell walls: study of an anomalous strain exhibiting a pink-colored cell phenotype, FEMS Microbiol. Lett. 197 (2001) 179–186.

Annexe 3

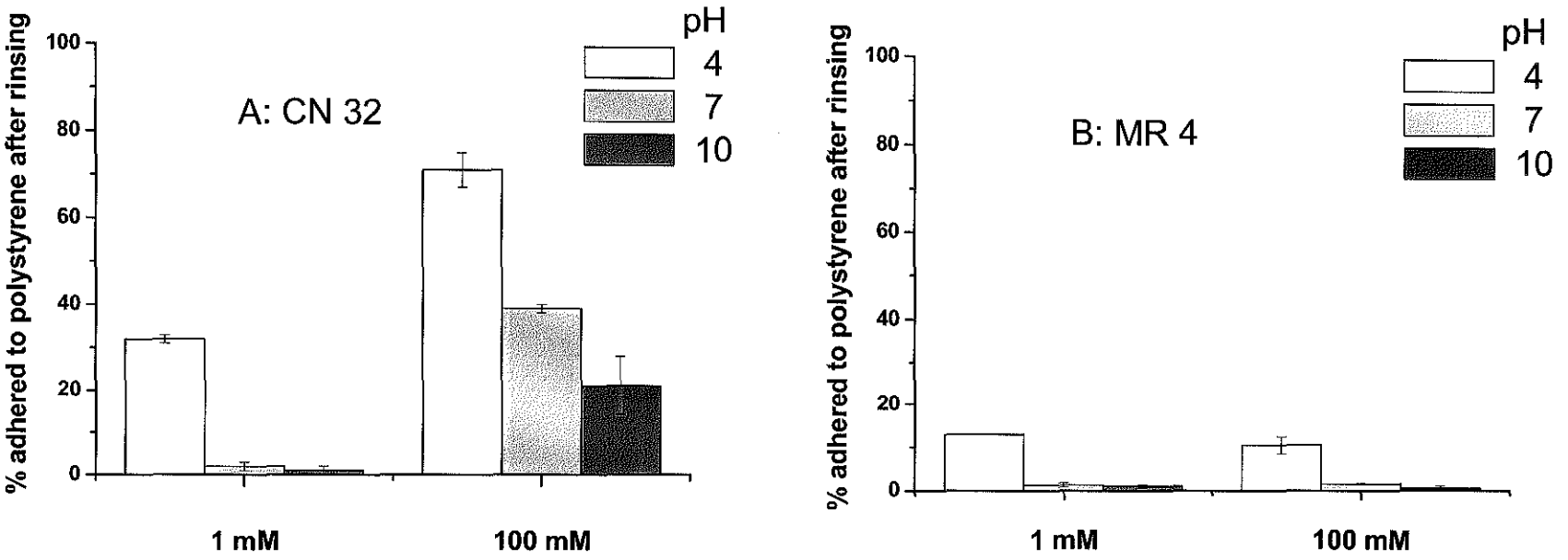

Pourcentage d'adhésion de *Shewanella* spp. (A : *S. putrefaciens* CN32, B : *Shewanella oneidensis* MR4) au polystyrène. Expérience réalisée selon le protocole décrit au chapitre quatre.

Nancy-Université

Université Henri Poincaré

Prénom, Nom : **Etienne DAGUE**

Nature de la thèse :

Doctorat de l'Université Henri Poincaré, Nancy 1
en Biologie - Santé - Environnement

VU, APPROUVE et PERMIS D'IMPRIMER N° 1308

Nancy, le 29/11/06

Le Président de l'Université Henri Poincaré, Nancy I

UNIVERSITÉ HENRI POINCARÉ, NANCY LE PRÉSIDENT

Jean-Pierre FINANCE

Résumé

L'interface entre les bactéries et leur milieu environnant est impliquée dans de nombreux phénomènes : adhésion, biominéralisation, reconnaissance de surface. Les propriétés physico-chimiques de ces interfaces cellulaires sont le plus souvent qualifiées à des échelles macroscopiques (test d'adhésion à une surface ou à des solvants, mesure d'angle de contact...) ne permettant pas de décrire toute la complexité de ces interfaces. Afin de quantifier ces propriétés aux différentes échelles : micrométrique et nanométrique, nous avons mis en œuvre une approche basée sur des techniques microscopiques et spectroscopiques. Quatre souches du genre *Shewanella* ont été choisies pour la variabilité structurale de leurs enveloppes (présence détectable ou non de polymères en surface).

Nous avons pu quantifier par spectroscopie de force l'effet du pH et de la force ionique sur les enveloppes bactériennes. Cette analyse des courbes de force obtenues par AFM a permis de quantifier, *in situ*, le module d'Young (élasticité) et aussi la constante de raideur (en relation avec la pression de turgescence de la cellule) des bactéries. L'augmentation du pH et/ou de la force ionique induit une augmentation de la souplesse nanomécanique des bactéries.

D'autre part, l'analyse électrocinétique, par le biais d'outils théoriques récemment développés, a montré des relations complexes entre la mobilité électrophorétique des quatre souches bactériennes, la charge effective des cellules et leurs propriétés hydrodynamiques, jusque là ignorées en microbiologie. Ainsi, nous avons pu démontrer que les cellules sans polymère présentent une densité de charge beaucoup plus importante avec une perméabilité faible alors que les cellules avec polymères sont peu chargées mais fortement perméables.

La combinaison complémentaire de ces différentes approches constitue l'originalité de notre travail et a permis d'ores et déjà, d'interpréter les phénomènes observés aux échelles macroscopiques. Par conséquent, ces nouvelles données permettent une meilleure compréhension mécanistique de la réactivité des bactéries, notamment de leur capacité d'adhésion. Ainsi, nous proposons une hypothèse expliquant les propriétés d'adhésion, au polystyrène, des cellules modèles de notre étude. Les cellules présentant un polymère important adhèrent moins bien que celles sans polymère en raison du caractère hydrodynamique mou de leur interface et des différences de densité de charge. Les évolutions des interfaces bactériennes avec le pH et la force ionique, démontrées dans ce travail, induisent des modifications des capacités d'adhésion renforçant cette hypothèse.

Mots-clefs : AFM, Bioadhésion, Electrocinétique des particules molles, Interface bactérienne, *Shewanella* spp., Spectroscopie de force.